AGU ADVANCING EARTH AND SPACE SCIENCES

Reviews of Geophysics

REVIEW ARTICLE
10.1029/2023RG000804

Multi-Scale Soil Salinization Dynamics From Global to Pore Scale: A Review

Nima Shokri[1,2], **Amirhossein Hassani**[3], **and Muhammad Sahimi**[4]

[1]Institute of Geo-Hydroinformatics, Hamburg University of Technology, Hamburg, Germany, [2]United Nations University Hub on Engineering to Face Climate Change at the Hamburg University of Technology, United Nations University Institute for Water, Environment and Health (UNU-INWEH), Hamburg, Germany, [3]The Climate and Environmental Research Institute NILU, Kjeller, Norway, [4]Mork Family Department of Chemical Engineering and Materials Science, University of Southern California, Los Angeles, CA, USA

Key Points:

- Soil salinization poses existential threat to sustainable agriculture, food security, and soil fertility
- We synthesized recent advances on soil salinization at different length scales, ranging from pore to global scale
- We offer new insights and present future outlook on the key challenges and open questions related to soil salinization

Correspondence to:

N. Shokri, A. Hassani and M. Sahimi,
nima.shokri@tuhh.de;
ahas@nilu.no;
moe@usc.edu

Citation:

Shokri, N., Hassani, A., & Sahimi, M. (2024). Multi-scale soil salinization dynamics from global to pore scale: A review. *Reviews of Geophysics*, *62*, e2023RG000804. https://doi.org/10.1029/2023RG000804

Received 5 DEC 2023
Accepted 20 AUG 2024

Abstract Soil salinization refers to the accumulation of water-soluble salts in the upper part of the soil profile. Excessive levels of soil salinity affects crop production, soil health, and ecosystem functioning. This phenomenon threatens agriculture, food security, soil stability, and fertility leading to land degradation and loss of essential soil ecosystem services that are fundamental to sustaining life. In this review, we synthesize recent advances in soil salinization at various spatial and temporal scales, ranging from global to core, pore, and molecular scales, offering new insights and presenting our perspective on potential future research directions to address key challenges and open questions related to soil salinization. Globally, we identify significant challenges in understanding soil salinity, which are (a) the considerable uncertainty in estimating the total area of salt-affected soils, (b) geographical bias in ground-based measurements of soil salinity, and (c) lack of information and data detailing secondary salinization processes, both in dry- and wetlands, particularly concerning responses to climate change. At the core scale, the impact of salt precipitation with evolving porous structure on the evaporative fluxes from porous media is not fully understood. This knowledge is crucial for accurately predicting soil water loss due to evaporation. Additionally, the effects of transport properties of porous media, such as mixed wettability conditions, on the saline water evaporation and the resulting salt precipitation patterns remain unclear. Furthermore, effective continuum equations must be developed to accurately represent experimental data and pore-scale numerical simulations.

Plain Language Summary Soil salinization refers to the excess accumulation of salt in soil to a level that affects crop production and ecosystem functioning. This poses existential threat to sustainable agriculture, food security, and soil fertility. Soil salinization is considered as one of the major drivers for desertification, resulting in a persistent loss of ecosystem services. It also imposes nutritious imbalances in plants that may induce significant alterations in Earth's organisms, ecosystems, and biodiversity. We synthesized recent advances on soil salinization at different length and time scales, ranging from pore to global scale, offering new insights, and presenting future perspective on the key challenges and open questions on soil salinization.

1. Introduction

Soil, a complex and dynamic ecosystem, plays a fundamental role in supporting life on Earth. It functions as a carbon sink, storing large amounts of carbon, and serves as a medium for plant growth, providing anchorage, water, and nutrients. Soil acts as a reservoir for water, regulating its availability to plants and playing a vital role in the hydrological cycle. Soil also supports a diverse community of organisms, ranging from microorganisms, such as bacteria and fungi to larger organisms such as earthworms and insects, all of which contribute to nutrient cycling and organic matter decomposition.

Soil also plays a vital role in the livelihood of human beings. It not only provides the ground for growing part of the food that we eat every day, and the grass that livestock needs to feed itself, its quality also affects the air that we breathe, and the water that we drink. The significance of soil, though acknowledged and appreciated throughout history, is being increasingly recognized in our era due to the rapidly growing world's population and the ongoing global changes. The ability to feed the people relies heavily on our actions and limitations concerning soil. In fact, an important issue over the past few decades has been food security, to which soil, and more specifically agricultural lands, are critical. At the same time, the ongoing climate challenges are increasing the risk of

prolonged droughts in some areas around the globe, which can adversely impact soil health (A. Dai, 2011; Vicente-Serrano et al., 2020).

Due to a variety of factors, the arable land resources, and in particular fertile soils, have been decreasing rapidly, causing worldwide concerns. According to several reports (see, for example, European Commission Report et al., 2020; Olsson et al., 2019; Wild, 2003) around 15% of the world's land has been degraded. However, other sources report higher figures with some estimating as much as one-third of the Earth's land surface is affected by degradation (see, for example, UNEP factsheet, 2017). Soil degradation, as a subset of land degradation, refers to the deterioration of soil quality. A degraded soil is one that has undergone a decline in its physical, chemical, or biological properties, resulting in diminished fertility, productivity, and ecosystem services compared to its natural state (Blum, 2020). Degraded soils often exhibit erosion, compaction, loss of organic matter, nutrient depletion, salinization, or contamination with pollutants. Human-induced factors, such as unsustainable land use practices, deforestation, overgrazing, and poor irrigation management are among the reasons for soil degradation (Hopmans et al., 2021). Preserving soil is, therefore, crucial, since the aforementioned factors are relentlessly at work. Soil preservation implies that the causal factors that contribute to soil degradation must be recognized, understood, and to the extent possible mitigated. Among such factors are erosion of soil by wind and excess water, contamination by industrial and agricultural processes, and soil salinization.

The last factor, namely, soil salinization, is the subject of the present review. Soil salinization refers to the excess accumulation of soluble salts in soil. Excessive levels of soil salinity adversely influence vegetation, food security, and environmental health. Salt stress in soils may cause reduced plant transpiration, which influences the surface water-energy partitioning (Perri, Suweis, et al., 2018) and impedes long-term plant growth (Runyan & D'Odorico, 2010; Parihar et al., 2015). Moreover, excessive soil salinity influences functioning of the soil microbial community (L. Liu et al., 2023) that disturbs its nitrogen cycle and respiration (Rath & Rousk, 2015). Salt storms from saline soils (Hassani, Azapagic, D'Odorico, et al., 2020), desertification (D'Odorico et al., 2013; Perri et al., 2020), disrupting soil organic carbon (OC) cycle (Wong et al., 2010), and deterioration of economic opportunities that may lead to human migration (J. Chen & Mueller, 2018) are among other consequences of soil salinization. Soil salinization spreads through various types of land, moving beyond national borders and impacting areas such as deserts, farmlands, or coastal areas (Hassani, Azapagic, & Shokri, 2020; Tully et al., 2019; Werner et al., 2013). The environmental consequences of soil salinization, including loss of biodiversity and habitat degradation (Sahab et al., 2021), necessitate global attention to conserving natural ecosystems.

Understanding the mechanisms of soil salinization is essential to addressing such a growing environmental challenge. Motivated by the importance of soil salinization, the goal of this review is to describe mechanisms and models of soil salinization, from the large to pore scale. In the context of this review, salinization at large or global scale refers to a broad range of processes and interactions that go well beyond the boundaries of individual agricultural fields. In essence, while molecular, pore, and core scales deal with intricate and minute details of soil and salinity processes at a small and localized level, the large scales that we mean here encompass processes that operate at a much larger scope that consider the patterns of soil salinization across a collection of farmlands, regions, countries, and even globally. Yet, these pore to large-scale processes are connected, and linking them is the real challenge in the field.

We will start by defining the salinity and its global extent (Sections 2 and 3) and describing its drivers and impacts. Section 4 reviews key drivers of soil salinity, discussing inland and coastal soil salinity interactions with factors such as climate change, rising sea levels, saline dust and aerosols, and soil morphology. Section 5 discusses the negative environmental and socio-economic impacts of soil salinity, highlighting their implications for plant ecosystems, plant growth, and human livelihoods. Following this, we will discuss various aspects of soil salinity, starting from the largest scale, which is the global level, and then progressing to the core, pore, and molecular scales. Sections 6 and 7 focus on monitoring and modeling soil salinity at large scales, discussing the methods and challenges involved, while Section 8 introduces soil salinization at the core to pore scale, discussing evaporation process as a factor which could lead to soil salinization. In Section 9, the molecular mechanisms of salt formation in soil will be covered. Some fundamental aspects of soil salinization chemistry in soil are discussed in Section 10, while the final section highlights potential future research directions (Section 11).

2. Salinity and Sodicity

Salinity is the amount of salt dissolved in a body of water, commonly known as saline water, and is measured usually in g L^{-1} or g kg^{-1}, that is, grams of salt per liter or kilogram of water. Important aspects of the chemistry of natural water are controlled or influenced by salinity. If biological processes also occur in the water, they are also influenced by salinity. Salinity is, in fact, a thermodynamic state variable that, in addition to temperature and pressure, governs physical characteristics of water, such as its density and heat capacity. *Isohalines* or *isohales* are lines (or contours) that connect points with the same salinity in an aquatic system.

Although conceptually simple, practical definition of salt depends on the water content, especially natural water —water in natural systems, such as soil—which usually contains a complex mixture of various elements contributed by different sources with distinct molecular structures. At the same time, the chemical properties of such molecular structure depend on temperature and pressure. To circumvent such difficulties, salinity is usually linked to the sum of masses of a subset of the dissolved chemical constituents, which is usually referred to as *solution salinity*. For practical purposes, the sum is often limited to a set of eight major ions in natural waters (Pawlowicz & Feistel, 2012), but to define with high precision of seawater salinity, additional seven minor ions are also included; see the International Thermodynamic Equation of Seawater (TEOS, 2010).

As for soil salinity, one usually estimates the concentration of total soluble salts of the soil solution by measuring the Electrical Conductivity EC or g with units dS m^{-1} or mmho cm^{-1}. Note that 1 dS m^{-1} corresponds to a salt concentration of about 680 mg L^{-1} of total dissolved solids in soil solution. For comparison, seawater conductivity is about 50 dS m^{-1}. Although in principle we are interested in field measurements of the EC, which represents the bulk soil, the more accepted measurement of soil salinity uses the EC of the extracted solution of a saturated soil paste, denoted by EC_e, or g_e (US Soil Salinity Laboratory, 1954). The reasons for advocating EC_e are twofold. One is that the chemistry of the saturated soil extract is close to that of the soil water; the second reason is that the chemistry may vary if larger soil water dilutions is employed, dissolution and precipitation of sulfate and carbonate minerals may occur, which explains why EC_e is preferred to other soil-water ratios for measuring EC.

On the other hand, soil sodicity is one that is characterized by concentrations of Na^+ relative to other cations, positively charged ions, in the soil exchange complex. As sodium salts are leached through the soil, some Na^+ remains bound to clay particles, and displace other cations. When the amount of sodium reaches a certain level that influences soil structure, it is considered "sodic" soil. Sodicity degrades the properties of soil by weakening the bond between soil particles. When soil contains high levels of Na^+, these ions attach to soil particles, particularly clay particles, through electrostatic forces. This causes the clay particles to repel each other, leading to dispersion. Sodicity negatively affects soil infiltration (Wong et al., 2010), raises the risk of water and wind erosion (De la Paix et al., 2013), and accelerates the decomposition of soil organic matter (K. Singh, 2016; P. Singh et al., 2023). In fact, Sodicity is a form of salinity characterized by a higher concentration of Na^+ ions compared to other cations.

According to Abrol et al. (1988) and Richards (1954), if $EC_e < 4$ dS m^{-1}, the soil is classified as non-saline, whereas soils with $4 \leq EC_e < 8$, $8 \leq EC_e \leq 16$ and $EC_e > 16$ dS m^{-1} should be viewed, respectively, as moderately, strongly and very strongly saline soils. Abrol et al. (1988) labelled soils with the salinity range of $2 \leq EC_e < 4$ as slightly saline soils where yields of sensitive crops may be restricted. Note that depending on the soil classification system, the salinity threshold can be other values such as 15 (R. K. Gupta et al., 2008) referred to as "Solonchaks" (soils with a high concentration of soluble salts at some time of the year) or even as high as 30 dS m^{-1} (Soil Survey Staff, 2022)—called "salic."

The corresponding levels for exchangeable sodium percentage (ESP), representative of sodicity severity, are 6% (Isbell, 2016; Northcote & Srene, 1972) or 15% (R. K. Gupta et al., 2008; Richards, 1954; Soil Survey Staff, 2022), in which case the soil is called "solonetz" or "natric." Moreover, the distinguishing characteristics of saline and sodic soils are not limited only to the values of EC_e and ESP; other soil physico-chemical properties, such as pH, salt content, sodium absorption ratio (SAR), and permeability, should also be taken into consideration. For example, according to the Soil Science Society of America (Soil Science Glossary Terms Committee, 2008), sodic soils are non-saline soils with enough concentrations of exchangeable sodium that can adversely affect crop productivity with a saturation extract SAR ≥13, rather than adopting any ESP threshold. We should also note that, although these are widely used, they do have some shortcomings. For example, EC_e may

underestimate the in-situ salinity for unsaturated soils. Moreover, soil wetting in the laboratory often results in dissolution of precipitated salts, thereby overestimating EC of the natural soil.

3. Salt-Affected Soils: A Global Overview

Soil salinity and sodicity levels fluctuate spatially and dynamically, particularly in the top 0–30 cm layer, which is sensitive to climate drivers (Ivushkin et al., 2019; Mulder et al., 2011; Zaman et al., 2018). Figure 1 presents the global distribution of salt-affected soils, excluding the frigid zones (after Hassani, Azapagic, & Shokri, 2020). The maps and predictions of saline and sodic soils are generated using Machine Learning (ML) algorithms that are trained based on ground-based measurements and predictive variables. Natural events, such as flash floods, and climate events, such as El Niño, can significantly impact salt levels in the soil, affecting both short- and long-term dynamics (Hassani, Azapagic, & Shokri, 2020). Numerous data sets related to the global occurrence of salt-affected soils have been compiled through a combination of soil survey data and statistical extrapolation. Global studies indicate that salt-affected soils (which primarily include the saline, sodic, and saline-sodic soils) are present across every climate zone and continent, covering an estimated area of approximately 4.2 to even 17 million km^2, depending on the measurement, modeling, mapping, and vertical averaging methods used (FAO, 2000; FAO-Itps, 2015; Ghassemi et al., 1995; Hassani, Azapagic, & Shokri, 2020; Ivushkin et al., 2019; Nachtergaele et al., 2008; Negacz et al., 2022; Oldeman et al., 1990; Squires & Glenn, 2011; Szabolcs, 1989; Wicke et al., 2011).

In addition, the range of estimates for salt-affected soils can vary widely between different studies partly due to differences in the soil classification systems and the threshold values used to define salt-affected conditions (Hassani, Azapagic, & Shokri, 2020). As mentioned earlier, the EC_e, the key measure of soil salinity, has various threshold values in different classification systems (see Section 2). Some systems use a threshold value of 4 dS m^{-1} for EC_e (Abrol et al., 1988; Richards, 1954), while others use 2 dS m^{-1} (as in the case of Harmonized World Soil Database (HWSD)—to be detailed in Section 6.4). As an example, Negacz et al. (2022) indicated that soils with an EC_e exceeding 4 dS m^{-1} covered a total area of 16.6 million km^2. The extent of such salt-affected soils was determined using the ECOCROP model in their study.

Estimates of Kraamwinkel et al. (2021) indicate that 20% of total cultivated and 33% of irrigated agricultural lands around the globe have been afflicted by high salinity. According to a report by the United Nations' Food and Agricultural Organization (FAO) and the Intergovernmental Technical Panel on Soils (ITPS) (FAO-ITPS, 2015; Hopmans et al., 2021), about one-third of the world's irrigated land—70 Mha—is affected by salt. A more recent Global Map of Salt-Affected Soils (GSASmap) (FAO, 2021a), a collaborative effort involving contributions from 118 countries offering data from 257,419 locations and involving over 350 national experts in its creation, maps salt-affected soils in two depth intervals (0–30 and 30–100 cm), including parameters such as EC, ESP, and pH (salt-affected soils: $EC_e > 2$ dS m^{-1}, ESP > 15% and pH > 8). Covering 85% of the world's land area, the map indicates that over 4.24 million km^2 of topsoil (0–30 cm) and 8.33 million km^2 of subsoil (30–100 cm) are affected by salt. The data reveals that 3% of global topsoils and 6% of subsoils are impacted by salinity or sodicity. Eighty-five percent of salt-affected topsoils are saline ($EC_e > 2$ dS m^{-1}), while this is 62% for salt-affected subsoils.

It is widely agreed, however, that saline and salt-affected soils, which include sodic soils, are predominantly located in drylands (Abrol et al., 1988; Fischer et al., 2008; Richards, 1954). In these regions, the evaporation rate surpasses the water input rate into the soil, leading to salt accumulation in the top layer. Drylands are defined by a multi-year aridity index below 0.65 mm mm^{-1}, calculated as the ratio of total annual precipitation to potential evapotranspiration (Sorensen, 2007). These areas form approximately 45% of the Earth's land surface (Prăvălie, 2016; Schimel, 2010). For example, according to GSASmap (FAO, 2021a), over two-thirds of the world's salt-affected soils are in arid and semi-arid climates. Specifically, 37% of these soils are found in arid desert regions, while 27% are located in arid steppes, evenly split between cold and hot arid steppe areas.

In Europe, a continent not typically associated with deserts and arid areas, soil salinization has been acknowledged as a contributing factor to soil degradation. According to a report by the European Commission Report et al. (2020), 60%–70% of Europe's soil is classified as “unhealthy,” prompting the need for significant action to move toward sustainable land and soil management. For soil preservation in Europe, the Mission Board's proposal defines reducing desertification and salinization through restoration of 50% of the degraded land by 2030 as the first

objective. However, it is important to note that salinization is just one of many drivers of soil degradation in Europe and other factors such as biochemical degradation, erosion, and the loss of OC and nutrients should not be neglected.

National-scale studies that quantify trends in soil salinity are relatively rare. That being said, the global map tracking soil salinity changes from 1986 to 2016 by Ivushkin et al. (2019) found that soil salinity is globally increasing. On the other hand, a study by Hassani, Azapagic, and Shokri (2020) that estimated trends in areas with soils with an EC_e of 4 dS m^{-1} or larger found the trends in salinity to be dependent upon location, which cannot be generalized to state that soil salinity is increasing or decreasing globally. Their findings were statistically significant ($P < 0.05$) for only 117 of the 256 countries or states examined. The countries with the highest rates of annual increase in areas with high salinity were Brazil, Peru, Sudan, Colombia, and Namibia. It is, however, worth noting that these estimates were generated using ML techniques partially trained using remote sensing data. The study cautioned that such data, particularly vegetation indices, can be unreliable in regions with frequent cloud cover, such as the Amazon basin.

Even more alarming is the estimation by Abbas et al. (2013). The annual rate of increase in the salinized areas is estimated to be around 10%, equivalent to 2 million hectares (Mha) per year (Abbas et al., 2013). Such a rapid increase is caused by rock weathering, drought or low precipitation, irrigation with saline water, evaporation, and poor agricultural practices. Moreover, it has been estimated that, if the current trends continue, over 50% of the arable land would be salinized by the year 2050 (Jamil et al., 2011).

At a more regional scale, a study by Herrero and Pérez-Coveta (2005) aimed at identifying trends in soil salinization or desalinization in the Flumen irrigation district in Aragón, Spain, by directly measuring soil salinity over time. Soil samples were collected in 1975, 1985–1986, and 1999, with important findings indicating a decrease in soil salinity over the 24 years. Specifically, the median EC_e in saline areas dropped from 5.9 dS m^{-1} in 1975 to 1.9 dS m^{-1} in 1999.

4. Drivers of Soil Salinization at Different Scales

It is important to emphasize the distinction between soil salinity and soil salinization, as they are distinct but interconnected concepts in soil science. Soil salinity refers to the existing presence of salts within the soil, which can originate from natural or human-related processes. Conversely, soil salinization refers to the ongoing process resulting in the build-up of salt in the soil both due to natural and anthropogenic drivers. Human activities, such as irrigation with saline water, improper land management, or industrial processes are examples of anthropogenic drivers. Soil salinization is a specific process that falls under the broader category of soil degradation processes (Intergovernmental Panel on Climate Change, 2022).

Salt transport in soil is governed by complex interplay of various factors, each of which contributes to the distribution of salts in soils. Such factors include climate, geomorphology, hydrology, vegetation response to salinity (e.g., Barrett-Lennard, 2002), and human activities, and their roles in shaping soil salinity patterns are crucial to understanding the various aspects of salinity at different spatial and temporal scales. In general, all such factors that act as sources of salt in soil may be put into two groups: they are either natural (primary) or man-made (anthropogenic; secondary) (Ding et al., 2011). Of course, the two types of drivers interact with each other. Hence, natural causes of salt salinization are amplified by the anthropogenic ones that act faster and cause effects that may persist over very long time scales.

Primary, or natural, salinization refers to development and natural deposition of weathered minerals that contain high concentration of salt. The weathering produces such ions as sodium, calcium, magnesium, and potassium, which are dissolved in freshwater. If precipitation is insufficient to leach the ions from the soil profile, salts accumulate and salinize the soil (Blaylock, 1994). Global warming has also been intensifying weathering of rocks (Gong et al., 2023). The changes in salinity that are associated with the weathering occur over a time scale of about 100,000 years, although variations over shorter cycles of 23,000–41,000 years may also occur (Neukom et al., 2014). Anthropogenic, or secondary, sources of soil salinization include industrial processes that increase salt content of soil, and agricultural practices that are not sustainable.

4.1. Agricultural, Mining, and Industrial Activities

While modern irrigation methods have increased plants productivity, they can also salinize soil. For example, the volume of water used for irrigation is usually such that it can reach no deeper than plants' root zone. Thus, even

small amounts of salt in the water can deposit and accumulate over time (Greene et al., 2016). A meta-analysis of 74 studies by Du et al. (2023) revealed that drip irrigation typically reduced soil salinity in the root zone by 37.7% and boosted crop yield by 37.4%, when compared with flooding irrigation. On the other hand, if too much water is used in irrigation, it may cause the water table to rise, causing capillary rise of saline groundwater. Extensive use of chemical fertilizers can also be a contributing factor to soil salinization (Maas & Grattan, 1999). Khasanov et al. (2023) monitored and mapped nationwide cropland and soil salinity changes in Uzbekistan using the Google Earth Engine platform for the period from 2000 to 2020. Their study found that phosphorus-based mineral fertilizers contributed to soil salinity, while other agrochemical applications showed no significant effect on soil salinity.

Another major anthropogenic factor that contributes to increasing salt in soil is irrigation of agricultural land by brackish water, that is, water in natural settings whose level of salt is higher than that of fresh water, but lower than seawater. In its natural state, brackish water is used primarily as a cooling agent in the power, oil, and gas, and the mining industries and, therefore, as discussed above, at least some of such water will eventually reach soil and increase the salt level. Its unregulated use for irrigation in a practice known as saline agriculture also leads to increased salinity in soil, although certain crops, such as cabbage and oats, are salt tolerant and can grow on salt-affected land and irrigated with brackish water. Use of brackish water in countries with scarce fresh water resources is quite common; see, for example, Pang et al. (2010).

Two major industrial processes that increase salt in soil are oil extraction, and adding salt to roads in order to lower freezing point of water. Oil reservoirs are formed over geological time scales in marine environments that contain brine. Thus, when crude oil is extracted, it always contains salt water, whose salt content can be as high as 200,000 ppm (A.-M. O. Mohamed et al., 2003), which must be removed from oil. Often, the saline water is injected back into the reservoirs in order to increase oil production, but it must eventually be disposed of, which poses great difficulty to site remediation (Leung et al., 2003; McFarland et al., 1987). Salts used in drilling mud and channelization in coastal oil fields (Ko et al., 2004) can also cause increased soil salinity levels. Other industrial sources of salt for soil salinization include wastes from mines, paper, pulp, food, textiles, cement, and steel production (Morudu, 2009; Muller et al., 2009), and from power generation. For example, pouring saline drainage water from mines into rivers is a common practice in many parts of the world.

Although applying salt to roads for lowering the freezing temperature of water is a common practice, it also salinizes soil and freshwater (Chernousenko et al., 2003; Daley et al., 2009). Salt added to roads migrates to their sides and accumulate on the ground. When the snow melts, it carries with it the salt to water streams. Precipitation, flooding, and even wind can transfer the salt to soil (Seltenrich, 2023). According to Church and Friesz (1993), 55% of all the salts applied to roads end up in water bodies, while the rest accumulates in soil, and may even enter groundwater. If the applied salt is NaCl, as it often is, the Cl ions do not easily associate with soil particles, which is a source of concern.

Note that, as discussed by Mazhar et al. (2022), land drainage (Valipour, 2014), accelerated subsidence (Daliakopoulos, Tsanis, et al., 2016), groundwater extraction (White and Kaplan, 2017), and land use changes (Gopalakrishnan et al., 2019) must also be considered as anthropogenic drivers of soil salinization.

4.2. Drivers of Salinization in Freshwater Inland and Coastal Wetlands

Apart from the local cases documented in literature, no precise estimates are available for the current or future salinization of freshwater wetlands in both inland and coastal areas at the global scale (Herbert et al., 2015). However, it is evident that this is a widespread global issue that is expected to worsen over time. Salinization in freshwater inland and coastal wetlands is driven by multiple factors, shaped by natural processes or human activities. In arid and semi-arid environments, the salinity levels in wetlands fluctuate naturally due to factors such as intense evaporation, irregular rainfall, groundwater influx, and freshwater input following rain or flooding events (Jolly et al., 2008). Vegetation clearance, intensive irrigation, river regulation, mining and extraction, and de-icing salts are among the main factors that contribute to secondary salinization in inland freshwater wetlands (Herbert et al., 2015). The removal of deep-rooted vegetation, such as trees and grasses, disrupts the hydrological balance of wetlands. With fewer plants to absorb water, evapotranspiration decreases (Perri, Suweis, et al., 2018), which leads to elevated saline water tables. This disrupts pre-existing hydrological conditions, causing salt to move upwards through the soil. This phenomenon, known as dryland salinization, is particularly prevalent in landscapes with shallow saline aquifers (Greiner & Cacho, 2001; John et al., 2005). Interactions between

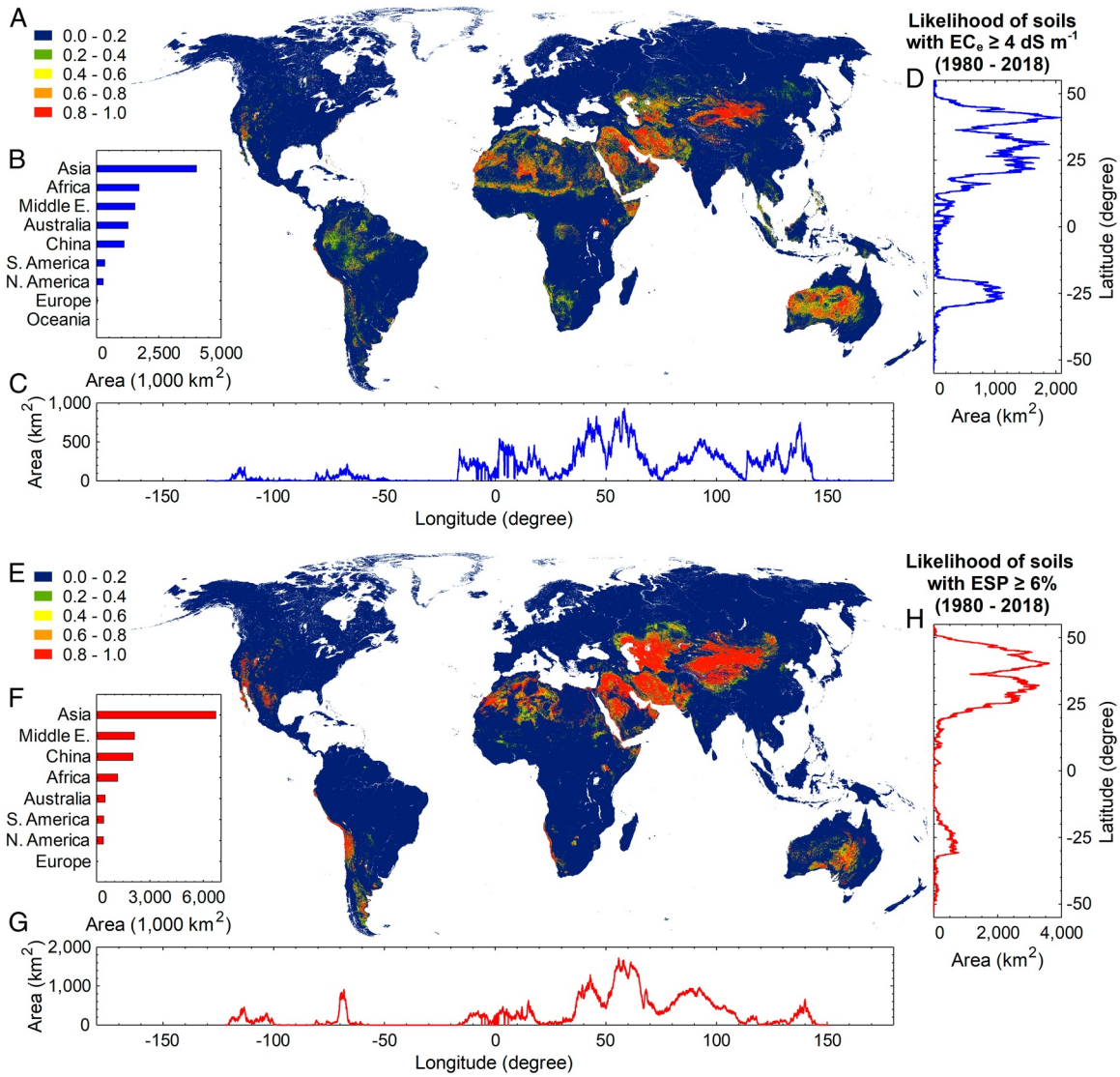

Figure 1. Global distribution of salt-affected soils, excluding the frigid zones (after Hassani, Azapagic, & Shokri, 2020). (a) and (e) Likelihood of the surface soils with an EC_e ≥ 4 dS m^{-1} and exchangeable sodium percentage (ESP) $\geq 6\%$ between 1980 and 2018, respectively (the likelihood is dimensionless, calculated by dividing the number of years with EC_e ≥ 4 dS m^{-1} or ESP $\geq 6\%$ by the total number of studied years). (d, h) and (c, g) Show the total area of soils with an annual predicted EC_e ≥ 4 dS m^{-1} and ESP $\geq 6\%$, respectively, in at least 75% of the period between 1980 and 2018 for various longitudes and latitudes at 30 arc-second resolution (about 1 km). (b, f) Total area of the soils with an annual predicted EC_e ≥ 4 dS m^{-1} and ESP $\geq 6\%$, respectively, in at least 75% of the period from 1980 to 2018 at the continental level.

groundwater and surface water in wetlands are primarily influenced by factors such as variations in hydraulic head between the wetland surface water and groundwater, the specific geomorphology of the wetland (especially the composition and characteristics of the wetland bed and banks), and the configuration of wetland and groundwater flow paths (Jolly et al., 2008).

Alterations to natural river flow patterns, such as dams and channelization, impact floodplain wetlands (see e.g., Álvarez-Cobelas et al., 2010). Such changes disrupt the natural wetting and drying cycles, resulting in desiccation of wetlands (Lane et al., 2018). Saline groundwater then penetrates the dried wetland beds, leading to salinization (Herbert et al., 2015).

Industries that discharge saline wastewater into aquatic systems contribute to salinization. For example, traditional drilling and oil extraction methods (Zabbey & Olsson, 2017) or surface mining activities can expose marine sediments and shallow saline aquifers, leading to salinization (see, e.g., Trites & Bayley, 2009). Among the

drivers of inland wetlands salinization, the role of salts used for de-icing cannot be neglected (Hernandez Gonzalez et al., 2023; Hintz et al., 2022). In colder climates, the application of de-icing salts on roads and airports introduces salt into nearby waterways and wetlands. These salts, primarily sodium chloride, magnesium chloride, and calcium chloride, accumulate in wetlands and streams, leading to salinization.

In coastal wetlands, mechanisms such as surface or subsurface seawater intrusion, reductions in riverine freshwater flow, alterations of subsurface freshwater, anthropogenic alteration of coastal geomorphology (including dredging, land reclamation, and channelization), and storm surges contribute to salinization (Herbert et al., 2015). Rising sea levels push seawater further inland, intruding into historically freshwater wetlands (see e.g., Parker & Boyer, 2019). We will detail the rising sea level effects in the Section 4.3.2. Anthropogenic activities, such as dam construction and water diversion, reduce freshwater flows into coastal estuaries and embayments (Sahavacharin et al., 2022; White & Kaplan, 2017; Zamrsky et al., 2024). This reduction alters hydrologic gradients, allowing saltwater to penetrate further upstream, leading to salinization. Dredging, land reclamation, and channelization modify coastal landscapes, facilitating seawater intrusion into freshwater areas. This alteration of coastal geomorphology contributes to salinization.

Extraction of freshwater from coastal aquifers involves the removal of groundwater from underground reservoirs located near the coast (Tully et al., 2019). This process is often necessary to meet growing water demands for agricultural, industrial, and municipal purposes in coastal regions. However, excessive extraction can lead to salinization of nearby wetlands and surface water bodies. Coastal aquifers are typically charged by both freshwater from precipitation and seawater from the nearby ocean. When freshwater is extracted at a faster rate than it can be naturally charged, the balance between freshwater and seawater within the aquifer shifts, resulting in saltwater intrusion. Saltwater intrusion occurs when the natural boundary between freshwater and saltwater in the aquifer, known as the freshwater-saltwater interface, moves inland due to decreased freshwater pressure (Gollo et al., 2024). In regions where saltwater intrusion occurs in aquifer, saline aquifer water can eventually discharge into surrounding soils. This discharge can occur through natural processes, such as groundwater flow toward the land or human activities, such as pumping groundwater for agricultural or industrial use. A comprehensive set of hydrogeochemical parameters is essential for accurately modeling the impact of salinity intrusion into coastal aquifers (Oude Essink et al., 2010). However, acquiring this extensive data set is often difficult, particularly on larger scales.

4.3. The Effect of Climate Change

The state of the climate is a fundamental factor that influences the accumulation of salt in soil. It determines the amount of precipitation a region receives and the evaporation rates it experiences. The changes in frequency, intensity, spatial extent and duration of extreme events, such as the 2023 European severe summer heat waves and drought, will lead to changes in many drivers that influence soil salinization. Rising temperature in summer will lead to higher evapotranspiration, which in turn increases salt concentration in soil solution. Moreover, frequency and intensity of the precipitation will directly influence salt leaching through soil profile that affects salinization (J. Han et al., 2024).

Regions with low rainfall and high evaporation, such as arid and semi-arid areas, are particularly susceptible to salt accumulation (Sahab et al., 2021). In these regions, limited water availability reduces salt's leaching from soil, allowing it to concentrate near the surface (Karmakar et al., 2016). The high evaporation rates further exacerbate this effect, which could lead to the crystallization and deposition of salts on the soil surface (Szabolcs, 1990). However, the solubility and concentration of salts significantly shape the interaction between climate and salt transport. In other words, the influence of climate on salt transport is contingent upon the presence of soluble salts within the system. The current literature on the relationship between climate and large-scale soil salinization is predominantly focused on primary salinization (there is no saline irrigation or salt uptake from the aquifer) and consists of descriptive accounts with limited quantitative predictions regarding the future state of salt-affected soils based on current trends.

In contrast to other dynamic soil properties, such as the availability of organic matter content, there has been notably less focus on predicting how global-scale soil salinity responds to climate variability (Corwin, 2021). Szabolcs (1990) was one of the early researchers to project that, in reaction to a 1°C rise in average annual temperature, the salt-affected areas in North Mediterranean regions will double by the year 2050. Hassani et al. (2021) undertook a study using AI-driven approaches to project how primary soil salinity would respond to

changes in various climatic variables, including temperature, precipitation amount, frequency, and intensity, and the dry and wet deposition rate of sea salt aerosols. Their research aimed to identify areas prone to salinization due to climate change which was one of the first of its kind to provide detailed quantitative information on a global scale. Although their study offered predictions about areas at risk under different climate scenarios, it did not provide precise cause-and-effect relationships between climatic variables and the extent of salinization which remained an open question.

Employing a combination of observations and ecohydrological models, Perri et al. (2022) investigated the hydrological feedback on and from salinity, considering the impact of plant transpiration. They found that the impact of climate varies: arid regions with low rainfall tend to enhance salinization because they reduce soil moisture and limit salt removal. On the other hand, areas with rainfall seasonality, particularly those with a strong mismatch between when water is available (wet season) and when it is needed (water demand), such as Mediterranean climates, experience less salt accumulation due to more effective salt removal during the wet season.

4.3.1. Feedback Loops Between Salinization and Climate Change

Anticipated hydrological changes due to climate change could lead to various soil degradations, encompassing physical, biological, biochemical, and chemical aspects (Brevik, 2013). Soil salinity stands out as a significant concern for soil biodiversity, fertility, and stability, and is expected to become increasingly problematic in a warming climate (Daliakopoulos, Pappa, et al., 2016; Hassani et al., 2021; Talat, 2020; Tomaz et al., 2020). Perhaps the most critical aspect of the relationship between soil salinization and climate change is the presence of feedback loops that can exacerbate both issues. For example, soil salinization impacts vegetation health and reduces plant cover (Bui, 2013; Greenway & Munns, 1980). In this context, salinization can be assumed to act like aridity, which can influence the hydrological distribution and the intensity of interactions among land, vegetation, and the atmosphere on a catchment scale (Perri et al., 2020). The degree of influence depends on how well vegetation can handle salt stress through functional characteristics, such as salt tolerance (Perri, Entekhabi, et al., 2018; Perri, Suweis, et al., 2018; Perri et al., 2020). As a result, these degraded ecosystems become less effective at sequestering carbon dioxide, a greenhouse gas contributing to climate change. This, in turn, amplifies the warming effect of climate change.

Conversely, climate change-induced factors, such as increased temperatures and altered precipitation patterns, can intensify soil salinization (Corwin, 2021). The Intergovernmental Panel on Climate (IPCC) (Shukla et al., 2019) report warns that climate change will likely affect all the key processes leading to soil salinization. They include shifts in hydrological balance, the intrusion of sea salt, and the deposition of salt carried by the wind. Such changes disrupt the delicate balance of soil moisture and salt concentration, favoring salt accumulation (Bates et al., 2008; Karmakar et al., 2016). Thus, soil salinization and climate change create a self-perpetuating cycle with adverse consequences for both ecosystems and global climate stability. In addition, changes in land use and extreme climate events, such as prolonged droughts and severe floods, can mobilize salts from geological formations, and increase the risk of soil salinization in new areas (Daliakopoulos, Tsanis, et al., 2016; van Weert & van der Gun, 2012). Rising sea levels also can cause saltwater-induced soil salinization in coastal regions (J. Chen & Mueller, 2018).

The investigation of the interconnected response of climate change and soil salinity at large scales has often been constrained by the unavailability of detailed microdata. Typically, research in this area has primarily concentrated on primary soil salinization. A study by Hassani et al. (2021) identifies areas in South America, southern and western Australia, Mexico, the southwest U.S., and South Africa as future hotspots for increased soil salinization (Figure 2). In contrast, it projects a decline in soil salinity in such places as the northwest U.S., the Horn of Africa, Eastern Europe, Turkmenistan, and west Kazakhstan, due to climate change.

The Australian National Land and Water Resources Audit (2001) suggests that the area of Australia's drylands at risk for soil salinity due to dryland management could grow to 170,000 km^2 by 2050, up from around 57,000 km^2 in 2000. Schofield and Kirkby (2003) designed indicators, such as low relief, high annual moisture flux in both directions, and local flow deficits in large catchments, in order to identify both current and future locations (from 2079 to 2099) susceptible to salinization. They concluded that the regions at risk for soil salinity are increasing globally. A review conducted by Kumar and Sharma (2020) indicates that each year, almost an additional 10% of land becomes salt-affected in India. The research predicts that by the year 2050, approximately half of India's arable land will be impacted by salinity.

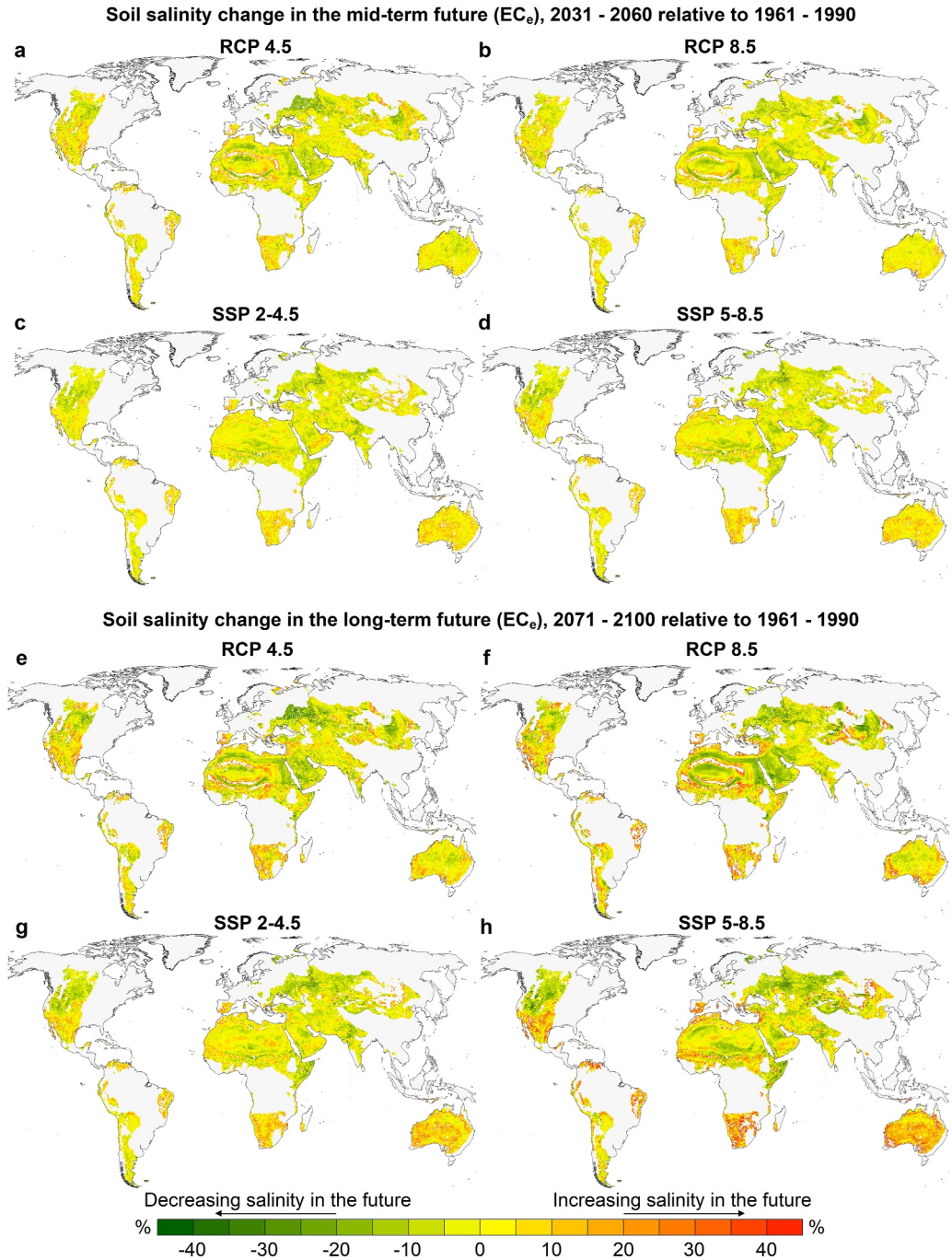

Figure 2. (a–d) Mid-term predictions of changes in EC_e (2031–2060). (e–h) Long-term predictions of changes in EC_e (2071–2100), after Hassani et al. (2021). The average predictions of data-driven models down to a depth of 1 m were used to calculate salinity changes. For each map cell (pixel) and based on the data-driven models trained using different Global Circulation Models (GCMs), Hassani et al. (2021) computed the mean soil salinity for the reference, mid-, and long-term future periods. The relative change was calculated as (Future mean-Reference mean)/Reference mean. The percentage value of each cell represents the multi-GCM mean of these relative changes, shown by the color map. Positive values indicate an increase in soil salinity, while negative values indicate a decreasing trend.

Conversely, examination of secondary soil salinization has been limited in scope. These studies typically look at salinization due to unsustainable irrigation methods or the intrusion of seawater into soil as a result of over-extraction of freshwater from the coastal aquifer or rising sea levels—see Daliakopoulos, Pappa, et al. (2016), Corwin (2021), Colombani et al. (2015), Zanchi and Cecchi (2010), Oude Essink et al. (2010), Gollo et al. (2024). Secondary soil salinization studies have predominantly operated at smaller spatial scales, such as individual fields or local regions. The limitation arises from the need for fine-resolution data to capture the nuanced dynamics of secondary salinization processes, which can be influenced by local factors, such as land management practices, irrigation methods, and hydrological conditions.

One other feedback loop between soil salinity and climate is its influence on the global carbon cycle, which plays a vital role in climate change dynamics (Hassani et al., 2024; Setia et al., 2013). At the heart of this relationship is the soil's capacity to store and release OC, directly impacting atmospheric carbon dioxide levels. Soil serves as one of the largest terrestrial carbon pools, storing more carbon than the atmosphere and vegetation combined (Bhattacharya et al., 2016). The relationship between soil salinity and soil OC is complex and varies, depending on environmental conditions, land management practices, and the specific soil type (Wong et al., 2010). Salinity affects the activity and composition of microbial communities responsible for organic matter breakdown—for example, L. Liu et al. (2023) observed that microbial diversity generally decreased as EC increased, with the bacterial community being more sensitive to changes in EC than the fungal community. Elevated salt levels disrupt these communities, decreasing decomposition rates (Rath & Rousk, 2015). On the other hand, soil salinity can negatively impact plant growth and vegetation cover (Hailu & Mehari, 2021). When salt concentrations in the soil exceed plant tolerance levels, it reduces plant biomass and root exudates. This, in turn, limits the inputs of organic matter into the soil, as dead plant material and root exudates are primary sources of soil OC.

Using a modified Rothamsted Carbon model, a model for the turnover of OC in non-waterlogged topsoils that takes into account the effects of soil type, temperature, moisture content, and plant cover on the turnover process, Setia et al. (2013) project that global soils may lose 6.8 Pg of organic content by 2100, due to increasing soil salinity. The collective findings from various studies indicate that soil salinity is expected to lead to a global reduction in the level of soil OC levels (Haj-Amor et al., 2022). Analyzing 43,459 mineral soil samples (SOC < 150 g kg^{-1}) collected across various land covers since 1992 (Figure 3), Hassani et al., 2024 estimate that an increase in soil salinity from 1 to 5 dS m^{-1} in croplands would result in a decline in mineral soil SOC from 0.14 g kg^{-1} above the mean predicted SOC ($\overline{\text{SOC}} = 18.47$ g kg^{-1}) to 0.46 g kg^{-1} below ($\sim -430\%$). For non-croplands, this decline is even more, dropping from 0.96 above ($\overline{\text{SOC}} = 35.96$ g kg^{-1}) to 4.99 below ($\sim -620\%$).

4.3.2. The Effect of Rising Sea Levels

The rise of sea level is another key driver of soil salinization, which is considered as a direct consequence of climate change and the resulting global warming. Given its substantial impact on soil salinization in coastal regions, however, we describe it separately.

Approximately 40% of the world's population lives in coastal areas, withn 100 km of the coastline (Barbier, 2015; Nevermann et al., 2023). According to the Intergovernmental Panel on Climate Change (IPCC, 2022), by the year 2100 the projected global climate change could increase the mean sea levels between 0.26 and 0.82 m, with some researchers projecting even higher rise of mean sea level (Richardson et al., 2011; Rignot et al., 2011; Vermeer & Rahmstorf, 2009). Due to gravitational effects that are the result of land ice mass changes, thermal expansion, and ocean dynamics, the sea level rise will be neither uniform everywhere around the globe, nor will it be linear. Some regions, such as Mediterranean coasts and lands that face the Red Sea, as well as the Persian Gulf area that faces the northern part of the Indian Ocean, both of which have high salinity water, may be more vulnerable, with the salinity level projected to be more than 40% or higher.

The rise in the sea level has at least three important consequences. One is that it threatens the drinking water resources through intrusion of wetlands and freshwater sources by brine (Bosserelle et al., 2022). The second effect is salinization of coastal agricultural lands, while the third effect is the threat sea level rise poses to biodiversity. According to Blankespoor et al. (2014), 1 m rise in sea level will cause loss of 64% of freshwater coastal wetlands and its conversion to saline systems. Even higher losses are predicted for the Middle East and North Africa (at 100%), Latin America and the Caribbean (74%), sub-Saharan Africa (72.5%), and East Asia and

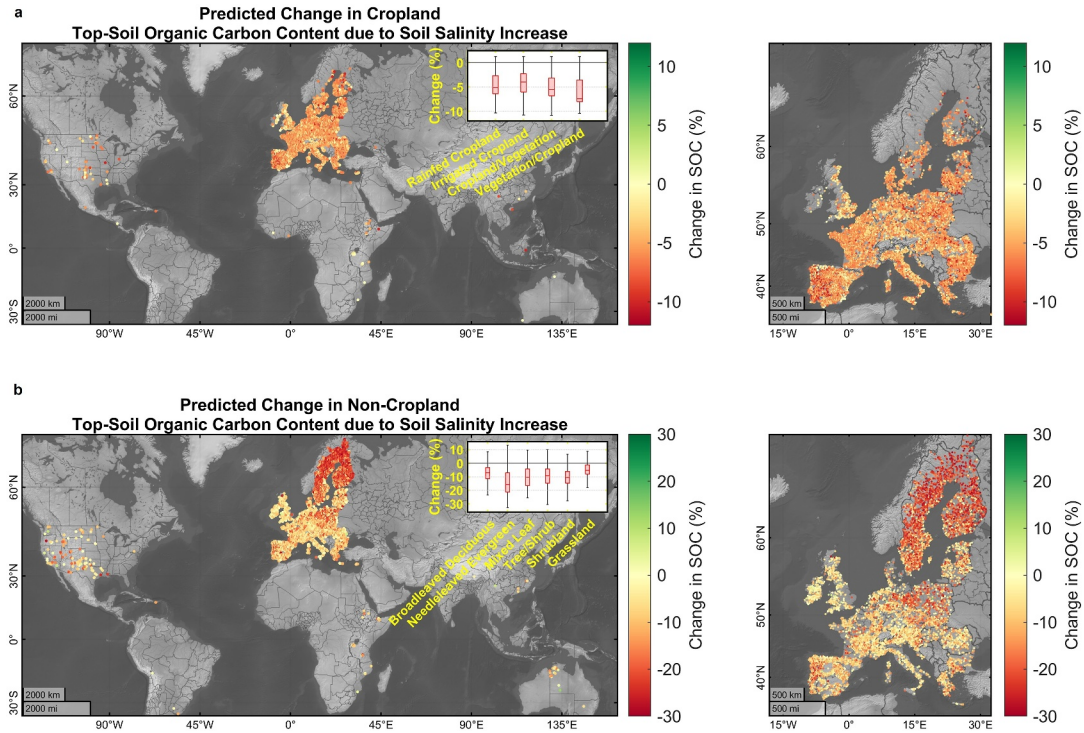

Figure 3. Impact of a 1 Standard Deviation (SD) increase in soil salinity on topsoil (0–7 cm) organic carbon (OC) content at the locations of soil profiles/samples (after Hassani et al., 2024): (a) in croplands and (b) in non-croplands. The maps show the Generalized Additive Models predictions of topsoil OC changes due to a 1 SD rise in soil salinity. The right-side panels provide a closer view of Europe, where the majority of the data from the LUCAS topsoil data sets (2015 and 2018) are concentrated. The box plots illustrate the median, lower, and upper quartiles, and the non-outlier minimum and maximum change values for major land cover types. Outliers are identified as values exceeding 1.5 times the inter-quartile range from the top or bottom of the box.

the Pacific (62.2%) regions. Since there are about 15 Mha coastal wetlands that are below 5 m elevation above the mean sea level (Henman & Poulter, 2008), they are highly vulnerable to the estimated sea level rise.

What are the spatio-temporal drivers of soil salinization in the presence of rising sea levels? Mazhar et al. (2022) provide a detailed discussion of this issue, which we summarize. To begin with, we first note that the time and spatial scales over which natural drivers of coastal soils salinization act vary widely. For example, the time scale may be less than a year, in which case the affected areas would be relatively limited, or it could be a much longer time scale in which case the affected areas could extend to a global scale (White & Kaplan, 2017). In addition, although transient drivers, such as tsunamis or hurricanes, can cause salinization of groundwater and soils in coastal areas, restoration of the salt level to the level before occurrence of such drivers may occur within a year, because intense seasonal rains can leach away the added salt (Kume et al., 2009). This process is affected by the local climate and the permeability of soil. If the permeability is small, then the effect of marine inundation caused by transient events may last much longer.

The impact of storms and high tides on salt transfer from the sea to inland areas is also a critical aspect of global salt transport, particularly in coastal regions (Pezeshki et al., 2022). Extreme weather, combined with rising sea levels, generate tides of large heights, which, together with frequent inundation, dramatically increase the likelihood of soil salinization. Storms, especially tropical cyclones and hurricanes, generate powerful surges that are temporary, rapid sea-level increases caused by the low atmospheric pressure and strong winds associated with storms. A storm approaching a coastline can push seawater inland, causing flooding in low-lying coastal areas. During high tides, the water level in coastal areas rises significantly. When they coincide with storm events or heavy rainfall, they exacerbate saltwater intrusion into coastal soil and groundwater. The rising tide can push saline water further inland through channels, rivers, and estuaries. Coastal aquifers, underground layers of water-bearing rock or sediment near the coast, are particularly vulnerable to saltwater intrusion during storms and high

tides (Heiss et al., 2022; Huizer et al., 2017). The increased water pressure from storm surges or high tides can force saline seawater into these aquifers. Once the salty water infiltrates the aquifer, it can contaminate freshwater resources used for drinking and agriculture. The influence of storms and tides on soil salinization has received relatively limited attention in the existing literature, especially considering large-scale implications.

Strong winds drive water waves of high tides deep into land. If the land is suffering drought, that salt will begin to accumulate. In addition, evaporation in inundated soil could also result in deposition of large amounts of salt, further salinizing the soil close to its surface. The inundation pattern depends on the geographical characteristics of the land, as well as the direction of winds. In particular, the frequency of inundation depends on such landscape characteristics as the length and tortuosity of tidal creeks, as well as the distance from the shore.

4.4. The Effect of Saline Dust and Aerosols

In addition to precipitation and evaporation rates, the movement and dry/wet (through precipitation) deposition of saline dust and aerosols play a significant role in soil salinity and salt movements at large or global scales (Reheis, 2006). Saline dust consists of larger (typically between 20 and 70 μm) solid particles of salt or saline compounds, which is associated with dry, dusty environments. These particles settle out of the air relatively quickly. It is, however, worth noting that smaller particulate matter (typically less than 10 μm), including fine salt aerosols, can also be entrained and transported over significant distances, potentially spanning hundreds of km (Randall et al., 2021) and contributing to the dispersal of salt into the atmosphere. Typically, inland saline dust or saline dust storms originate from the saline playa of the dried-up inland saline lakes (Abuduwaili et al., 2010; Duan et al., 2022; Hassani, Azapagic, D'Odorico, et al., 2020). Such secondary landscapes arise from hydrological imbalances, reduction in saline lake size, evaporation of highly saline lake water solution, and accumulation of salt on the desiccated lake beds within drainage basins, primarily due to human activities (Blank et al., 1999; Wurtsbaugh et al., 2017). Examples of lakes facing salt dust problems include the Aral Sea, the Salton Sea, Owens Lake, and the Dead Sea, primarily due to declining water levels and arid conditions.

Studies on the consequences of saline lakebed desiccation on the surrounding soil areas, such as those of Gillette et al. (1997), King et al. (2011), and Reynolds et al. (2007), are primarily focused on the release of saline dust into the atmosphere through field or wind tunnel studies. Studies concerning drying of hypersaline lakes, such as Iran's Lake Urmia, have indicated that the thick salt layer left behind during the lake's drying process may not be the primary origin of saline dust emissions (Mardi et al., 2018). Instead, the saline soils in the vicinity of the lake have been identified as more significant contributors to the release of fine saline particles into the atmosphere. There is, however, a scarcity of studies that specifically quantify the deposition rate of airborne saline particles and variations in soil salinity levels resulting from the deposition of the airborne saline dust (e.g., D. Liu et al., 2011). The complex interactions between hydrological and climatic factors hinder accurate assessment of the geographical distribution of nearby populations and industrial centers exposed to saline particle emissions, as well as impede the ability to make reliable estimates of deposition rates in the face of climate change. Accordingly, deposition rates are limited to short-term extreme events (see for example Figure 4 by Hassani, Azapagic, D'Odorico, et al., 2020).

In the realm of aeolian processes, the rate at which dust is emitted—vertical dust flux—from soil beds is subjected to the influence of multiple factors, including wind speed, surface characteristics (including the presence of rough elements), soil texture, particle-size distribution, moisture content, and the extent of vegetation cover. The literature on aeolian processes and the physical principles governing the movement of wind-blown sand and dust extensively explores the interplay and interactions among these parameters, recognizing their combined effects on dust emissions (Kok et al., 2012).

In estimating vertical dust flux, two critical parameters must be determined: (a) the threshold friction velocity, which marks the onset of soil particle movement (saltation), and (b) the horizontal saltation flux $Q(d_s)$ (kg m^{-2} s^{-1}). The threshold friction velocity (u^*_{ft}) is defined as the minimal friction velocity necessary to initiate the movement of soil particles and trigger the saltation process. An expression for u^*_{ft} at the point of saltation initiation is given by:

$$u^*_{ft} = A_{ft}\sqrt{\frac{(\rho_p - \rho_a)\, gD_p}{\rho_a}}, \tag{1}$$

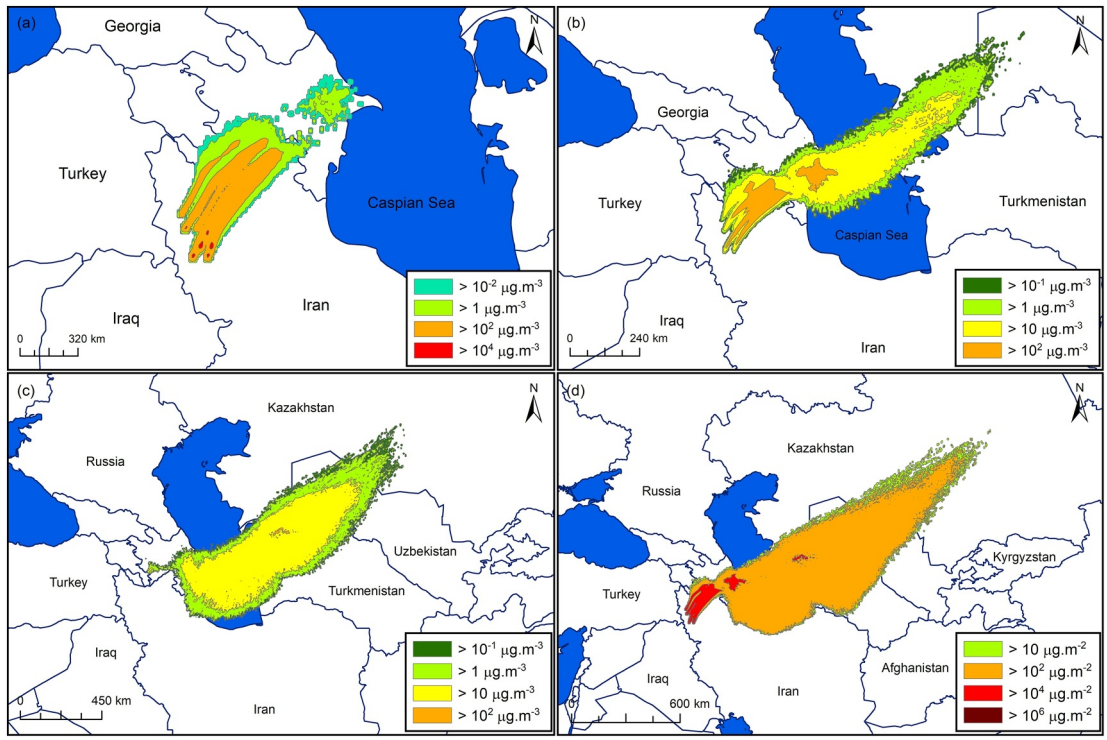

Figure 4. (a–c) the mean concentrations of PM_{10} (particulate matter with a diameter of 10 µm or less) measured from ground level up to a height of 100 m, recorded at respective intervals of 6, 12, and 18 hr from the start of a storm nearby Lake Urmia (Hassani, Azapagic, D'Odorico, et al., 2020). (d) The total rate of PM_{10} deposition observed 24 hr after initiating the simulation. Hassani, Azapagic, D'Odorico, et al. (2020)'s model projects the spread of PM_{10} particles from the saline playa of Lake Urmia, assuming a scenario where the lake has completely dried up, during a dust storm that occurred on 24 March 2018, at 14:00 UTC. The average results from 27 ensemble members, each differing slightly by one meteorological grid point horizontally and 0.01 sigma units vertically, were used to compute the dispersion over an 18-hr period in the simulation.

where A_{ft} is a constant that depends on interparticle forces, the lift force, and the flow's Reynolds number (Kok et al., 2012). Here, D_p represents the diameter of a sphere equivalent in volume to the irregularly shaped sand particle, and g is the gravitational acceleration constant. The particle density (ρ_p), which varies based on the sand's composition, is approximately 2,650 $kg\ m^{-3}$ for quartz sand on Earth, while ρ_a denotes the air density.

Saltation commences when the wind stress, denoted as τ, reaches a level capable of elevating surface particles into the fluid flow. This phenomenon typically occurs at a wind stress of approximately 0.05 $N\ m^{-2}$ for loose sand (Kok et al., 2012). Once initiated, the particles that are lifted are then accelerated by the wind into ballistic trajectories. The subsequent impacts of these particles on the soil bed have the potential to dislodge or splash additional particles into the fluid stream, thereby perpetuating the saltation process. The steady-state saltation mass flux, (Q), is quantified using the following equation (Kok et al., 2012):

$$Q = \rho_a \left(u_*^2 - u_{*sfc}^2\right) \frac{L}{\Delta v}. \tag{2}$$

In this equation, L, is the particle's hop length, v represents the average difference between the particle's impact and lift-off speeds, u_* is the shear velocity above the saltation layer, and u_{*sfc} is the shear velocity at the surface. It is important to note that different assumptions about the dependencies of L, v, and u_{*sfc} on u_* have led to various formulations relating Q to u_*. The equations presented in Table 1 of Kok et al. (2012) represent some of the most commonly used saltation Q relations.

Particles undergoing saltation can initiate the mobilization of other particles across various size ranges through their impact on the soil surface. Dust particles are typically not directly uplifted by wind forces. This is due to the dominance of inter-particle cohesive forces over aerodynamic forces, as noted by Kok et al. (2012). Instead, these

particles are predominantly dislodged and elevated from the soil surface as a result of impacts from saltating particles (Gillette, 1974). This ejection leads to a vertical flux of dust particles into the atmosphere, resulting in their suspension.

Various analytical and semi-analytical approaches have been developed to estimate vertical dust flux. Hassani, Azapagic, D'Odorico, et al. (2020) employed a simplified model for calculating dust flux (F) from Iran's Lake Urmia saline playa. The model was originally developed by H. Lu and Shao (1999), simulating the plowing action of individual saltating particles, based on the assumption that a saltating particle impacts at an angle of 13°. H. Lu and Shao's (1999) model is expressed as:

$$F = \frac{C_\alpha g f \rho_b}{2p}\left(0.24 + C_\beta u_* \sqrt{\rho_b / p}\right) Q_{\text{tot}}. \quad (3)$$

In this equation, p represents the plastic pressure of the soil surface in Pascals (indicating surface hardness; varying as 500 for silty clay loam, 10,000 for loam, and 50,000 for sand dune). The variable f denotes the fraction of dust in the soil volume, while ρ_b and ρ_p are the densities of the bulk soil and particles, respectively. C_α and C_β are constants. Q_{tot} is the total saltation flux intensity, calculated by the integral $Q_{\text{tot}} = \int_{d_1}^{d_2} q(ds)p(ds)\,\delta ds$, where d_1 and d_2 are the respective lower and upper limits of particle diameters contributing to the saltation flux and $p(ds)$ is the soil particle size distribution (Shao, 2001; Shao et al., 2002).

The presence of salts adds, however, an extra layer of complexity when estimating the vertical dust flux from saline soils. For example, soil salinity can act as a particle-binding cement (as suggested by Schatz & Herrmann, 2006, for dunes) and impact the threshold friction velocity (the wind speed at which saltation of the particles starts), such as higher soil moisture levels or the presence of non-erodible elements such as rocks (Raupach, 1992; Raupach et al., 1993). There are, however, fewer studies in the literature that sought to quantify the role of soil salinity on threshold friction velocity. Among them, Khatei et al. (2024) used wind tunnel experiments to investigate how soil salinity affects the wind erosion threshold velocity and dust production in dry soils of varying textures treated with water enriched with different concentrations of salt. The results indicated that the wind erosion threshold velocity can increase by up to 100% with higher soil salinity concentrations, ranging from 0.5 to 7.0 dS m^{-1}, depending on the soil texture. Khatei et al. (2024) attribute the increased wind erosion threshold to the soil aggregation and crust formation due to presence of salts. Conversely, sodicity causes soil dispersion, breaking down soil aggregates and making the soil more susceptible to erosion by wind. Various factors influence the vertical emission of saline dust, making it difficult to establish universal parameters that are applicable to all scenarios. Consequently, research in this field tends to be case-specific, relying on empirical or semi-analytical methods.

The primary source of saline aerosols or fine particulate matter is, however, sea spray (Monahan et al., 1986) or nebulization of a saline solution (e.g., from the ocean surface or a saline lake). While approximately two-thirds of the observed variations in sea spray concentrations can be attributed to wind speed (Hoppel et al., 1990), it is essential to acknowledge that other factors, such as salinity, wave conditions, surfactants, and sea surface temperatures (Saliba et al., 2019; Soares et al., 2016) also play a role in shaping sea surface conditions and, consequently, affect sea salt emissions.

Saline aerosols are not the primary aerosol type, except in the oceans, coastal areas, and the vicinity of dried inland saline lakes (Ge et al., 2019). These aerosols can originate from coastal regions with high salinity levels, and wind patterns can transport them far inland. As these aerosols settle out of the atmosphere, they deposit salt particles onto the soil surface. Over time, repeated deposition events can lead to the accumulation of salts in the soil. The extent of deposition and subsequent salt accumulation depends on such factors as the frequency and intensity of aerosol events, local wind patterns, and the proximity to aerosol sources (Suweis et al., 2010). In coastal regions, the usual salt contributions to the soil range from 100 to 200 kg per hectare per year, whereas in inland areas, these figures decrease by approximately a factor of ten (Hillel, 2000).

The majority of modeling efforts suggests that changes in climate may have a limited impact on global sea salt emissions (Paulot et al., 2020), which is attributed mainly to the limited response of surface oceanic wind speed, the primary driver of sea salt emissions, to climate variations (Tegen & Schepanski, 2018). The presence of saline

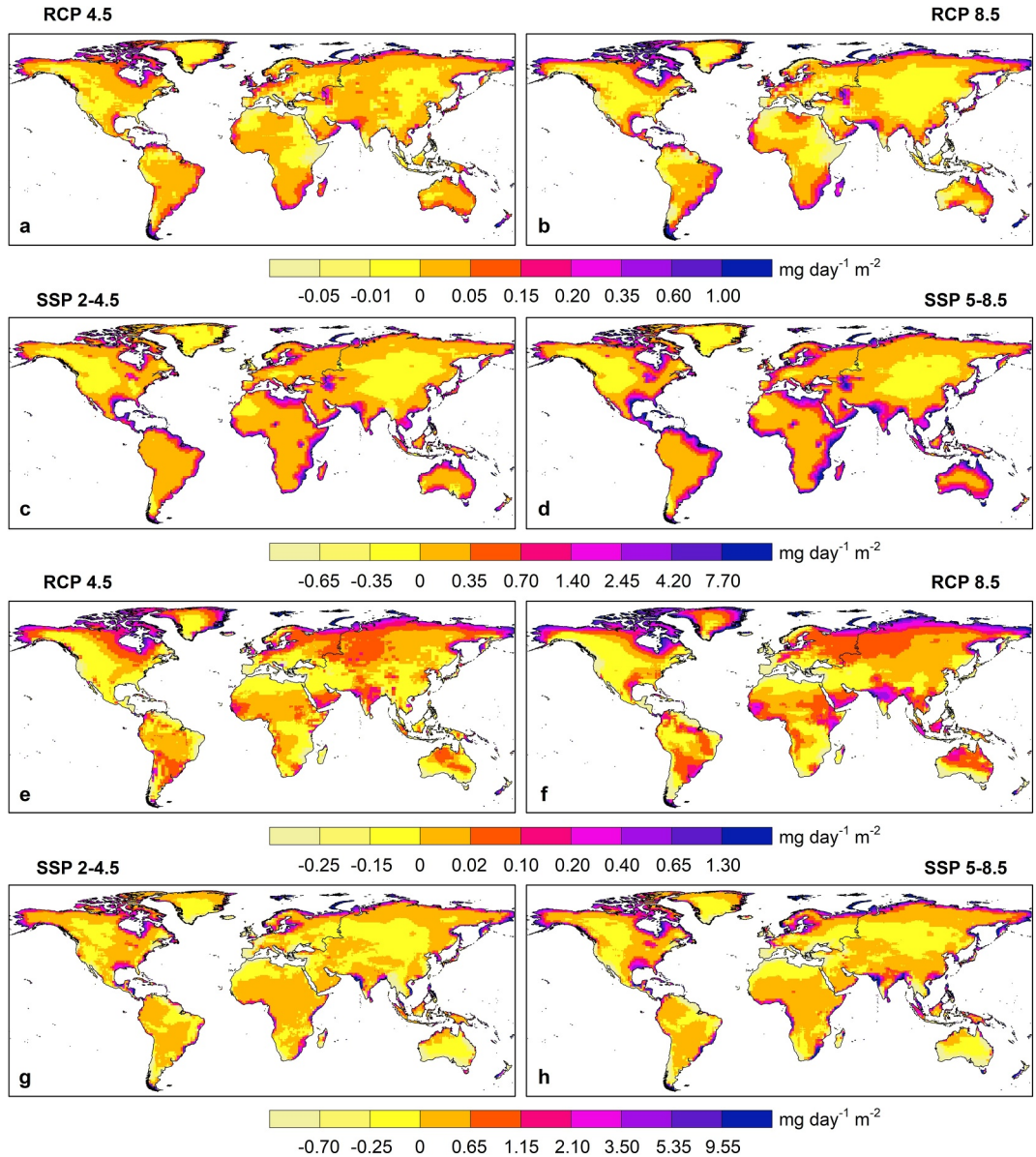

Figure 5. Projected changes in sea salt deposition rates by the 21st century's end (2071–2100), compared to the baseline period (1961–1990), under various greenhouse gas emission scenarios (Hassani et al., 2021). The multi-model ensemble mean is represented in the panels. (a–d) Show alterations in the 5-year rolling average of daily dry salt deposition, while (e–h) depict changes in the 5-year rolling average of daily wet salt deposition. Representative Concentration Pathways are relevant to CMIP5 Global Circulation Models (GCMs), while Shared Socioeconomic Pathways are relevant to CMIP6 GCMs.

aerosols in the atmosphere can also have feedback effects on climate. Sea salt aerosols have the potential to influence climate directly through their ability to scatter light, resulting in a negative radiative effect, ranging from −0.3 to −1.2 at the top of the atmosphere (Paulot et al., 2020, and references therein). Aerosols can impact cloud formation and reflectivity (Rosenfeld et al., 2008), affecting regional and global climate patterns. Climate changes can also influence the frequency and distribution of saline aerosol dry and wet deposition, creating a complex interplay between aerosols, climate, and soil salinity at larger scales. The rate at which saline aerosol deposition will change, however, due to climate change being uncertain, because it depends on the specific Global Circulation Model used, and different models may provide different predictions; see Figure 5.

4.5. The Effect of Soil Texture and Geomorphology

Soil texture and geomorphology also represent the spatial drivers of soil salinization. Soil texture, as characterized by the fraction of sand, silt, and clay particles in the fine earth fraction (soil particles < 2 mm), affects both the movement of water and salts. Soil particle size and shape influence pore morphology, affecting interactions between gravity, viscous, and capillary forces. This controls water flow pathways, discharge speed, pore water exchange, and tidal range, all of which impact salt transport and crystallization dynamics (Li et al., 2014; Sadeghi et al., 2012; Shokri-Kuehni et al., 2020). In addition, the thickness of capillary fringe is determined by soil texture (Vogelbacher et al., 2024), as is the maximum flux of solutes to the surface of soil (Fiola et al., 2020). Soil texture also influences the succession and composition of soil horizon in estuarine and former floodplain areas. The pore connectivity of soil is also controlled by its texture, which can reduce the flow of water and solute transport to the surface (L. R. Gardner, 2005). The importance of pore connectivity to solute transport in porous media was first pointed out by Sahimi et al. (1983), Sahimi, Heiba, et al. (1986), Sahimi, Hughes, et al. (1986), and further studied later on by Sahimi and Imdakm (1988), Sahimi (2012), and Ghanbarian-Alavijeh et al. (2012). The discharge flow is also limited by such stratigraphic constraints as mud layers. Such effects are particularly strong in low-lying soils where the depth of the water table is shallow. Thus, the steepness of the banks may zonally reduce the effect of infiltration of salty groundwater.

Furthermore, geomorphological features, elements of the Earth's surface, govern the movement and distribution of salts in soils (Schofield & Kirkby, 2003). Topography is a geomorphological factor that influences salt transport (Celleri et al., 2022). The topography of a landscape dictates how water flows across the terrain and how it interacts with the soil. In hilly or sloping regions, water tends to follow the natural contours of the land, which can lead to rapid drainage and reduced salt accumulation. On the other hand, the salts accumulated in the root zone are more effectively leached on gentler hill slopes. Flat or poorly-drained landscapes may create conditions where water pools or stagnates, increasing the potential for salt accumulation (Suweis et al., 2010). In such low-lying areas, water may infiltrate the soil, but it will struggle to move away efficiently, allowing salts to accumulate over time. Such salt-affected regions are often referred to as “saline flats” or “salt pans.”

Rivers are another geomorphological feature that affect salt transport dynamics and soil salinity across different landscapes. In areas where rivers flow through salt-affected landscapes, ion leaching processes in the upstream soils may increase salt concentrations in water bodies, impacting soil salinity, water quality, and the health of aquatic ecosystems in the downstream regions. In the Hetao Irrigation District along the Yellow River in China, a noticeable trend of soil salinity increase (16.4 mg kg^{-1} per km) was reported along the river (X. Wang et al., 2023). Conversely, rivers can also play a mitigating role in soil salinization under certain conditions. In regions where rivers flow through salt-affected areas and then continue into the sea, transporting salts from the land to the ocean can help reduce salt accumulation in the soil. Groundwater, on the other hand, may contain dissolved salts and can discharge into rivers or infiltrate into soils, affecting salt transport patterns (Fan et al., 2012; Rengasamy, 2006).

When saltwater intrudes into rivers' freshwater systems (due to, e.g., high tides or rising sea levels, see Section 4.3.2), it increases their salinity levels (Bellafiore et al., 2021; Gollo et al., 2024). The elevated salinity can then affect salt transport dynamics, both locally and over larger scales. As saltwater intrudes into rivers from their mouths and estuaries, it can travel upstream due to freshwater flow from upstream areas. A study in Vietnam's Mekong Delta on the impact of sea level rise on salinity intrusion (Vu et al., 2018) projected a sea level increase of 25–30 cm by 2050, with salinity intrusion affecting up to 50–60 km into the river and negatively impacting rice yields due to salinity levels exceeding 4 g L^{-1}. Approximately 30,000 hectares of agricultural land could be affected if sea levels rise by 30 cm.

5. Adverse Impacts of Soil Salinization

Before describing the mechanisms of soil salinization and its modeling, it is essential to first consider the severe adverse impact of soil salinization on the environment, ecosystem, and human life.

5.1. Salinity and Plants

Soil salinity has various negative effects on plants, impacting their growth, through causing osmotic stress, ion toxicity, and nutrient Imbalance (Flowers & Colmer, 2008; Greenway & Munns, 1980; Kibria & Hoque, 2019;

Munns, 1993, 2002; Munns & Gilliham, 2015; Munns & Tester, 2008). High levels of salts in the soil solution create an osmotic imbalance between the soil solution and the plant's root cells (Osmotic Stress), making it difficult for the plant to uptake water, which leads to water stress or dehydration. As a result, plants may wilt, exhibit reduced growth, and manifest symptoms of water stress such as leaf rolling or curling. Additionally, the excess ions in the soil, particularly sodium (Na^+) and chloride (Cl^-), can be taken up by the plant along with water, disrupting various physiological processes (Ion Toxicity). High concentrations of Na^+ and Cl^- ions interfere with the uptake of essential nutrients such as potassium (K^+), calcium (Ca^{2+}), and magnesium (Mg^{2+}), disrupting the balance of essential nutrients within the plant and leading to deficiencies in key nutrients (Munns, 2002). Sodium ions can replace K^+ ions in enzyme systems, resulting in enzyme dysfunction and metabolic disruption, while Cl^- ions can disrupt photosynthesis by damaging chloroplast structure and inhibiting enzyme activity. This reduces the plant's ability to produce energy and assimilate carbon dioxide, resulting in reduced growth and yield. Moreover, soil salinity significantly reduces plant phosphorus uptake because the phosphate ions precipitate with Ca ions (Bano & Fatima, 2009).

Endocellular and intracellular microorganisms colonize the natural environment of plants (Gray & Smith, 2005). In addition, beneficial bacteria and fungi, such as rhizosphere microorganisms, enhance plants' performance and productivity. However, if the soil is stressed by the presence of excess salt, it will affect practically all aspects of the plants' physiology and growth (Paul, 2013). High soil salinity can disrupt the symbiotic relationships between plants and beneficial microbes, reducing their ability to support plant health and growth. Furthermore, salt stress can alter the composition and activity of microbial communities in the rhizosphere, affecting nutrient cycling, disease suppression, and other essential functions.

In coastal wetlands or rivers, evapotranspiration of plants of riparian species is reduced by salt, whereas rising soil salinity may lead to the die back of the riparian vegetation (Zeng et al., 2020), favoring instead the establishment of halophytes and salt-tolerant woody species. A major source of nutrients to many riparian communities is plant matter (Litalien & Zeeb, 2020). Most plants cannot, however, tolerate toxic levels of salts, as a result of which they fail to complete a life cycle in salinized soil. When the amount of plant matter decreases and salts also enters freshwater systems, the diversity and richness of odetritivores, macroinvertebrates, and fish suffer (Dowse et al., 2017; East et al., 2017; Kefford et al., 2011), which affects the nutrient cycling.

In tidal environments, Salt stress limits mangrove tree height. Higher salinity favors species that can tolerate salt better (Perri et al., 2023). Mangroves adapted to salt have lower rates of photosynthesis and growth, leading to decreased productivity and smaller size compared to less salt-tolerant species. This suggests a link between salinity, biodiversity, and tree height, as higher salinity promotes the growth of less productive, shorter, salt-tolerant species (Perri et al., 2023).

Excessive deposition of fine saline particles (<2.5 μm) on plant leaves can have negative effects. Burkhardt's (2010) review explains how the deposition of aerosols on plant leaves can act as both nutrients and desiccants. Most fine aerosols are hygroscopic, meaning they absorb moisture from the air, and often become liquid on transpiring leaves. These concentrated solutions can be absorbed by both the cuticle (outer layer) and stomata (small pores) of the leaves. The establishment of a continuous liquid water connection along stomatal walls affects individual stomata, known as the "hydraulic activation of stomata" (HAS). HAS enables efficient bidirectional transport of water and solutes between the leaf interior and surface, making stomatal transpiration partly independent of stomatal aperture (opening). Normally, HAS affects only a few stomata, but if too many are activated due to excessive particle accumulation or additional surfactants, hygroscopic particles may act as "desiccants," reducing the plants' drought tolerance. This property is utilized when hygroscopic salts and acids are sprayed to kill aggressive weeds (e.g., potato vine). Excessive particle accumulation may also result from air pollution.

The detrimental effects of soil salinity on plant growth at the molecular and plant levels also have been extensively discussed in previous literature reviews—see for example, Litalien and Zeeb (2020), Kibria and Hoque (2019), or Safdar et al. (2019). However, plants exhibit a wide range of tolerance levels to salinity, and some species can increase their tolerance to a certain extent when exposed to salinity over extended periods (B. Gupta & Huang, 2014; C. Zhao et al., 2020). The salt tolerance among plants is diverse, with glycophytes being most sensitive to salt. Conversely, xerophytes, which are drought tolerant, can withstand high salinity but often exhibit stunted growth. Halophytes, on the other hand, are salt tolerant, with some even requiring salt for optimal growth. They make up less

than 2% of all terrestrial flora and exist in various saline habitats, including coastal regions, salt marshes, drylands, and salt flats (Flowers & Colmer, 2008).

Various adaptive mechanisms are used by plants to survive in saline environments (see, e.g., a recent review by Muhammad et al., 2023). Xerophytes employ metabolic regulation to survive in saline environments, such as Crassulacean acid metabolism, limiting water loss by opening stomata only at night when evapotranspiration is lowest (Lüttge, 1993), thereby reducing the soil water requirement. Halophytes often exclude salts from their roots, preventing toxic levels of ions within root cells (Litalien & Zeeb, 2020). They may have specialized ion transporters favoring potassium over sodium, reducing sodium toxicity and potassium deficiency. Other species rely on ion exporters to remove salts from their roots (B. Wang et al., 2006).

To counteract low water or high salt content within cells, plants perform osmotic adjustment by producing compatible solutes (so-called osmoprotectants) (Flowers & Colmer, 2008), which encourage water movement into roots without interfering with protein function. These solutes vary between species, with some accumulating sugars while others rely on salts (M. Singh et al., 2015). Soluble osmolytes that are stored in the cell vacuoles regulate the osmotic stress (Flowers et al., 2015), allowing salt-tolerant plants to take up water at very low soil water potential. Some plants increase the tolerance to salinity through sequestration of ions in the central vacuoles of their cells. Sequestration of ions in vacuoles helps reduce cytoplasmic ion concentrations below toxic levels. Halophytes often have larger vacuoles than glycophytes, allowing them to store larger amounts of salts. Some plants secrete salts through specialized glands in the shoot epidermis (Litalien & Zeeb, 2020).

On the other hand, the capacity of plants to cope with salinity affects the distribution of soluble salts. The spatial distribution of salts is greatly affected by plants, whose nutrient uptakes usually exclude Cl^-, leading to its accumulation in soil and groundwater. Thus, the concentration gradient of Cl^- in soil decreases with depth. The spatial distribution of Cl^- in soil is also affected by roots of neighboring trees, which can increase the likelihood of soil salinization during drought. Except for very dry seasons, when leaf stomata close and reduce transpiration, evapotranspiration increases salt accumulation and reduces the vegetation cover in halophytic communities relative to riparian ones. This increases soil temperature that further increases salt accumulation through evaporation (B. Liu et al., 2019), which also changes the structure of the bacterial community (Y. Zhao et al., 2022).

Perri et al. (2020) investigated how river-basin salinization and plant salt tolerance affect soil water balance at the catchment scale. Using data from the AWAP data set and a salinity-dependent soil water budget model (the S-D SWB), their study showed that salinity has a significant impact on hydrological processes. In salinized basins, salinity acts as an aridity enhancer, reducing evapotranspiration and increasing the demand limit of the S-D SWB compared to baseline conditions. The extent of this effect depends largely on vegetation's ability to tolerate salinity (Perri, Suweis, et al., 2018). Halophytes, which thrive in saline environments, maintain higher transpiration rates in salty soils, while glycophytes, which are salt-sensitive, experience reduced transpiration even at low soil salinity levels. Ignoring these effects could lead to inaccuracies in estimating hydrological processes, surface-energy partitioning, and interactions within the land-vegetation-atmosphere system at the catchment scale (Perri et al., 2020).

The characteristics of sodic soils impede root penetration, and the decrease in soil pores limits root access to water and oxygen. It is known (Brown, 1982; Mooney et al., 1952) that clays and clay-mineral soils swell in the presence of Na+. If the ions accumulate on the surface of such soil, the resulting swelling reduces water infiltration and soil drainage, causing flooding and waterlogging in soil, further degrading it.

5.2. Socio-Economic Impacts of Soil Salinity

Soil salinization has serious societal and political consequences (Alkharabsheh et al., 2021; Wondim et al., 2020). A study released by the U.S. Defense Department (USDD, 2014) stated unequivocally that climate change is a threat to the national security of many countries. Drought and soil salinization, among other factors, have led to emergence of *environmental refugees*, that is, the people forced to leave their region and even homeland because the land in which they live can no longer sustain them due to prolonged drought and soil salinization or other severe environmental conditions. According to a study by Storlazzi et al. (2018), based on the greenhouse gas emission rates, the nonlinear interactions between sea-level rise and wave dynamics over reefs will lead to the annual wave-driven overwash of most atoll islands by the mid-21st century. This annual flooding will result in the islands becoming uninhabitable because of frequent damage to infrastructure and the inability of their freshwater

aquifers to recover between overwash events by seawater. Based on the same study, the U.S. Geological Survey declared that low-lying Pacific islands may become uninhabitable because their fresh water turns salty long before the waves engulf them. A study by J. Chen and Mueller (2018) indicated that in much of Bangladesh, particularly in the Ganges, Brahmaputra, and Meghna river delta, it is salinization, rather than the generally accepted notion of migration by floods, tsunamis, and other natural disasters, which is a more significant driver of migration. Mass migration at such scales may cause political instability and upheaval, and may even lead to transboundary conflicts between the affected nations.

Quantifying the socio-economic impact of soil salinization is an essential yet complex task with far-reaching implications (Rahman et al., 2019). For agriculture-dependent economies, soil salinization can significantly reduce crop yield, affecting farmers' income, and potentially leading to food scarcity issues (Kumar & Sharma, 2020). The economic loss can extend beyond agriculture, affecting related industries, such as food processing and distribution. In extreme cases, soil salinity can disturb human health and economic welfare, which finally leads to unemployment, migration, and collapse of societal stability.

There are direct costs to consider, such as those needed for soil remediation techniques (Bello et al., 2021), or the importation of water with lower salinity levels for irrigation (Sahab et al., 2021). Introducing salt-tolerant crop varieties might require investment in research and development, as well as costs for farmers to adopt new agricultural practices (Nouri et al., 2017). Tripathi (2011) calculated that approximately 55,000 Indian rupees (Rs.) per hectare is needed to rehabilitate saline soils. Assessments of Qadir et al. (2014) indicate that the yearly expenses for soil salinization range between US $250 to $500 per hectare. Qadir et al. (2014) extrapolated this to estimate a global annual crop loss of around US $27 billion in irrigated areas. Then, there are indirect costs, including potential rural-to-urban migration, loss of livelihood, and subsequent social challenges that could arise from such changes (J. Chen & Mueller, 2018; Eswar et al., 2021). In many instances, the burden of salinization falls disproportionately on small-holder farmers who have fewer resources to adapt to the challenges presented by saline soils (da Silva Dias et al., 2021; Oo et al., 2017), as those most affected are often the most vulnerable populations.

To adequately quantify the socio-economic impacts of soil salinization, multi-disciplinary approaches that combine soil science with economics, social science, and environmental studies are required. These could include cost-benefit analyses of adopting different salinity management practices, surveys to understand the social impacts on affected communities (such as Zekri et al., 2010), and environmental assessments to understand the long-term sustainability of such practices (Inam et al., 2017). Oo et al. (2013) assessed the impact of soil salinity on crop yield, food security, and socio-economic conditions in three selected villages in Northeast Thailand, known for varying levels of soil salinity. Using a multi-method approach that included a questionnaire, semi-structured interviews, and direct observation from January to June 2012, the study collected data from 90 randomly selected households. The rice production system was found to be similar across the villages, with farmers using organic fertilizers and manure to combat salinity. Despite their efforts, average rice yields were low, at about 1.5 tons per hectare.

Salvati and Ferrara (2015) examined the relationship between soil salinization and socio-economic factors in Italy using a range of territorial indicators. They explored the spatial correlation between vulnerability to soil salinization and six socioeconomic domains: population structure/dynamics and human settlements, labor market and human capital, economic specialization and competitiveness, quality of life, agriculture and rural development, and landscape and environment. The findings suggest that municipalities at risk for soil salinization typically experience higher human pressure, manifested through intensified agriculture, high population density, a younger population, discontinuous urban settlements, higher unemployment rates, higher crime levels, and medium to high financial prosperity.

Szabo et al. (2016) examined the long-term environmental risk of soil salinization in coastal areas, specifically the Ganges-Brahmaputra delta in Bangladesh, and its impact on food security. Using data from the 2010 Household Income and Expenditure Survey and the Soil Resource Development Institute, their research focused on the relationship between soil salinity, household wealth, and food security measures, namely, calorie availability and household food expenditure. They found that while soil salinity negatively affects food security, the impact becomes statistically insignificant when household wealth is considered. In addition, education and remittance inflows, rather than the gender or employment status of the household head, are significant factors influencing food insecurity in the region.

A review of salt-affected reclamation trends in India (Tripathi, 2011) showed reclamation efforts are economically feasible, with a benefit-cost ratio of 1.5 and an internal rate of return of 20%. The initiatives have led to 15 million additional tons of food grain production and 250 million person-days of employment annually. However, challenges such as small and fragmented land holdings, high reclamation costs, flawed irrigation practices, and insufficient water pricing policies, hinder further progress. Technologies successfully adopted in India for soil reclamation include using gypsum to rehabilitate sodic soils, installing sub-surface drainage systems for waterlogged saline areas, developing salt-resistant crop strains, and enhancing agroforestry methods. A review by Kumar and Sharma (2020) suggested, however, that the remediation of approximately 2.18 million hectares of salt-impaired soil, which includes 2.07 million hectares of unproductive sodic soil and 0.11 million hectares of saline soil, has added an excess of 17 million tons of food grains to India's annual food supply, increased the yearly income by Rs. 15.5 billion, and created 2.8 million workdays per year.

6. Large Scale Monitoring of Soil Salinity

Large-scale soil salinization cannot be fully addressed using isolated regional interventions, necessitating a comprehensive global perspective, since soil salinization is a transboundary and global issue that calls for international solutions and collaboration. Large-scale monitoring (a) provides a holistic view of soil salinity distribution over extensive regions, allowing for the identification of hotspots and trends that may not be apparent at smaller scales (Omuto et al., 2013), (b) facilitates the early identification of areas at risk of salinization, enabling in-time intervention (Oldeman et al., 1990), (c) helps allocate resources where they are most needed for soil amelioration and conservation, and (d) allows for observing long-term trends and changes in soil salinity, essential for adapting to evolving environmental conditions. Timely detection of soil salinity changes is crucial for proactive management. Decision-makers in agriculture, land management, and environmental protection benefit from data-supported insights (Mukhopadhyay et al., 2021; Zhang et al., 2017). Large-scale monitoring data inform policy development and land-use planning. Efficient resource allocation is possible when the extent and severity of soil salinity are known (Hassani, Azapagic, & Shokri, 2020). Moreover, monitoring soil salinity in the context of changing climate conditions is crucial for adaptation and mitigation strategies.

Monitoring soil salinity involves estimating the salinity (measured typically as the EC of the soil paste; see 2) across geographical areas and over time (Zaman et al., 2018). The process typically begins with collecting in-field ground-based measurements of soil salinity, which can vary in spatial distribution and the timeframes over which they are collected. They may be structured in a grid pattern or randomly sampled across a study area. Monitoring soil salinity through ground-based measurements can provide accurate data about salt levels in specific locations. There are, however, practical limitations to conducting ground measurements at a large scale. Performing ground-based measurements involves significant time, expenses, and labor. Collecting soil samples, preparing the soil-water paste, and using specialized equipment to measure EC can be resource-intensive. To comprehensively monitor soil salinity across a large area, many soil samples must be collected and analyzed. This becomes logistically challenging, especially for regions with extensive agricultural or environmental monitoring needs (Juan et al., 2011). Soil salinity can vary over time due to such factors as irrigation, rainfall, and land management practices. Obtaining frequent and continuous ground-based measurements to capture the temporal changes is impractical. Achieving a high spatial resolution with ground measurements would require collecting samples at very short intervals, which may not be feasible in terms of both time and resources.

Due to such difficulties, soil salinity monitoring typically combines ground-based measurements at selected points with other techniques, such as remote sensing and geostatistical modeling in soil salinity mapping (Allbed & Kumar, 2013). Ground measurements provide essential calibration and validation data. Geostatistical models then interpolate and extrapolate the information from the measured points to create continuous salinity maps (Goovaerts, 1997). Recently, satellite imagery, particularly from sensors with thermal and multispectral capabilities, has been also used as a tool for assessing soil salinity over large areas (Allbed & Kumar, 2013; Gorji et al., 2019; Metternicht & Zinck, 2003). Remote sensing can provide data on land surface temperature (LST), vegetation indices, and reflectance patterns, which are indirect indicators of soil salinity levels. Data from satellites, such as Landsat, Sentinel, and MODIS (Moderate Resolution Imaging Spectroradiometer), are commonly used for this purpose. We will discuss the remote sensing applications for soil salinity mapping in detail later in this Review.

The monitoring and mapping process of soil salinity encapsulates the core principles of digital soil mapping, wherein data collected from the field serve as inputs to generate spatially continuous representations of soil properties (Zhang et al., 2017).

6.1. Ground-Based Measurements

Ground-based measurements play a crucial role in assessing soil salinity, and are essential to its monitoring and mapping efforts. They provide reference data that can be used to calibrate and validate remote sensing and modeling efforts. Remote sensing data, such as satellite or airborne imagery, may not directly measure soil salinity, but can be correlated with ground-based measurements, and help assess the accuracy and reliability of remote sensing data and models.

The first step is to design a sampling plan that determines where and how soil samples are to be collected. The selection of sampling locations should aim at capturing the spatial variability of salinity within the study area. Then, soil samples are collected from predetermined sites using specialized tools, such as soil augers or coring equipment. Samples are typically collected at various depths to assess salinity profiles. The collected soil samples are transported to a laboratory for analysis. The primary parameter of interest is the soil-water mixture EC, which is a standard indicator of salinity, since it reflects the soil's ability to conduct an electrical current, which increases with higher salt concentrations (Richards, 1954). Various ratios of soil to water paste can be used for this purpose, depending on the specific requirements of the analysis.

Saturated Paste: This method measures the electrical conductivity of the saturated soil paste extract (EC_e; see Section 2). The saturated soil paste extract—which shines under light, exhibits a slight flow when the container is tilted, and smoothly slides off the spatula, unless the soil is rich in clay content—is usually extracted using a vacuum pump (FAO, 2021b). The EC_e is often used as a reference metric for quantifying soil salinity (see Section 2).

Other Ratios: Depending on the specific objectives of the analysis, various ratios may be used, such as 1:1, 1:2, 1:5, 1:10, and 1:20 soil-to-water ratios (Sonmez et al., 2008). Ratios of 1:2 and 1:5 are more common, mainly when conducting a large number of soil tests. The more diluted extracts are suitable for preliminary assessments, or when only a rough estimate of soil salinity is needed. They are less sensitive to slight variations in salinity, but can still provide valuable information.

The choice of soil-to-water ratio should align with the analysis' goals, the available resources, and the desired level of precision. Saturated paste is widely accepted (Richards, 1954). It is, relatively speaking, the most representative method for determining the maximum salinity potential of the soil as it closely replicates the root zone moisture and reflects conditions that plants experience (Datta et al., 2019), but it may not always be practical due to the time needed for saturation. In addition, preparing an ideal saturated paste might be subjective, requiring expertise as soil texture (clay content) and organic matter can change the properties of the prepared saturated paste. Specifically, the soil's clay content can affect its water-holding capacity and consistency, while organic matter influences the soil's structure and water retention. Conversely, some studies have evaluated the effects of various combinations of soil physical parameters, such as EC, pH, soil water content, and temperature, on predicting soil salinity metrics like total dissolved salts, potential salinity, sodium adsorption ratio, or ESP (e.g., Xiao et al., 2023, using ML techniques).

Converting EC measurements obtained at various soil-water extract ratios to EC_e can be difficult. The relationship between such measurements is not straightforward and can vary significantly based on soil properties and geographic locations (Kargas et al., 2022). While there have been attempts to empirically convert EC values from various extract ratios to the EC of the saturated paste (Aboukila & Norton, 2017; Hogg & Henry, 1984; Matthees et al., 2017), the conversions are often site-specific and depend on such factors as soil composition, texture, and local hydrology. Therefore, interpreting and comparing the EC data obtained at various extract ratios should be done with caution, considering the specific characteristics of the study area.

The results of field surveys are typically documented and disseminated through scientific papers, reports, or, in the case of government or geological survey institutes, saved as geodatabases. Scientific articles and reports typically include detailed descriptions of the study area, sampling locations, soil sampling and analysis methods, and quality assurance/quality control procedures. In the case of agricultural/governmental agencies or geological survey institutes, which often undertake large-scale and ongoing surveys of soil salinity, the data collected may be

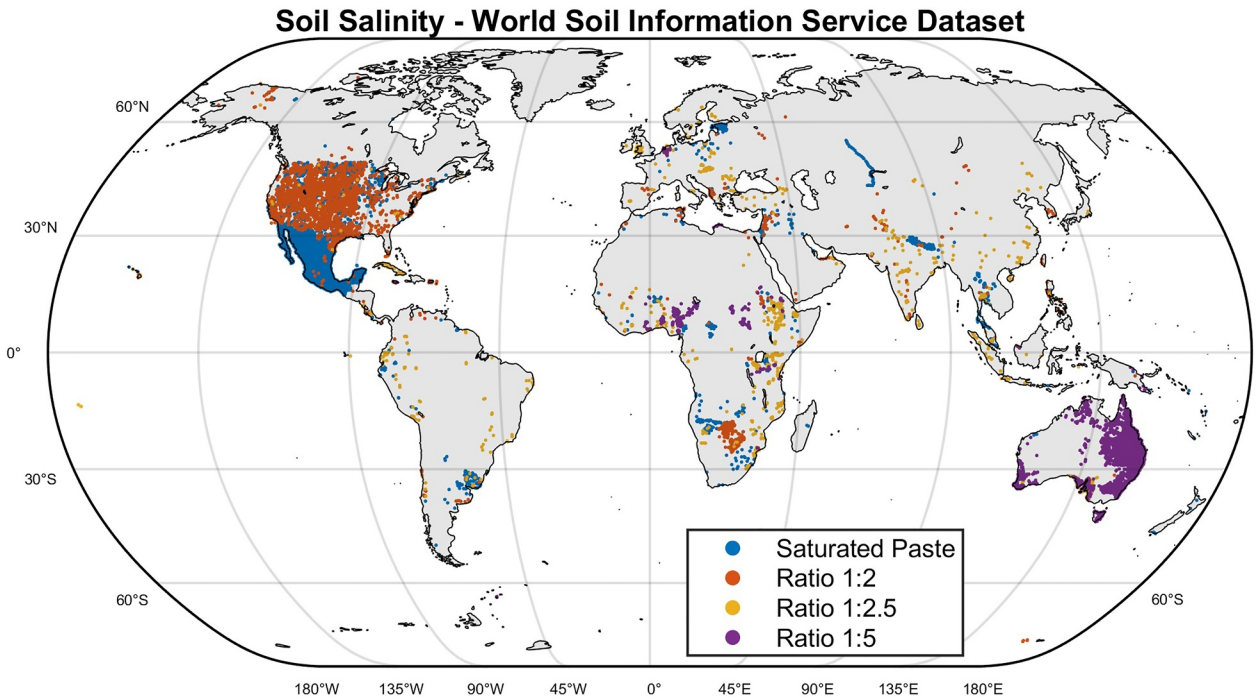

Figure 6. Soil salinity measurements provided by the World Soil Information Service, a database developed and maintained by the International Soil Reference and Information Center.

organized and stored in soil databases, which allow for integrating soil salinity data with other geospatial information, such as land use, hydrology, and climate data. The integration enables a holistic understanding of soil salinity's interaction with various environmental factors.

Regional and national databases may use different measurement methods, units, and data formats, making it difficult to combine and compare data from various sources. Standardization involves establishing standard protocols, measurement units, and data structures to ensure consistency across data sets (Ribeiro et al., 2015). Once regional and national databases are standardized and harmonized, they can be aggregated to create more extensive, often global, data sets. ISRIC-WoSIS Standardized soil profile data is a prominent example of a globally-recognized and widely-used data set for soil information (https://www.isric.org/explore/wosis/accessing-wosis-derived-datasets, accessed October 2023). ELCO20 (electrical conductivity—ratio 1:2, dS m^{-1}), ELCO25 (electrical conductivity—ratio 1:2.5, dS m^{-1}), ELCO50 (electrical conductivity—ratio 1:5, dS m^{-1}), and ELCOSP (electrical conductivity—saturated paste, dS m^{-1}) are the soil salinity measurements provided by WoSIS data set at different soil depths globally; see Figure 6 (Batjes et al., 2017).

The LUCAS Topsoil Survey (typically 0–20 cm), coordinated by the European Soil Data Center (https://esdac.jrc.ec.europa.eu, accessed October 2023)—Joint Research Center of the European Commission, is another valuable source of soil data at the European scale (Orgiazzi et al., 2018). It involves multiple survey rounds in the years 2009, 2015, and 2018. While this survey provides data on various soil properties and characteristics across Europe, such as soil texture, pH, and OC content, the LUCAS Topsoil Survey conducted in 2009, unfortunately does not include measurements of soil salinity. The soil salinity data measured in LUCAS topsoil surveys are obtained using the ISO 11265:1994 method (https://www.iso.org/standard/19243.html, accessed October 2023). The method involves using metal electrodes in an aqueous soil-water mixture with a 1:5 mass-to-volume ratio. Figure 7 shows the 2018 survey.

6.2. Electromagnetic Induction

Electromagnetic Induction (EMI) is sometimes employed as an alternative or complement to traditional ground-based measurements for assessing soil salinity (Doolittle & Brevik, 2014; Eltarabily et al., 2024). EMI offers a non-invasive and efficient way to gather information about depth-averaged soil salinity over larger areas (Corwin

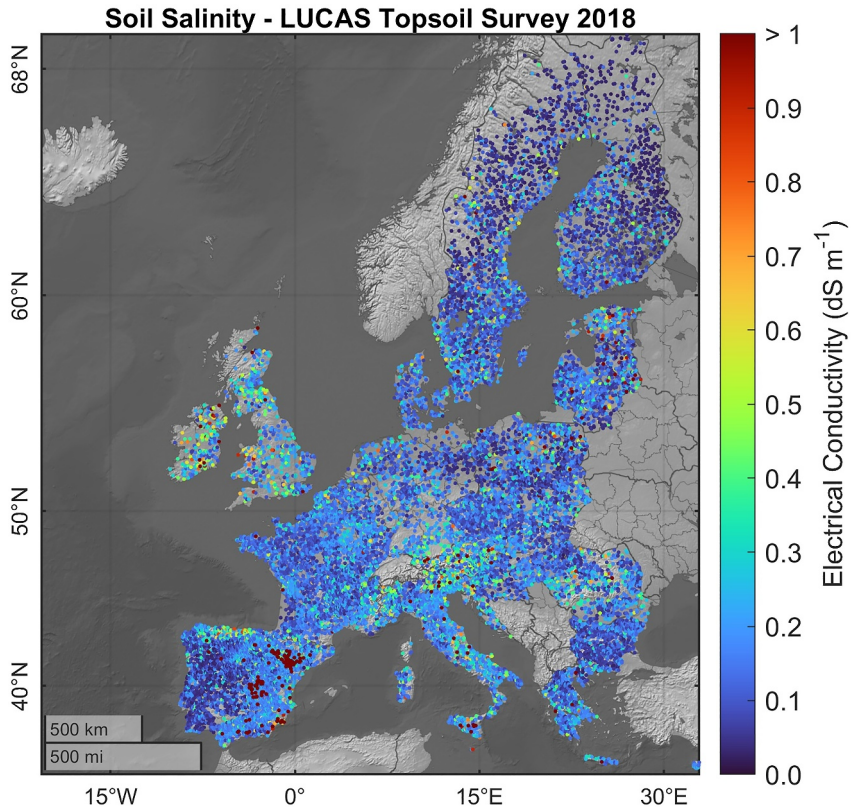

Figure 7. Soil salinity measurements from the 2018 LUCAS Topsoil Survey. The data were collected using the ISO 11265:1994 method, which employs metal electrodes in a 1:5 mass-to-volume soil-water mixture (Orgiazzi et al., 2018).

& Lesch, 2013). Instead of extracting soil samples, EMI instruments quickly scan the ground and provide a spatially continuous picture of soil EC. The method is particularly advantageous for large-scale surveys, where collecting numerous soil samples may be time-consuming and cost-prohibitive. Even at smaller scales, EMI can help identify depth-averaged spatial variability in soil salinity within a field, which is valuable for optimizing fertilizer and irrigation strategies to improve crop yield and reduce resource use (Scudiero et al., 2017).

Frequency-domain electromagnetics (FDEMI) works based on the interaction of electromagnetic fields with the conductive properties of the soil (McNeill, 1980). A FDEMI instrument, which typically consists of a transmitter and a receiver coil, is deployed in the study area. The transmitter coil emits an electromagnetic signal into the soil, while the receiver coil detects the response signal. The transmitter coil emits alternating current, generating an electromagnetic wave propagating into the soil. The electromagnetic wave consists of alternating electric and magnetic fields. As the electromagnetic wave travels through the soil, it induces eddy currents within conductive materials that are present in the soil. The most conductive materials in soil are typically soil moisture and dissolved salts (ions), which respond to the changing electromagnetic fields by creating eddy currents. The electromagnetic wave propagates through the soil, and its strength diminishes with depth due to its attenuation as it interacts with the conductive materials. The depth to which the electromagnetic wave penetrates depends on its frequency; higher frequencies are more sensitive to shallow depths (see below). The receiver coil at the surface detects the response signal generated by the eddy currents induced in the subsurface. The response signal, known as the secondary electromagnetic field, carries information about the soil's EC.

A data logger measures the secondary field's components: the in-phase component that aligns with the primary transmitted field, and the quadrature component, which is 90 degrees out of phase. In typical subsurface scenarios, the in-phase component is significantly influenced by the presence of buried metallic objects, whereas the quadrature component directly reflects the sub-surface's conductivity (Callegary et al., 2007; McNeill, 1980). When operating under what are termed “low induction numbers,” the secondary electromagnetic field is directly

related to the current in the ground. This relationship is exploited for determining the "apparent" or "bulk" electrical conductivity (ECa) of the soil volume being profiled (see McNeill, 1980, and references therein).

The depth to which an EM system can investigate the subsurface, known as the skin depth (δ), is determined by the electromagnetic properties of the medium. It is calculated using the equation, $\delta = \sqrt{2/\sigma\mu\omega}$, where σ is the conductivity of the subsurface (half-space conductivity), μ is magnetic permeability, and ω is the angular frequency of the wave plane (De Carlo et al., 2021). μ is a property of materials that describes their ability to conduct magnetic flux and respond to magnetic fields. In the context of electromagnetic waves, angular frequency defines how rapidly the wave oscillates in radians per unit time. Angular frequency is closely related to a wave's frequency f through the relationship, $\omega = 2\pi f$. In addition, the depth of investigation is influenced by both the distance between the transmitter and receiver coils and their orientation in relation to the ground (McNeill, 1980). When the distance between the coils increases, the depth of the investigated soil also increases. Two standard coil configurations are horizontal coplanar (HCP) and vertical coplanar (VCP) (McNeill, 1980). They determine the orientation of the coils concerning the ground surface. In the HCP configuration, the coils are aligned in a horizontal plane, which is analogous to a vertical dipole orientation. Conversely, the VCP configuration involves rotating the instrument 90 degrees with respect to the HCP orientation, which corresponds to a horizontal dipole orientation. The choice between these configurations and the transmitter-receiver distance affects how the electromagnetic signal propagates into the subsurface.

The EMI instrument provides measurements of the soil's ECa, which represents the composite conductivity of the soil, considering both the pore water (moisture) and any dissolved salts present. ECa is influenced by the conductivity of the soil's liquid phase and the distribution of conductive materials. Calibration is typically performed to convert ECa to soil salinity (Corwin & Scudiero, 2019), which involves taking direct soil samples at measurement locations and measuring their EC_e or other ratios in the laboratory. A relationship can be established between the ECa measurements and the actual soil salinity, typically considering the local soil properties, depth variations, and instrument-specific factors (see, e.g., Gu et al., 2023). Y. Wang et al. (2024) assessed various approaches to reduce the impact of soil moisture on soil salinity prediction through laboratory simulations of in-situ Vis-NIR spectra. They concluded that for certain soils, moisture correction is unnecessary to achieve relatively high accuracy.

Soil moisture sensors (L. Yu et al., 2021) are also valuable tools for monitoring soil salinity, because they provide insights into the water content of the soil, which is intimately linked to salinity levels. These sensors are typically buried at various depths within the soil profile, allowing them to track changes in moisture content over time. When used in conjunction with other salinity assessment methods, such as EMI or remote sensing, soil moisture sensors enhance our understanding of the interactions between salinity, soil moisture distribution and plant health (Metternicht & Zinck, 2003).

6.3. Soil Salinity Mapping: From Ground-Based Pointwise to Continuous Maps

In the context of soil salinity, mapping involves the integration of various data sources to create informative maps that depict the continuous distribution of soil salinity across a geographic area (Silatsa & Kebede, 2023; Zhang et al., 2017). Geospatial models leverage the available data to estimate soil salinity levels at locations where direct measurements or samples were not taken. This process is referred to as spatial interpolation, whose goal is to create a continuous map of soil salinity across an entire area, even in places where no specific measurements were collected.

Mapping starts with a data set that includes soil salinity measurements at specific sampled locations. Using various mathematical and statistical techniques, geostatistical models are generated, which analyze the relationship between the known data points and the spatial characteristics of the landscape, such as climate, topography, and land use. It looks for patterns and trends in how soil salinity varies across space. For example, it may identify that salinity tends to increase in areas closer to a saltwater source, such as a coastline. Geospatial tools and techniques are not limited to mapping the spatial distribution of soil salinity; they can also monitor and map its temporal variations over time. In this context, the values of predictors used in modeling must be known as a function of time. A common approach in the recent literature involves using two types of predictors: one set comprising spatially static variables, such as soil properties assumed to remain constant over extended periods of

salinity variations (e.g., decades), and another set containing more spatially and temporally dynamic predictors, such as climate or vegetation data (e.g., Hassani, Azapagic, & Shokri, 2020).

Before geostatistical modeling can commence, it is essential to preprocess the data, which involves cleaning and standardizing them, dealing with missing values, and converting different data formats into a standard reference system. Integration of other data sets is common in geospatial modeling. Such data sets typically include remote sensing data, such as satellite imagery and aerial photographs, which may have different spatial and temporal resolutions.

Remote sensing, in the context of soil salinity mapping and monitoring, primarily involves collecting data from space-borne instruments or sensors mounted on satellites (Gorji et al., 2019; Metternicht & Zinck, 2003). EMI devices can also fall under the category of remote sensors (Corwin & Scudiero, 2019). For the purpose of this Review, however, when we refer to "remote sensing," we are explicitly referring to satellite imagery. Remote sensing can be employed in two primary ways in this context:

6.3.1. Direct Mapping or Monitoring

Remote sensing data can be used directly to map and monitor soil salinity (e.g., Das et al., 2023; Y. Han et al., 2023; Kaplan et al., 2023; S. A. Mohamed et al., 2023; Sarkar et al., 2023). The approach involves analyzing satellite imagery and sensor data to detect and quantify salinity levels in the soil. Elevated soil salinity levels often lead to reduced vegetation cover, which, in turn, affects LST. Therefore, LST can be related to soil salinity (Ivushkin et al., 2019; L. Yang et al., 2015). Remote sensing data can be used to calculate vegetation indices, such as the normalized difference vegetation index (NDVI) (Alqasemi et al., 2021), which measures the greenness and health of vegetation. High soil salinity can cause vegetation stress, leading to lower NDVI values, and making it an indirect but informative indicator of salinity. Moreover, surface reflectance patterns can be directly used to monitor and detect soil salinity and salinization hot spots. Different soil properties, including soil salinity, affect how soils reflect and absorb light at different wavelengths. Soil salinity can influence the spectral signature of the soil, causing variations in reflectance patterns (R. P. Singh & Sirohi, 1994). In areas with salt-affected soils, the high concentration of salts in the soil can alter its reflectance properties. Saline soils often appear brighter or have a higher reflectance in specific spectral bands due to the presence of salt crystals on the soil surface. These patterns can be indicative of soil properties, including salinity. Anomalous reflectance patterns in certain bands may suggest the presence of saline soils.

6.3.2. Indirect Use as Predictors in Geostatistical Models of Soil Salinity Mapping

Remote sensing data can also be used indirectly as predictor variables in geostatistical models of soil salinity (e.g., Hassani, Azapagic, & Shokri, 2020; Ivushkin et al., 2019; S. Ma et al., 2023; N. Wang et al., 2024). Instead of directly mapping salinity levels, remote sensing data, such as vegetation indices and soil moisture content, or land cover information, are integrated into geostatistical models. These models combine remote sensing variables with other spatial data sources and ground-based measurements to predict regional soil salinity levels. Microwave sensors on satellites can measure soil moisture content, closely related to soil salinity (Wagner et al., 2007). Accordingly, soil moisture data can serve as a predictor variable for salinity modeling. Remote sensing data provide information on land cover types and land use practices. More importantly, satellite-derived climate data, including temperature, precipitation, and evapotranspiration, can be incorporated into the models. Climate variables influence the hydrological processes that affect soil salinity.

Commonly-used satellite platforms in soil salinity modeling include Landsat, MODIS, and Sentinel and their onboard instruments (W. Wu, 2019). However, new platforms are becoming more and more available. A recent study by J. Wang et al. (2023) has used Cyclone Global Navigation Satellite System (CYGNSS) data (CYGNSS L1 v3.0) to develop a novel salinity retrieval model, for example, Or H. Yang et al. (2023) used Gaofen-2 (GF-2) imagery data to map salinity in Yellow River Delta. The choice between direct mapping and indirect use as predictors depends on the specific goals of a study, data availability, and the desired level of detail. Direct mapping using remote sensing provides immediate insights into the spatial distribution of soil salinity, but its use with remote sensing does have several shortcomings, as direct remote sensing primarily provides information about the surface properties of the soil, but provides limited depth information. Soil salinity at deeper layers, affecting root zones and groundwater, may not be accurately represented. One limitation of direct soil salinity monitoring through satellite data is that the vegetation signals detected by the satellite, such as NDVI, may not

distinguish between salt-tolerant and salt-intolerant crops. This means that satellite imagery cannot detect stress caused by salinity, which is misleading in monitoring the soil salinity levels. As a result, additional ground-based information or field surveys may be needed to differentiate between different crop types and assess their specific responses to soil salinity.

Moreover, the availability of suitable satellite data may be limited in some regions or during specific periods, restricting the frequency and coverage of direct mapping efforts (Metternicht & Zinck, 2003). The spatial resolution of remote sensing data may not be sufficient to capture fine-scale variations in soil salinity, especially in heterogeneous landscapes. Similarly, remote sensing data capture the state of the landscape at a specific point in time. Soil salinity can exhibit temporal variations due to seasonal changes, irrigation practices, or natural processes (Mulder et al., 2011). Direct mapping may not capture such dynamic changes effectively. More importantly, remote sensing signals can be influenced by factors other than soil salinity, such as vegetation cover, soil moisture, and atmospheric conditions, which introduce noise and make it difficult to isolate the impact of salinity alone. Direct mapping methods using remote sensing require extensive calibration and validation processes to ensure accuracy. Ground-based measurements and field campaigns are typically needed to validate the remote sensing-derived salinity values, adding complexity and cost to the process.

Aerial surveys by drones that are equipped with specialized sensors have emerged as new tools for monitoring and mapping soil salinity at large scales (Qi et al., 2021; Xie et al., 2022). While not typically suitable for comprehensive, large-scale mapping on their own, they can complement other soil salinity assessment methods, such as satellite remote sensing. Drones equipped with various sensors, such as multispectral cameras and EMI devices, can capture high-resolution data over specific regions of interest. The advantage of aerial surveys lies in their ability to offer fine-grained, site-specific insights into soil salinity dynamics, making them particularly useful for precision agriculture, environmental studies, and localized salinity assessment (X. Yu et al., 2022).

As a geostatistical model makes soil salinity estimations across the entire study area (and time), it effectively creates a continuous soil salinity map. Various techniques are employed to generate spatially explicit maps, which include geostatistical methods (such as kriging and cokriging) (W. Zhao et al., 2019), ML regression algorithms, such as random forests or support vector machines (Hassani et al., 2021; Ivushkin et al., 2019; Zarei et al., 2021), and other interpolation methods. Such models use the available data to estimate soil salinity at unsampled locations, generating a continuous salinity map. To ensure the accuracy of the continuous map, it is typically validated by comparing the model's estimated values with independent measurements or samples that were not used during the model's development.

Taxotransfer is an alternative approach to mapping soil salinity (Batjes, 2003). A taxotransfer function is a method for predicting soil parameters using typical characteristics of soil units identified by their classification name or taxon, which inherently suggests a specific range of soil attributes. This estimation process combines expert knowledge, empirical rules, and statistical analysis of numerous profiles that belong to a particular taxon. Once these functions are established, they can be applied to soil classification maps that are already available. The accuracy of such estimates depends not only on the quality and representativeness of the original soil profile data and the taxotransfer functions, but also on the accuracy and resolution of the soil classification map being used.

6.4. Currently Available Maps of Soil Salinity

Soil Salinity Map of the HWSD (Fischer et al., 2008) is a global-scale data set that compiles ground-based soil salinity measurements from various sources worldwide. It was established through collaboration in 2008 by the International Institute for Applied Systems Analysis, the Food and Agriculture Organization (FAO), the International Soil Reference and Information Center (ISRIC), the European Soil Bureau Network, and the Institute for Soil Sciences at the Chinese Academy of Sciences. Subsequently, HWSD underwent updates in 2013 (HWSD v1.2), which provides estimates of soil salinity for various spatial map units at two specific depths: topsoil (0–30 cm) and subsoil (30–70 cm). The measurements are expressed in units of EC_e. HWSD v1.0 and v1.2 primarily compiled data from various sources, including the Soil Map of the World of FAO—The Digitized Soil Map of the World (V3.5), the FAO-UNESCO Soil Map, SOTER regional studies, the European Soil Database, the Northern Circumpolar Soil Map, the Soil Map of China, and the World Inventory of Soil Emission Potential (WISE) database (Version 2.0, including 9,607 profiles). In HWSD, every map unit is composed of individual soil units or combinations of them. A soil map unit represents a distinct, naturally occurring portion of the terrain including one or more predominant soil types (West, 2004). Compound map units can consist of a primary soil unit along

with as many as nine additional associated soils. Each soil unit is named based on the Revised FAO soil classification legend from 1988, except for regions that continue to use the original soil classification legend from the Digital Soil Map of the World in 1974. For those units, the names of soil units were associated with those found in the Revised Legend.

The WISE30sec data set (Batjes, 2016), which stands for "WISE derived soil properties on a 30 by 30 arc-seconds global grid," is also a global data set that provides the soil salinity represented as EC (measured in either a saturated soil paste or a diluted soil-water suspension). This Geographic Information System data set was generated by overlaying soil map unit delineations from the HWSD version 1.2 with climate zone data (Köppen-Geiger) as a co-variate (Beck et al., 2018). Soil property estimates are provided at fixed depth intervals, ranging from 20 to 100 cm, with 50 cm intervals between 100 and 200 cm at 0.93 km × 0.93 km spatial resolution at the equator. These property estimates were derived from statistical analyses of approximately 21,000 soil profiles stored in ISRIC-WISE database (Batjes, 2008, 2009, 2011). The data set provides means and standard deviations for each attribute. Similar to HWSD, WISE30 employed a taxotransfer scheme to derive best estimates for soil properties.

HWSD v1.2 and WISE30sec differ in several key aspects. While both share a 30 by 30 arc-second grid size and are suitable for continental and global-scale applications, HWSD offers data for soil depths up to 1 m in two layers and threee textural classes, with 16 soil attributes per layer. In contrast, WISE30sec provides data up to 2 m in seven layers, covers five textural classes, and includes 20 soil attributes per layer. WISE30sec also incorporates climate data (Köppen-Geiger) as a co-variate, allowing a more comprehensive analysis of soil properties and associated uncertainties. In contrast, HWSD's taxotransfer procedures can vary depending on source materials. Additionally, WISE30sec provides uncertainty of estimations and emphasizes flagging the nature of taxotransfer rules, enhancing transparency in data interpretation, whereas HWSD lacks uncertainty information.

HWSD v1.2, while valuable, does come with two significant limitations. The mapping within the database adopts a polygon-based approach, where soil salinity values are associated with distinct map units (including 16,327 unique units). The method does not offer salinity values at precise spatial resolutions, despite the overall map being presented as a raster at a 1 km resolution. Furthermore, the database is primarily static spatial information, but does not provide insights into the dynamic variations of soil salinity over time. To overcome the limitations and obtain more up-to-date, detailed, and dynamic information on soil salinity, Ivushkin et al. (2019) provided another continuous global soil salinity map, addressing the limitations of the HWSD. Their study employed the computational capabilities of Google Earth Engine and utilized a random forest classifier trained on seven soil properties maps, thermal infrared remote sensing imagery, and EC_e point data from the WoSIS database. The result was the generation of six maps covering the years 1986, 2000, 2002, 2005, 2009, and 2016 at 250 m resolution. The validation accuracy of the maps fell within the range of 67%–70%.

The maps created by Ivushkin et al. (2019) have their own limitations. A notable one is that they provide soil salinity classes, rather than a continuous prediction of soil EC_e. In addition, the maps are limited to specific years, which means they represent a snapshot in time and may not capture full trends in soil salinity. The role of soil depth was also neglected in the analysis. For a more comprehensive understanding of soil salinity dynamics, especially in terms of continuous variations and changes over time, Hassani, Azapagic, and Shokri (2020) created a global-scale data set that quantified various aspects of soil salinity variability (EC_e) over the past four decades. Their data set provided detailed information at a resolution of approximately 1 km for each year and various soil depths. They employed ML techniques and a predictor data set that included climatic, topographic, soil, and remote sensing data. The data were used to develop predictive models capable of estimating soil salinity and sodicity at various geographical locations, soil depths, and time periods on a global scale.

The revised edition of HWSD (HWSD v2.0), released in 2022 (Nachtergaele et al., 2023), builds on its predecessors, HWSD v1.2, with several enhancements, including (a) expanded data sources from various national soil databases, (b) a larger array of soil attributes accessible for seven distinct soil depth layers, and (c) the implementation of a unified soil reference system, FAO1990 and the World Reference Base for Soil Resources. Figure 8 presents EC of the topsoil (0–20 cm) and deepsoil (150–200 cm) dominant soil types in HWSD v2.0 soil mapping units.

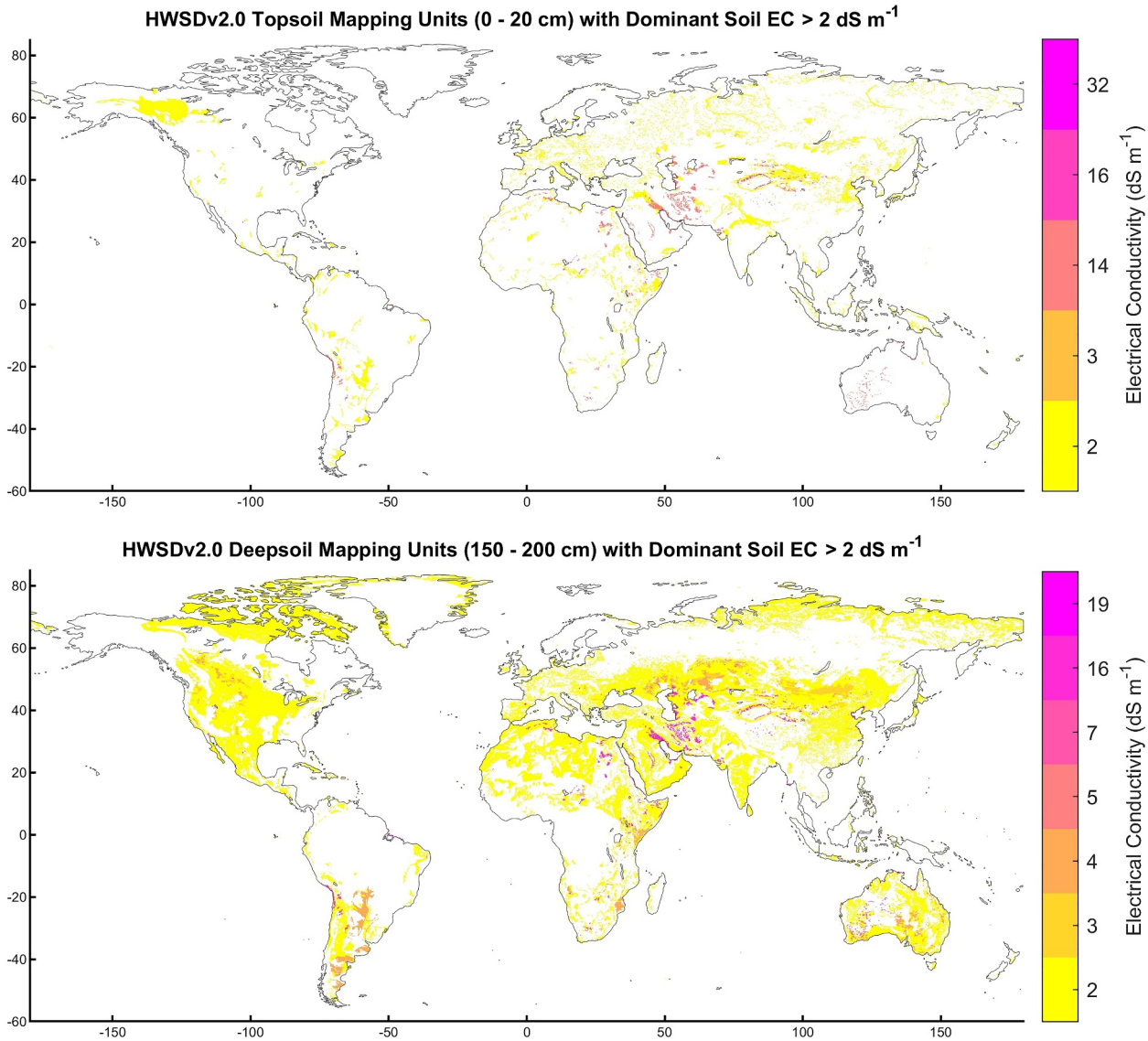

Figure 8. Electrical Conductivity of the topsoil (0–20 cm) and deepsoil (150–200 cm) dominant soil types in Harmonized World Soil Database v2.0 soil mapping units. The input data were obtained directly from the WISE30sec database (data source: Nachtergaele et al., 2023).

7. Minimalist Models of Soil Salinity

It is important to note that modeling soil salinity at a large scale—beyond a collection of agricultural fields—rarely rely on analytical or physics-based models. Physical models—such as those of Corwin et al. (2007), El-Din et al. (1987), or Oude Essink et al. (2010)—that are used to estimate soil salinity dynamics require a range of parameters and data inputs. Initial soil salinity, soil properties (soil texture, structure, and hydraulic properties, such as soil porosity, hydraulic conductivity, and cation exchange capacity), climate data (meteorological data, including precipitation, temperature, humidity, wind speed, and solar radiation), irrigation data (information on the timing, rate, and frequency of irrigation events), data on crop types and evapotranspiration rates, hydrological boundary conditions (information on groundwater levels, depth to the water table, and the presence of perched water tables), boundary conditions on salt (data on the concentration of salts in irrigation water or groundwater sources that may be used for irrigation), root zone characteristics (parameters related to root depth, density, and distribution, which affect water and salt uptake by plants), land use and management practices (information on land use, crop rotations, tillage practices, and the use of soil amendments or gypsum to mitigate salinity), solute transport parameters (those related to salt transport processes, such as dispersion coefficients and

data on the equilibrium between the soil solution and solid phases—cation exchange capacity), the temporal resolution at which the model operates (which affects the simulation of salt dynamics over time), boundary conditions for modeling drainage (data on drainage conditions or the presence of subsurface drains, which influence the removal of excess salts from the root zone), soil profile depth (the depth of the profile being modeled, as salt dynamics can vary with depth), crop/plant growth parameters (parameters related to crop growth, including growth stages, planting and harvesting dates, and yield expectations), topography (information on the spatial distribution of the land surface, which affects surface water flow and salt movement), and continuous salinity measurements (ground-truth salinity measurements for model calibration and validation) are among such data and parameters. Obtaining accurate data for these parameters can be very difficult, especially at large scales, which is why empirical and data-driven approaches are often preferred to physical models for soil salinity monitoring and mapping at large scales. We discussed salinity monitoring and mapping in Section 6.

Minimal models for evaluating soil salinity levels do exist, such as the vertically-averaged soil moisture and salt balance equations proposed by such studies as those of Suweis et al. (2010). In their study, Suweis et al. (2010) developed a set of equations to quantify the mass balance of soil moisture and salt within the root zone, considering specific environmental inputs and disregarding the salt input due to irrigation or ground-water. The model assumes a consistent concentration of salt in rainwater (C_R) and a steady flux of salt mass per unit area over time (M_d) due to dry deposition. The proposed equations are (Perri et al., 2022; Suweis et al., 2010):

$$nZ_r\frac{ds}{dt} = -ET(s) - L(s) + R_t, \tag{4}$$

$$\frac{dm}{dt} = C_R R_t + M_d - CL(s). \tag{5}$$

Here, $nZ_r\frac{ds}{dt}$ represents the change in soil moisture, where n is the porosity, Z_r is the root depth, and s is the soil moisture content. The term $ET(s)$ denotes the combined loss of water due to evapotranspiration, while $L(s)$ represents the deep percolation, and R_t represents rainfall. In the second equation, $\frac{dm}{dt}$ denotes the change in salt mass within the root zone, with C being the salt concentration in this zone. Rainfall (R_t) was conceptualized as a marked Poisson process characterized by a frequency or mean arrival rate λ_P (events d^{-1}). The daily depths of rainfall follow an exponential distribution, the mean of which was represented by $1/\gamma_P$ (Rodríguez-Iturbe & Porporato, 2007; Rodriguez-Iturbe et al., 1999). The parameter γ_P is equivalent to $\frac{nZ_r}{\alpha}$ (α is the mean storm depth, cm per event), and $1/\gamma_P$ can also be interpreted as the mean storm depth weighted by the root zone.

The model simplifies the dynamics of soil moisture by assuming constant average values for soil and eco-hydrological parameters, including root depth (Z_r), porosity (n), and the maximum rate of evapotranspiration $(ET_{\max})$. The concept presented by Porporato et al. (2004) relates to the behavior of evapotranspiration (ET) in response to varying soil moisture levels. In their model, ET_s—where "s" represents soil moisture—is assumed to have a linear relationship within a specific range of soil moisture. This range is defined between two critical points: the Wilting Point (denoted as s_w) and a certain Soil Moisture Threshold (denoted as s_1).

Wilting Point (s_w) is the lower limit of soil moisture in the model. At the wilting point, the soil moisture is so low that plants cannot sufficiently extract water, leading to wilting. Below this point, ET is significantly reduced or practically nonexistent because there is not enough moisture to support evapotranspiration. However, the Soil Moisture Threshold (s_1) is an upper limit defined as an effective field-capacity threshold. At this threshold, the soil moisture is at an optimal level that allows ET to occur at its maximum rate, denoted as $ET_{\max}$. The model implies that as soil moisture increases from the wilting point (s_w) to the threshold (s_1), ET increases linearly. This linear increase continues until it reaches $ET_{\max}$ at s_1. Beyond this point, if additional rainfall occurs and the soil moisture exceeds s_1, the excess water is assumed to be lost as deep percolation, denoted as $L(s)$ at s_1.

By solving the aforementioned equations under a set of assumptions, Suweis et al. (2010) calculated the probability distribution for the salt mass in the root zone, expressed as:

$$p(m) = N\exp\left(-\frac{m\lambda}{\Upsilon}\right)m^{1/\nu}. \tag{6}$$

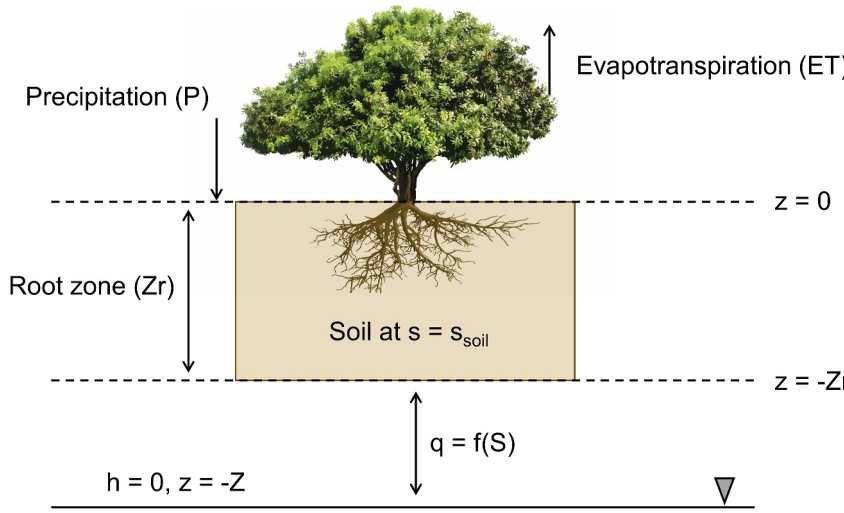

Figure 9. Conceptual model for groundwater uptake by vegetation in a semiarid system, adopted from Shah et al. (2011).

Here, N is a normalization constant defined as $N = (\lambda/\Upsilon)^{\frac{1+\nu}{\nu}}/\Gamma\left(\frac{1+\nu}{\nu}\right)$, where $\Gamma(x)$ is the Gamma function.

The leaching frequency, denoted as λ, is derived from the formula $\lambda = \eta \exp(-\gamma)\gamma^{\lambda_P}/\eta/\Gamma(\lambda_P/\eta,\gamma)$, where $\gamma(x,y)$ is the lower incomplete gamma function. The parameters η and γ are defined as $\eta = ET_{\max}/(nZ_r(s_1 - s_w))$ and $\gamma = \gamma_P nZ_r(s_1 - s_w)$, respectively. Additionally, ν is given by $\nu = b/(nZ_r s_1 \lambda_P)$. The leaching-efficiency parameter, denoted as b, is incorporated to reflect the incomplete dissolution of salt in the soil. It is also assumed that the typical soil moisture level during leaching events can be reasonably approximated by the value s_1. s_1 and b the free parameters that require to be fitted.

In a following research, Shah et al. (2011) expanded upon the work of Suweis et al. (2010) by incorporating the impact of capillary rise from groundwater into the existing water flow model. This model originally accounted for water flow dynamics including precipitation or irrigation (P), leaching (L), capillary upflow (U), and evapotranspiration (ET). The integration of these factors resulted in the formulation of a water balance equation as:

$$nZ_r\frac{ds}{dt} = P - ET(s) + U(s) - L(s), \tag{7}$$

where s represents soil saturation, bounded between 0 and 1 (Figure 9). However, it is noteworthy that Shah et al. (2011)'s analysis did not consider the effects of poor-quality irrigation water and salt deposition through rainfall.

Mau and Porporato (2015) advanced the understanding of soil salinity in irrigated lands by integrating irrigation into a dynamical system framework, and formulating an equation that expresses mass balance for a unit soil area under irrigation, given by:

$$nZ_r\frac{ds}{dt} = P(t) + I(t) - ET(s) - L(s) - Q(s). \tag{8}$$

In this model, water inputs include P and irrigation (I), while outputs are through ET, L, and surface runoff (Q). Mau and Porporato (2015) assumed a deep water table relative to the rooting zone, omitting a water upflow term for simplicity. They also focused on a scenario typical of a dry season in semiarid or arid regions, characterized by minimal precipitation in comparison to irrigation (effectively considering $P = 0$). They posited that under these conditions, relative soil moisture reaches a steady state, denoted as s^*, when subjected to constant rates of I and ET. Additionally, they assumed that Q was negligible. Consequently, this simplification led to the modification of their balance equation to $L(s) = I - ET$, effectively linking the deep percolation directly to the difference between irrigation and evapotranspiration (ET) rates.

Mau and Porporato (2015) derived an equation for salt concentration (C) dynamics as $\frac{dC}{dt} = \frac{IC_i}{w^*} - \frac{L^*}{w^*}C$. L^* is L at s^*, C_i is the irrigation water salt concentration $\left(mmolc\ L^{-1}\right)$, and C $\left(mmolc\ L^{-1}\right)$ is defined by the equation $C = m_{salt}/w*$ (w^* is volume of water in the root zone at s^*). This concentration is also referred to as the electrolyte concentration. This equation describes the evolution of soil salinity, factoring in the salt input from irrigation and the rates of irrigation and percolation. Under constant irrigation parameters C and C_i, the equation simplifies to:

$$C(t) = C^* + (C_0 - C^*)\, e^{-\frac{t}{\tau_C}}, \tag{9}$$

where $C^* = \frac{Ci}{L^*/I}$, $\tau_C = \frac{w^*}{L^*}$, and C_0 is the initial concentration (at $t = 0$). τ_C represents the typical time scale for reaching equilibrium. The leaching fraction (LF), defined as L^*/I, is the proportion of irrigation water that infiltrates beyond the root zone. The steady-state concentration can thus be expressed as $C^* = \frac{Ci}{LF}$. Given that $LF \leq 1$, it follows that $C^* \geq Ci$.

Salt tolerance is crucial in managing the soil water budget within irrigated agricultural ecosystems (Yin et al., 2023). Perri, Suweis, et al. (2018) proposed a minimalist probabilistic estimation of soil moisture in the root zone by integrating the interplay between soil salinity, vegetation, and its impact on the rate of evapotranspiration ET, based on the model of Suweis et al. (2010). The reduction in transpiration due to osmotic and ionic stress largely depends on the plant's salt tolerance, which varies considerably among species. This variation leads to species-specific salinity impacts on the soil water budget, as highlighted by Shah et al. (2011). They introduced the concept of virtual or equivalent moisture content, expressed as:

$$s = s_s \psi_s^b \left[\psi_s \frac{s^{-1/b}}{s_s} + \kappa C\right]^{-b}. \tag{10}$$

In this equation, b is a parameter linked to soil connectivity and tortuosity, ψ_s is the soil matric potential at saturation, and s_s is the relative soil moisture at saturation, with $s_s = 1$. However, this equation, primarily accounting for osmotic effects, does not fully capture the diverse adaptations and transpiration patterns of different plant species under salt stress.

Perri, Suweis, et al. (2018) proposed a simple parameterization of the relationship between ET and root-zone salt concentration, C, drawing on the proportionality between crop yield and transpiration as suggested by Homaee et al. (2002). Experimental studies indicate that beyond a certain salt endurance threshold, all species exhibit a roughly linear decrease in relative crop yield, Y_r (the ratio of actual to potential yield), with increasing C. Given the linear relationship between ET and plant growth over extended salt exposure, it is reasonable to equate Y_r with $ET/ET_{\max}$ or ET_r, and to describe the ET-C relationship as a piece-wise linear function, with a salt-stress threshold C_T and a rate of transpiration decline above C_T, denoted as β (see Perri, Suweis, et al. (2018) and references therein):

$$ET(C) = \begin{cases} ET_{\max}\left[1 - \beta(C - C_T)\right] & \text{if } C \geq C_T, \\ ET_{\max} & \text{if } C < C_T. \end{cases} \tag{11}$$

This equation reflects the observed ET-C relationship. Plants begin experiencing salt stress at varying C_T levels based on their salt tolerance, with transpiration decreasing as salt concentration increases beyond C_T. Similar to the approach adopted by Porporato et al. (2004), water losses, $\rho(s)$, are assumed to be a linear function of s between the wilting point, s_w, and well-watered conditions $(s = s_1)$. Rainfall exceeding s_1 is lost through deep percolation at $s = s_1$. Integrating Equation 5 into this loss function, one can derive an expression for salinity-dependent water losses as a function of relative soil moisture, soil salt mass m, and vegetation salt tolerance (C_T, β):

$$\rho(s,m) = \begin{cases} \eta\chi(s - \theta) & \theta \leq s \leq s_T, \\ \eta s & s_T < s \leq s_1. \end{cases} \tag{12}$$

Here, $\eta = ET_{\max}/nZ_r s_1$ is the normalized ET loss under well-watered conditions. The dependence of ρ on m and salt tolerance is embedded in $\theta = C_{sat}\beta/\chi = C_{sat}/C_{\max}$ (with $C_{sat} = m/nZ_r$ being the concentration at saturation) and $s_T = C_{sat}/C_T$, representing the minimum relative water content of the soil and the soil moisture level at which salt stress first occurs, respectively, for given salinization and salt-tolerance levels. The minimum relative soil moisture, θ, acts as a virtual wilting point, corresponding to water unavailable for root uptake and transpiration due to the combined effects of osmotic and ionic stress.

To develop their model, Perri, Suweis, et al. (2018) had to make an assumption regarding the temporal dynamics of salt mass in the root zone relative to precipitation and wet deposition. They posited that the timescales governing salt mass dynamics are significantly longer than those of precipitation forcing and wet deposition. This implies that soil moisture s can achieve a steady-state value within a time frame where the variability of salt concentration in the root zone m is minimal, the so-called quasi-steady-state. Based on this assumption, they calculated the steady-state probability density distribution (pdf) of soil moisture, conditional to a given level of salinization m and prescribed plant salt tolerance, as follows:

$$p(s|m) = \begin{cases} N_T \dfrac{e^{-\gamma s}}{(s-\theta)}\left(\dfrac{s-\theta}{s_T-\theta}\right)^{\frac{\lambda}{\eta\chi}} & \theta \le s \le s_T, \\ N_T \chi \dfrac{e^{-\gamma s}}{s}\left(\dfrac{s}{s_T}\right)^{\frac{\lambda}{\eta}} & s_T < s \le s_1. \end{cases} \tag{13}$$

In this formulation, N_T represents a normalization constant that is specific to species with high salt tolerance.

These minimalist models focus on primary salinization, while dynamical system approaches (Mau & Porporato, 2015) are available for irrigated lands, and are advantageous because they are parsimonious, offering mechanistic insights into how different variables, such as climate or vegetation, influence soil salinity levels in the root zone (see e.g., Perri et al., 2022). They are, however, still not readily applicable for large-scale monitoring despite their value. One reason for this limitation is that they require extensive parameterization, particularly for the root zone. Moreover, the availability of comprehensive soil data, on which these models rely, is often limited. Instead, empirical approaches that utilize available ground-based measurements in combination with statistical or ML models are more commonly employed for effective soil salinity monitoring and mapping.

The models mentioned in this section, that is, those of Suweis et al. (2010), Shah et al. (2011), Mau and Porporato (2015), and Perri, Suweis, et al. (2018), are categorized as process-based and low-complexity models of soil salinization. These models primarily focus on understanding the temporal evolution of the idea that vegetation actively regulates salinization through ET. For instance, in Perri, Suweis, et al. (2018), ET is not solely dependent on soil moisture but also on salinity. Over the long term, this can influence both the water and salt mass balance of the soil. These minimalistic models (some of which are stochastic) aim to understand processes that are not yet integrated into more complex models of land-atmosphere interactions, such as the land modules of Earth System Models. Their scope includes probing the interactions between vegetation, soil salinity, and ET, shedding light on how vegetation dynamics influence soil salinity dynamics over time.

8. Soil Salinization at the Core Scale

Another important length scale, smaller than the large scale described so far, over which soil salinization must be understood is the core or laboratory scale, and in fact the vast majority of experimental data for soil salinization have been obtained over such a scale. Soil salinization is closely tied with evaporation of salt-containing liquids, and subsequent drying of the pore space. As a globally significant process, evaporation consumes nearly 25% of the solar energy (Trenberth et al., 2009), but also feeds into the global hydrological cycle about 60% of the terrestrial precipitation, 20% of which is by direct soil evaporation, while the rest is by plant transpiration (Oki & Kanae, 2006). Thus, before we describe soil salinization at the core scale (porous samples of linear size of at most 30–90 cm), we must first gain a clear understanding of drying of soil and factors that affect it. In this section, first we describe evaporation and drying of soil at the core scale, after which we will discuss soil salinization at the same length scale.

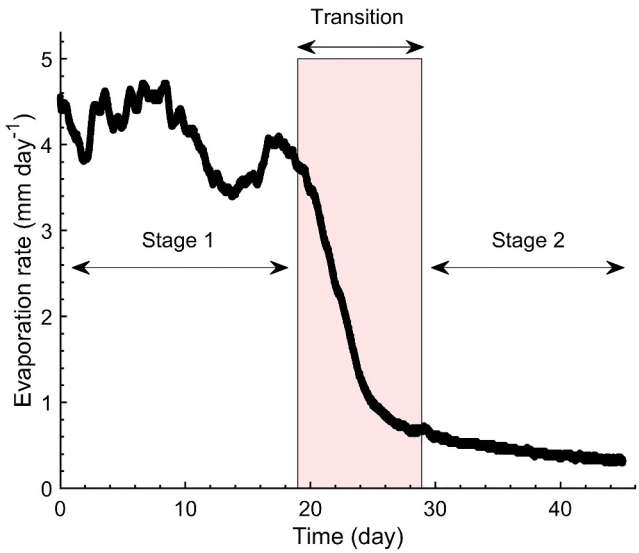

Figure 10. Evaporation dynamics of an initially saturated sand column that exhibits the two stages of evaporation (adopted from Shokri and Or, 2011): Stage I (constant rate period), followed by falling rate period, or vapor diffusion-controlled Stage II. During Stage I, the drying front (i.e., the interface between saturated and unsaturated zone) connects the wet zone to the vapourization plane at the surface. When the hydraulic connection with the surface is interrupted, the drying front recedes from the surface leading to formation of a dry layer close to the surface.

8.1. Evaporation and Drying at Core Scale

Or et al. (2013) reviewed and comprehensively described factors that contribute to evaporation in soil and other types of porous media. Drying of a porous medium is not only important to salt transport and precipitation, the subject of this Review, but also to many other phenomena, ranging from agriculture and soil physics (Aydin et al., 2008; Ben-Noah & Friedman, 2018), to remediation and recovery of soil contaminated with hydrocarbons (Hosseini & Alfi, 2016; Nadim et al., 2000; Soltanian et al., 2016), recovery of volatile hydrocarbons from oil reservoirs, cosmetics, building restoration, and material processing such as the production of food, wood, paper, textiles, pharmaceuticals, and washing powders. In addition, water evaporation influences the availability, transport, and partitioning of nutrients, as it controls the transfer of heat, air, and humidity between the atmosphere and subsurface.

8.1.1. Experiment-Based Insights Into Evaporation From Porous Media

There are two distinct stages in a typical evaporation process in soil. One is an initially high and relatively constant rate, which is usually referred to as Stage I evaporation—also called the constant rate period (CRP)—and is supported by internal capillary flow (van Brakel, 1980; Yiotis et al., 2006), followed by Stage II or the falling rate period (FRP), one in which evaporation occurs at a lower and gradually decreasing rate. Stage II represents a transition from capillary flow to diffusion-limited vapor transport in porous media. Figure 10 presents the two stages.

Qualitative features of both stages have been known for over a century, after the pioneering work of Buckingham (1907) and Sherwood (1929a, 1929b, 1930, 1931). The former described the role that capillary flow along "films" plays in sustaining high evaporation rates, as well as the eventual effect of breakup of "water films" on reduced evaporation rates. Buckingham (1907) also proposed that breakup of liquid connections under high atmospheric demands was the key to the counter-intuitive observation of reduced evaporative rates relative to fluxes under low atmospheric demand for surfaces with a constant water table below. This phenomenon, now known as the "Buckingham effect" (Bond & Willis, 1970; Covey & Bloodworth, 1965) represents a percolation effect (Sahimi, 2011, 2023) that describes the role of connectivity in fluid flow and transport processes in porous media. Sherwood, a pioneering chemical engineering faculty at MIT, identified two mechanisms that contribute to the FRP, namely, the limited vapor diffusion across a surface air film, and resistance due to internal flow in a porous medium in which evaporation occurs. Modeling of the transition from capillary-flow dominated

evaporation to diffusion-limited vapor transport is a formidable challenge (Kalma et al., 2008; Mohanty & Skaggs, 2001).

Similar to most mass-transfer processes, the driving force for evaporation is the vapor concentration gradient between the concentration of the nearly saturated vapor at water menisci and that of the air vapor. As water is lost during evaporation from wet soils, it induces invasion of air into emptied pores. The manner by which this occurs is determined by the pores' size and the capillary pressure P_c needed to invade them, namely, $P_c \propto \sigma/r$, where σ is the surface tension, and r is the pore's effective radius. Thus, large pores are invaded first, because they require the least capillary pressure. This is completely similar to invasion percolation (Wilkinson & Willemsen, 1983; for a comprehensive review see Sahimi, 2023; for a simple introduction see Ebrahimi, 2010) that describes drainage of a wetting front, and was first noted by Shaw (1987). Shokri, Lehmann, Vontobel, and Or (2008) and Shokri et al. (2010) noted that the capillary pressure at a receding drying front into a saturated porous medium remains essentially constant, with a value that is about the entry capillary pressure for air.

Stage I evaporation ends (Lehmann et al., 2008) when, with gradual drying of the top surface, the drying front recedes deeper into the soil, and the associated capillary pressure takes on larger negative values in order to drive capillary flow from the deeper front, and a critical value of the capillary force is reached at which the pores at the surface have either been invaded, or the capillary flow network is disrupted elsewhere. Therefore, the time over which Stage I evaporation occurs is controlled by the values of two capillary pressures P_c, namely, the pressure needed for the air to invade the saturated soil pore space, and the critical capillary pressure at which the network of liquid-filled pores loses its macroscopic connectivity, signaling a percolation transition at which water exists only at its residual saturation in disconnected clusters of pores. If the evaporation rate, as well as the two capillary pressures, are known, one can predict the critical depth h_c of the drying front and the duration of Stage I evaporation at which the transition to Stage II evaporation begins. Although the pore space of soil is an interconnected network of pores, by considering two parallel capillary pores of radii r_1 and r_2 $(r_1 < r_2)$ that communicate with each other (Krischer, 1956; Lehmann et al., 2008; Scherer, 1990), one could obtain an expression for h_c, given by

$$h_c = \frac{h_G}{h_G/h_V + 1}, \tag{14}$$

which provides a qualitative estimate of h_c, where h_G is a gravity characteristic length equivalent to maximal pressure head difference between the two capillary pores, given by

$$h_G = \left(\frac{2\sigma}{\rho g}\right)\left(\frac{1}{r_1} - \frac{1}{r_2}\right), \tag{15}$$

with ρ and g being, respectively, liquid density and gravitational acceleration constant. h_V, on the other hand, is a characteristic viscous length for a cylindrical capillary in the absence of gravity. Assuming the Hagen-Poiseuille (laminar) flow in the capillary, h_V is given by

$$h_V = \frac{\rho g r_1^4}{8q\mu\left(r_1^2 + r_2^2\right)}\Delta h_{\text{cap}}. \tag{16}$$

Here, q is the evaporation rate, μ is the liquid's viscosity, and Δh_{cap} is pressure head difference between the two capillaries. If K_e is the effective hydraulic conductivity of the region that connects the drying front with the surface (defined by $K_e = J/\Delta P$, with J and ΔP being, respectively, the macroscopic flux and pressure difference), then the combined evaporative characteristic length h_c considering viscous and gravity effects is given by Lehmann et al. (2008)

$$h_c = \frac{h_G}{1 + q/K_e}. \tag{17}$$

Since K_e depends on the pore-size distribution of soil, Equation 17 takes into account its effect on h_c. h_c is relatively short for coarse-textured soil due to low capillary driving forces that are the result of coarse and narrow pore-size distribution. Also, h_c could be relatively short for very fine-textured soil due to high viscous losses

(short h_V). An important implication of the existence of h_c is that it limits inferences on evaporation dynamics from studies that have been carried in columns that are shorter that the characteristic length (Shokri & Or, 2010).

Two other important factors that affect Stage I evaporation are soil heterogeneity (Lehmann & Or, 2009; Nachshon, Shahraeeni, et al., 2011; Nachshon, Weisbrod, et al., 2011) and wettability (Bachmann et al., 2001; Doerr et al., 2000; Ritsema & Dekker, 2012; Shokri, Lehmann, & Or, 2008; Shokri et al., 2009). The wettability of porous media, which determines how easily a liquid spreads on or adheres to a surface, can alter by various natural and human-induced phenomena (see Ustohal et al., 1998 and the references therein), influencing processes at larger ecological and hydrological scales. Forest fires, for instance, could lead to the formation of hydrophobic layers (Varela et al., 2005), resulting in affected soil becoming water-repellent, leading to increased runoff, increased leaching, reduced plant growth, and increased soil erosion (Chau et al., 2012). Similarly, coatings of surfaces by organic compounds such as oils, waxes, and resins can alter the surface chemistry of soil grains. Fungal hyphae also contribute by coating soil particles and forming hydrophobic mycelial networks (Chau et al., 2012; Feeney et al., 2006). A wide range of natural and artificial chemicals are surface-active and degrade slowly, capable of altering the wetting properties of the subsurface matrix over the long term (Ustohal et al., 1998). If the wettability changes at the pore scale, it will affect the effective properties at the core scale. Bachmann et al. (2001) and Shahidzadeh-Bonn et al. (2007) demonstrated that evaporation in mixed soils with both hydrophobic and hydrophilic grains is suppressed compared to uniformly wetting porous media. Chapuis and Prat's (2007) pore-network simulations showed shorter drying times in hydrophilic networks than in hydrophobic ones.

Stage II evaporation begins when hydraulic continuity between primary drying front and evaporating surface at the end of Stage I is lost, and the last menisci pinned at the surface recede into the porous medium, forming a new vapourization plane from which water vapor diffuses through the overlying dry layer to the atmosphere (see Shokri & Salvucci, 2011; Or et al., 2013, and references therein). The vapourization plane, which represents a secondary drying front, recedes slowly, but remains hydraulically connected to the primary drying front below through capillary-induced liquid flow. As the process advances, the length of the diffusion path from the receding vapourization plane to the surface increases gradually, resulting in commensurate decrease in drying rate during Stage II (Shokri & Or, 2011).

Experimental data of Shokri et al. (2012) indicated that the drying front traces exhibit roughness in hydrophobic sand that is larger than what is predicted based on the mean wettability properties of hydrophobic surfaces (Tsimpanogiannis et al., 1999). In a separate study, Shokri and Sahimi (2012) studied the structure of propagating drying front in a three-dimensional sand column, using synchrotron x-ray tomography. Their results indicated that the liquid phase has a self-similar fractal structure, with its fractal dimension D_f in all the cross sections of the column being a function of the water content or saturation. These results have important implications for modeling the drying of porous media, as well as salinization. If the drying front and the liquid clusters both have fractal structures, the implication is that continuum models cannot predict them, unless the effects of heterogeneity and fractal structures that are built up by the dynamics of front propagation, on the flow and transport coefficients that appear in such models are explicitly taken into account. Doing so is, however, a difficult problem on its own.

Kharaghani et al. (2021) carried out an experimental study of convective drying of capillary porous media under slow isothermal conditions. Dense packings of particles filled with monodisperse spherical glass beads, initially saturated with distilled water (or with a salt solution) were used, and in-situ tomograms provided the time evolution of three-dimensional structures of liquid (and salt deposit) in the packings during drying. The data demonstrated clearly the formation of capillary liquid rings at the wedge-shaped pores near the contacts between the particles, which remained connected over a long distance to the packing surface during a significant period of drying. Such rings have a great influence on drying, since they act as additional hydraulic pathways for moisture transport from the interior of the pore/particle network to the surface, accelerating the drying process considerably. The same effect was observed during evaporation of brine in the same packing of particles, implying its significance to soil salinization.

8.1.2. Continuum Models of Drying of Porous Media

Continuum modeling of drying of porous media has a long and rich history that goes back to the early decades of the twentieth century. The papers by Lewis (1921) and Fisher (1923), and the work of Sherwood (1929a, 1929b,

1930, 1931) represent some of the pioneering works on evaporation, and in particular evaporation in a porous medium. The first comprehensive model for non-isothermal evaporation from porous media was developed by Whitaker (1977). Starting from the mass, momentum, and energy conservation equations, and assuming the ideal gas law for the vapor phase and Darcy's law for the liquid phase, Whitaker (1977) used the volume-averaging method to derive a complete set of equations for describing the drying process in both the liquid and vapor phases in a periodic unit cell representing the porous medium. Whitaker (1977) also showed, subject to several assumptions, that the density of the vapor phase is described by a diffusion equation. Whitaker did not, however, make any attempt to compare the predictions of his theory of drying of porous media with any relevant experimental data. As he himself stated, "What appears to be an extremely difficult problem at this time is the comparison of theory with experiment in order to determine the value of the various parameters that appear in the governing equations." In addition, it is known that, although the volume-averaging method leads to elegant derivation of equations for describing flow and transport in porous media, its predictions for many cases are only qualitative, as the method cannot take into account the effect of the heterogeneity of the porous medium, particularly when the medium is strongly disordered. Whitaker's paper (1977), which provides the references to earlier works, was followed by that of Scherer (1990).

Attari Moghaddam, Prat, et al. (2017) and X. Lu et al. (2021) developed a mixed model for evaporation in porous media. They utilized the diffusion equation (Equation 18), to model evaporation of water and diffusion of its vapor, but used a pore-network model to obtain the saturation dependence of the diffusivity $D_v(S_v)$. Attari Moghaddam, Prat, et al. (2017) compared the performance of the continuum model, including the pore network-supplied diffusivity, with the results of direct pore-network simulation of drying. There was an agreement between the two, but an objective approach for testing the validity of the mixed continuum model would be comparing its predictions with the experimental data, not with pore-network simulation, since the latter was used to estimate the diffusivity $D_v(S_v)$ in the continuum equation. In other words, the issue with using the continuum model is not that they do not provide a valid theoretical framework for the phenomenon under study; they represent ensemble averages of the equations that describe the fundamental laws of mass, momentum, and energy conservation. Rather, the issue is that such models contain transport and other coefficients that depend on the morphology of the pore space.

8.1.3. Pore-Network Modeling of Evaporation in Porous Media

As first pointed out by Shaw (1987), drying of a wet porous medium is analogous to invasion percolation. Percolation theory (for a simple introduction to percolation theory see Stauffer and Aharony (2018) or Ebrahimi (2010), and for its various applications see Sahimi (2023)) quantifies the effects of the morphology of a pore space—that is, its pore connectivity, and pore-size or pore-conductance distribution—on the phenomena that occur in a porous medium. In particular, as a pore space is dried, the liquid-filled pores lose their connectivity, and eventually exist only in isolated clusters. During salt transport, as salt crystals nucleate and grow, and brine evaporates, salt precipitates on the surface of the pores and, hence, reduces their flow capacity, which can eventually lead to their closure. There are experimental methods based on nitrogen adsorption and the concepts of percolation theory that provide accurate estimates of the mean connectivity of a pore space, defined as the mean coordination number, that is, the average number of pores that are connected to the same pore. Such methods are described in detail by Sahimi (2011). In a more refined pore-network model, one distinguishes between pore throats—the narrow passages through which fluid flow and transport take place—and pore bodies—the large chambers to which the throats are connected and in which most of the porosity of the pore space resides.

Continuum models are not capable of taking into account the effect of the pore connectivity, unless the various flow, transport, and other coefficients that appear in the continuum models, and depend on the morphology of the pore space, are estimated, computed, or measured separately. Pore-network models with suitable pore connectivity and pore-size distribution take into account the effect of the morphology. Pore-network models offer another advantage over the continuum models: Whereas the latter models assume the existence of a representative elementary volume (REV) in order to arrive at the volume- or ensemble-averaged equations, pore-network models make no such assumption. Thus, they may be used at length scales smaller than the REV in order to understand the evolution of the phenomenon as the length scale of interest increases or decreases.

Similar to other flow and transport processes in heterogeneous porous media, the spatio-temporal dynamics of a fluid—liquid or vapor—distribution and the drying front in porous media are controlled by two sets of distinct factors:

(i) One set includes the morphological properties of the porous medium and, if they are present, the fractures (Borgman et al., 2017; Fantinel et al., 2017; Prat, 2002). Such properties include the pore-size distribution, pore connectivity, pore surface structure, and correlations between the sizes of the pores. Large-scale porous media in which evaporation occurs are also normally anisotropic, with the anisotropy caused by stratification, a key feature of rock on a scale from micrometer up to hundreds of meters. Stratification is caused by a variety of processes, such as weathering, deposition, cementation, and compaction that, together, form sedimentary rock. Small-scale stratification is due to alternately operating depositional processes. Vorhauer et al. (2018) showed that the impact of nonuniform distribution of evaporation rate becomes increasingly less important with increasing the number of porous layers.

(ii) The second set includes dynamic factors, such as capillarity-driven flow (D. Le et al., 2009; Scherer, 1990; Shokri, Lehmann, & Or, 2008), pore-scale evaporation and vapor diffusion (Hajirezaie et al., 2017; Lehmann & Or, 2009; Miri et al., 2015), and formation of liquid films on the pores' surface (Chauvet et al., 2009; Lehmann & Or, 2009; Yiotis et al., 2001). In addition, wettability also plays a prominent role. The combination of the effects of all the main factors mentioned in (i) and here gives rise to ramified preferential flow paths and the spatial distribution of the fluids.

Since evaporation from a pore space is essentially a drainage process in which the non-wetting vapor or gas displaces the evaporating wetting liquid (with the caveat that it is not driven by external injection, but by internal diffusion in the gas phase, i.e., one in which a non-wetting fluid—air or any other gas—expels a wetting one—water, brine, or other liquids—from a pore space), in the absence of viscous effects, that is, when the interface between the liquid and vapor moves slowly, the receding interface is described by the invasion percolation process. Pore-network models of drying took advantage of the link between drying and the invasion percolation (Le Bray & Prat, 1999; Pham et al., 2022; Prat, 1995, 2002, 2011; Rahimi et al., 2016; Shaw, 1987; Surasani et al., 2008; Yiotis et al., 2001). The models range from relatively simple to relatively advanced pore networks (e.g., Kharaghani et al., 2012; Mahmood et al., 2021), although most of them have been developed for two-dimension porous media (Dashtian et al., 2018; K. H. Le et al., 2017; Rahimi et al., 2016; Yiotis et al., 2001), but three-dimensional models have also been developed (Dashtian et al., 2019; D. Le et al., 2009; Pham et al., 2022; Vorhauer et al., 2018; Yiotis et al., 2015; Attari moghadam, Kharaghani et al., 2017). Note, however, that the aforementioned constant-rate period (CRP) of drying can be reproduced only with three-dimensional pore networks. This is due to trapping effect: As the gas phase advances, it can surround clusters of liquid-filled pores. They are, therefore, trapped since the liquid phase can move only if it is connected to the external face of the pore space. The trapping effect is very strong in two dimensions, but not so in three dimensions, since in three dimensions the liquid phase remains connected and form a sample-spanning cluster, even when the gas phase also becomes macroscopically connected.

A few points are worth mentioning here:

(i) Simulating invasion percolation in a large three-dimensional pore network is highly time-consuming. However, Sheppard et al. (1999) and Knackstedt et al. (2000) developed highly efficient algorithms for simulating invasion percolation.

(ii) In a typical drying process, flow through thin wetting films on the surface of the pores plays a major role in the transport process during the drying of porous materials and, in fact, its effect is dominant when capillarity controls the process, which is the case in many soil evaporation processes. In the presence of the films the gas phase remains saturated, with little or no evaporation occurring in such pores and, therefore, the transport of the fluid is through strong capillary flow, which is effective in transporting the fluid closer to the evaporation surface. To include the effect of film flow, one must modify the invasion percolation algorithm (Hashemi et al., 1998, 1999). In addition, while in many pore-network models of drying it was assumed that the pore throats are cylindrical, including the effect of film flow entails using non-cylindrical pores, and in fact one must use pores with triangular cross sections that allow flow of films at the corners of the pores. Yiotis et al. (2004) and R. Wu et al. (2020) developed a two-dimensional pore-network model that included the effect of film flow.

(iii) Even if one wishes to simulate, for example, transport in the vapor phase through a diffusion equation,

$$\phi \frac{\partial C_v}{\partial t} = \nabla \cdot [D_v(S_v)\nabla C_v] + q, \tag{18}$$

where C_v and S_v are, respectively, the concentration and saturation of the vapor, D_v is its diffusion coefficient that depends on vapor saturation, and q is the drying rate, one can use percolation theory and the associated concepts in order to compute the saturation-dependence of $D_v(S_v)$ and utilize it in the continuum equation (Ghanbarian et al., 2015).

(iv) Most of the previous works on modeling of evaporation in porous media were based on the assumption of isothermal condition. Under non-isothermal conditions, one must also (a) use an equation of state for the densities of both the liquid and the gas in order to compute them at various temperatures and pressures; (b) utilize correlations for the temperature-dependence of other coefficients, such as the viscosity of the two fluids, which appear in the governing equations, and (c) solve the energy equation along the mass and momentum conservation equations (see Whitaker, 1977). One very recent example of this approach is the work of Benilov (2023) who studied evaporation of a liquid layer on a substrate under non-isothermal condition. His analysis indicated that under non-isothermal condition the evaporation rate depends on the substrate's conditions.

8.1.4. Lattice-Boltzmann Simulation

Since drying of soil is a two-phase flow phenomenon, one can use a lattice-Boltzmann (LB) approach to simulate the process (Márkus & Házi, 2011). Use of the LB approach is particularly useful, and even necessary, if one has a three-dimensional digitized image of the pore space. The approach then allows simulating the phenomenon directly in the image, hence avoiding any assumption regarding the structure of the pore space. Such simulations are, however, time-consuming. Aljasmi and Sahimi (2021) proposed a novel method whereby one first pre-processes the image using three-dimensional curvelet transformations in order to remove all its non-essential features, and then utilizes it in the LB simulation. They showed that the approach reduces the computation time by at least one order of magnitude, while producing accurate results.

8.2. Soil Salinization at Core Scale

Salt precipitation and evaporation in porous media are closely tied. Therefore, now that a good understanding of drying of porous media has been gained, we turn our attention to dynamics of salt precipitation in drying porous media. We point out that solute transport, with the dissolved salt ions being the solute, plays a fundamental role in evaporation of porous media and salt precipitation in the pore space. The presence of salt influences osmotic pressure, which in turn affects matric potential, thereby impacting flow and transport processes (Hu et al., 2023). Since solute transport is highly sensitive to the morphology of a pore space (see Sahimi, 2011), so also is salt transport and precipitation. To understand soil salinization at core scale, we first discuss the most important features of the phenomenon, obtained through experiments, and then describe modeling of salt precipitation in soil at core scale. Note, however, that salt precipitation is also important during injection of a gas, such as supercritical CO_2, into an oil reservoir, and production from it, as it has important consequences for upstream operations. In particular, there is strong evidence indicating that, due to the complexity of the pore space, microscopic capillary-driven solute transport plays a key role in the relationship between the permeability and porosity of the pore space when salt precipitates in the pore space. This was studied through careful experiments by Ott et al. (2014).

Generally speaking, in a porous medium saturated with brine and drying out by evaporation, salt crystallization occurs at the surface of the solid matrix, which is where most of the evaporation takes place (see, for example, Gran et al., 2011; Nachshon, Shahraeeni, et al., 2011; Rodriguez-Navaro and Doehne, 1999). The patterns of salt precipitation could alter dynamics of evaporation, with two common patterns of salt precipitation in porous media usually emerging: *subflorescence*, which develops when the evaporation front is within the porous medium and salt precipitates below the matrix surface in the pores if the solution is supersaturated, and *efflorescence*, which occurs when the liquid-vapor interface remains on the porous medium surface and supersaturation leads to precipitation there, representing a pattern formed in a crust above the surface. Formation of the two patterns depends on salt's chemical composition, humidity, thermal conditions, and other factors, such as wind. Efflorescent crusts (porous packings of salt crystals) deposit during Stage I evaporation (see Section 8.1.1), which is

when the liquid evaporates at the surface. The primary effect of subflorescence is through altering the pore space available for flow, decreasing the unsaturated hydraulic conductivity (Wissmeier & Barry, 2008), and the diffusion coefficient of vapor in the matrix by reducing the matrix porosity, an effect that was pointed out by Millington and Quirk (1961), and was demonstrated by pore-network simulation of Dashtian et al. (2018).

8.2.1. Experiment-Based Insights Into Salinization of Porous Media

Naillon et al. (2015) studied the molecular mechanism of nucleation of salt crystals in clay at length scale of a capillary tube (representing a pore) in which salt crystals nucleate and grow as a result of evaporation of an aqueous solution.

Salt precipitation in a pore: In their experiments, circular capillary tubes that were made of borosilicate glass with an interior diameter of 1 mm were used. They were soaked in an ultrasound bath with detergent solution, followed by being rinsed in deionized water and ethanol, and passing in an O_2 plasma oven. The concentration of NaCl in the solution was close to the solubility value. Each tube was set in an enclosure at fixed temperature and relative humidity, which were measured and recorded during the experiment. Successive images of the capillary tubes during the evaporation experiment were used for collecting the data. The receding meniscus during evaporation was followed so as to (a) measure its kinetics, and (b) determine the size of liquid plug that is used for estimating saturation values. In addition, the crystallization kinetics were also measured.

The position $z_m(t)$ of the receding meniscus in the tube, measured from its entrance, at time t that represents the solution of the Stefan tube problem, is given by

$$z_m(t) = \left[\left(\frac{2M_w P D_v}{\rho_w R T}\right)\ln\left(\frac{1-x_\infty}{1-x_e}\right)(t-t_0) + z_m^2(t_0)\right]^{1/2}, \tag{19}$$

where M_w and ρ_w are, respectively, the molecular weight and density of water, and x_∞ and x_e are, respectively, the mole fraction of vapor in the air and at equilibrium, R is the ideal gas constant, P and T are, respectively, the gas total pressure and temperature with the rest of notation being the same as before. Index 0 refers to the intial time. Note, however, that Equation 19 neglects the variation in the equilibrium vapor partial pressure and the density. Despite such shortcomings, all the qualitative features of evaporation in an actual tube are reproduced by Stefan's equation. Naillon et al. (2015) carried out a more careful numerical analysis in order to take into account the features neglected in the Stefan's solution. The experiments indicated that, generally speaking, the growth of salt crystals takes place at the meniscus. In addition, the structure of liquid velocity field in the vicinity of an evaporating meniscus is complex, because depending on a variety of factors such as variations of temperature along the meniscus generated by the preferential cooling near the contact line—which is the place of the highest evaporation flux—one may have rotating vertices adjacent to the meniscus (Buffone et al., 2005).

The most important result of the Naillon et al.'s (2015) study was that the onset of crystallization of NaCl salt occurs at a significant supersaturated state. This was contrary to the previous claims (Bouzid et al., 2011; Flatt, 2002; Sekine et al., 2011; Steiger, 2005) that no high supersaturations can be reached for NaCl, and that the pore size has a profound influence on the concentration at which the nucleation is first observed, even though the typical pore sizes are orders of magnitude larger than the size of a critical NaCl salt nucleus. Earlier, Desarnaud et al. (2014) had also shown that supersaturation can be reached for NaCl in micro-capillary tubes which spanned several orders of magnitude in volume. In all their experiments, nucleation of salt crystals happened at a very high supersaturation S_s, defined by

$$S_s = \frac{N_c}{N_s}, \tag{20}$$

where N_c and N_s are, respectively, the number of moles of solute by unit mass of solvent when crystallization occurs, and its value at saturation. In their experiments, $S_s \approx 1.6$, and was independent of the size, shape and surface properties of the microcapillaries. Desarnaud et al. (2014) also showed, based on the classical nucleation theory, that this is expected, as $S_s \approx 1.6$ corresponds to the point at which nucleation becomes observable on experimental time scales for the first time. A consequence of the high supersaturation at the onset of nucleation is the very rapid growth of a single skeletal (Hopper) crystal. Experiments on porous media also reveal the formation

of such crystals in the entrapped liquid pockets in the pore network and, therefore, underline the fact that NaCl can easily reach high supersaturation. As for the kinetics of salt crystal growth, Naillon et al. (2015) distinguished two main phases, namely, a first phase in which the growth was quite fast, followed by the second phase in which the growth was much slower. Moreover, the kinetics of salt crystal growth is expressed by

$$\frac{dh}{dt} = K_c(S_s - 1)^{g_c}, \tag{21}$$

where h is the height of the crystal, K_c is kinetic coefficient, and g_c is the crystal growth exponent whose value for NaCl is 1.

Using square capillaries, Shahidzadeh-Bonn et al. (2008) addressed an important problem, namely, whether there is a relationship between the interfacial properties and the location of crystallization that leads to the efflorescence or subflorescence. They studied the problem for two salts, sodium sulfate, Na_2SO_4, and NaCl. Their experiments indicated that NaCl crystals are formed preferentially in contact with a nonpolar area, for example, air or a hydrophobic solid. Hydrophobic treatments have been used to prevent crystallization and damage to buildings, whereas Shahidzadeh-Bonn et al.'s (2008) experiments indicated that the practice can be counterproductive because NaCl tends to crystallize on nonpolar surfaces. On the other hand, their experiments also indicated that hydrated sodium sulfate and anhydrous NaCl crystals form *within* the square capillary at the liquid-vapor interface of both the meniscus within the tube and in the thick wetting films in the corners. Thus, most of such crystals remain within the pore at the end of the evaporation, causing subflorescence. Formation of the crystals at the liquid-vapor interface also enhances the spreading of the solution, since they lower the interfacial tension during crystallization and evaporation, which leads to the wetting of the solution on the outer surface of the capillaries and consequently to efflorescence. The size of anhydrous crystals of Na_2SO_4 is smaller than that of the hydrated crystals. They grow directly at the contact line of the liquid films toward the exit of capillary, exhibiting efflorescence-like behavior. These experiments pointed to an important aspect of salinization: It is a combination of transport properties of saline liquids, namely, the diffusion and dispersion coefficients, and the interfacial properties of the various crystalline phases that govern the dynamics of crystallization, and determines whether the salt solution will effloresce—crystallize on the outer surface of the system—or subfloresce, that is, crystallize within the pores during evaporation.

Experiments in circular capillary tubes have shown that salt precipitation is also affected by the boundary conditions imposed on the system. When the two ends of capillary tubes are open, salt crystals tend to migrate even outside the tube and form a patchy packing. In closed-end capillaries, however, salt crystallization occurs inside the tubes (Miri et al., 2015). Therefore, the question of whether salt precipitates mainly on the external surface of a porous medium, or more uniformly in its pore space, depends on the medium's morphology, the competition between convection and diffusion—as quantified by the Péclet number—and the boundary conditions.

Salt precipitation in porous media: We now turn our attention to salt precipitation at scales larger than a capillary tube or a single pore, specifically within core-scale porous media. One of the earliest studies on evaporation of saline water in actual soil was that of Hassan and Ghaibeh (1977), who studied evaporation in homogeneous and stratified columns in the presence of shallow water table, using soils from Syria and Egypt. They measured the hydraulic conductivity-moisture tension curves for the soils, as well as the evaporation rates and the salt profiles. The salt profiles in the top dry layer indicated flow of multiphase water in that zone. They measured the dispersion coefficient of the ions with the solution and correlated the data with the flow velocity.

Depending on the application, efflorescence might be less damaging than subflorescence, but it is an important issue for preserving old paintings and frescoes. It is also an important problem in soil physics, as well as the role that it plays in soil health, as well as sequestration of CO_2 in underground reservoirs (Peysson et al., 2011). M. Kim et al. (2013) reported on two distinct salt crystallization in synthetic porous media. One type consisted of large, bulky crystals that form away from the vapor-liquid interface, while the second type comprised aggregated, randomly oriented crystals that form near the drying interface.

One key issue is understanding why efflorescence crusts do not form everywhere on the surface of a porous medium, but only at some specific locations. In other words, why is efflorescence *discrete*? In addition, the fact that there exists an exclusion zone around an efflorescence in which no new efflorescence forms, was puzzling for quite sometime. Carrying out wicking experiments, Veran-Tissoires et al. (2012) addressed these issues. They

utilized a packing of glass beads with a diameter of 1 mm in a 50 mm long hollow cylinder that formed a porous medium. The packing was in contact at its bottom with a nearly saturated aqueous NaCl solution. The liquid level in the reservoir was at any time such that, due to the capillary effects, the wick remained fully saturated. The system was isothermal, and the evaporation rate at the wick surface was varied by changing the distance between the wick surface and the entrance to the hollow cylinder.

Experiments by Veran-Tissoires et al. (2012) produced discrete efflorescence that was localized, that is, it was discrete with its localization varying with the distance between the porous medium surface and the entrance to the hollow cylinder. To explain the experimental results, Veran-Tissoires et al. (2012) noted that the evaporation induces flow within the pore space, and since the menisci stay at the surface because the medium remains saturated, the evaporation rate J_e from a meniscus is balanced by capillarity-induced liquid flow rate q_ℓ toward the meniscus between the surface of the porous medium surface and the entrance of the hollow cylinder. Because of the flow (velocity) field within the pore space with an average velocity directed toward the surface, convection transports the salt ions to the evaporation surface, as a result of which a salt peak builds up and salt concentration gradients develop. But molecular diffusion levels off the accumulation of salt and shrinks the concentration gradient, so that there is a competition between diffusion, on the one hand, and convection that transports the ions to the top of the porous medium, on the other hand, causing salt accumulation. The competition is characterized by the Péclet number Pe, with Pe $\gg$1 indicating strong convection. The ion distribution, generated by convection, is characterized by a narrow region of high salt concentration adjacent to the porous medium surface, with a size that increases with time but remains narrow, which explains why crystallization was observed at the surface and not inside the porous medium since it occurs when the saturation concentration is first reached at the sample surface. In addition, efflorescence appears preferentially in regions where evaporation is the greatest—hence, in the surface periphery—because greater evaporation flux implies greater flow velocities in that region. This, together with the fact that the heterogeneity of the random packing induces spatial fluctuations in the velocity field within the pore space, explains why efflorescence is discrete.

In another set of experiments that studied the discrete nature of efflorescence, Eloukabi et al. (2013) reported that, by varying the average size of the beads in the packings that were utilized by Veran-Tissoires et al. (2012), formation of the crystal layer does not significantly affect the drying process, and can even enhance the drying rate when the beads are sufficiently large, since larger beads give rise to larger pores in the packing that increase the rate of flow and transport, whereas if the beads are sufficiently small, the crystal layer can greatly affect the drying process, leading even to blocking or severely limiting evaporation. Thus, there exist two regimes, namely, the blocking and the enhanced drying rate regimes, with each corresponding to a different type of efflorescence, which were dubbed, respectively, crusty and patchy. Varying the initial salt concentration for a given bead-size indicated that the interplay between drying and the efflorescence formation causes *non-monotonous* variation of the drying rate with the initial salt concentration, if the efflorescence is patchy, but not when it is crusty.

To study the effect of soil heterogeneity on evaporation of saline water, Nachshon, Shahraeeni, et al. (2011) measured evaporation rates from transparent polyvinyl chloride sand columns, which were packed with three different morphologies. One was a homogeneous (same size) fine sand; the second system was homogeneous coarse sand, while the third column represented a heterogeneous porous medium, a mixture of sands with 50% each of fine and coarse sands with a sharp vertical interface between the two textures. The sands were poured into the columns from the top. In the case of the heterogeneous columns, thin cardboard spacers were used to separate fine and coarse sands segments during packing, after which, the cardboards were removed and the columns were gently shaken to create a tight packing. Nachshon, Shahraeeni, et al. (2011) utilized infrared thermography (IRT) to quantify partitioning of the evaporation rate from various parts of the sand columns. The technique is based on thermal signature arising from the phase change in order to estimate mass flux during evaporation (Shahraeeni & Or, 2010).

Experiments by Nachshon, Shahraeeni, et al. (2011) demonstrated that most of the evaporation occurs in the fine sand sections, with more than 90% of salt accumulating in or above the sections with small pores, which reduced the evaporation rate in the fine texture by almost an order of magnitude, whereas the rate in the coarser texture that was relatively free of salt was reduced by at most 50%. The diffusion coefficient of vapor through the salt crust depends on salt precipitation pattern, that is, its morphology, which is strongly affected by environmental conditions, and more specifically the potential evaporation rate (Sahimi, 2011). Conditions that create high evaporation rates produce denser efflorescent crusts, which offer higher resistance to vapor transport. Such evaporation

conditions also result in precipitation of amorphous and homogeneously distributed salt crystals in the evaporating media.

Using the same sand columns, together with X-ray computed tomography, Nachshon, Weisbrod, et al. (2011) studied evaporation of saline water when salinity was high. They identified three new stages of evaporation for saline water. One exhibited a low and gradual decrease in evaporation rate, which was caused by increasing osmotic potential. In the second stage, formation of salt crust caused progressive decrease in the evaporation rate. The third stage represented a constant low evaporation rate. Despite their apparent similarities to the classical evaporation stages for pure water that were described above, the saline stages represent different mechanisms of evaporation. The experiments by Nachshon, Weisbrod, et al. (2011) indicated that the second and third stages occur as long as water in the matrix can support first-stage evaporation. In addition, their experiments indicated that, when the porous medium is more homogeneous, salinity suppresses evaporation more strongly than in a heterogeneous medium. Salt precipitation occurred preferentially in the fine-textured regions of the heterogeneous sand columns; the fluctuations in spatial distribution of salt precipitated in the pore space enabled vapor transport through large pores, whereas small pores were clogged with precipitated salts.

Experimental studies of Roels et al. (2014) with core samples indicated that capillary-driven flow does not have substantial effect on salt precipitation, because of which accumulation of salt near the core surface was small. Their computed-tomography images after drying indicated uniform salt distribution inside the core. Börnhorst et al. (2016) reported that high evaporation rates limit transport of solutes to the external surface, leading to a more uniform precipitation distribution, whereas low drying rates result in strong solid accumulation on the porous medium's external surface, but that small pore throats reduce the solute transport and restrict solid accumulation on the surface. One must also recognize the self-enhancing of salt growth and salt transport in water films (Miri et al., 2015). Aggregated salt crystals form a microporous medium (Malmir et al., 2016a, 2016b, 2017) with a high degree of capillarity in each pore throat that enhances solute transport through imbibing brine over long distances. Such phenomena as the growth of salt crystals at the drying interface occur at the molecular scale (Dashtian et al., 2017).

Another set of experiments was carried out by Norouzi Rad et al. (2013), which demonstrated the essence and some features of soil salinization. They carried out a series of experiments in cylindrical plastic columns, packed with sand grains with various sizes and saturated with NaCl of various molar concentration, ranging from 3.5 M (moles of NaCl/kg of water) to 6 M. The drying of the porous medium was visualized by means of a HMXST X-ray microtomography system with spatial and temporal resolutions of 0.021 mm and 30 min, respectively. The duration of each round of the experiments was nearly 24 hr. Each three-dimensional scan included 1,500 horizontal cross sections. The ML technique of support vector machine (Cortes & Vapnik, 1995) was used with a quadratic kernel in order to segment each cross section into solid, liquid, and air phases. The SVMs were trained using sequential minimal optimization. To distinguish the precipitated salt from the sand grains, each two-dimensional cross section was compared to its corresponding image obtained at the beginning of the experiment, when there was no precipitated salt in the sample.

Figure 11 shows the patterns and distribution of precipitated salt on the surface of the sand column at various times, saturated with the 4 M NaCl solution. The most striking feature of these images is the nonuniform distribution of the precipitated salt on the surface of the grains, which is due to the distribution of the pore sizes. As Figure 11 indicates, over time, each evaporating spot is turned into a precipitation spot, when the salt concentration exceeds its solubility limit in water. Therefore, the number of precipitation spots increases with time, as indicated by Figure 11a–11c. After the NaCl concentration exceeds the solubility limit at all the evaporation spots, the number of active pores that contributed to salt precipitation remains constant. It should be emphasized that the patterns of precipitated salt shown in Figure 11 is solely related to the flow of the liquid toward the evaporating surface, either in the bulk or by film flow, and driven by capillary.

An analysis by Norouzi Rad et al. (2013) demonstrated the feasibility of the hydraulic connection between the wet zone and evaporation surface even after salt crystallization. They considered a fully-saturated cylindrical pore of radius r with complete evaporation within it. In the absence of convective transport to replenish the evaporating liquid, the volume per unit length occupied by the precipitated salt is $\pi r^2\gamma/\rho_s$, with γ being the solubility and ρ_s the salt density. Thus, assuming that salt precipitates uniformly on the pore's surface, the available pore volume is $\pi r^2\left(1-\gamma/\rho_s\right)$, implying a relative reduction $-\gamma/\rho_s$ of the pore volume. Given that $\gamma \approx 0.36$ g cm^{-3} and

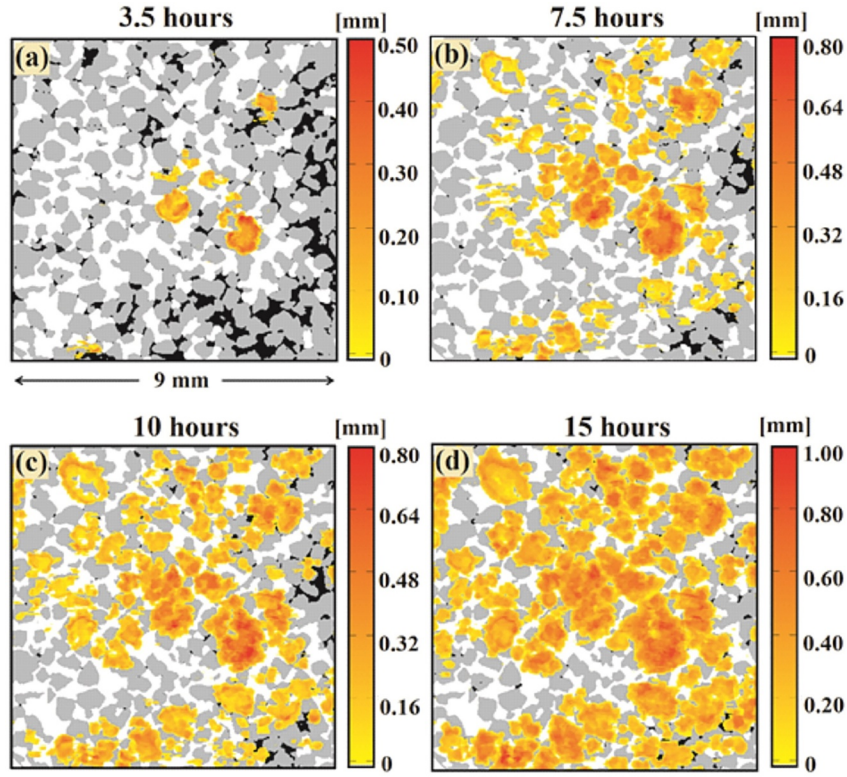

Figure 11. Patterns and distribution of precipitated salt on the surface of the sand column saturated with a 4 M NaCl solution at various times from the onset of the experiment including (a) 3.5, (b) 7.5, (c) 10, and (d) 15 hours. The color scale indicates the height of the precipitated salt. Black, gray, and white indicate, respectively, the regions filled with the liquid, sand grains, and the air phase. All other colors correspond to the precipitated salt and the color spectrum indicates the thickness of the precipitated salt such that the closer the color is to orange (darker color), the thicker is the salt crust (after Norouzi Rad et al., (2013) with the license agreement and permission to use granted by American Physical Society, https://doi.org/10.1103/PhysRevE.88.032404).

$\rho_s \approx 2.165$ g cm^{-3}, the fraction is about 0.17, indicating that even after salt precipitation, a part of the pore volume at the surface is still open, which is through the pores in the packing of the salt crystals accumulated in the pore, that is, the evaporating pore is still hydraulically connected to the wet zone at the bottom via the capillary-induced liquid flow supplying the evaporative demand.

Using their data, Norouzi Rad et al. (2013) also estimated the salt growth rate at the evaporating surface in each three-dimensional sand column. Figure 12a presents the cumulative precipitated salt as a function of the cumulative mass of liquid water, lost due to drying. When the sand column was initially saturated with a high salt concentration, more salt precipitated on the surface for the same mass loss. Figure 12b presents the dynamic evolution of the precipitated salt in each sand column, which indicates that, in the cases of sand columns saturated with 3.5 and 4 M NaCl solutions, the precipitation rate (the slope of the line in the figures) initially changes with time, followed by a nearly constant value. The transition point corresponds to the time at which all evaporation spots served as the precipitation spots, hence giving rise to a relatively constant precipitation rate. In other words, prior to the transition time, as water evaporates, salt concentration continuously increases at the surface until it reaches the solubility limit, implying that evaporation spots continually turn into precipitation spots at the early stages, producing higher precipitation rates, even though the evaporative flux remains nearly constant. After the transition, however, the number of the precipitation spots is constant, and salt continues to deposit on the already existing spots and, hence, its precipitation rate remains relatively constant.

Norouzi Rad and Shokri (2014) used X-ray microtomography to study the effect of grain angularity on salt precipitation dynamics and patterns during evaporation from saline porous media. They used packings of quartz sand and glass beads with nearly similar average particle sizes and porosities, which enabled them to constrain the

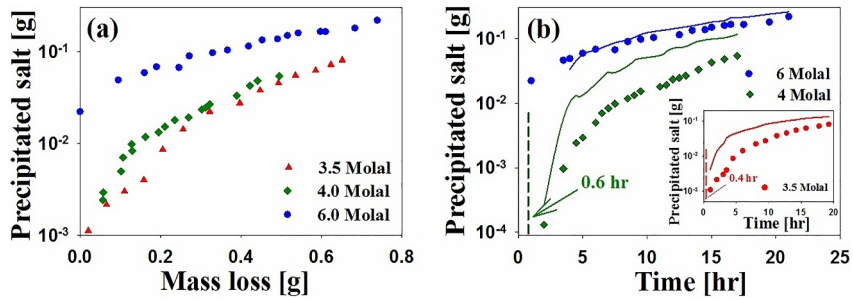

Figure 12. (a) Cumulative precipitated salt as a function of the cumulative mass of liquid water lost by evaporation. The legend indicates the initial salt concentration in each evaporating sand column. (b) Dynamic evolution of the cumulative precipitated salt in each sand column. The precipitation rate (the slope of the curves) changes with time until it becomes nearly constant in the cases of the columns saturated with 3.5 and 4 M solutions. The transition time to a constant precipitation rate is the time at which all the evaporation spots at the surface turn into precipitation spots. Solid lines correspond to the precipitated salt at the surface over time, as predicted by convection (see below). The vertical dash lines indicate the onset of NaCl precipitation on the surface predicted by the numerical solution of the convective-diffusion equation described in below, which is in qualitative agreement with the experimental data (after Norouzi Rad et al., (2013), with the license agreement and permission to use granted by American Physical Society, https://doi.org/10.1103/PhysRevE.88.032404).

effects of grain angularity on salt precipitation, as the glass beads were spherical and smooth, whereas the sand consisted of irregularly shaped grains. Their experiments indicated that the presence of angularity leads to a wider pore-size distribution, as well as range of pore shapes, which influences the dynamics of evaporation and salt precipitation. In particular, the experiments demonstrated that the existence of preferential evaporation exclusively in fine pores at the surface of the porous media produces discrete efflorescence. Cumulative salt precipitation, when the porous medium was made of glass beads, was higher at the early stages of precipitation, presumably due to the presence of a fewer number of evaporation spots at the surface, resulting in formation of a salt crust that, compared with that in sand grains, was thicker and more discrete at the surface of the glass beads. Moreover, the water saturation profiles indicated formation of a wider unsaturated zone above the receding drying front in the sand compared to glass beads, because of the presence of finer pores that affect capillary flow through the partially wet zone. See also a third paper from the same group (Rad et al., 2015) in which salt precipitation in packings of quartz particles was investigated in order to study the effect of particle-and pore-size distributions on salt patterns, and reached the same conclusions as those reported by Norouzi Rad and Shokri (2014).

Solute (salt ions) transport through a pore space is also sensitive to the morphology of the pore space. To study the effect of the morphology, Shokri-Kuehni et al. (2018) utilized four-dimensional (space plus time) synchrotron X-ray tomography for iodine *k*-edge dual energy imaging, and measured solute concentration profiles in every single pore during saline water evaporation from coarse- and fine-grained sands, which were fully saturated with a salt solution containing 5% calcium iodide (by weight) and packed in cylindrical plastic columns. The columns were closed at all boundaries, except at the top that was open to air for water evaporation. The external conditions—ambient temperature and relative humidity—were similar and constant in both experiments. Image reconstruction was carried out using programs that convert X-ray attenuation to three-dimensional volumetric data. The top part of the sand column that included 1,103 reconstructed images of the two-dimensional horizontal cross sections was used, with gray-scale values representing density distribution within the pore space. The sand packs were visualized twice, once with X-rays with energies immediately above the *k*-edge (33.1694 keV) value of Iodide, and a second time with X-rays with energies immediately below the *k*-edge value at 33.069 keV. The difference in the gray value of the two scans yielded the salt concentration at the pore scale.

Figure 13 presents the solute concentration along the sand profiles over time. They illustrate a sharper gradient of solute concentration closer to the surface of the coarse sands when compared with the fine one. Although both porous media had similar porosity and initial salt concentration, and were placed under similar evaporative conditions, the pore-scale solute distributions through the two sand columns were remarkably different, which in turn affect the macroscopic response. The results indicated that, relative to the coarse sand, the solute is distributed more uniformly through the fine sand packing, suggesting that the effective dispersion coefficient is higher in the fine sand. As illustrated in Figures 13a and 13b, there are more tortuous capillary pathways in the

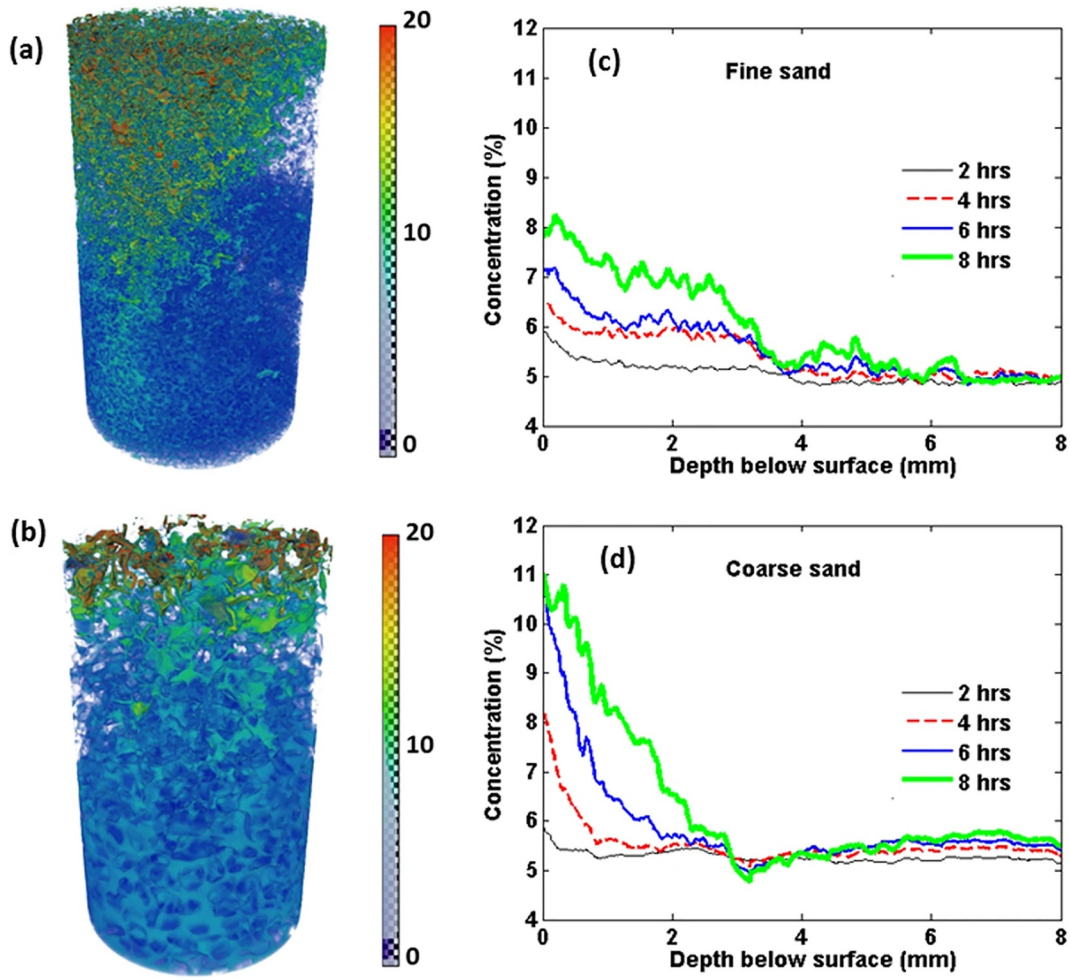

Figure 13. Reconstruction of the liquid phase in the top 5 mm of the (a) fine and (b) coarse sand, 8 hr after the onset of evaporation, with the color map representing the solute concentration percentages. Colors closer to red indicate higher concentrations. Dynamics of solute distribution in (c) fine and (d) coarse sand at various times from the onset of the experiments (after Shokri-Kuehni et al., 2018).

fine sand, leading to more mixing, as a result of the existence of higher connectivity in the complex liquid network and the longer lengths of the flow paths. This implies higher effective dispersion coefficients that influence solute transport during evaporation. When the concentration profiles were fitted to a one-dimensional convective-diffusion equation,

$$\frac{\partial(\phi\rho_\ell SC)}{\partial t} = \frac{\partial}{\partial z}\left(\rho_\ell \phi S D_L \frac{\partial C}{\partial z} - \rho_\ell \phi S C V\right), \tag{22}$$

where C is the solute mass fraction, ϕ is the porosity, D_L is the effective dispersion coefficient, and V is the average flow velocity (with the rest of the notation being as before), it was found that D_L is a strong function of the saturation of the liquid. Although saturation-dependence of the effective dispersion coefficient has been known for a long time in the oil reservoirs literature (Sahimi et al., 1986a; Salter & Mohanty, 1982), in the literature on salt transport, D_L had been mostly assumed to be constant (see, for example, Eloukabi et al., 2013; Sghaier et al., 2007). More interestingly and importantly, when D_L was plotted as a function of S/L, where L is the length of the unsaturated zone, the data for both types of porous media converged onto a single universal curve.

Fujimaki et al. (2006) proposed that precipitation of NaCl and KCl crusts above the matrix—efflorescence salt crust (ESC)—leads to reduced evaporation, because the precipitated ESC acts as a barrier with a small vapor

diffusion coefficient, reducing vapor diffusion toward the atmosphere. These studies assumed, and then concluded by measurements, that a phase transition, that is, transition of water from liquid to vapor, occurs at the matrix upper surface, below the ESC, and that evaporation is reduced because of reduction by the ESC of vapor diffusion from the soil surface to the atmosphere. Nachshon et al. (2018) studied this issue by measuring evaporation rates from saturated porous media covered by the ESC and comparing the data to theoretical calculations by Nachshon and Weisbrod (2015). They showed, in agreement with the aforementioned previous studies (Fujimaki et al., 2006; Gran et al., 2011; Nachshon, Weisbrod, et al., 2011) that, for NaCl under the conditions in which they carried out their experiments, most of the water evaporates below the ESC. Using various imaging methods, Nachshon et al. (2018) demonstrated that the salt crust grows out of specific nucleation centers (see also Veran-Tissoires et al., 2012 discussed above) and creates an elevated crust approximately slightly above the matrix surface, with most of the crust being disconnected from the matrix, indicating that evaporation from a porous medium that is covered by NaCl ESC may occur below the crust at the soil surface.

On the other hand, Shokri-Kuehni, Vetter et al. (2017; see also Licsandru et al., 2022) showed through careful experiments that formation of salt crusts at the top of porous media not only does not stop or even slow down the evaporation, but in fact could increase the evaporation rate and the cumulative mass loss, hence exemplifying the complex interplay of various factors. In their experiments, cylindrical glass columns were packed with quartz sand grains, and were wetted with NaCl solutions of various concentrations. In addition, one column was packed with solid NaCl grains and wetted with saturated NaCl solution. The columns were mounted on high-resolution digital balances to record the mass loss due to evaporation over a period of time. For comparison, one column was filled with pure water to measure the potential evaporation rate in the absence of any salt in each round of experiments. Metal halide lamps were directed to the surface of the packed columns in order to boost the evaporation process. To record the temporal and spatial evolution of the surface temperature, a thermal camera was fixed above the sand columns to record images over a number of time steps, and visual snapshots of the surface of sand columns were also recorded.

The microscopic images, taken during the experiments by Shokri-Kuehni, Vetter, et al. (2017), revealed that the salt crust formed at the surface of the porous media is itself porous—as it is a packing of salt crystals—and evolves dynamically due to the complex interplay of crystallization and evaporation at the crystal-liquid, crystal-crystal, liquid-air, and the crystal-air interfaces, as was suggested by Shahidzadeh et al. (2015). S. Dai et al. (2016) had also suggested that NaCl "preferentially precipitates in cubic-shaped crystals, which are packed heterogeneously to form a highly porous structure," a morphology that was later studied by Malmir et al. (2016a, 2016b, 2017). Microscopic analysis of Shokri-Kuehni, Vetter, et al. (2017) also suggested that the salt at the surface causes top-supplied creeping of the solution, helping the growth of subsequent crystals.

As discussed by Shokri-Kuehni, Vetter, et al. (2017), the drying of porous media saturated with salt solutions is usually described in terms of three stages (Jambhekar et al., 2015), namely, the first stage that includes a decreasing drying period due to increasing salt concentration at the surface, when the drying rate is relatively high, followed by the second stage, the transition period, to a third stage in which the evaporation flux is much smaller than in the first stage, since it is limited by vapor diffusion through the salt crust. Experimental data of Shokri-Kuehni, Vetter, et al. (2017) suggested, however, one should perhaps add an additional stage, in which the evaporation rate is largely controlled by liquid transport and evaporation through the evolving porous salt layer at the surface.

The effects of external conditions and the salt type on the drying behavior of saline water in porous media, as well as on the dynamics of surface salt precipitation, were studied by Shokri-Kuehni, Rad, et al. (2017). Thirty three columns of sand (as well as Hele-Shaw cells), saturated with various salt solutions, were utilized; a digital camera was mounted at the surface of the sand packs to record the dynamics of salt precipitation at the surface, and the effect of relative humidity, ambient temperature, and type of salt on the evaporation process was studied. Three types of salts, namely, sodium chloride, calcium chloride, and potassium iodide with a wide range of concentration were used to saturate the sand columns and investigate the evaporation process. They found increasing salt concentration led to decreasing cumulative evaporative losses in three types of salt. To understand whether the presence of precipitated salt limits the evaporation process under the boundary conditions tested in their experiments, they scaled the time (t_s) according to

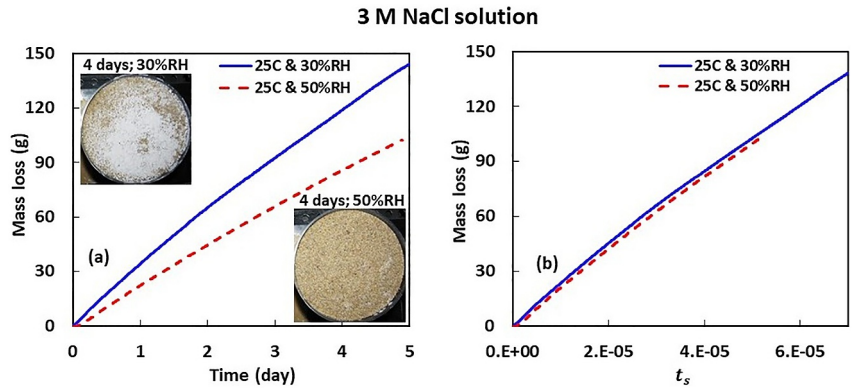

Figure 14. (a) The cumulative mass loss was measured during evaporation from cylindrical columns filled with sand saturated with 3 M NaCl solutions. These experiments were performed at a constant temperature of 25°C and relative humidity levels of 30% and 50%. (b) The cumulative mass losses presented in section (a) are plotted against the scaled time t_s (in days), as introduced in Equation 23. The insets show the precipitation patterns on the surface after 4 days from the start of the experiment, with white indicating precipitated salt (after Shokri-Kuehni, 2018).

$$t_s = \frac{M(1 - RH)P_s}{\rho RT} t, \tag{23}$$

where M is water molecular mass, P_s is water saturated vapor pressure, RH is the relative humidity, ρ is the density of liquid, R is the gas constant, T is the temperature and t is the time. Figure 14 shows a typical example of their results illustrating the measured cumulative mass losses from sand columns saturated with 3 M NaCL solution under two different evaporation conditions in terms of the ambient relative humidity. Lower relative humidity of 30% resulted in more evaporation compared to the case of 50% relative humidity, Figure 14a. This led to precipitation of more salt at the surface of the column placed under external conditions with lower relative humidity. However, when the evaporative mass losses were plotted against the scaled time, Equation 23, the two columns demonstrated very similar evaporation behavior. This confirms that the varying cumulative mass losses shown in Figure 14a are caused by differing external conditions, rather than the presence or absence of precipitated salt on the surface. Additionally, these findings suggest that the porous nature of the precipitated salt does not necessarily restrict liquid transfer to the surface.

In the case of $CaCl_2$, Shokri-Kuehni et al. (2018) observed a different evaporation behavior than those for NaCl and KI. Their results showed that, in the case of $CaCl_2$, the cumulative mass losses, when plotted in re-scaled form, do not converge, either in the early or later stages of the evaporation. Moreover, variation of the evaporative mass losses as a function of salt concentration were much more significant in the case of $CaCl_2$, when compared to the other two salts (NaCl and KI). One reason for such behavior may be the significant dependence of the saturated vapor pressure P_s on salt concentration in the case of $CaCl_2$, compared to NaCl and KI. As evaporation proceeds, the salt concentration increases close to the surface, hence the saturated vapor pressure decreases over time, which influences the driving force for evaporation, particularly in the early stages of the process when the process is still limited by the external conditions. If P_s changes significantly with the concentration, the driving force for liquid vapourization in the early stages of the process also changes notably, which continuously lowers the evaporation rates.

Another important issue is the relationship between saline water evaporation from soil surfaces and the depth of the water table. Several studies (Assouline et al., 2013; Kamai & Assouline, 2018; Sadeghi et al., 2012; Shokri-Kuehni et al., 2020) provided evidence for the influence of the depth of water tables on surface evaporative fluxes. As first pointed out by W. Gardner and Fireman (1958), shallow water tables, supply water to the surface through capillarity-induced flow pathways to meet the demand for evaporation. Shallow water tables also affect functioning of the ecosystem and evaporation of water from land surfaces (Muwamba et al., 2018; Shokri & Salvucci, 2011). If, however, the water tables are deeper than the maximum length of capillary liquid continuity in the soil above the table, capillary liquid pathways may not be connected all the way to the surface (Vogelbacher et al., 2024), and a vapourization plane forms below the surface. In which case the water table meets the

evaporative demand by the capillary liquid flow to the vapourization plane. Subsequently, water vapor diffuses through the overlying dry layer (Cahill & Parlange, 1998; Kamai & Assouline, 2018; Milly, 1986; Ross et al., 1991; Saravanapavan & Salvucci, 2000; Shokri & Or, 2011; Shokri & Salvucci, 2011; Smits et al., 2012).

Despite its significance, very few studies have been devoted to the relationship between the depth of water table and evaporation of saline water in soil (X. Chen, 1992; Hassan & Ghaibeh, 1977; Jalili et al., 2011; Nulsen, 1981; Rose et al., 2005; Shimojimaa et al., 1996). One recent comprehensive study was reported by Shokri-Kuehni et al. (2020). They carried out laboratory experiments, and linked their data to two global-scale databases for topsoil salinity, soil texture, and water table depths. They used cylindrical columns packed with sand with various particle-size distributions and saturated with NaCl solutions. Three samples of quartz sand particles, representing fine, medium, and coarse textures were employed, and the relationship between water content and capillary pressure was measured. Then, five series of evaporation experiments were carried out. Packed columns with medium-size sands were used in the first three series that were connected to steady-state water tables fixed at various distances below the surface. Pure water and NaCl solutions with two different salt concentrations were used in the three series of experiments, with two additional rounds of experiments conducted with fine and coarse sand particles in order to evaluate the effect of the texture of porous media and the depth of water table on solute precipitation patterns at the surface. To boost evaporation and enhance salt precipitation at the surface, metal halide lamps were directed onto the surface of the columns during the fourth and fifth series of measurements.

The experiments demonstrated that if the water table is shallow and hydraulically connected to the evaporating surface, capillary-induced liquid flow is the primary supplier of the evaporative flux and vaporization at the surface, whose rates are influenced by external conditions and properties of the evaporating fluid. As for salt precipitation on the surface, one expects intuitively more precipitation on the surface if water table depth is shallow, but Shokri-Kuehni et al. (2020) reported the opposite trends, namely, in both fine- and coarse-textured sand columns, deeper water tables produced more salt precipitation at the surface after the same elapsed time from the onset of the evaporation experiments. The reason is that when the surface is uniformly wet, a stratified vapor concentration field forms at the surface that drives the evaporative fluxes. But, if the surface is only partially saturated, formation of liquid patches causes the initially one-dimensional layered vapor concentration field above the surface to evolve into a collection of three-dimensional vapor density shells over the remaining wet patches at the evaporation surface. As the spacing between the liquid clusters on the surface decreases, the spherical vapor shells formed above the wet patches overlap with each other, reducing the lateral component of diffusive fluxes that eventually reduces the evaporation rate per cluster compared to the case in which the wet patches are separated on the surface (Assouline & Or, 2013; Shahraeeni et al., 2012). Since deeper water tables produce fewer liquid clusters at the surface, which increases the spacing between the evaporating clusters, there is more evaporation per liquid cluster at the surface. Numerical simulation of the process by Shokri-Kuehni et al. (2020) based on the convective-diffusion equation supported the assumptions made in order to interpret the experimental data.

Another important aspect of saline water evaporation from porous media is the dynamics of salt *re-crystallization* as a result of cycling, which, in general, is different from crystallization because in direct crystallization the process is rapid, and when the phase transition (from liquid to solid) occurs, the solid may contain trapped impurities, as demonstrated by Sunagawa (1999). Moreover, depending on whether the nucleation is primary, that is, one that occurs directly in the solution, or secondary—one that is the result of pre-existing crystallites present in the solution—one may have distinct growth rates and crystallization patterns (see, for example, Desarnaud et al., 2013, 2014; Shahidzadeh and Desarnaud, 2012). High supersaturation can be achieved in primary crystallization such as, for example, what happens during evaporation of homogeneous salt solutions in confined systems. This contrasts with secondary nucleation that typically happens around the saturation concentration. These aspects make it clear that the dynamics of salt crystallization in porous media depends not only on the thermodynamics of the system, but also on the morphology of the pore space that controls flow and transport processes therein.

Desarnaud et al. (2015) studied the behavior of sandstones (with porosity of 0.29 and pore diameter of about 30 μm) that had been contaminated with NaCl and exposed to various relative humidities. The main advantage of using NaCl salt is that its solubility depends weakly on temperature. Therefore, the main driving force for (re-) crystallization is the variations in the relative humidity. Their experiments studied the crystallization patterns and the drying kinetics of saturated sandstones, as well as the re-crystallization behavior and the drying of the salt-

contaminated sandstones, once they were rewetted with liquid water or brought in contact with water vapor (i.e., at 100% relative humidity). Their experiments demonstrated that the kinetics of crystal growth, and in particular whether the nucleation is primary or secondary, has a strong influence on the drying behavior. Desarnaud et al. (2015) identified three possible regimes, which may also depend on external factors, such as the relative humidity and the sample size. The three regimes were, (a) a capillary regime that is characterized by a constant evaporation rate, (b) a regime in which the evaporation rate decreases exponentially fast due to the crystal growth that reduces the surface area for evaporation, and (c) a diffusive regime in which the evaporative flux scales as $\sqrt{t}$ (typical of diffusive processes). In the last regime, the porous medium is almost completely covered with salt while, at the same time, the speed of the capillary flow through the small pores of the crust (packing of salt crystals) is not high enough to meet evaporative demand. Moreover, it was shown that re-crystallization caused by subsequent cycling decreases progressively the surface coverage by the salt crust and, hence, the evaporation rate increases. After several cycles, the intermediate regime associated with the formation of the salt crust disappears completely. The experiments also clarified the difference between dissolution by adding liquid water or deliquescence (by water vapor): liquid water progressively extracts the salt from the porous medium and forms a few large microcrystallite assemblies on its surface, due to the secondary nucleation of crystals on incompletely dissolved crystals on the stone surface.

R. Wu and Chen (2023) carried out visualization experiments with microfluidic pore networks in order to study the interplay between salt precipitation, the corner liquid film flow, and gas-liquid displacement during evaporation. They reported observation of two types of salt precipitation. One was aggregated polycrystalline structures, while the second type was large bulk crystals. Moreover, their experiments indicated that, due to imbibition of liquid into aggregated polycrystalline structures, gas bubble can form. Thin liquid films formed in the corner of pores and their length can affect the direction of growth of the aggregated polycrystallines that are connected to the film. If discontinuous corner liquid films are touched by growing aggregated polycrystalline, they can form long and continuous films. The polycrystalline structures that aggregate at the open surface of the pore network, that is, efflorescence, can continue to grow if they come into contact with the growing aggregated polycrystalline structures within the pore network, referred to as subflorescence. Due to efflorescence, the evaporation rate from the pore network first increases and then decreases.

An important issue that has not been studied as much as other salinization-related problems is *salt creeping*. In this phenomenon, salt crystals precipitate from evaporating salt solutions, climb onto solid surfaces, and spread far away from the solution. The spreading is very rapid and has been likened to superfluid flow of helium films. A material in a superfluid state, such as Helium-4, behaves like a zero-viscosity fluid and flows without friction past any surface, circulates over obstructions, and flows through pores in containers that hold it. It stops only if it loses its own inertia. Transport of saline solution in a porous medium by creeping can lead to the physiological aridness of the soil above ground water level (see, for example, Green et al., 2008; Hird & Bolton, 2016). Salt creeping can also damage materials severely by creating cracks and causing delamination. Despite its significance, not much attention has been paid to salt creeping, ever since it was first discussed by Washburn (1926) almost a century ago, followed by Hazlehurst et al. (1936).

Qazi et al. (2019) studied salt creeping experimentally. They used a vertical smooth glass substrate, either as a cylinder or a flat surface, which was in contact with a reservoir of an evaporating and initially undersaturated salt solution (with supersaturation $S_s = 0.9$). The setup provided a continuous supply of the salt solution. The glass substrates were cleaned with ultra-pure water and ethanol to avoid problems associated with surface chemistry and wettability, with aging of the treatments, such as Piranha cleaning or plasma treatment. Qazi et al. (2019) then followed the evolution of the contact line of the evaporating salt solution on the substrate, as well as its contact angle with the glass surface. Time-dependence of the mass of the suspended vertical cylinder was also recorded, if creeping initiated, and the rate of growth and precipitation on the substrate) could be determined. Three types of salts, NaCl, KCl, and Na_2SO_4, were also used, as not only are they important to various natural and industrial processes, but they also possess distinct crystalline structures and interfacial properties. While NaCl and KCl form cubic anhydrous crystals, Na_2SO_4 has anhydrous, usually referred to as thenarditem, and hydrated crystalline polymorphs. Thus, their effect on salt creeping could be studied. NaCl, KCl, and hydrated crystals of Na_2SO_4 precipitated at the liquid/air interface.

Qazi et al.'s (2019) experiments indicated that at a relative humidity φ of 40% at 21°C, no salt creeping on the cylindrical substrate occurred with any of the solutions. When the relative humidity was lowered to 6% at the

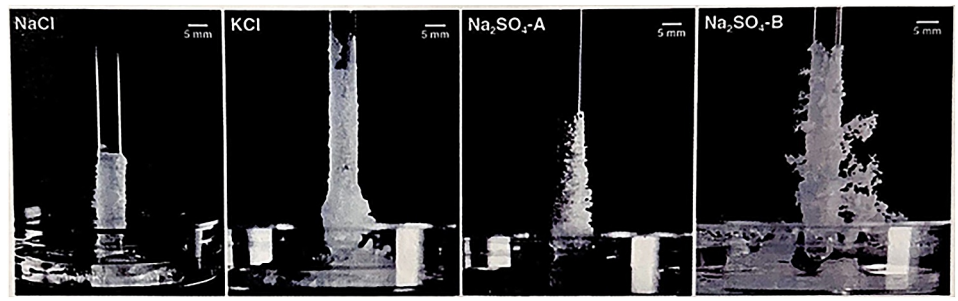

Figure 15. Salt creep at the end of the creeping process, when all the solution has evaporated. Solutions (from left to right) are NaCl, KCl, Na_2SO_4-A, and Na_2SO_4-B. In all experiments the relative humidity was 6% and $T = 21°C$ (after Qazi et al., 2019).

same temperature, however, which allowed high evaporation rates and multiple nucleation at the contact line, salt creeping emerged for all salt solutions. Figure 15 presents the patterns of salt creeping. Before creeping, the solution reached saturation, triggering crystal precipitation and growth in the reservoir. As evaporation continued, however, creeping on the vertical glass substrate began with the precipitation of new crystals at the liquid/air interface close to the contact line, with a chain of crystals growing outside of the contact line and moving upward onto the glass substrate. It is due to the existence of multiple nucleation sites that salt crystals could grow beyond the evaporation front, where they provided a platform for a film of solution to extend well beyond the creeping front. In turn, evaporation from the film induces the precipitation of nanocrystals far away from the creeping front. Therefore, salt crystallization can act as a probe for revealing the extent of precursor nanofilms ahead of a macroscopic front, although as Qazi et al. (2019) pointed out, this possibility is rather unexpected, because one expects the high evaporation rates to disrupt any thin films of solution. This implies that after salt creeping is initiated, it becomes a self-amplifying process with an exponential growth rate for all salts used in the study, indicating the universality of the process. Qazi et al. (2019) also provided theoretical justification for their observation and data.

8.2.2. Continuum Models of Salt Transport

Models of brine evaporation and salt transport and precipitation in porous formations can be divided into two groups. In one group are thermodynamic models of salt deposition in Earth's crust; see, for example, Toner et al. (2015). We do not review the thermodynamic models, as they cannot take into account the effect of a variety of important factors, in particular the morphology of soil, as well as the competition between convection and diffusion. The second group of models consists of two subgroups: pore network models and continuum models. In this section, we describe the continuum models. Continuum models of fluid flow and transport (Guglielmini et al., 2008; Huinink et al., 2002)—those that are based on the classical averaged equations of hydrodynamics and transport—are capable of modeling evaporation and salt precipitation at the field scale, assuming that the dependence on the pore space morphology of the flow, transport, and other coefficients that appear in the governing equations can be adequately accounted for. They include models for the evolution of salt crystals (D. Le et al., 2009) and salt concentration in liquids (Mahadevan et al., 2006) in porous media, which, however, predict mostly the location of the maximum salt concentration inside the porous medium. Salt precipitation and invasion of the pore space by a gas (e.g., air) are not included in such models. The second subgroup consists of pore-network models.

Continuum models of salt transport in fluid flow through porous media are based on the convective-diffusion equation, which for a three-dimensional pore space, takes on the following form:

$$\phi \frac{\partial C}{\partial t} + \mathbf{V} \cdot \nabla C = \frac{\partial}{\partial x}\left(D_L \frac{\partial C}{\partial x}\right) + \nabla_2 \cdot (D_T \nabla_2 C). \tag{24}$$

Here, C is the salt molar concentration, $\mathbf{V}$ is the mean fluid velocity vector, and ∇_2 represents the gradient in the transverse direction (perpendicular to the direction x of the mean flow). D_L and D_T are, respectively the longitudinal (parallel to the direction of mean flow) and transverse dispersion coefficients with $D_L \gg D_T$. Both D_L and

D_T depend not only on the saturation state of the systems, but also on the mean flow velocity, although many researchers have taken them to be constant, which might be incorrect and gives rise to spurious predictions. Often, one writes, $C = \rho_\ell yS$, with y being the mass fraction, ρ_ℓ the density of the liquid, and S its saturation, in which case the one-dimensional version of the convective-diffusion equation becomes identical to Equation 22.

Using synchrotron X-ray microtomography, Shokri (2014) investigated the pore-scale dynamics of dissolved salt distribution in drying saline porous media. In his experiments, a cylindrical column packed with sand particles and saturated with CaI_2 solution was employed. The drying sand column was imaged during the entire process, using synchrotron X-rays energies immediately above and below the k-edge value of Iodine. In agreement with many of the experiments described above, Shokri's (2014) data indicated that during early stages of evaporation, air preferentially invades large pores at the surface, since it is a non-wetting fluid, while smaller pores remain saturated and connected to the wet zone at bottom via capillary-induced liquid flow acting as evaporating spots. As a result, the salt concentration increases preferentially in smaller pores. Shokri (2014) then solved numerically a one-dimensional convective-diffusion equation, Equation 22, and compared the solution with his data. The comparison indicated that the convective-diffusion equation does capture the overall trend of the measured salt profiles, but the agreement between the data and the solution of the convective-diffusion equation was only qualitative. One possible reason for the quantitative disagreement was that the dependence of the dispersion coefficient on the flow velocity was not considered.

Evaporative soil salinization is, in general, a non-isothermal process. There is also interaction between flow in the porous medium and free flow above the vaporization plane, therefore, fluid flow in the porous medium must be coupled to the free flow for accurate description of the process. Most of the past continuum modeling of evaporative salt transport and precipitation only focused on the porous media aspect of the problem (see, for example, Bechtold et al., 2011; Derluyn et al., 2014; R. M. Espinosa et al., 2007; Gamazo et al., 2012; Koniorczyk, 2012; Mosthaf et al., 2011; Nicolai et al., 2007). The continuum model represents the averaged equations of mass, momentum, and energy equations, with the averaging taken over a REV, that is, a portion of the pore space over which the averaged continuum equations are representative of what happens in the pore space and, more importantly, if the equations are solved in domains larger than an REV, the results will not change and will be independent of the size of the domain. Implicit in the assumption of the existence of a REV is that the porous medium over the scales comparable with the REV is stationary.

In general, evaporative salt transport and precipitation in a porous medium represents a multiphase fluid flow problem, due to the presence of water, its vapor, and air. Jambhekar et al. (2015) developed a full numerical model, based on the continuum equation of mass, momentum, and energy conservation, as well as the coupling between the porous media and free flow outside the media. They assumed a non-isothermal condition, and considered the solid matrix as rigid. Thus, any deformation related to salt precipitation, was neglected. Jambhekar et al. (2015) assumed single-phase gas flow in the free-flow domain outside the porous medium, and solved the convective-diffusion equation along with Stokes' equation to determine the state of the system outside the pore space. The two domains—the pore space and the free-flow domain—were then coupled based on the continuity of fluxes across the interface between the two, as well as the assumption of thermodynamic equilibrium.

Figure 16 compares the computed cumulative mass loss of water and dissolved NaCl obtained using the model developed in Jambhekar et al. (2015) with the experimental data (Norouzi Rad et al., 2013) for initial NaCl concentrations of 3.0, 4.0, and 6.0 M. The numerical model could not reproduce fluctuations in the experimental data. The reason may be twofold: (a) formation of primary evaporation spots at the sand surface due to heterogeneity in the pore space, and (b) fluctuations in the free-flow humidity and temperature during evaporation experiments (Norouzi Rad et al., 2013). The slopes of the cumulative mass loss curves were, however, in agreement with the experimental data. The cumulative salt precipitation was marginally overestimated, which might be due to the preferential salt precipitation in the fine pores at the surface of the porous medium, as illustrated experimentally by Shokri (2014). Recall that during the initial stage of drying, larger pores at the surface of the porous medium are invaded by air rather quickly, but the model was unable to capture the preferential salt deposition, which may have resulted in the overestimation of the precipitated salt.

In another paper, Jambhekar et al. (2016) extended their model in order to study reactive fluid flow and transport during soil salinization. Salt ions in solutions react and interact with each other strongly, which affect its precipitation in the pore space. Jambhekar et al. (2016) defined the ionic activity $[i]$, also called thermodynamically effective concentration (Domenico & Schwartz, 1997) by $[i] = \gamma_i(m_i/m_0)$, where γ_i is the ionic activity

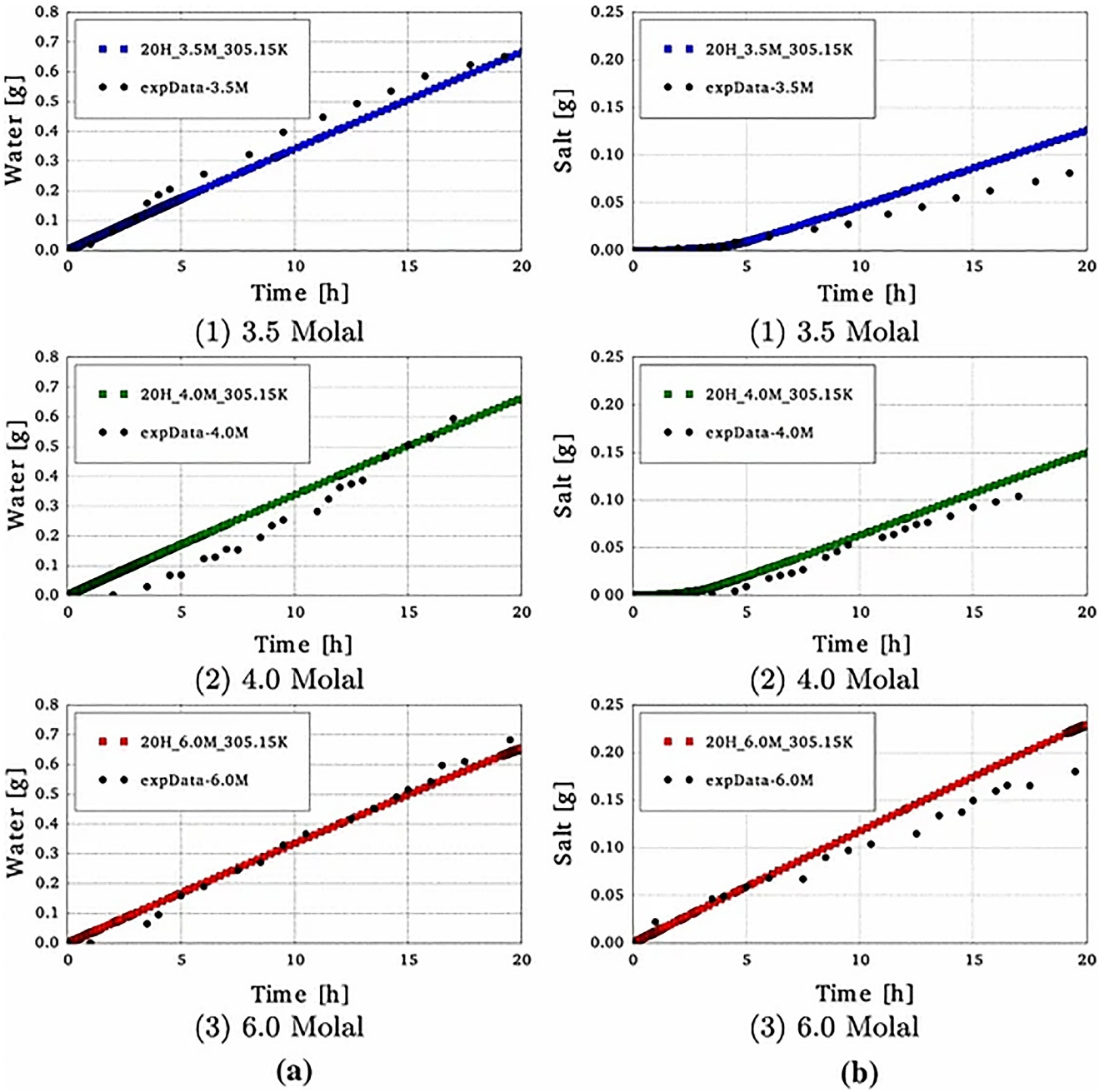

Figure 16. (a) Cumulative mass of liquid water reduced by evaporation from the saline sand columns initially saturated with various concentrations of NaCl solution. The sand columns were subjected to identical free flow and porous media conditions. (b) The corresponding cumulative NaCl precipitation during evaporation from saline sand columns. Black dotted lines represent the experimental data, while the color plots are the numerical results (after Jambhekar et al. (2015), with the license agreement and permission to use granted by Springer Nature).

coefficient, m_i (in mol kg^{-1}) is the molality, and m_0 is the standard state molality of 1 mmol kg^{-1}, with the purpose of making the equation dimensionless. As is well-known, γ_i for dilute solutions is close to unity and decreases with salinity, but at higher salinities, γ_i increases in many cases and may even exceed unity. An accurate equation for γ_i is the Debye-Hückle model, according to which, $\ln(\gamma_i) = -az_i^2 I^{1/2}$, with z_i being the electrical charge of the ion, and I the ionic strength, $I = \frac{1}{2}\sum_i (m_i/m_0)\, z_i^2$. If we consider the chemical reaction (ionic dissociation), $\mathrm{Na} \rightarrow \mathrm{Na}^+ + \mathrm{Cl}^-$, then, one defines an equilibrium constant, $K_{\mathrm{eq}} = [\mathrm{Na}^+]\,[\mathrm{Cl}^-]/[\mathrm{NaCl}]$, which usually depends

on temperature. Since both reaction and transport occur in the system, the Damkühler number, $\mathrm{Da} = \mathcal{R}_R/\mathcal{R}_T$ plays a key role, where $\mathcal{R}_R$ and $\mathcal{R}_T$ are the rates of reaction and transport.

In practice, the precipitation-dissolution reactions in geochemical systems are usually kinetically controlled; the equilibrium concept is applicable only if the reaction processes are significantly more rapid than transport (i.e., large Damkühler number Da), and the reactive surface area between the solid and the liquid phase is a critical parameter that controls the overall rate of reaction. Thus, A_n, the solid-liquid interfacial area, is correlated with the porosity of the system, which evolves dynamically. One such correlation due to Clement et al. (1996) is given by, $A_n = 500\left(1 - \phi_s/\phi_0\right)^{2/3} S_w$, in which ϕ_s and ϕ_0 are, respectively, the volume fraction of the pore space occupied by salt, and the initial porosity of the porous medium, and S_w is the liquid saturation.

Given these preliminaries, Jambhekar et al. (2016) simulated reaction and transport during salt precipitation by extending the model developed by Jambhekar et al. (2015) described above. They first applied the equilibrium approach to the numerical simulation and analysis of precipitation dynamics. The equilibrium condition implies immediate precipitation since the dissolved salt concentration exceeds its solubility limit. Aside from some minor deviations, the simulation results were in agreement with experimental data of Norouzi Rad et al. (2013).

Jambhekar et al. (2016) then simulated the kinetic case for the mixture of NaCl and NaI, for which, in the simulations within the pore space, in addition to Na^+ and Cl^-,I^- was also considered. The simulation results for the saline water saturation distribution and the pore space occupied by precipitated NaCl and NaI indicated that most of the salt precipitates near the interface between the two domains, and that the initiation of NaI precipitation is delayed. Moreover, because NaCl and NaI precipitate, the concentrations of Na^+ and Cl^- decrease significantly at the interface, but even though NaI also precipitates, the concentration of I^- continued to increase at the evaporation front, hence indicating the potential of NaI precipitation for longer drying periods.

It has been known since 1850s (Lavalle, 1853) that the growth of salt crystals in pores generates stress on the pores' walls, implying that it can deform the porous medium, in addition to changing its morphology by salt precipitation (Becker & Day, 1905). Thus, the concept of crystallization pressure P_{cryst} was introduced (Taber, 1916; see also Rijniers et al., 2005). The following expression for P_{cryst} was proposed (Scherer, 1990; Steiger, 2005):

$$P_{\mathrm{cryst}} = \left(\frac{2RT}{V_m}\right)\left(\ln S_s + \ln \frac{\gamma_{\pm}}{\gamma_{\pm,0}}\right), \tag{25}$$

where V_m is the molar volume of the solid phase forming the crystal (e.g., $V_m = 27.02\ \mathrm{cm}^3/\mathrm{mol}$ for NaCl), $\gamma_{\pm}$ is the ion mean activity coefficient, with subscript 0 representing the reference state where the salt crystal is in equilibrium with the solution. As Naillon et al. (2018) discussed, the precise mechanism by which salt crystals generate stress on the walls is not completely clear. For example, Equation 25 predicts that, $P_{\mathrm{cryst}} = 160$ MPa, whereas the tensile strength of glass is about 40 MPa, yet no damage was observed in the experiments with glass capillary tubes (Desarnaud et al., 2014; Naillon et al., 2015). Naillon et al. (2018) carried out experimental studies of the problem, as well as continuum modeling of the same, in order to shed light on the mechanism of stress generation by salt crystals precipitated on a surface.

In their experiments, Naillon et al. (2018) used a large channel that supplied the fluids, either a salt solution or nitrogen. Smaller pore channels were positioned perpendicular to the supply channel. The experiments were carried out by a NaCl solution with two different initial sodium chloride molalities. The experiments indicated significant channel deformation and rapid growth, which was dependent upon the initial dissolved salt mass. The higher the initial salt mass, the higher was the deformation. Naillon et al. (2018) developed a continuum model of the same phenomenon, based on solving the mass and momentum conservation equations, coupled to the convective-diffusion equation for solute (salt) transport, assuming purely elastic materials for the walls of the pores. The numerical results indicated that a pressure of about $P_{\mathrm{cryst}} = 0.5$ MPa was sufficient to induce the maximum deformation observed in the experiment. Using this value in Equation 25, P_{cryst} corresponds to a supersaturation of only $S_s = 1.005$, much lower than the supersaturation at the crystallization onset, which was about 1.7. To explain the discrepancy, Naillon et al. (2018) argued that one must use the supersaturation at the interface between the crystal and the solution, not the average supersaturation. Numerical simulations also indicated that the supersaturation is in fact quite weak (slightly larger than 1) in the vicinity of the crystal, when it

is about to touch the walls on opposite sides of the channel. Moreover, the numerical simulations indicated that the generation of stresses on the pore walls due the growth of a single crystal of NaCl is a highly transient non-equilibrium process that occurs over a very short period, since the precipitation reaction is fast. Consequently, the supersaturation at the crystal interface rapidly decreases during its growth. Naillon et al. (2018) also pointed out that the process eventually leads to *permanent* deformation, and is not reversible.

8.2.3. Pore-Network Models of Salt Precipitation

Similar to drying, to develop a physically-based pore-network model, one must take into account the mechanism by which the precipitated salt accumulates. Moreover, the type of salt also plays a role in its precipitation and the location where it occurs, as well as the extent of changes to the pore space, as experimental studies by Shahidzadeh-Bonn et al. (2010) demonstrated. They showed that the formation of hydrated sodium sulfate crystals enhances the spreading power of the salt solution in the pore space of sandstone, giving rise to very rapid growth of the hydrated phase of sulfate and forming clusters. Sodium chloride, on the other hand, only forms anhydrous crystals, which explains why less efflorescence is observed compared to sodium sulfate.

Salt precipitation at field scale is influenced by the initial spatial distributions of the porosity and permeability of the porous formation (Celia et al., 2011; Zeidouni et al., 2009), and provides insights into the factors that are relevant to modeling of salt precipitation at the core scale. Several experimental studies of salt precipitation in geological formations during CO_2 injection have also been reported (e.g., Ott et al., 2011; Peysson et al., 2011), indicating that salt precipitation reduces permeability and porosity in Berea sandstone, that is, subflorescence, supporting the view that, in such formations, crystallization occurs *inside* the pore throats in the pore space, rather than migrating to the outside surface.

Development of the pore-network model of evaporation-induced salt precipitation entails simulating the drying process in the same model. Pore-network models of drying of porous media were already described in Section 8.1.3. We now describe the same type of models for salt transport and precipitation within the pore space, that is, subflorescence. Transport of salt through a porous medium is by convection and diffusion. The electro-neutrality of brine implies that the concentration C of the salt at time t is governed by the convective-diffusion equation, Equation 24. One can also show that the salt concentration near the liquid-vapor interface is maximum (Guglielmini et al., 2008; Huinink et al., 2002). Thus, salt precipitates mostly at the interface throats. In the liquid-filled pores i, the net accumulation of salt at time step n is given by

$$\sum_{\{ij\}} S_{ij} J_{ij} = \sum_{\{ij\}} v_{ij} \frac{C_i^{n+1} - C_i^n}{\Delta t}, \tag{26}$$

where v_{ij} is the velocity in the pore throat ij, $J_{ij} = v_{ij}C_i - D_L \partial C_i/\partial z = v_{ij}C_i - D_L(C_j - C_i)/\ell_{ij}$ is the mass flux in the pore throat ij over a time step Δt, with z being the axial direction in pore throat ij and D_L being the longitudinal dispersion coefficient that depends in general on flow velocity and saturation. If a throat contains partially the vapor that can escape (i.e., it is connected to other pores and throats that are filled with vapor), then, mass balance will take the mass flow rate of the vapor in that throat into account. Writing the brine mass balance for each pore i yields a set of equations for the concentrations C_i of the salt that is solved numerically. Thus, the pore-network model for subflorescence may be summarized as follows (Dashtian et al., 2018):

(i) The pressure distribution in the vapor phase is computed.
(ii) The mass evaporation rate in each throat and that from the boundary layer are calculated.
(iii) The pressure distribution in the liquid phase and, therefore, the mean flow velocity and the local dispersion coefficient D_L in each throat are computed.
(iv) The time step for advancing the vapor-liquid interface by an invasion percolation algorithm is selected, following Hekmatzadeh et al. (2016). There are two time scales in the problem. One is associated with evaporation, while the second one is the time scale over which one solves the convective-diffusion equation. The smaller of the two is used, since that is the relevant time scale. Thus, the evaporated mass from all the throats in the drying front containing liquid throats, which leaves the pore netwrok, is computed. The throat at the interface with the lowest capillary pressure is one with the largest radius. The time step for emptying that throat is given by

$$\Delta t = \frac{\rho^{(l)} V_{ij}}{\sum_{\{ij\} \in \mathcal{L}_D} M_{ij}}, \tag{27}$$

where V_{ij} is the volume of the throat ij, M_{ij} is the mass rate of evaporation, and the sum is over all the throats $\{ij\}$ that are at the drying front $\mathcal{L}_D$.

(v) The convective-diffusion equation is solved in the brine part of the pore network in order to compute the salt concentration in the throats.

(vi) As drying continues, salt concentration in the liquid phase increases. The solution of the convective-diffusion equation for salt transport in porous media indicates that salt concentration at the drying front is maximum (Guglielmini et al., 2008; Huinink et al., 2002). Thus, salt concentrations in the throats next to the drying front $\mathcal{L}_D$ are compared with a threshold concentration for its precipitation. If they exceed the threshold, which, in principle, is the solubility limit of salt in water at room temperature (about 36% in mass), then, salt precipitates in such throats. Desarnaud et al. (2014) reported that the precipitation threshold may be as high as 1.5 times the solubility limit. But, this would not make any difference to the pore-network model, as the precipitation threshold may be set at any value. Pore-network simulations (Dashtian et al., 2018) indicated that the salt content of practically no throat away from the interface exceeds the saturation limit. Then, the amount of precipitated salt in the throats is calculated as the *difference* between the current salt concentration in the throats and the saturation concentration. The precipitated salt forms a porous packing of its crystals and therefore, it would take some time to plug a throat mostly or completely. Thus, the volume of the precipitated salt in each throat is calculated and subtracted from the throat's volume, and its radius is updated, assuming that salt precipitates uniformly. Depending on its size and the amount of precipitated salt, the throat can either become partially or completely plugged.

(vii) The drying algorithm—the invasion percolation procedure—advances further the drying front in the pore-network by one or a few throats, and the procedure is repeated until the evaporation rate from the boundary layer is negligible.

Dashtian et al. (2018) showed that such a pore-network model reproduces all the important features of sub-florescence in soil. In particular, the three stages of evaporation of saline water and salt precipitation that were described above were reproduced by the pore-network model. Dashtian et al. (2018) also studied the effect of anisotropy (stratification) and the correlations between pore sizes, and demonstrated that they are relevant to the patterns of salt precipitation.

Similar pore-network models of saline water evaporation and salt precipitation were developed by Börnhorst et al. (2016), Ahmad et al. (2021), and Kharaghani et al. (2021). If the pore-size distribution is narrow and populated by small pores, solute migration during drying is reduced, as a result of which uniform salt distributions are developed, with the drying conditions having no influence (Shokri-Kuehni et al., 2018). A higher initial concentration of the solution leads to significant surface accumulation of salt. To characterize the degree of heterogeneity in the liquid phase structure during saline water evaporation, Ahmad et al. (2021) carried out Monte Carlo simulations in order to distinguish the percolating (sample-spanning) liquid cluster from the isolated clusters. The Monte Carlo data were used to estimate the probability that the first solid crystals appear in the respective liquid phase elements. The simulations also indicated that solute enrichment (as a result of evaporation) is more pronounced in the isolated single liquid throats and isolated clusters, due to lack of significant hindrance to back-diffusion caused by discontinuity in the liquid phase and the emergence of isolated liquid clusters. Ahmad et al. (2021) also solved the continuum convective-diffusion equation and compared its predictions with the results of pore-network simulations.

8.2.4. Lattice-Boltzmann Approach

Also LB models have been developed to simulate salt precipitation in porous media (J. Yang et al., 2023). The approach is particularly useful for simulating the phenomenon in the image of an actual porous medium in which salt precipitation occurs, since the pore space is not approximated by any particular model, such as a pore network, as a result of which the effect of the morphology of the pore space on the transport, salt crystal formation and growth, and precipitation can be studied. One must not only solve the convective-diffusion equation by the LB method, but also account for salt dissolution and precipitation, implying that one must have extra sets of particle

distribution functions that are used in LB simulations. In addition, mass balance at the fluid-vapor interface must be accounted for.

The most straightforward of doing so is by using a source/sink term, incorporated in the particle distribution function for the *i*th species (depending on how many species are included in the LB simulations). Thus, a flag variable is introduced that indicates whether a point is at the fluid-vapor or the fluid-solid interface, or is away from them. Nucleation of salt crystals, their growth, and transport are accounted by three variables, namely, one that accounts for the reduction in the concentration of the dissolved salt in water due to nucleation of salt crystals, a second variable that takes into account the reduction in the concentration of the dissolved salt because its crystals grow, while the third variable represents the *increase* in the concentration of the dissolved salt due to water evaporation at the fluid-vapor interface. In addition, one also needs to include a mechanism for the nucleation of the salt crystals. This can be done, for example, by a probabilistic approach (Masoudi et al., 2021; Nooraiepour et al., 2021), whereby one assumes a probability density function (PDF) for nucleation of salt crystals during a lattice time step. The PDF may be parameterized, with its parameters estimated by the classical theory of nucleation mentioned earlier. Alternatively, one can use the results of molecular dynamics (MD) simulations of Dashtian et al. (2017) in order to construct a functional form for the PDF. LB simulations require, however, intensive and long computations.

9. Molecular Mechanisms of Formation of Salt in Soil

Nucleation and growth of salt crystals from supersaturated solutions by evaporation of water, which is an important factor in soil salinization, is actually quite common and occurs both on Earth's surface (Desarnaud et al., 2015, 2016) and in geological formations. Salt weathering that damages rock and the soil profile (Sabbioni et al., 2008) is an important contributing factor to landscape degradation, infrastructure damage, and the loss of agricultural productivity. This process, driven by environmental factors such as temperature fluctuations, humidity, and water movement, leads to the mechanical disruption of materials through crystallization pressure, significantly impacting both natural and human-made structures. In addition, sequestration of CO_2 in rock, a promising way of mitigating global warming, suffers from salt precipitation both near and far from the injection wells that hampers flow of CO_2 in the rock, because it gives rise to pressure build-up and reduces the permeability and porosity and, ultimately, the capacity of the formations for holding CO_2. Thus, nucleation of salt crystals in soil is important, and understanding this process in pores and confined spaces is necessary for controlling it and preventing salt weathering.

Nucleation of crystals, including those of salt, and their growth in liquids is an ubiquitous phenomenon in the nature (Billinge, 2009), which has been studied both theoretically and by experiment (for a review see Karthika et al., 2016). In the classical theory of nucleation, first proposed by Volmer and Weber (1926), the free energy for producing a nucleus of *n* particles is divided into a favorable term, which is proportional to the number of particles in the nucleus, and an unfavorable term proportional to the surface between the nucleus and the solution. Putting it another way, one can express the total free energy as the sum of two terms, with one expressing the contribution of the bulk free energy (ΔG) gain, which clearly depends on the number of molecules in the cluster, and a loss term since the area of the crystal-liquid interface increases as nucleation proceeds. Despite its success in providing a qualitative picture of nucleation of crystals in liquids, the classic theory fails to predict homogeneous nucleation (i.e., when the particles are formed in the vapor phase, as opposed to heterogeneous nucleation in which the formation of the crystals is aided by impurities in the solution) rates, as its predictions are at least 10 orders of magnitude smaller than experimental data. Statistical theory of nucleation (Binder & Stauffer, 1976; Stauffer, 1976) provides a much more accurate description of the nucleation phenomenon.

Experiments over the past decade or so (see, for example, Gebauer et al., 2008; Loh et al., 2017; Smeets et al., 2015) provided strong evidence for the existence of an intermediate phase, which is relevant to the solidification pathway of solutes. This is in agreement with a two-step mechanism of nucleation of crystals in solution, first proposed by Wolde and Frenkel (1997) according to which amorphous nuclei are formed first, with their surface energy being lower than that of crystalline nuclei, which is a consequence of their disordered interface with the solution. Then, in the second step, an amorphous-to-crystalline transition occurs in the middle of the amorphous phase.

Since nucleation of salt crystals, and in particular NaCl crystals, is relevant to a wide variety of phenomena, many studies have been undertaken in order to gain insights into the process. In particular, Giberti et al. (2013) reported

on identifying a wurtzite-like polymorph, which they suggested to be an intermediate route from brine to the final salt structure. But, the questions is, what is the mechanism of nucleation of salt crystals in soil's pores? The confined environment of the pores, the chemical heterogeneity of soil, and the resulting molecular interactions between Na and Cl ions and the pores' wall imply that the process of salt crystal nucleation in soil is quite complex. Thus, one must resort to MD simulations in order to not only account for the molecular-scale interactions, but also the effect of the confined structure of the pores. Although MD simulations of salt crystal nucleation in bulk solutions have been carried out in the past (see, for example, Alejandre & Hansen, 2007; Chakraborty & Patey, 2013; J. R. Espinosa et al., 2015; Giberti et al., 2013; Lanaro & Patey, 2016; Mendoza & Alejandre, 2013; Sun et al., 2020; Zahn, 2004; Zimmermann et al., 2015), Dashtian et al. (2017) appear to be among the first to utilize MD simulations to study nucleation of salt crystals in soil, and in particular in clays. The utility of MD simulation is manifested by the fact that water near the pores' wall—the so-called *bound water*—and its properties are completely different from those under bulk conditions, leading to the so-called *dual water model*. Macroscopic theories cannot differentiate between the two types of water and, hence, are incapable of describing accurately the process that occurs there. It is, of course, imperative to include the interactions of all atoms and molecules in any model of clays, if accurate MD simulation is to be carried out.

Clay minerals, water, and sodium chloride, the most abundant salt on Earth, co-exist everywhere. Nucleation, growth and, ultimately, precipitation of salt crystals in soil is more severe when it contains a significant amount of clay minerals. Kaolinite, illite, vermiculite, and smectite are the four major clay groups (Freedman, 2015), which consist of parallel tetrahedral and octahedral structures that are further divided into subgroups based on the type of the isomorphic cation substitution that they contain. Surface chemistry at the clay-brine interface plays a critical role in salt precipitation. Clay particles are phyllosilicates that consist of numerous combinations of bonded tetrahedral and octahedral sheets stacked together. Silicon-oxygen ions, SiO_4^{4-}, are linked together by sharing the basal oxygen atoms and form a tetrahedral sheet, referred to as the T layer. Such layers do not exist by themselves, as they are always bonded to the octahedral sheets—the O layers that are formed from aluminum-oxygen ions, AlO_4^{5-}, with shared apical and basal oxygen. Hydrogen bonding bridges the T and/or O sheets.

The 1:1 clay particles, such as kaolinite, are formed by binding of one T and one O sheet. Their structure does not contain additional cations and, thus, they are electrically neutral. The 2:1 clay particles are formed by bonding of two T and one O sheets. Due to isomorphic substitution in their structure, they have a net negative charge on their surfaces. Such clays, which includes the well-known montmorillonites (MMT), also have high surface area and adjustable spacing between their layers that contribute to their swelling and/or shrinkage and reactions. The differences in the chemical compositions and structures of clay minerals determine their diverse behavior under similar conditions. For example, clay-water interaction is completely different for kaolinite and the MMT (see, for example, the experimental data reported by DeCarlo & Shokri, 2014a, 2014b; Shokri et al., 2015).

As the model of clay particles, Dashtian et al. (2017) used kaolinite and the Na-MMTs, whose molecular modeling has been studied extensively in the past (see, for example, Ghassemzadeh & Sahimi, 2004; N. Kim et al., 2005, 2007). The Na-MMT model is based on a triclinic pyrophillite structure (Bickmore et al., 2003). The chemical structure of the MMT is characterized by random isomorphic substitution of Al by Mg atoms. Dashtian et al. (2017) utilized a MMT for which the chemical composition of its unit cell was $Na_3[Si_{31}Al_1][Al_{14}Mg_2]O_{80}(OH)_{16}$, while that of the kaolinite that they simulated was $Al_2Si_2O_5(OH)_4$. The structures of the MMT and kaolinite are shown in Figure 17. Note the differences in the thickness of two types of clay. Clay minerals swell when they come into contact with water, either pure or salinized with NaCl. To prevent swelling, KCl is added, which does not hydrate. Both phenomena can influence nucleation and growth of salt crystals.

To carry out MD simulations, one must have an accurate force field that describes the interactions between all the atoms. Dashtian et al. (2017) used the CLAYFF force field (Cygan, 2001; Cygan et al., 2004) to generate the molecular structures of both clays, which contains a single bond-stretching parameter for the structural O-H groups. A smectite particle, such as the MMTs, holds a net negative structural charge, due to isomorphic substitution by elements of lower valences in the T and O sheets. The charge deficiency caused by the isomorphic substitution of Mg is compensated by inserting four Na^+ ions in the structure. According to CLAYFF the total energy E of the material is given by,

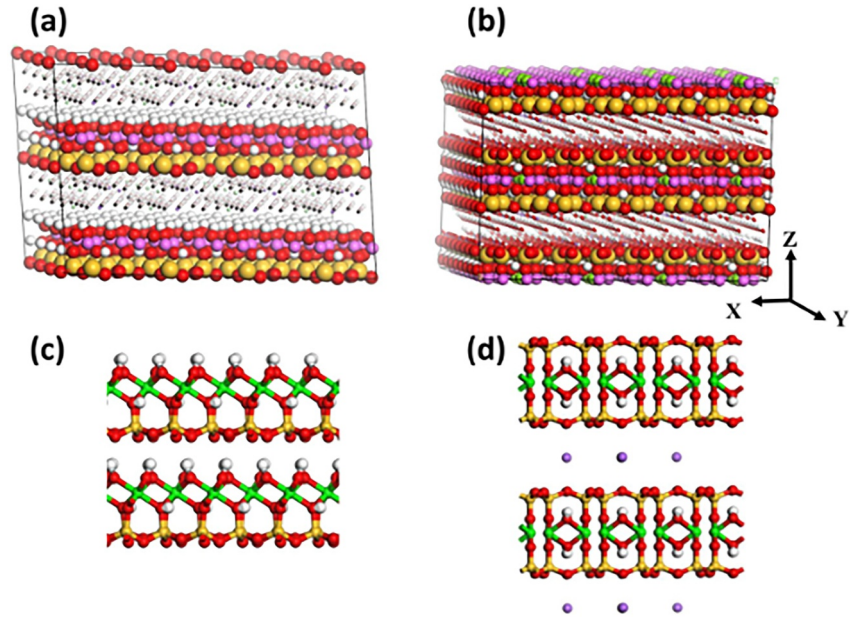

Figure 17. (a) and (c): The kaolinite molecular structure. (b) and (d) molecular structure of Na-MMT clays. Water molecules in (a) and (b) are shown by sticks. Colors represent oxygen (red), hydrogen (white), Si (yellow), Mg (green, only in (b)), Al, pink in (a) and (b) and green in (c) and (d), Na (purple), and Cl (green; very small) (after Dashtian et al. (2017), reprinted with the permission from https://doi.org/10.1021/acs.jpclett.7b01306. Copyright © 2017, American Chemical Society).

$$E = \sum_{\text{bonds}} k_1(r_{ij} - r_0)^2 + \sum_{\text{angle}} k_2(\theta_{ijk} - \theta_0)^2 + \sum_{ij} \epsilon_{ij}\left[\left(\frac{\sigma_{ij}}{r_{ij}}\right)^{12} - 2\left(\frac{\sigma_{ij}}{r_{ij}}\right)^{6}\right] + \frac{e^2}{4\pi\varepsilon_0}\sum_{i,j}\frac{q_i q_j}{r_{ij}}. \quad (28)$$

Here, k_1 and k_2 are two force constants, θ_{ijk} is the angle between bonds ij and jk, e is the electron's charge, q_i is the partial charge of atom i, ε_0 is the dielectric permittivity of vacuum, and r_0 and θ_0 are the equilibrium values of the corresponding quantities. ϵ_i and σ_i are the usual Lennard-Jones (LJ) energy and size parameters. Sodium chloride was used to represent salt, with its molecular structure and parameters given by CLAYFF. The complete details of the simulations are given by Dashtian et al. (2017).

Figure 18 shows the top view of the nucleation and growth of NaCl crystals in the interlayer space of kaolinite and Na-MMT, as they evolve with time. For clarity the water molecules and clay sheets are not shown. In the case of Na-MMT, there is no distinct order among the ions at early times. At longer times, the local ion density around some particular sites increases, but there is still no distinguishable order between Na^+ and Cl^-. Moreover, by this time some water molecules have left the interlayer region. At still longer times some initial small nuclei of crystals form, but they are still not stable, after which larger crystals form. The final stage is marked by stable crystals, filling some portions of the interlayer space of the clay, on the one hand, and some empty regions with essentially zero ion density, on the other hand. Note since the Na-MMT has extra Na^+ in its structure, they are attached to the clay or the salt crystal lattice.

The MD simulations of Dashtian et al. (2017) indicated that crystallization in both the MMT and kaolinite follow qualitatively the aforementioned two-step mechanism. In addition, the MD simulations indicated that the spatial distribution of the ions and water in soil, and in particular in the interlayer space of clays, is an important factor in nucleation and growth of the salt crystals.

One may be tempted to describe the crystal nucleation based on the aforementioned classical nucleation theory that views the formation of salt crystals as a single-step process. As discussed above, however, recent studies have shown that the phase diagrams of systems experiencing nucleation and crystallization involve a phase transition region between two stable disordered states with distinct concentration densities, implying that before formation of stable salt crystal, the system transitions to an intermediate state in which the ions form disordered aggregates. As Figure 18 indicates, MD simulations of Dashtian et al. (2017) indicated that even in a pore, small size

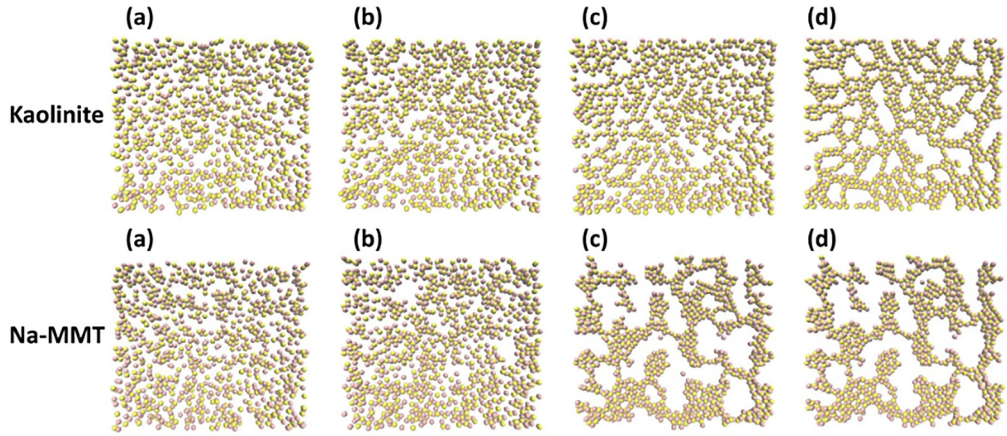

Figure 18. Top view of the positions of Na^+ (red) and Cl^- (yellow) within the interlayer space of kaolinite and Na-MMT. Time increases from (a) to (d). (a) Early positions (after 0.1 ns) of the ions after the system reached equilibrium. (b) The initial spatial ordering of the ions after 7 ns for kaolinite and 6 ns for Na-MMT. (c, d) Show the nucleation steps and spatial ordering after 30 and 40 ns for, respectively, kaolinite and Na-MMT. Colors show Na^+ (pink) and Cl^- (yellow) (after Dashtian et al. (2017), reprinted with the permission from https://doi.org/10.1021/acs.jpclett.7b01306. Copyright © 2017, American Chemical Society).

aggregates or clusters of ions form initially, with their number increasing with time, giving rise to a locally supersaturated state, that is, a state in which the concentration of a solute (the salt ions in this case) exceeds the concentration specified by the value of solubility at equilibrium. Initially, the solution tends to form several small nuclei because it is entropically more favorable for the NaCl solution plus the clay minerals. Then, the small clusters combine gradually and form larger aggregates that are referred to as the critical nuclei.

Another way of looking at the evolution of formation of salt crystals is through studying the time-dependence of the mean-square displacements (MSDs) of the ions, as nucleation of salt crystals is approached. Dashtian et al. (2017) calculated the MSDs and averaged them over all the ions with respect to a reference position. In Figure 19, we show the resulting MSDs for both clay types. In both cases the MSDs increase over time, albeit with different rates for two types of clay, and approach saturation, indicating that the ions eventually stop moving since nucleation of salt crystals has commenced and they have begun to form. The rate of approach to the saturation limit is higher in the Na-MMT case, indicating that the spatial ordering of the nucleation in kaolinite under the conditions that was studied was not as stable as that in the Na-MMT.

We note that after salt crystals form, whose shape is typically in the form of a cubic lattice, and precipitate on a surface or in pores, they form a packing of cubic particles whose morphology, porosity, and permeability have been studied extensively (Malmir et al., 2016a, 2016b, 2017). Figure 20 presents a typical configuration of packing of salt crystals. The structure of packing of salt crystals precipitated on the pores is crucial to modeling of salt precipitation in soil, because it still provides flow and transport paths through the pores between the crystals.

10. Chemical Processes in Soil and Salinization

In addition to brine evaporation in soil under the right conditions, soil salinization is influenced by several in-situ processes within the soil itself, such as dissolution and precipitation reactions of minerals in soil that are predominantly gypsum and calcite, which are affected by soil pH, alkalinity, and such organic constitutions as wastewater, soil redox reactions, and gas exchange. Such factors constitute what is usually referred to as geochemical weathering of rock that occur over geologic time scales and releases various types of salts onto the surface and into groundwater. Thus, soil chemistry plays a fundamental role in its salinization and, therefore, it is essential to obtain a comprehensive understanding of the chemical aspects of soil.

Soil chemistry is complex, particularly when it comes to reactions that produce salt. Oster and Tanji (1985) and Suarez and Jurinak (2011) provided extensive reviews of the important aspects of chemical processes in soil that are affected by the presence of salt. Several models have been developed in order to study transport and chemical reactions of ions, which contain accurate kinetic models for the reactions. In particular, Šimůnek et al. (1996) and

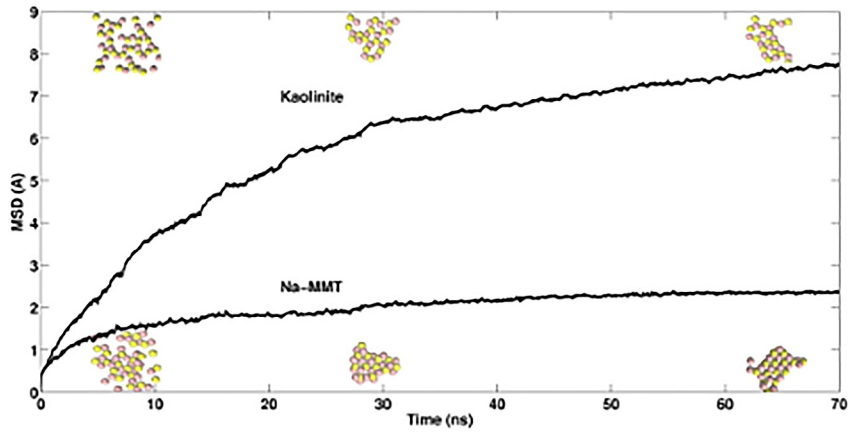

Figure 19. Evolution with time of the mean-square displacements of the ions in the interlayer space. The shapes of the salt aggregates are also shown (after Dashtian et al., (2017), reprinted with the permission from https://doi.org/10.1021/acs.jpclett.7b01306. Copyright © 2017, American Chemical Society).

Suarez and Šimůnek (1997) proposed the UNSATCHEM model (for chemistry of unsaturated soil) and considered eight major aqueous components in soil, namely, Ca, Mg, Na, K, SO_4, Cl, B, and Si, and defined their concentrations by the sum of the individual species that contain each component. For Ca, for example, one has

$$[\mathrm{Ca}] = \left[\mathrm{Ca}^{2+}\right] + \left[\mathrm{CaSO_4}^{0}\right] + \left[\mathrm{CaCO_3}^{0}\right] + \left[\mathrm{CaHCO_3}^{+}\right], \tag{29}$$

and for B one has

$$[\mathrm{B}] = \left[\mathrm{B(OH)_3}\right] + \left[\mathrm{B(OH)_4}^{-}\right], \tag{30}$$

where $[\cdot]$ indicates concentration. Alkalinity of soil was defined by

$$\begin{aligned}\text{Alkanility} = {} & \left[\mathrm{HCO_3}^{-}\right] + 2\left[\mathrm{CO_3}^{2-}\right] + 2\left[\mathrm{CaCO_3}^{0}\right] + \left[\mathrm{CaHCO_3}^{+}\right] + 2\left[\mathrm{MgCO_3}^{0}\right] \\ & + \left[\mathrm{MgHCO_3}^{+}\right] + 2\left[\mathrm{NaCO_3}^{-}\right] + \left[\mathrm{NaHCO_3}^{0}\right] + \left[\mathrm{B(OH)_4}^{-}\right] - \left[\mathrm{H}^{+}\right] + \left[\mathrm{OH}^{-1}\right].\end{aligned} \tag{31}$$

The precipitation or dissolution of calcite in the presence of CO_2 is described by the reaction

$$\mathrm{CaCO_3} + \mathrm{CO_2(g)} + \mathrm{H_2O} \Leftrightarrow \mathrm{Ca}^{2+} + 2\mathrm{HCO_3}^{-}, \tag{32}$$

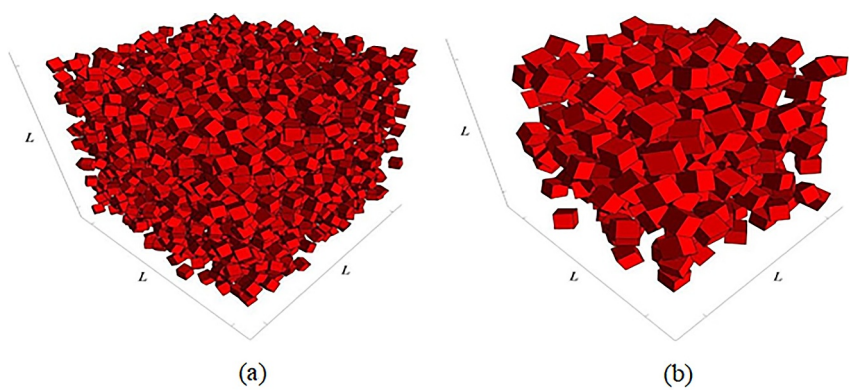

Figure 20. Packings of salt crystals with (a) 2,600 particles with the size 0.05L, and (b) with 400 particles with the size 0.1L, where L is the linear size of the packing system (after Malmir et al., 2016a).

while the precipitation or dissolution of sepiolite in the presence of CO_2 is described by

$$Mg_2Si_3O_{7.5}(OH).3H_2O + 4.5H_2O + 4CO_2(g) \Leftrightarrow 2Mg^{2+} + 3H_4SiO_4{}^0 + 4HCO_3{}^-, \quad (33)$$

where g denotes the gas phase. Suarez and Šimůnek (1997) also derived the kinetic rate expressions for all the important reactions. One must also take into account the effect of cation exchange. Although several models have been proposed for this purpose, two major models that are widely used are those of Gapon and Vanselow. The Gapon equation (Gapon, 1933) has been used widely to describe the cation exchange capacity of soil, which is a measure of how many cations can be retained on the soil particle surface, and is commonly used to study binary heterovalent exchange reactions, which helps to maintain the ratio Na/Ca on the soil colloid surface content. It was pointed out, however, that the Gapon equation (Gapon, 1933) is not consistent with thermodynamics of exchange reactions. Instead, the Vanselow exchange equation (Vanselow, 1932) has been shown (Evangelou & Phillips, 1988) to be consistent with thermodynamics of exchange reactions.

Another simulator is the so-called HP1 model (Jacques & Šimůnek, 2005; Šimůnek et al., 2006), which combines two simulators, namely, HYDRUS-1D, a one-dimensional variably-saturated water flow and solute transport model (Šimůnek et al., 1998), and PHREEQC-2, which is a geochemical code (Parkhurst & Appelo, 1999). HYDRUS-1D carries out simulation of flow of water and solute transport, plus the heat effects (non-isothermal) in a one-dimensional model of porous media, and includes several types of boundary conditions, such as precipitation and evaporation, as well as a sink term that accounts for water uptake by roots. Solutes may be exchanged between the water and gas phase and interact linearly or non-linearly with the solid phase, through either equilibrium or nonequilibrium reactions between the dissolved and adsorbed solutes. The interaction between the different solutes is allowed by only a consecutive chain reaction in which the solutes are sequentially transformed along the chain by means of first-order reactions (Jacques & Šimůnek, 2005).

On the other hand, PHREEQC-2 package simulates a large number of geochemical reactions in low-temperature water, soil, and groundwater aquifers, including interactions with minerals, gasses, solid solutions, exchangers, and sorption surfaces, all based on thermodynamic equilibrium, kinetics, or mixed equilibrium-kinetic reactions (see, for example, Appelo et al., 2002). The code also simulates one-dimensional reactive transport using a mixing cell solution approach (see, for example, Appelo et al., 1998; Postma and Appelo, 2000), and can be used to simulate reactive transport during steady-state flow with a wide variety of geochemical reactions.

Such simulators have been widely used in the simulation of flow of water, solute transport, and geochemical reactions in porous media. For example, UNSATCHEM simulator was utilized by Schoups et al. (2005, 2006) in order to study and evaluate the relevance of the complex salinity chemistry for the sustainability and long-term regional salt balance in San Joaquin Valley, California. In their simulations, groundwater salinity was taken into account. We should, however, point out that such studies do not incorporate the effect of specific ion chemistry on plant growth or salinity management, but consider only the total soil solution salinity. Thus, much remains to be done for understanding the effect of specific salt ions that are relevant to improving plant salt tolerance, crop salt tolerance breeding, and to soil hydraulic and transport characteristics.

11. Challenges and Open Research Directions

The recent improvements in soil salinity maps are commendable, but they largely remain extrapolated estimates based on geostatistical models. Furthermore, soil salinity observations from diverse global locations are still lacking. High uncertainty in such estimations is highlighted by the wide range of total areas reported for salt-affected soils. Although some data-driven attempts exist in the literature for globally quantifying the impact of primary soil salinization due to climate change, further evaluations are necessary, given the range of processes and uncertainties involved (El-Ramady et al., 2024; Y. Ma & Tashpolat, 2023).

Regarding secondary salinization, existing research is primarily at the local or national level; studies at broader scales could provide more insights. Open research questions include the response of soil salinity to rising sea levels in coastal regions, the salinization of coastal aquifers, water logging, and brackish irrigation. The role of salt deposition from dried saline lake beds under various climate and emission scenarios can also be worthy of research. To accurately project the processes affecting secondary salinization, high-resolution climate data is essential, both temporally and spatially (Shokri et al., 2023). In this regard, the forthcoming climate informatics

system from projects such as the "Destination Earth" promises to be a resource (Bauer et al., 2021). The project aims to create "digital twins" of the Earth at a spatial resolution of about 1 km, and such a data set could significantly enhance accuracy and effectiveness.

To achieve high-resolution climate data, including variables such as precipitation, temperature, humidity, and wind speed, a data assimilation system is required that continuously integrates real-time, highly detailed, high-resolution simulations of the Earth system with observational data from various sources (Bauer et al., 2021). This includes traditional instruments as well as new remote sensing technologies, crowd-sourced meteorological data (such as NetAtmo weather stations), undersea cables (Levin et al., 2019), drones, and smart sensors in croplands (Ullo and Sinha, 2021). This system helps estimate uncertain model parameters and fill in missing process details. With advances in high-performance computing, it is possible now to model the Earth system with much greater accuracy and detail than before.

There is still a lack of detailed maps quantifying or projecting the socio-economic impacts of soil salinization, particularly in arable lands or highly productive areas. While the ecological implications of soil salinity are relatively well understood, its socio-economic impacts have been less studied. Soil salinity can lead to abandoning traditional agricultural practices, economic decline, forced immigration, and social instability. A comprehensive understanding of soil salinity socio-economic impacts should include its effects on aspects like gender roles, income inequality, immigration, and community health.

Globalization has had various effects on agriculture, yet its impact on soil salinity remains underexplored. Such practices as the growth of export-focused monocultures can worsen soil salinity and increase the use of irrigation and fertilizers. They can create a cycle of soil degradation and increased reliance on imports, affecting areas far beyond the immediate location.

There are several open questions regarding the remediation and reclamation of salt-affected soils. One key question is the most effective and sustainable remediation techniques for different types of salt-affected soils (Qadir et al., 2000; Shaygan & Baumgartl, 2022). Unfortunately, there is not enough data to offer detailed recommendations on the most effective and eco-friendly techniques for salinity remediation to improve crop production (Mishra et al., 2023). While methods such as leaching, addition of inorganic (such as Gypsum; Elsherpiny, 2023; Xu et al., 2023) and organic (Leogrande & Vitti, 2019) amendments, revegetation using halophytes, and phytoremediation have been used (Shankar & Evelin, 2019), their long-term effectiveness and environmental impacts require further investigation. There is a need to understand the factors influencing the success of these remediation techniques, such as soil properties, climate conditions, and plant species (Shaygan & Baumgartl, 2022). Many remediation projects focus on short-term outcomes, but the long-term resilience of treated soils to salt re-accumulation and other stressors remains uncertain. Longitudinal studies are needed to track the effectiveness of remediation techniques over time and identify any potential challenges or limitations.

Another important question revolves around the development of cost-effective and scalable remediation technologies suitable for large-scale application. Many existing techniques may not be economically viable or practical for widespread use, particularly in resource-constrained regions. Research into innovative and low-cost approaches is necessary to address this challenge. Evaluating the impact of rehabilitation processes on carbon cycling and carbon stocks in salt-affected areas is also important (Amini et al., 2016). It is especially important to determine how to enhance carbon stock accumulation in these lands, which typically have low soil OC levels. Further research issues requiring immediate attention in soil salinization reclamation are provided by Kumar et al. (2022), which we do not reiterate here.

The role of land use and land cover change in soil salinity is a crucial yet under-researched area, especially in the context of climate change and global scale studies. Changes in land use, such as converting natural landscapes to agricultural fields or urban areas, can dramatically alter a region's hydrology and soil characteristics. For example, deforestation or the development of irrigated agriculture can lead to a rise in groundwater, bringing naturally occurring salts to the soil surface. Similarly, certain agricultural practices, such as excessive irrigation without proper drainage, exacerbate soil salinization.

In the area of core-scale salinization, there are several open questions. The governing equations for brine evaporation, as well as salt transport and precipitation at the macro-scale, are not well understood at different levels of porous media heterogeneity. Also, how exactly the precipitated salt with evolving porous structure at the surface of porous media influences the evaporation rate is poorly understood (Shokri-Kuehni et al., 2022).

Moreover, additional research is required to understand how the intermediate wet-condition, which may occur in the natural environment, influences saline water evaporation and corresponding salt precipitation patterns in porous media. Under intermediate wet-condition, the pore geometry has a strong influence on interface dynamics, leading to co-existence of concave and convex interfaces which will affect the subsequent flow and transport processes in porous media (Rabbani et al., 2017, 2018). Pore-network simulations can be used to generate numerical data, which can be combined with experimental data in the same type of porous media. Then, a physics-based, data-driven approach, either based on ML algorithms or a symbolic regression and stochastic optimization (see Sahimi, 2024) can be used to discover the governing equation. If such an equation is discovered, then, it can also be upscaled to a much larger scale, which will be a very significant advancement, and can be used for modeling the phenomenon at much larger scales.

Our understanding of salinization at molecular scale is also incomplete. For example, in the molecular simulation of Dashtian et al. (2017), evaporation of water was simulated by simply removing the water molecules. In reality, water vapourization is a phase transition. Thus, one must simulate the true liquid-vapor phase transition in order to understand in depth salt nucleation and crystallization, and how the restricted environment of a pore affects the transition. In addition, molecular simulation should be used to study the effect of wettability of the pore space on the same phenomenon.

Citizen science can significantly enrich soil salinity research by expanding the scope of data collection, offering real-time monitoring, and providing localized insights that may otherwise be overlooked. Moreover, involving local communities in data gathering raises awareness about the issue, leading to better land and water management practices. Increased public awareness can enhance efforts to advocate for sustainable farming and soil management policies.

Potential citizen scientists in soil salinity research include farmers, gardeners, students, teachers, community groups, nature enthusiasts, outdoor recreationists, citizen science networks, environmental advocates, retirees, and urban residents. These individuals can contribute in some specific ways to soil research (Head et al., 2020). Citizen scientists can be involved in soil sampling campaigns across various regions to provide a wide geographic coverage of soil salinity data (Rossiter et al., 2015). Citizens also can assist in deploying soil sensors in their local areas and monitoring soil salinity levels over time. Additionally, citizen scientists can participate in data analysis tasks (Pino et al., 2022), such as interpreting soil salinity measurements, identifying trends, and contributing to scientific discussions on the findings. Citizen scientists can collaborate with researchers in defining research questions (Head et al., 2020). More importantly, engaging citizen scientists in advocacy efforts can help raise awareness about soil salinity issues among policymakers and the public (Dörler et al., 2021; Mourad et al., 2020; Pino et al., 2022). Developing user-friendly mobile apps and online platforms can enable citizens to report soil salinity observations, upload photos, and share their findings with the research community.

Finally, although governments and international organizations increasingly acknowledge the gravity of soil salinization, a globally accepted policy and regulatory framework is still missing. Strategies, such as more sustainable irrigation practices, investment in mitigating technologies, and land reform focused on sustainability are potential areas for further investment. However, the effectiveness of these strategies often hinges on multi-disciplinary cooperation involving soil scientists, climatologists, agronomists, and social scientists.

Acknowledgments
N.S. would like to acknowledge funding from the European Union's Horizon Europe research and Innovation Program under grant agreement No. 101086179 as well as funding from the Deutsche Forschungsgemeinschaft (DFG, German Research Foundation), project number 497539130. A.H. gratefully acknowledges the funding provided by the SIS-EO project (NILU B121004). Parts of the work by M.S. described in this review were supported by the Center for Geologic Storage of CO_2, an Energy Frontier Research Center funded by the U.S. Department of Energy, Office of Science, Basic Energy Sciences, under Award DE-SC0C12504, as well as by the Petroleum Research Fund. Open Access funding enabled and organized by Projekt DEAL.

Data Availability Statement

Soil salinity measurements provided by the World Soil Information Service (WoSIS), can be accessed via the following: https://www.isric.org/explore/wosis/accessing-wosis-derived-datasets. Similarly, data concerning soil salinity from the 2018 LUCAS Topsoil Survey (Figure 7) are accessible at: https://esdac.jrc.ec.europa.eu/content/lucas-2018-topsoil-data. The Harmonized World Soil Database (HWSD) version 2.0 (Figure 8), is accessible through the ISRIC—World Soil Information data hub https://data.isric.org/geonetwork/srv/eng/catalog.search#/home, with the identifier: 54aebf11-ec73-4ff8-bf6c-ecff4b0725ea.

References

Abbas, A., Khan, S., Hussain, N., Hanjra, M. A., & Akbar, S. (2013). Characterizing soil salinity in irrigated agriculture using a remote sensing approach. *Physics and Chemistry of the Earth, Parts A/B/C*, *55*, 43–52. https://doi.org/10.1016/j.pce.2010.12.004

Aboukila, E. F., & Norton, J. B. (2017). Estimation of saturated soil paste salinity from soil-water extracts. *Soil Science*, *182*(3), 107–113. https://doi.org/10.1097/ss.0000000000000197

Abrol, I., Yadav, J. S. P., & Massoud, F. (1988). *Salt-affected soils and their management* (Vol. 39). Food & Agriculture Org.
Abuduwaili, J., DongWei, L., & GuangYang, W. (2010). Saline dust storms and their ecological impacts in arid regions. *Journal of arid land*, *2*(2), 144–150. https://doi.org/10.3724/sp.j.1227.2010.00144
Ahmad, F., Rahimi, A., Tsotsas, E., Prat, M., & Kharaghani, A. (2021). From micro-scale to macro-scale modeling of solute transport in drying capillary porous media. *International Journal of Heat and Mass Transfer*, *165*, 120722. https://doi.org/10.1016/j.ijheatmasstransfer.2020.120722
Alejandre, J., & Hansen, J.-P. (2007). Ions in water: From ion clustering to crystal nucleation. *Physical Review E*, *76*(6), 061505. https://doi.org/10.1103/physreve.76.061505
Aljasmi, A., & Sahimi, M. (2021). Speeding-up image-based simulation of two-phase flow in porous media with lattice-Boltzmann method using three-dimensional curvelet transforms. *Physics of Fluids*, *33*(11), 113313. https://doi.org/10.1063/5.0065857
Alkharabsheh, H. M., Seleiman, M. F., Hewedy, O. A., Battaglia, M. L., Jalal, R. S., Alhammad, B. A., et al. (2021). Field crop responses and management strategies to mitigate soil salinity in modern agriculture: A review. *Agronomy*, *11*(11), 2299. https://doi.org/10.3390/agronomy11112299
Allbed, A., & Kumar, L. (2013). Soil salinity mapping and monitoring in arid and semi-arid regions using remote sensing technology: A review. *Advances in Remote Sensing*, *2*, 373–385.
Alqasemi, A. S., Ibrahim, M., Fadhil Al-Quraishi, A. M., Saibi, H., Al-Fugara, A., & Kaplan, G. (2021). Detection and modeling of soil salinity variations in arid lands using remote sensing data. *Open Geosciences*, *13*(1), 443–453. https://doi.org/10.1515/geo-2020-0244
Álvarez-Cobelas, M., Sánchez-Carrillo, S., Cirujano, S., & Angeler, D. (2010). A story of the wetland water quality deterioration: Salinization, pollution, eutrophication and siltation. In *Ecology of threatened semi-arid wetlands: Long-term Research in Las Tablas de Daimiel* (pp. 109–133).
Amini, S., Ghadiri, H., Chen, C., & Marschner, P. (2016). Salt-affected soils, reclamation, carbon dynamics, and biochar: A review. *Journal of Soils and Sediments*, *16*(3), 939–953. https://doi.org/10.1007/s11368-015-1293-1
Appelo, C., Van der Weiden, M., Tournassat, C., & Charlet, L. (2002). Surface complexation of ferrous iron and carbonate on ferrihydrite and the mobilization of arsenic. *Environmental Science & Technology*, *36*(14), 3096–3103. https://doi.org/10.1021/es010130n
Appelo, C., Verweij, E., & Schäfer, H. (1998). A hydrogeochemical transport model for an oxidation experiment with pyrite/calcite/exchangers/organic matter containing sand. *Applied Geochemistry*, *13*(2), 257–268. https://doi.org/10.1016/s0883-2927(97)00070-x
Assouline, S., & Or, D. (2013). Plant water use efficiency over geological time–evolution of leaf stomata configurations affecting plant gas exchange. *PLoS One*, *8*(7), e67757. https://doi.org/10.1371/journal.pone.0067757
Assouline, S., Tyler, S. W., Selker, J. S., Lunati, I., Higgins, C., & Parlange, M. (2013). Evaporation from a shallow water table: Diurnal dynamics of water and heat at the surface of drying sand. *Water Resources Research*, *49*(7), 4022–4034. https://doi.org/10.1002/wrcr.20293
Attari Moghaddam, A., Kharaghani, A., Tsotsas, E., & Prat, M. (2017). Kinematics in a slowly drying porous medium: Reconciliation of pore network simulations and continuum modeling. *Physics of Fluids*, *29*(2), 022102. https://doi.org/10.1063/1.4975985
Attari Moghaddam, A., Prat, M., Tsotsas, E., & Kharaghani, A. (2017). Evaporation in capillary porous media at the perfect piston-like invasion limit: Evidence of nonlocal equilibrium effects. *Water Resources Research*, *53*(12), 10433–10449. https://doi.org/10.1002/2017wr021162
Aydin, M., Yano, T., Evrendilek, F., & Uygur, V. (2008). Implications of climate change for evaporation from bare soils in a mediterranean environment. *Environmental Monitoring and Assessment*, *140*(1–3), 123–130. https://doi.org/10.1007/s10661-007-9854-4
Bachmann, J., Horton, R., & Van Der Ploeg, R. (2001). Isothermal and nonisothermal evaporation from four sandy soils of different water repellency. *Soil Science Society of America Journal*, *65*(6), 1599–1607. https://doi.org/10.2136/sssaj2001.1599
Bano, A., & Fatima, M. (2009). Salt tolerance in zea mays (l). following inoculation with rhizobium and pseudomonas. *Biology and Fertility of Soils*, *45*(4), 405–413. https://doi.org/10.1007/s00374-008-0344-9
Barbier, E. B. (2015). Climate change impacts on rural poverty in low-elevation coastal zones. *Estuarine, Coastal and Shelf Science*, *165*, A1–A13.
Barrett-Lennard, E. (2002). Restoration of saline land through revegetation. *Agricultural Water Management*, *53*(1–3), 213–226. https://doi.org/10.1016/s0378-3774(01)00166-4
Bates, B., Kundzewicz, Z., & Wu, S. (2008). *Climate change and water*. Intergovernmental Panel on Climate Change Secretariat.
Batjes, N. H. (2003). *A taxotransfer rule-based approach for filling gaps in measured soil data in primary soter databases. Technical report*. ISRIC.
Batjes, N. H. (2008). *Isric-wise harmonized global soil profile dataset*. ISRIC-World Soil Information, Wageningen.
Batjes, N. H. (2009). Harmonized soil profile data for applications at global and continental scales: Updates to the wise database. *Soil Use & Management*, *25*(2), 124–127. https://doi.org/10.1111/j.1475-2743.2009.00202.x
Batjes, N. H. (2011). Soil organic carbon stocks under native vegetation–revised estimates for use with the simple assessment option of the carbon benefits project system. *Agriculture, Ecosystems & Environment*, *142*(3–4), 365–373. https://doi.org/10.1016/j.agee.2011.06.007
Batjes, N. H. (2016). Harmonized soil property values for broad-scale modelling (wise30sec) with estimates of global soil carbon stocks. *Geoderma*, *269*, 61–68. https://doi.org/10.1016/j.geoderma.2016.01.034
Batjes, N. H., Ribeiro, E., Van Oostrum, A., Leenaars, J., Hengl, T., & Mendes de Jesus, J. (2017). Wosis: Providing standardised soil profile data for the world. *Earth System Science Data*, *9*(1), 1–14. https://doi.org/10.5194/essd-9-1-2017
Bauer, P., Stevens, B., & Hazeleger, W. (2021). A digital twin of Earth for the green transition. *Nature Climate Change*, *11*(2), 80–83. https://doi.org/10.1038/s41558-021-00986-y
Bechtold, M., Haber-Pohlmeier, S., Vanderborght, J., Pohlmeier, A., Ferré, T., & Vereecken, H. (2011). Near-surface solute redistribution during evaporation. *Geophysical Research Letters*, *38*(17), L17404. https://doi.org/10.1029/2011gl048147
Beck, H. E., Zimmermann, N. E., McVicar, T. R., Vergopolan, N., Berg, A., & Wood, E. F. (2018). Present and future köppen-geiger climate classification maps at 1-km resolution. *Scientific Data*, *5*(1), 1–12. https://doi.org/10.1038/sdata.2018.214
Becker, G., & Day, A. (1905). The linear force of growing crystals, and an interesting pseudo-solid. In *Proceedings of the Washington Academy of sciences, VII* (pp. 251–300).
Bellafiore, D., Ferrarin, C., Maicu, F., Manfè, G., Lorenzetti, G., Umgiesser, G., et al. (2021). Saltwater intrusion in a mediterranean delta under a changing climate. *Journal of Geophysical Research: Oceans*, *126*(2), e2020JC016437. https://doi.org/10.1029/2020jc016437
Bello, S. K., Alayafi, A. H., Al-Solaimani, S. G., & Abo-Elyousr, K. A. (2021). Mitigating soil salinity stress with gypsum and bio-organic amendments: A review. *Agronomy*, *11*(9), 1735. https://doi.org/10.3390/agronomy11091735
Benilov, E. (2023). Nonisothermal evaporation. *Physical Review E*, *107*(4), 044802. https://doi.org/10.1103/physreve.107.044802
Ben-Noah, I., & Friedman, S. P. (2018). Review and evaluation of root respiration and of natural and agricultural processes of soil aeration. *Vadose Zone Journal*, *17*(1), 1–47. https://doi.org/10.2136/vzj2017.06.0119

Bhattacharya, S. S., Kim, K.-H., Das, S., Uchimiya, M., Jeon, B. H., Kwon, E., & Szulejko, J. E. (2016). A review on the role of organic inputs in maintaining the soil carbon pool of the terrestrial ecosystem. *Journal of Environmental Management*, *167*, 214–227. https://doi.org/10.1016/j.jenvman.2015.09.042

Bickmore, B. R., Rosso, K. M., Nagy, K. L., Cygan, R. T., & Tadanier, C. J. (2003). Ab initio determination of edge surface structures for dioctahedral 2:1 phyllosilicates: Implications for acid-base reactivity. *Clays and Clay Minerals*, *51*(4), 359–371. https://doi.org/10.1346/ccmn.2003.0510401

Billinge, S. J. (2009). How do your crystals grow? *Nature Physics*, *5*(1), 13–14. https://doi.org/10.1038/nphys1172

Binder, K., & Stauffer, D. (1976). Statistical theory of nucleation, condensation and coagulation. *Advances in Physics*, *25*(4), 343–396. https://doi.org/10.1080/00018737600101402

Blank, R., Young, J., & Allen, F. (1999). Aeolian dust in a saline playa environment, Nevada, USA. *Journal of Arid Environments*, *41*(4), 365–381. https://doi.org/10.1006/jare.1998.0491

Blankespoor, B., Dasgupta, S., & Laplante, B. (2014). Sea-level rise and coastal wetlands. *Ambio*, *43*(8), 996–1005. https://doi.org/10.1007/s13280-014-0500-4

Blaylock, A. D. (1994). *Soil salinity, salt tolerance, and growth potential of horticultural and landscape plants*. University of Wyoming, Cooperative Extension Service, Department of Plant, Soil, and Insect Sciences, College of Agriculture.

Blum, W. E. (2020). Basic concepts: Degradation, resilience, and rehabilitation. In *Methods for assessment of soil degradation* (pp. 1–16). CRC Press.

Bond, J., & Willis, W. (1970). Soil water evaporation: First stage drying as influenced by surface residue and evaporation potential. *Soil Science Society of America Journal*, *34*(6), 924–928. https://doi.org/10.2136/sssaj1970.03615995003400060030x

Borgman, O., Fantinel, P., Lühder, W., Goehring, L., & Holtzman, R. (2017). Impact of spatially correlated pore-scale heterogeneity on drying porous media. *Water Resources Research*, *53*(7), 5645–5658. https://doi.org/10.1002/2016wr020260

Börnhorst, M., Walzel, P., Rahimi, A., Kharaghani, A., Tsotsas, E., Nestle, N., et al. (2016). Influence of pore structure and impregnation–drying conditions on the solid distribution in porous support materials. *Drying Technology*, *34*(16), 1964–1978. https://doi.org/10.1080/07373937.2016.1147048

Bosserelle, A. L., Morgan, L. K., & Hughes, M. W. (2022). Groundwater rise and associated flooding in coastal settlements due to sea-level rise: A review of processes and methods. *Earth's Future*, *10*(7), e2021EF002580. https://doi.org/10.1029/2021ef002580

Bouzid, M., Mercury, L., Lassin, A., & Matray, J.-M. (2011). Salt precipitation and trapped liquid cavitation in micrometric capillary tubes. *Journal of Colloid and Interface Science*, *360*(2), 768–776. https://doi.org/10.1016/j.jcis.2011.04.095

Brevik, E. C. (2013). The potential impact of climate change on soil properties and processes and corresponding influence on food security. *Agriculture*, *3*(3), 398–417. https://doi.org/10.3390/agriculture3030398

Brown, G. (1982). *Crystal structures of clay minerals and their X-ray identification* (Vol. 5). The mineralogical society of Great Britain and Ireland.

Buckingham, E. (1907). Studies on the movement of soil moisture.

Buffone, C., Sefiane, K., & Christy, J. (2005). Experimental investigation of self-induced thermocapillary convection for an evaporating meniscus in capillary tubes using micro–particle image velocimetry. *Physics of Fluids*, *17*(5), 052104. https://doi.org/10.1063/1.1901688

Bui, E. (2013). Soil salinity: A neglected factor in plant ecology and biogeography. *Journal of Arid Environments*, *92*, 14–25. https://doi.org/10.1016/j.jaridenv.2012.12.014

Burkhardt, J. (2010). Hygroscopic particles on leaves: Nutrients or desiccants? *Ecological Monographs*, *80*(3), 369–399. https://doi.org/10.1890/09-1988.1

Cahill, A. T., & Parlange, M. B. (1998). On water vapor transport in field soils. *Water Resources Research*, *34*(4), 731–739. https://doi.org/10.1029/97wr03756

Callegary, J. B., Ferré, T. P., & Groom, R. (2007). Vertical spatial sensitivity and exploration depth of low-induction-number electromagnetic-induction instruments. *Vadose Zone Journal*, *6*(1), 158–167. https://doi.org/10.2136/vzj2006.0120

Celia, M. A., Nordbotten, J. M., Court, B., Dobossy, M., & Bachu, S. (2011). Field-scale application of a semi-analytical model for estimation of CO_2 and brine leakage along old wells. *International Journal of Greenhouse Gas Control*, *5*(2), 257–269. https://doi.org/10.1016/j.ijggc.2010.10.005

Celleri, C., Pratolongo, P., & Arena, M. (2022). Spatial and temporal patterns of soil salinization in shallow groundwater environments of the bahía blanca estuary: Influence of topography and land use. *Land Degradation & Development*, *33*(3), 470–483. https://doi.org/10.1002/ldr.4162

Chakraborty, D., & Patey, G. (2013). How crystals nucleate and grow in aqueous nacl solution. *The Journal of Physical Chemistry Letters*, *4*(4), 573–578. https://doi.org/10.1021/jz302065w

Chapuis, O., & Prat, M. (2007). Influence of wettability conditions on slow evaporation in two-dimensional porous media. *Physical review E*, *75*(4), 046311. https://doi.org/10.1103/physreve.75.046311

Chau, H. W., Goh, Y. K., Vujanovic, V., & Si, B. C. (2012). Wetting properties of fungi mycelium alter soil infiltration and soil water repellency in a γ-sterilized wettable and repellent soil. *Fungal Biology*, *116*(12), 1212–1218. https://doi.org/10.1016/j.funbio.2012.10.004

Chauvet, F., Duru, P., Geoffroy, S., & Prat, M. (2009). Three periods of drying of a single square capillary tube. *Physical Review Letters*, *103*(12), 124502. https://doi.org/10.1103/physrevlett.103.124502

Chen, J., & Mueller, V. (2018). Coastal climate change, soil salinity and human migration in Bangladesh. *Nature Climate Change*, *8*(11), 981–985. https://doi.org/10.1038/s41558-018-0313-8

Chen, X. (1992). Evaporation from a salt encrusted sediment surface-field and laboratory studies. *Soil Research*, *30*(4), 429–442. https://doi.org/10.1071/sr9920429

Chernousenko, G., Yamnova, I., & Skripnikova, M. (2003). Anthropogenic salinization of soils in Moscow. *Eurasian Soil Science C/C Of Pochvovedenie*, *36*(1), 92–100.

Church, P. E., & Friesz, P. J. (1993). *Effectiveness of highway drainage systems in preventing road-salt contamination of groundwater: Preliminary findings* (Vol. 1420). The National Academies Press.

Clement, T., Hooker, B., & Skeen, R. (1996). Macroscopic models for predicting changes in saturated porous media properties caused by microbial growth. *Groundwater*, *34*(5), 934–942. https://doi.org/10.1111/j.1745-6584.1996.tb02088.x

Colombani, N., Mastrocicco, M., & Giambastiani, B. M. S. (2015). Predicting salinization trends in a lowland coastal aquifer: Comacchio (Italy). *Water Resources Management*, *29*(2), 603–618. https://doi.org/10.1007/s11269-014-0795-8

Cortes, C., & Vapnik, V. (1995). Support-vector networks. *Machine Learning*, *20*(3), 273–297. https://doi.org/10.1007/bf00994018

Corwin, D., & Scudiero, E. (2019). Review of soil salinity assessment for agriculture across multiple scales using proximal and/or remote sensors. *Advances in Agronomy*, *158*, 1–130. https://doi.org/10.1016/bs.agron.2019.07.001

Corwin, D. L. (2021). Climate change impacts on soil salinity in agricultural areas. *European Journal of Soil Science*, *72*(2), 842–862. https://doi.org/10.1111/ejss.13010

Corwin, D. L., & Lesch, S. M. (2013). Protocols and guidelines for field-scale measurement of soil salinity distribution with eca-directed soil sampling. *Journal of Environmental & Engineering Geophysics*, *18*(1), 1–25. https://doi.org/10.2113/jeeg18.1.1

Corwin, D. L., Rhoades, J. D., & Šimůnek, J. (2007). Leaching requirement for soil salinity control: Steady-state versus transient models. *Agricultural Water Management*, *90*(3), 165–180. https://doi.org/10.1016/j.agwat.2007.02.007

Covey, W., & Bloodworth, M. (1965). The buckingham effect in the drying of soil (p. 61). In *Agronomy abstracts*. ASA.

Cygan, R. T. (2001). Molecular modeling in mineralogy and geochemistry. *Reviews in Mineralogy and Geochemistry*, *42*, 1–36. https://doi.org/10.2138/rmg.2001.42.1

Cygan, R. T., Liang, J.-J., & Kalinichev, A. G. (2004). Molecular models of hydroxide, oxyhydroxide, and clay phases and the development of a general force field. *The Journal of Physical Chemistry B*, *108*(4), 1255–1266. https://doi.org/10.1021/jp0363287

Dai, A. (2011). Drought under global warming: A review. *Wiley Interdisciplinary Reviews: Climate Change*, *2*(1), 45–65. https://doi.org/10.1002/wcc.81

Dai, S., Shin, H., & Santamarina, J. C. (2016). Formation and development of salt crusts on soil surfaces. *Acta Geotechnica*, *11*(5), 1103–1109. https://doi.org/10.1007/s11440-015-0421-9

Daley, M. L., Potter, J. D., & McDowell, W. H. (2009). Salinization of urbanizing New Hampshire streams and groundwater: Effects of road salt and hydrologic variability. *Journal of the North American Benthological Society*, *28*(4), 929–940. https://doi.org/10.1899/09-052.1

Daliakopoulos, I. N., Pappa, P., Grillakis, M. G., Varouchakis, E. A., & Tsanis, I. K. (2016). Modeling soil salinity in greenhouse cultivations under a changing climate with saltmed: Model modification and application in timpaki, crete. *Soil Science*, *181*(6), 241–251. https://doi.org/10.1097/ss.0000000000000161

Daliakopoulos, I. N., Tsanis, I., Koutroulis, A., Kourgialas, N., Varouchakis, A., Karatzas, G., & Ritsema, C. (2016). The threat of soil salinity: A European scale review. *Science of the Total Environment*, *573*, 727–739. https://doi.org/10.1016/j.scitotenv.2016.08.177

Das, A., Bhattacharya, B. K., Setia, R., Jayasree, G., & Das, B. S. (2023). A novel method for detecting soil salinity using aviris-ng imaging spectroscopy and ensemble machine learning. *ISPRS Journal of Photogrammetry and Remote Sensing*, *200*, 191–212. https://doi.org/10.1016/j.isprsjprs.2023.04.018

Dashtian, H., Shokri, N., & Sahimi, M. (2018). Pore-network model of evaporation-induced salt precipitation in porous media: The effect of correlations and heterogeneity. *Advances in Water Resources*, *112*, 59–71. https://doi.org/10.1016/j.advwatres.2017.12.004

Dashtian, H., Shokri, N., & Sahimi, M. (2019). Pore-network simulation of drying of heterogeneous and stratified porous media. In *Convective heat transfer in porous media* (pp. 87–101). CRC Press.

Dashtian, H., Wang, H., & Sahimi, M. (2017). Nucleation of salt crystals in clay minerals: Molecular dynamics simulation. *The Journal of Physical Chemistry Letters*, *8*(14), 3166–3172. https://doi.org/10.1021/acs.jpclett.7b01306

da Silva Dias, N., da Silva, J. F., Moreno-Pizani, M. A., Lima, M. C. F., da Silva Ferreira, J. F., Linhares, E. L. R., et al. (2021). Environmental, agricultural, and socioeconomic impacts of salinization to family-based irrigated agriculture in the Brazilian semiarid region. In *Saline and alkaline soils in Latin America: Natural resources, management and productive alternatives* (pp. 37–48).

Datta, A., Mandal, A., & Yadav, R. (2019). Proper measurement of electrical conductivity and other parameters influence profile salinity and sodicity under different land uses. *Ecological Indicators*, *101*, 1004–1006. https://doi.org/10.1016/j.ecolind.2019.02.012

DeCarlo, K. F., & Shokri, N. (2014a). Effects of substrate on cracking patterns and dynamics in desiccating clay layers. *Water Resources Research*, *50*(4), 3039–3051. https://doi.org/10.1002/2013wr014466

DeCarlo, K. F., & Shokri, N. (2014b). Salinity effects on cracking morphology and dynamics in 3-D desiccating clays. *Water Resources Research*, *50*(4), 3052–3072. https://doi.org/10.1002/2013wr014424

De Carlo, L., Vivaldi, G. A., & Caputo, M. C. (2021). Electromagnetic induction measurements for investigating soil salinization caused by saline reclaimed water. *Atmosphere*, *13*(1), 73. https://doi.org/10.3390/atmos13010073

De la Paix, M., Lanhai, L., Xi, C., Varenyam, A., Nyongesah, M., & Habiyaremye, G. (2013). Physicochemical properties of saline soils and aeolian dust. *Land Degradation & Development*, *24*(6), 539–547. https://doi.org/10.1002/ldr.1148

Derluyn, H., Moonen, P., & Carmeliet, J. (2014). Deformation and damage due to drying-induced salt crystallization in porous limestone. *Journal of the Mechanics and Physics of Solids*, *63*, 242–255. https://doi.org/10.1016/j.jmps.2013.09.005

Desarnaud, J., Bertrand, F., & Shahidzadeh-Bonn, N. (2013). Impact of the kinetics of salt crystallization on stone damage during rewetting/drying and humidity cycling. *Journal of Applied Mechanics*, *80*(2), 020911. https://doi.org/10.1115/1.4007924

Desarnaud, J., Bonn, D., & Shahidzadeh, N. (2016). The pressure induced by salt crystallization in confinement. *Scientific Reports*, *6*(1), 30856. https://doi.org/10.1038/srep30856

Desarnaud, J., Derluyn, H., Carmeliet, J., Bonn, D., & Shahidzadeh, N. (2014). Metastability limit for the nucleation of nacl crystals in confinement. *The Journal of Physical Chemistry Letters*, *5*(5), 890–895. https://doi.org/10.1021/jz500090x

Desarnaud, J., Derluyn, H., Molari, L., de Miranda, S., Cnudde, V., & Shahidzadeh, N. (2015). Drying of salt contaminated porous media: Effect of primary and secondary nucleation. *Journal of Applied Physics*, *118*(11), 114901. https://doi.org/10.1063/1.4930292

Ding, J.-L., Wu, M.-C., & Tiyip, T. (2011). Study on soil salinization information in arid region using remote sensing technique. *Agricultural Sciences in China*, *10*(3), 404–411. https://doi.org/10.1016/s1671-2927(11)60019-9

D'Odorico, P., Bhattachan, A., Davis, K. F., Ravi, S., & Runyan, C. W. (2013). Global desertification: Drivers and feedbacks. *Advances in Water Resources*, *51*, 326–344. https://doi.org/10.1016/j.advwatres.2012.01.013

Doerr, S. H., Shakesby, R., & Walsh, R. (2000). Soil water repellency: Its causes, characteristics and hydro-geomorphological significance. *Earth-Science Reviews*, *51*(1–4), 33–65. https://doi.org/10.1016/s0012-8252(00)00011-8

Domenico, P. A., & Schwartz, F. W. (1997). *Physical and chemical hydrogeology* (2nd ed.). John wiley & sons.

Doolittle, J. A., & Brevik, E. C. (2014). The use of electromagnetic induction techniques in soils studies. *Geoderma*, *223*, 33–45. https://doi.org/10.1016/j.geoderma.2014.01.027

Dörler, D., Fritz, S., Voigt-Heucke, S., & Heigl, F. (2021). Citizen science and the role in sustainable development. *Sustainability*, *13*(10), 5676. https://doi.org/10.3390/su13105676

Dowse, R., Palmer, C. G., Hills, K., Torpy, F., & Kefford, B. J. (2017). The mayfly nymph austrophlebioides pusillus harker defies common osmoregulatory assumptions. *Royal Society Open Science*, *4*(1), 160520. https://doi.org/10.1098/rsos.160520

Du, Y., Liu, X., Zhang, L., & Zhou, W. (2023). Drip irrigation in agricultural saline-alkali land controls soil salinity and improves crop yield: Evidence from a global meta-analysis. *Science of the Total Environment*, *880*, 163226. https://doi.org/10.1016/j.scitotenv.2023.163226

Duan, Z., Wang, X., & Sun, L. (2022). Monitoring and mapping of soil salinity on the exposed seabed of the Aral Sea, central Asia. *Water*, *14*(9), 1438. https://doi.org/10.3390/w14091438

East, J. L., Wilcut, C., & Pease, A. A. (2017). Aquatic food-web structure along a salinized dryland river. *Freshwater Biology*, *62*(4), 681–694. https://doi.org/10.1111/fwb.12893

Ebrahimi, F. (2010). Invasion percolation: A computational algorithm for complex phenomena. *Computing in Science & Engineering*, *12*(02), 84–93. https://doi.org/10.1109/mcse.2010.42

El-Din, M. N., King, I., & Tanji, K. (1987). Salinity management model: I. Development. *Journal of Irrigation and Drainage Engineering*, *113*(4), 440–453. https://doi.org/10.1061/(asce)0733-9437(1987)113:4(440)

Eloukabi, H., Sghaier, N., Nasrallah, S. B., & Prat, M. (2013). Experimental study of the effect of sodium chloride on drying of porous media: The crusty–patchy efflorescence transition. *International Journal of Heat and Mass Transfer*, *56*(1–2), 80–93. https://doi.org/10.1016/j.ijheatmasstransfer.2012.09.045

El-Ramady, H., Prokisch, J., Mansour, H., Bayoumi, Y. A., Shalaby, T. A., Veres, S., & Brevik, E. C. (2024). Review of crop response to soil salinity stress: Possible approaches from leaching to nano-management. *Soil Systems*, *8*(1), 11. https://doi.org/10.3390/soilsystems8010011

Elsherpiny, M. A. (2023). Maximizing faba bean tolerance to soil salinity stress using gypsum, compost and selenium. *Egyptian Journal of Soil Science*, *63*(2), 243–253. https://doi.org/10.21608/ejss.2023.203083.1582

Eltarabily, M. G., Amer, A., Farzamian, M., Bouksila, F., Elkiki, M., & Selim, T. (2024). Time-lapse electromagnetic conductivity imaging for soil salinity monitoring in salt-affected agricultural regions. *Land*, *13*(2), 225. https://doi.org/10.3390/land13020225

Espinosa, J. R., Vega, C., Valeriani, C., & Sanz, E. (2015). The crystal-fluid interfacial free energy and nucleation rate of NaCl from different simulation methods. *The Journal of Chemical Physics*, *142*(19), 194709. https://doi.org/10.1063/1.4921185

Espinosa, R. M., Franke, L., Deckelmann, G., & Gunstmann, C. (2007). Gekoppelter wärme-und stofftransport einschließlich der korrosionsprozesse in porösen baustoffen mit dem simulationsprogramm astra. *Bauphysik*, *29*(3), 187–193. https://doi.org/10.1002/bapi.200710026

Eswar, D., Karuppusamy, R., & Chellamuthu, S. (2021). Drivers of soil salinity and their correlation with climate change. *Current Opinion in Environmental Sustainability*, *50*, 310–318. https://doi.org/10.1016/j.cosust.2020.10.015

European Commission Report, Veerman, C., Pinto Correia, T., Bastioli, C., Biro, B., Bouma, J., et al. (2020). Caring for soil is caring for life—Ensure 75 healthy by 2030 for food, people, nature and climate—Report of the mission board for soil health and food. Technical report.

Evangelou, V., & Phillips, R. (1988). Comparison between the gapon and vanselow exchange selectivity coefficients. *Soil Science Society of America Journal*, *52*(2), 379–382. https://doi.org/10.2136/sssaj1988.03615995005200020014x

Fan, X., Pedroli, B., Liu, G., Liu, Q., Liu, H., & Shu, L. (2012). Soil salinity development in the yellow river delta in relation to groundwater dynamics. *Land Degradation & Development*, *23*(2), 175–189. https://doi.org/10.1002/ldr.1071

Fantinel, P., Borgman, O., Holtzman, R., & Goehring, L. (2017). Drying in a microfluidic chip: Experiments and simulations. *Scientific Reports*, *7*(1), 15572. https://doi.org/10.1038/s41598-017-15718-6

FAO. (2000). Extent and causes of salt affected soils in participating countries. Retrieved from http://www.fao.org/ag/agl/agll/spush/topic2.htm

FAO. (2021a). Global map of salt-affected soils gsasmap v1.0. Retrieved from https://www.fao.org/documents/card/en/c/cb7247en

FAO. (2021b). Standard operating procedure for saturated soil paste extract.

FAOITPS. (2015). Status of the world's soil resources (SWSR)—Main report. Technical report. In *Food and agriculture organization of the united nations and intergovernmental technical panel on soils, Rome, Italy*.

Feeney, D. S., Hallett, P. D., Rodger, S., Bengough, A. G., White, N. A., & Young, I. M. (2006). Impact of fungal and bacterial biocides on microbial induced water repellency in arable soil. *Geoderma*, *135*, 72–80. https://doi.org/10.1016/j.geoderma.2005.11.007

Fiola, J. C., Rabenhorst, M. C., Scaduto, E., Seitz, C. R., & Rankin, K. M. (2020). Soil biogeochemistry of the capillary fringe in laboratory mesocosms with contrasting soil textures. *Soil Science Society of America Journal*, *84*(3), 1011–1021. https://doi.org/10.1002/saj2.20076

Fischer, G., Nachtergaele, F., Prieler, S., Van Velthuizen, H., Verelst, L., & Wiberg, D. (2008). *Global agro-ecological zones assessment for agriculture (GAEZ 2008)* (Vol. 10). IIASA, Laxenburg, Austria and FAO.

Fisher, E. (1923). Some factors affecting the evaporation of water from soil. *The Journal of Agricultural Science*, *13*(2), 121–143. https://doi.org/10.1017/s0021859600003270

Flatt, R. J. (2002). Salt damage in porous materials: How high supersaturations are generated. *Journal of Crystal Growth*, *242*(3–4), 435–454. https://doi.org/10.1016/s0022-0248(02)01429-x

Flowers, T. J., & Colmer, T. D. (2008). Salinity tolerance in halophytes. *New Phytologist*, *179*(4), 945–963. https://doi.org/10.1111/j.1469-8137.2008.02531.x

Flowers, T. J., Munns, R., & Colmer, T. D. (2015). Sodium chloride toxicity and the cellular basis of salt tolerance in halophytes. *Annals of Botany*, *115*(3), 419–431. https://doi.org/10.1093/aob/mcu217

Freedman, M. A. (2015). Potential sites for ice nucleation on aluminosilicate clay minerals and related materials. *The Journal of Physical Chemistry Letters*, *6*(19), 3850–3858.

Fujimaki, H., Shimano, T., Inoue, M., & Nakane, K. (2006). Effect of a salt crust on evaporation from a bare saline soil. *Vadose Zone Journal*, *5*(4), 1246–1256. https://doi.org/10.2136/vzj2005.0144

Gamazo, P., Saaltink, M., Carrera, J., Slooten, L., & Bea, S. (2012). A consistent compositional formulation for multiphase reactive transport where chemistry affects hydrodynamics. *Advances in Water Resources*, *35*, 83–93. https://doi.org/10.1016/j.advwatres.2011.09.006

Gapon, E. (1933). Theory of exchange adsorption in soil. *Journal of General Chemistry USSR*, *3*, 144–149.

Gardner, L. R. (2005). Role of geomorphic and hydraulic parameters in governing pore water seepage from salt marsh sediments. *Water Resources Research*, *41*(7), W07502. https://doi.org/10.1029/2004wr003671

Gardner, W., & Fireman, M. (1958). Laboratory studies of evaporation from soil columns in the presence of a water table. *Soil Science*, *85*(5), 244–249. https://doi.org/10.1097/00010694-195805000-00002

Ge, Y., Abuduwaili, J., & Ma, L. (2019). Lakes in arid land and saline dust storms. In *E3S web of conferences* (Vol. 99, p. 01007). EDP Sciences. https://doi.org/10.1051/e3sconf/20199901007

Gebauer, D., Volkel, A., & Colfen, H. (2008). Stable prenucleation calcium carbonate clusters. *Science*, *322*(5909), 1819–1822. https://doi.org/10.1126/science.1164271

Ghanbarian, B., Daigle, H., Hunt, A. G., Ewing, R. P., & Sahimi, M. (2015). Gas and solute diffusion in partially saturated porous media: Percolation theory and effective medium approximation compared with lattice Boltzmann simulations. *Journal of Geophysical Research: Solid Earth*, *120*(1), 182–190. https://doi.org/10.1002/2014jb011645

Ghanbarian-Alavijeh, B., Skinner, T. E., & Hunt, A. G. (2012). Saturation dependence of dispersion in porous media. *Physical review E*, *86*(6), 066316. https://doi.org/10.1103/physreve.86.066316

Ghassemi, F., Jakeman, A. J., & Nix, H. A. (1995). Salinisation of land and water resources: Human causes, extent, management and case studies.

Ghassemzadeh, J., & Sahimi, M. (2004). Molecular modelling of adsorption of gas mixtures in montmorillonites intercalated with Al13-complex pillars. *Molecular Physics*, *102*(13), 1447–1467. https://doi.org/10.1080/00268970410001723037

Giberti, F., Tribello, G. A., & Parrinello, M. (2013). Transient polymorphism in NaCl. *Journal of Chemical Theory and Computation*, *9*(6), 2526–2530. https://doi.org/10.1021/ct4002027

Gillette, D. A. (1974). On the production of soil wind erosion aerosols having the potential for long range transport.

Gillette, D. A., Fryrear, D., Gill, T. E., Ley, T., Cahill, T. A., & Gearhart, E. A. (1997). Relation of vertical flux of particles smaller than 10 μm to total aeolian horizontal mass flux at owens lake. *Journal of Geophysical Research*, *102*(D22), 26009–26015. https://doi.org/10.1029/97jd02252

Gollo, V. S., Sahimi, M., González, E., Hajati, M.-C., Elbracht, J., Fröhle, P., & Shokri, N. (2024). Soil salinization due to saltwater intrusion in coastal regions: The role of soil characteristics and heterogeneity. *InterPore Journal*, *1*(1), ipj2604246. https://doi.org/10.69631/ipj.v1i1nr15

Gong, S., Bai, X., Luo, G., Li, C., Wu, L., Chen, F., et al. (2023). Climate change has enhanced the positive contribution of rock weathering to the major ions in riverine transport. *Global and Planetary Change*, *228*, 104203. https://doi.org/10.1016/j.gloplacha.2023.104203

Goovaerts, P. (1997). *Geostatistics for natural resources evaluation*. Oxford University Press.

Gopalakrishnan, T., Hasan, M. K., Haque, A. S., Jayasinghe, S. L., & Kumar, L. (2019). Sustainability of coastal agriculture under climate change. *Sustainability*, *11*(24), 7200. https://doi.org/10.3390/su11247200

Gorji, T., Yıldırım, A., Sertel, E., & Tanık, A. (2019). Remote sensing approaches and mapping methods for monitoring soil salinity under different climate regimes. *International Journal of Electronic Governance*, *6*(1), 33–49. https://doi.org/10.30897/ijegeo.500452

Gran, M., Carrera, J., Olivella, S., & Saaltink, M. W. (2011). Modeling evaporation processes in a saline soil from saturation to oven dry conditions. *Hydrology and Earth System Sciences*, *15*(7), 2077–2089. https://doi.org/10.5194/hess-15-2077-2011

Gray, E., & Smith, D. L. (2005). Intracellular and extracellular pgpr: Commonalities and distinctions in the plant–bacterium signaling processes. *Soil Biology and Biochemistry*, *37*(3), 395–412. https://doi.org/10.1016/j.soilbio.2004.08.030

Green, S. M., Machin, R., & Cresser, M. S. (2008). Long-term road salting effects on dispersion of organic matter from roadside soils into drainage water. *Chemistry and Ecology*, *24*(3), 221–231. https://doi.org/10.1080/02757540802032181

Greene, R., Timms, W., Rengasamy, P., Arshad, M., & Cresswell, R. (2016). Soil and aquifer salinization: Toward an integrated approach for salinity management of groundwater. In *Integrated groundwater management: Concepts, approaches and challenges* (pp. 377–412).

Greenway, H., & Munns, R. (1980). Mechanisms of salt tolerance in nonhalophytes. *Annual Review of Plant Physiology*, *31*(1), 149–190. https://doi.org/10.1146/annurev.pp.31.060180.001053

Greiner, R., & Cacho, O. (2001). On the efficient use of a catchment's land and water resources: Dryland salinization in Australia. *Ecological Economics*, *38*(3), 441–458. https://doi.org/10.1016/s0921-8009(01)00192-6

Gu, S., Jiang, S., Li, X., Zheng, N., & Xia, X. (2023). Soil salinity simulation based on electromagnetic induction and deep learning. *Soil and Tillage Research*, *230*, 105706. https://doi.org/10.1016/j.still.2023.105706

Guglielmini, L., Gontcharov, A., Aldykiewicz, A. J., & Stone, H. A. (2008). Drying of salt solutions in porous materials: Intermediate-time dynamics and efflorescence. *Physics of Fluids*, *20*(7), 077101. https://doi.org/10.1063/1.2954037

Gupta, B., & Huang, B. (2014). Mechanism of salinity tolerance in plants: Physiological, biochemical, and molecular characterization. *International Journal of Genomics*, *2014*, 1–18. https://doi.org/10.1155/2014/701596

Gupta, R. K., Abrol, I. P., Finkl, C. W., Kirkham, M. B., Arbestain, M. C., Macías, F., et al. (2008). *Solonchaks* (pp. 737–738). Springer Netherlands. https://doi.org/10.1007/978-1-4020-3995-9_566

Hailu, B., & Mehari, H. (2021). Impacts of soil salinity/sodicity on soil-water relations and plant growth in dry land areas: A review. *Journal of Natural Sciences Research*, *12*, 1–10.

Haj-Amor, Z., Araya, T., Kim, D.-G., Bouri, S., Lee, J., Ghiloufi, W., et al. (2022). Soil salinity and its associated effects on soil microorganisms, greenhouse gas emissions, crop yield, biodiversity and desertification: A review. *Science of the Total Environment*, *843*, 156946. https://doi.org/10.1016/j.scitotenv.2022.156946

Hajirezaie, S., Wu, X., & Peters, C. A. (2017). Scale formation in porous media and its impact on reservoir performance during water flooding. *Journal of Natural Gas Science and Engineering*, *39*, 188–202. https://doi.org/10.1016/j.jngse.2017.01.019

Han, J., Kim, M., Mammadov, Z., Lee, S., Elzinga, E. J., Mammadov, G., et al. (2024). Synergistic effect of climate change and water management: Historical and future soil salinity in the Kur-Araz lowland, Azerbaijan. *Science of the Total Environment*, *907*, 167720. https://doi.org/10.1016/j.scitotenv.2023.167720

Han, Y., Ge, H., Xu, Y., Zhuang, L., Wang, F., Gu, Q., & Li, X. (2023). Estimating soil salinity using multiple spectral indexes and machine learning algorithm in songnen plain, China. *IEEE Journal of Selected Topics in Applied Earth Observations and Remote Sensing*, *16*, 7041–7050. https://doi.org/10.1109/jstars.2023.3274579

Hashemi, M., Dabir, B., & Sahimi, M. (1999). Dynamics of two-phase flow in porous media: Simultaneous invasion of two fluids. *AIChE Journal*, *45*(7), 1365–1382. https://doi.org/10.1002/aic.690450702

Hashemi, M., Sahimi, M., & Dabir, B. (1998). Percolation with two invaders and two defenders: Volatile clusters, oscillations, and scaling. *Physical Review Letters*, *80*(15), 3248–3251. https://doi.org/10.1103/physrevlett.80.3248

Hassan, F., & Ghaibeh, A. S. (1977). Evaporation and salt movement in soils in the presence of water table. *Soil Science Society of America Journal*, *41*(3), 470–478. https://doi.org/10.2136/sssaj1977.03615995004100030008x

Hassani, A., Azapagic, A., D'Odorico, P., Keshmiri, A., & Shokri, N. (2020). Desiccation crisis of saline lakes: A new decision-support framework for building resilience to climate change. *Science of the Total Environment*, *703*, 134718. https://doi.org/10.1016/j.scitotenv.2019.134718

Hassani, A., Azapagic, A., & Shokri, N. (2020). Predicting long-term dynamics of soil salinity and sodicity on a global scale. *Proceedings of the National Academy of Sciences*, *117*(52), 33017–33027. https://doi.org/10.1073/pnas.2013771117

Hassani, A., Azapagic, A., & Shokri, N. (2021). Global predictions of primary soil salinization under changing climate in the 21st century. *Nature Communications*, *12*(1), 6663. https://doi.org/10.1038/s41467-021-26907-3

Hassani, A., Smith, P., & Shokri, N. (2024). Negative correlation between soil salinity and soil organic carbon variability. *Proceedings of the National Academy of Sciences*, *121*(18), e2317332121. https://doi.org/10.1073/pnas.2317332121

Hazlehurst Jr., T., Martin, H. C., & Brewer, L. (1936). The creeping of saturated salt solutions. *The Journal of Physical Chemistry*, *40*(4), 439–452. https://doi.org/10.1021/j150373a003

Head, J. S., Crockatt, M. E., Didarali, Z., Woodward, M.-J., & Emmett, B. A. (2020). The role of citizen science in meeting sdg targets around soil health. *Sustainability*, *12*(24), 10254. https://doi.org/10.3390/su122410254

Heiss, J. W., Mase, B., & Shen, C. (2022). Effects of future increases in tidal flooding on salinity and groundwater dynamics in coastal aquifers. *Water Resources Research*, *58*(12), e2022WR033195. https://doi.org/10.1029/2022wr033195

Hekmatzadeh, M., Dadvar, M., & Sahimi, M. (2016). Pore-network simulation of unstable miscible displacements in porous media. *Transport in Porous Media*, *113*(3), 511–529. https://doi.org/10.1007/s11242-016-0708-9

Henman, J., & Poulter, B. (2008). Inundation of freshwater peatlands by sea level rise: Uncertainty and potential carbon cycle feedbacks. *Journal of Geophysical Research*, *113*(G1), G01011. https://doi.org/10.1029/2006jg000395
Herbert, E. R., Boon, P., Burgin, A. J., Neubauer, S. C., Franklin, R. B., Ardón, M., et al. (2015). A global perspective on wetland salinization: Ecological consequences of a growing threat to freshwater wetlands. *Ecosphere*, *6*(10), 1–43. https://doi.org/10.1890/es14-00534.1
Hernandez Gonzalez, L. M., Rivera, V. A., Akosa, D., Phillips, C. B., Hatch, S. L., Miller, W. M., & Packman, A. I. (2023). Road salt intrusion dynamics in an ex-urban native wetland complex. *PLOS Water*, *2*(7), e0000148. https://doi.org/10.1371/journal.pwat.0000148
Herrero, J., & Pérez-Coveta, O. (2005). Soil salinity changes over 24 years in a mediterranean irrigated district. *Geoderma*, *125*(3–4), 287–308. https://doi.org/10.1016/j.geoderma.2004.09.004
Hillel, D. (2000). *Salinity management for sustainable irrigation: Integrating science, environment, and economics*. World Bank Publications.
Hintz, W. D., Fay, L., & Relyea, R. A. (2022). Road salts, human safety, and the rising salinity of our fresh waters. *Frontiers in Ecology and the Environment*, *20*(1), 22–30. https://doi.org/10.1002/fee.2433
Hird, R., & Bolton, M. D. (2016). Migration of sodium chloride in dry porous materials. *Proceedings of the Royal Society A: Mathematical, Physical and Engineering Sciences*, *472*(2186), 20150710. https://doi.org/10.1098/rspa.2015.0710
Hogg, T., & Henry, J. (1984). Comparison of 1: 1 and 1: 2 suspensions and extracts with the saturation extract in estimating salinity in saskatchewan soils. *Canadian Journal of Soil Science*, *64*(4), 699–704. https://doi.org/10.4141/cjss84-069
Homaee, M., Feddes, R., & Dirksen, C. (2002). Simulation of root water uptake: III. Non-uniform transient combined salinity and water stress. *Agricultural Water Management*, *57*(2), 127–144. https://doi.org/10.1016/s0378-3774(02)00073-2
Hopmans, J. W., Qureshi, A., Kisekka, I., Munns, R., Grattan, S., Rengasamy, P., et al. (2021). Critical knowledge gaps and research priorities in global soil salinity. *Advances in Agronomy*, *169*, 1–191. https://doi.org/10.1016/bs.agron.2021.03.001
Hoppel, W., Fitzgerald, J., Frick, G., Larson, R., & Mack, E. (1990). Aerosol size distributions and optical properties found in the marine boundary layer over the Atlantic Ocean. *Journal of Geophysical Research*, *95*(D4), 3659–3686. https://doi.org/10.1029/jd095id04p03659
Hosseini, S. A., & Alfi, M. (2016). Time-lapse application of pressure transient analysis for monitoring compressible fluid leakage. *Greenhouse Gases: Science and Technology*, *6*(3), 352–369. https://doi.org/10.1002/ghg.1570
Hu, S., Zhang, C., & Lu, N. (2023). Quantifying coupling effects between soil matric potential and osmotic potential. *Water Resources Research*, *59*(2), e2022WR033779. https://doi.org/10.1029/2022wr033779
Huinink, H., Pel, L., & Michels, M. V. A. (2002). How ions distribute in a drying porous medium: A simple model. *Physics of Fluids*, *14*(4), 1389–1395. https://doi.org/10.1063/1.1451081
Huizer, S., Karaoulis, M., Oude Essink, G., & Bierkens, M. (2017). Monitoring and simulation of salinity changes in response to tide and storm surges in a sandy coastal aquifer system. *Water Resources Research*, *53*(8), 6487–6509. https://doi.org/10.1002/2016wr020339
Inam, A., Adamowski, J., Prasher, S., Halbe, J., Malard, J., & Albano, R. (2017). Coupling of a distributed stakeholder-built system dynamics socio-economic model with sahysmod for sustainable soil salinity management—Part 1: Model development. *Journal of Hydrology*, *551*, 596–618. https://doi.org/10.1016/j.jhydrol.2017.03.039
Intergovernmental Panel on Climate Change. (2022). *Land degradation* (pp. 345–436). Cambridge University Press.
Isbell, R. (2016). *The Australian soil classification*. CSIRO publishing.
Ivushkin, K., Bartholomeus, H., Bregt, A. K., Pulatov, A., Kempen, B., & De Sousa, L. (2019). Global mapping of soil salinity change. *Remote Sensing of Environment*, *231*, 111260. https://doi.org/10.1016/j.rse.2019.111260
Jacques, D., & Šimůnek, J. (2005). *User manual of the multicomponent variably-saturated flow and transport model hp1. Technical report*. SCK-CEN.
Jalili, S., Moazed, H., Boroomand, N., & Naseri, A. (2011). Assessment of evaporation and salt accumulation in bare soil: Constant shallow water table depth with saline ground water. *Scientific Research and Essays*, *6*(29), 6068–6074. https://doi.org/10.5897/sre11.509
Jambhekar, V., Helmig, R., Schröder, N., & Shokri, N. (2015). Free-flow–porous-media coupling for evaporation-driven transport and precipitation of salt in soil. *Transport in Porous Media*, *110*(2), 251–280. https://doi.org/10.1007/s11242-015-0516-7
Jambhekar, V., Mejri, E., Schröder, N., Helmig, R., & Shokri, N. (2016). Kinetic approach to model reactive transport and mixed salt precipitation in a coupled free-flow–porous-media system. *Transport in Porous Media*, *114*(2), 341–369. https://doi.org/10.1007/s11242-016-0665-3
Jamil, A., Riaz, S., Ashraf, M., & Foolad, M. (2011). Gene expression profiling of plants under salt stress. *Critical Reviews in Plant Sciences*, *30*(5), 435–458. https://doi.org/10.1080/07352689.2011.605739
John, M., Pannell, D., & Kingwell, R. (2005). Climate change and the economics of farm management in the face of land degradation: Dryland salinity in Western Australia. *Canadian Journal of Agricultural Economics/Revue canadienne d'agroeconomie*, *53*(4), 443–459. https://doi.org/10.1111/j.1744-7976.2005.00029.x
Jolly, I. D., McEwan, K. L., & Holland, K. L. (2008). A review of groundwater–surface water interactions in arid/semi-arid wetlands and the consequences of salinity for wetland ecology. *Ecohydrology: Ecosystems, Land and Water Process Interactions, Ecohydrogeomorphology*, *1*(1), 43–58. https://doi.org/10.1002/eco.6
Juan, P., Mateu, J., Jordan, M., Mataix-Solera, J., Meléndez-Pastor, I., & Navarro-Pedreño, J. (2011). Geostatistical methods to identify and map spatial variations of soil salinity. *Journal of Geochemical Exploration*, *108*(1), 62–72. https://doi.org/10.1016/j.gexplo.2010.10.003
Kalma, J. D., McVicar, T. R., & McCabe, M. F. (2008). Estimating land surface evaporation: A review of methods using remotely sensed surface temperature data. *Surveys in Geophysics*, *29*(4–5), 421–469. https://doi.org/10.1007/s10712-008-9037-z
Kamai, T., & Assouline, S. (2018). Evaporation from deep aquifers in arid regions: Analytical model for combined liquid and vapor water fluxes. *Water Resources Research*, *54*(7), 4805–4822. https://doi.org/10.1029/2018wr023030
Kaplan, G., Gašparović, M., Alqasemi, A. S., Aldhaheri, A., Abuelgasim, A., & Ibrahim, M. (2023). Soil salinity prediction using machine learning and sentinel–2 remote sensing data in hyper–arid areas. *Physics and Chemistry of the Earth, Parts A/B/C*, *130*, 103400. https://doi.org/10.1016/j.pce.2023.103400
Kargas, G., Londra, P., & Sotirakoglou, K. (2022). The effect of soil texture on the conversion factor of 1: 5 soil/water extract electrical conductivity (EC 1: 5) to soil saturated paste extract electrical conductivity (ECE). *Water*, *14*(4), 642. https://doi.org/10.3390/w14040642
Karmakar, R., Das, I., Dutta, D., & Rakshit, A. (2016). Potential effects of climate change on soil properties: A review. *Science International*, *4*(2), 51–73. https://doi.org/10.17311/sciintl.2016.51.73
Karthika, S., Radhakrishnan, T., & Kalaichelvi, P. (2016). A review of classical and nonclassical nucleation theories. *Crystal Growth & Design*, *16*(11), 6663–6681. https://doi.org/10.1021/acs.cgd.6b00794
Kefford, B. J., Marchant, R., Schäfer, R. B., Metzeling, L., Dunlop, J. E., Choy, S. C., & Goonan, P. (2011). The definition of species richness used by species sensitivity distributions approximates observed effects of salinity on stream macroinvertebrates. *Environmental Pollution*, *159*(1), 302–310. https://doi.org/10.1016/j.envpol.2010.08.025

Kharaghani, A., Mahmood, H. T., Wang, Y., & Tsotsas, E. (2021). Three-dimensional visualization and modeling of capillary liquid rings observed during drying of dense particle packings. *International Journal of Heat and Mass Transfer*, *177*, 121505. https://doi.org/10.1016/j.ijheatmasstransfer.2021.121505

Kharaghani, A., Metzger, T., & Tsotsas, E. (2012). An irregular pore network model for convective drying and resulting damage of particle aggregates. *Chemical Engineering Science*, *75*, 267–278. https://doi.org/10.1016/j.ces.2012.03.038

Khasanov, S., Kulmatov, R., Li, F., van Amstel, A., Bartholomeus, H., Aslanov, I., et al. (2023). Impact assessment of soil salinity on crop production in Uzbekistan and its global significance. *Agriculture, Ecosystems & Environment*, *342*, 108262. https://doi.org/10.1016/j.agee.2022.108262

Khatei, G., Rinaldo, T., Van Pelt, R. S., D'Odorico, P., & Ravi, S. (2024). Wind erodibility and particulate matter emissions of salt-affected soils: The case of dry soils in a low humidity atmosphere. *Journal of Geophysical Research: Atmospheres*, *129*(1), e2023JD039576. https://doi.org/10.1029/2023jd039576

Kibria, M. G., & Hoque, M. A. (2019). A review on plant responses to soil salinity and amelioration strategies. *Open Journal of Soil Science*, *9*(11), 219–231. https://doi.org/10.4236/ojss.2019.911013

Kim, M., Sell, A., & Sinton, D. (2013). Aquifer-on-a-chip: Understanding pore-scale salt precipitation dynamics during CO_2 sequestration. *Lab on a Chip*, *13*(13), 2508–2518. https://doi.org/10.1039/c3lc00031a

Kim, N., Harale, A., Tsotsis, T. T., & Sahimi, M. (2007). Atomistic simulation of nanoporous layered double hydroxide materials and their properties. II. adsorption and diffusion. *The Journal of Chemical Physics*, *127*(22), 224701. https://doi.org/10.1063/1.2799985

Kim, N., Kim, Y., Tsotsis, T. T., & Sahimi, M. (2005). Atomistic simulation of nanoporous layered double hydroxide materials and their properties. I. structural modeling. *The Journal of Chemical Physics*, *122*(21), 214713. https://doi.org/10.1063/1.1902945

King, J., Etyemezian, V., Sweeney, M., Buck, B. J., & Nikolich, G. (2011). Dust emission variability at the Salton Sea, California, USA. *Aeolian Research*, *3*(1), 67–79. https://doi.org/10.1016/j.aeolia.2011.03.005

Knackstedt, M. A., Sahimi, M., & Sheppard, A. P. (2000). Invasion percolation with long-range correlations: First-order phase transition and nonuniversal scaling properties. *Physical Review E*, *61*(5), 4920–4934. https://doi.org/10.1103/physreve.61.4920

Ko, J.-Y., Day, J., Barras, J., Morton, R., Johnston, J., Steyer, G., et al. (2004). Impacts of oil and gas activities on coastal wetland loss in the Mississippi delta. *Environmental Analysis of the Gulf of Mexico*, *1*, 608–621.

Kok, J. F., Parteli, E. J., Michaels, T. I., & Karam, D. B. (2012). The physics of wind-blown sand and dust. *Reports on Progress in Physics*, *75*(10), 106901. https://doi.org/10.1088/0034-4885/75/10/106901

Koniorczyk, M. (2012). Salt transport and crystallization in non-isothermal, partially saturated porous materials considering ions interaction model. *International Journal of Heat and Mass Transfer*, *55*(4), 665–679. https://doi.org/10.1016/j.ijheatmasstransfer.2011.10.043

Kraamwinkel, C. T., Beaulieu, A., Dias, T., & Howison, R. A. (2021). Planetary limits to soil degradation. *Communications Earth & Environment*, *2*(1), 249. https://doi.org/10.1038/s43247-021-00323-3

Krischer, O. (1956). *Die wissenschaftlichen Grundlagen der Trocknungstechnik*. Springer.

Kumar, P., & Sharma, P. K. (2020). Soil salinity and food security in India. *Frontiers in Sustainable Food Systems*, *4*, 533781. https://doi.org/10.3389/fsufs.2020.533781

Kumar, R., Singh, A., Bhardwaj, A. K., Kumar, A., Yadav, R. K., & Sharma, P. C. (2022). Reclamation of salt-affected soils in India: Progress, emerging challenges, and future strategies. *Land Degradation & Development*, *33*(13), 2169–2180. https://doi.org/10.1002/ldr.4320

Kume, T., Umetsu, C., & Palanisami, K. (2009). Impact of the december 2004 Tsunami on soil, groundwater and vegetation in the nagapattinam district, India. *Journal of Environmental Management*, *90*(10), 3147–3154. https://doi.org/10.1016/j.jenvman.2009.05.027

Lanaro, G., & Patey, G. (2016). Birth of nacl crystals: Insights from molecular simulations. *The Journal of Physical Chemistry B*, *120*(34), 9076–9087. https://doi.org/10.1021/acs.jpcb.6b05291

Land, N., & Audit, W. R. (2001). *Australian dryland salinity assessment 2000: Extent, impacts, processes, monitoring and management options*. Commonwealth of Australia.

Lane, C. R., Leibowitz, S. G., Autrey, B. C., LeDuc, S. D., & Alexander, L. C. (2018). Hydrological, physical, and chemical functions and connectivity of non-floodplain wetlands to downstream waters: A review. *JAWRA Journal of the American Water Resources Association*, *54*(2), 346–371. https://doi.org/10.1111/1752-1688.12633

Lavalle, J. (1853). Comptes rendus hebdomadaires des séances de l'académie. *Des Sciences*, *36*, 493.

Le, D., Hoang, H., & Mahadevan, J. (2009). Impact of capillary-driven liquid films on salt crystallization. *Transport in Porous Media*, *80*(2), 229–252. https://doi.org/10.1007/s11242-009-9353-x

Le, K. H., Kharaghani, A., Kirsch, C., & Tsotsas, E. (2017). Discrete pore network modeling of superheated steam drying. *Drying Technology*, *35*(13), 1584–1601. https://doi.org/10.1080/07373937.2016.1264414

Le Bray, Y., & Prat, M. (1999). Three-dimensional pore network simulation of drying in capillary porous media. *International Journal of Heat and Mass Transfer*, *42*(22), 4207–4224. https://doi.org/10.1016/s0017-9310(99)00006-x

Lehmann, P., Assouline, S., & Or, D. (2008). Characteristic lengths affecting evaporative drying of porous media. *Physical Review E*, *77*(5), 056309. https://doi.org/10.1103/physreve.77.056309

Lehmann, P., & Or, D. (2009). Evaporation and capillary coupling across vertical textural contrasts in porous media. *Physical Review E*, *80*(4), 046318. https://doi.org/10.1103/physreve.80.046318

Leogrande, R., & Vitti, C. (2019). Use of organic amendments to reclaim saline and sodic soils: A review. *Arid Land Research and Management*, *33*(1), 1–21. https://doi.org/10.1080/15324982.2018.1498038

Leung, S. S., MacKinnon, M. D., & Smith, R. E. (2003). The ecological effects of naphthenic acids and salts on phytoplankton from the Athabasca oil sands region. *Aquatic Toxicology*, *62*(1), 11–26. https://doi.org/10.1016/s0166-445x(02)00057-7

Levin, L. A., Bett, B. J., Gates, A. R., Heimbach, P., Howe, B. M., Janssen, F., et al. (2019). Global observing needs in the deep ocean. *Frontiers in Marine Science*, *6*, 241. https://doi.org/10.3389/fmars.2019.00241

Lewis, W. K. (1921). The rate of drying of solid materials. *Industrial & Engineering Chemistry*, *13*(5), 427–432. https://doi.org/10.1021/ie50137a021

Li, X., Chang, S. X., & Salifu, K. F. (2014). Soil texture and layering effects on water and salt dynamics in the presence of a water table: A review. *Environmental Reviews*, *22*(1), 41–50. https://doi.org/10.1139/er-2013-0035

Licsandru, G., Noiriel, C., Geoffroy, S., Abou-Chakra, A., Duru, P., & Prat, M. (2022). Detachment mechanism and reduced evaporation of an evaporative nacl salt crust. *Scientific Reports*, *12*(1), 7473. https://doi.org/10.1038/s41598-022-11541-w

Litalien, A., & Zeeb, B. (2020). Curing the Earth: A review of anthropogenic soil salinization and plant-based strategies for sustainable mitigation. *Science of the Total Environment*, *698*, 134235. https://doi.org/10.1016/j.scitotenv.2019.134235

Liu, B., Zhao, W., Wen, Z., Yang, Y., Chang, X., Yang, Q., et al. (2019). Mechanisms and feedbacks for evapotranspiration-induced salt accumulation and precipitation in an arid wetland of China. *Journal of Hydrology*, *568*, 403–415. https://doi.org/10.1016/j.jhydrol.2018.11.004

Liu, D., Abuduwaili, J., Lei, J., & Wu, G. (2011). Deposition rate and chemical composition of the aeolian dust from a bare saline playa, Ebinur Lake, Xinjiang, China. *Water, Air, & Soil Pollution*, *218*(1–4), 175–184. https://doi.org/10.1007/s11270-010-0633-4

Liu, L., Wu, Y., Yin, M., Ma, X., Yu, X., Guo, X., et al. (2023). Soil salinity, not plant genotype or geographical distance, shapes soil microbial community of a reed wetland at a fine scale in the yellow river delta. *Science of the Total Environment*, *856*, 159136. https://doi.org/10.1016/j.scitotenv.2022.159136

Loh, N. D., Sen, S., Bosman, M., Tan, S. F., Zhong, J., Nijhuis, C. A., et al. (2017). Multistep nucleation of nanocrystals in aqueous solution. *Nature Chemistry*, *9*(1), 77–82. https://doi.org/10.1038/nchem.2618

Lu, H., & Shao, Y. (1999). A new model for dust emission by saltation bombardment. *Journal of Geophysical Research*, *104*(D14), 16827–16842. https://doi.org/10.1029/1999jd900169

Lu, X., Tsotsas, E., & Kharaghani, A. (2021). Drying of capillary porous media simulated by coupling of continuum-scale and micro-scale models. *International Journal of Multiphase Flow*, *140*, 103654. https://doi.org/10.1016/j.ijmultiphaseflow.2021.103654

Lüttge, U. (1993). The role of crassulacean acid metabolism (CAM) in the adaptation of plants to salinity. *New Phytologist*, *125*(1), 59–71. https://doi.org/10.1111/j.1469-8137.1993.tb03864.x

Ma, S., He, B., Ge, X., & Luo, X. (2023). Spatial prediction of soil salinity based on the google Earth engine platform with multitemporal synthetic remote sensing images. *Ecological Informatics*, *75*, 102111. https://doi.org/10.1016/j.ecoinf.2023.102111

Ma, Y., & Tashpolat, N. (2023). Current status and development trend of soil salinity monitoring research in China. *Sustainability*, *15*(7), 5874. https://doi.org/10.3390/su15075874

Maas, E. V., & Grattan, S. (1999). Crop yields as affected by salinity. *Agricultural Drainage*, *38*, 55–108. https://doi.org/10.2134/agronmonogr38.c3

Mahadevan, J., Sharma, M. M., & Yortsos, Y. C. (2006). Flow-through drying of porous media. *AIChE Journal*, *52*(7), 2367–2380. https://doi.org/10.1002/aic.10859

Mahmood, H. T., Tsotsas, E., & Kharaghani, A. (2021). The role of discrete capillary rings in mass transfer from the surface of a drying capillary porous medium. *Transport in Porous Media*, *140*(1), 351–369. https://doi.org/10.1007/s11242-021-01635-w

Malmir, H., Sahimi, M., & Tabar, M. R. R. (2016a). Microstructural characterization of random packings of cubic particles. *Scientific Reports*, *6*(1), 35024. https://doi.org/10.1038/srep35024

Malmir, H., Sahimi, M., & Tabar, M. R. R. (2016b). Packing of nonoverlapping cubic particles: Computational algorithms and microstructural characteristics. *Physical Review E*, *94*(6), 062901. https://doi.org/10.1103/physreve.94.062901

Malmir, H., Sahimi, M., & Tabar, M. R. R. (2017). Statistical characterization of microstructure of packings of polydisperse hard cubes. *Physical Review E*, *95*(5), 052902. https://doi.org/10.1103/physreve.95.052902

Mardi, A. H., Khaghani, A., MacDonald, A. B., Nguyen, P., Karimi, N., Heidary, P., et al. (2018). The lake Urmia environmental disaster in Iran: A look at aerosol pollution. *Science of the Total Environment*, *633*, 42–49. https://doi.org/10.1016/j.scitotenv.2018.03.148

Márkus, A., & Házi, G. (2011). Simulation of evaporation by an extension of the pseudopotential lattice Boltzmann method: A quantitative analysis. *Physical Review E*, *83*(4), 046705. https://doi.org/10.1103/physreve.83.046705

Masoudi, M., Fazeli, H., Miri, R., & Hellevang, H. (2021). Pore scale modeling and evaluation of clogging behavior of salt crystal aggregates in CO_2-rich phase during carbon storage. *International Journal of Greenhouse Gas Control*, *111*, 103475. https://doi.org/10.1016/j.ijggc.2021.103475

Matthees, H. L., He, Y., Owen, R. K., Hopkins, D., Deutsch, B., Lee, J., et al. (2017). Predicting soil electrical conductivity of the saturation extract from a 1:1 soil to water ratio. *Communications in Soil Science and Plant Analysis*, *48*(18), 2148–2154. https://doi.org/10.1080/00103624.2017.1407780

Mau, Y., & Porporato, A. (2015). A dynamical system approach to soil salinity and sodicity. *Advances in Water Resources*, *83*, 68–76. https://doi.org/10.1016/j.advwatres.2015.05.010

Mazhar, S., Pellegrini, E., Contin, M., Bravo, C., & De Nobili, M. (2022). Impacts of salinization caused by sea level rise on the biological processes of coastal soils-a review. *Frontiers in Environmental Science*, *10*, 909415. https://doi.org/10.3389/fenvs.2022.909415

McFarland, M. L., Ueckert, D. N., & Hartmann, S. (1987). Revegetation of oil well reserve pits in west Texas. *Rangeland Ecology & Management/Journal of Range Management Archives*, *40*(2), 122–127. https://doi.org/10.2307/3899202

McNeill, J. D. (1980). Electromagnetic terrain conductivity measurement at low induction numbers. Technical Note TN-6.

Mendoza, F. N., & Alejandre, J. (2013). The role of ion–water interactions in the solubility of ionic solutions. *Journal of Molecular Liquids*, *185*, 50–55. https://doi.org/10.1016/j.molliq.2012.09.020

Metternicht, G. I., & Zinck, J. (2003). Remote sensing of soil salinity: Potentials and constraints. *Remote Sensing of Environment*, *85*(1), 1–20. https://doi.org/10.1016/s0034-4257(02)00188-8

Millington, R., & Quirk, J. (1961). Permeability of porous solids. *Transactions of the Faraday Society*, *57*, 1200–1207. https://doi.org/10.1039/tf9615701200

Milly, P. (1986). An event-based simulation model of moisture and energy fluxes at a bare soil surface. *Water Resources Research*, *22*(12), 1680–1692. https://doi.org/10.1029/wr022i012p01680

Miri, R., van Noort, R., Aagaard, P., & Hellevang, H. (2015). New insights on the physics of salt precipitation during injection of CO_2 into saline aquifers. *International Journal of Greenhouse Gas Control*, *43*, 10–21. https://doi.org/10.1016/j.ijggc.2015.10.004

Mishra, A. K., Das, R., George Kerry, R., Biswal, B., Sinha, T., Sharma, S., et al. (2023). Promising management strategies to improve crop sustainability and to amend soil salinity. *Frontiers in Environmental Science*, *10*, 962581. https://doi.org/10.3389/fenvs.2022.962581

Mohamed, A.-M. O., El Gamal, M., & Zekri, A. Y. (2003). Effect of salinity and temperature on water cut determination in oil reservoirs. *Journal of Petroleum Science and Engineering*, *40*(3–4), 177–188. https://doi.org/10.1016/s0920-4105(03)00137-2

Mohamed, S. A., Metwaly, M. M., Metwalli, M. R., AbdelRahman, M. A., & Badreldin, N. (2023). Integrating active and passive remote sensing data for mapping soil salinity using machine learning and feature selection approaches in arid regions. *Remote Sensing*, *15*(7), 1751. https://doi.org/10.3390/rs15071751

Mohanty, B. P., & Skaggs, T. (2001). Spatio-temporal evolution and time-stable characteristics of soil moisture within remote sensing footprints with varying soil, slope, and vegetation. *Advances in Water Resources*, *24*(9–10), 1051–1067. https://doi.org/10.1016/s0309-1708(01)00034-3

Monahan, E. C., Spiel, D. E., & Davidson, K. L. (1986). A model of marine aerosol generation via whitecaps and wave disruption. In *Oceanic whitecaps: And their role in air-sea exchange processes* (pp. 167–174). Springer.

Mooney, R., Keenan, A., & Wood, L. (1952). Adsorption of water vapor by montmorillonite. II. Effect of exchangeable ions and lattice swelling as measured by X-ray diffraction. *Journal of the American Chemical Society*, *74*(6), 1371–1374. https://doi.org/10.1021/ja01126a002

Morudu, M. (2009). Saline waste information sheet. Retrieved from https://sawic.environment.gov.za/documents/5328.pdf

Mosthaf, K., Baber, K., Flemisch, B., Helmig, R., Leijnse, A., Rybak, I., & Wohlmuth, B. (2011). A coupling concept for two-phase compositional porous-medium and single-phase compositional free flow. *Water Resources Research*, *47*(10), W10522. https://doi.org/10.1029/2011wr010685

Mourad, K. A., Hosseini, S. H., & Avery, H. (2020). The role of citizen science in sustainable agriculture. *Sustainability*, *12*(24), 10375. https://doi.org/10.3390/su122410375

Muhammad, M., Waheed, A., Wahab, A., Majeed, M., Nazim, M., Liu, Y.-H., et al. (2023). Soil salinity and drought tolerance: An evaluation of plant growth, productivity, microbial diversity, and amelioration strategies. *Plant Stress*, *11*, 100319. https://doi.org/10.1016/j.stress.2023.100319

Mukhopadhyay, R., Sarkar, B., Jat, H. S., Sharma, P. C., & Bolan, N. S. (2021). Soil salinity under climate change: Challenges for sustainable agriculture and food security. *Journal of Environmental Management*, *280*, 111736. https://doi.org/10.1016/j.jenvman.2020.111736

Mulder, V., De Bruin, S., Schaepman, M. E., & Mayr, T. (2011). The use of remote sensing in soil and terrain mapping—A review. *Geoderma*, *162*(1–2), 1–19. https://doi.org/10.1016/j.geoderma.2010.12.018

Muller, M., Schreiner, B., Smith, L., van Koppen, B., Sally, H., Aliber, M., et al. (2009). Water security in South Africa. In *Development planning Division. Working paper series* (Vol. 12).

Munns, R. (1993). Physiological processes limiting plant growth in saline soils: Some dogmas and hypotheses. *Plant, Cell and Environment*, *16*(1), 15–24. https://doi.org/10.1111/j.1365-3040.1993.tb00840.x

Munns, R. (2002). Comparative physiology of salt and water stress. *Plant, Cell and Environment*, *25*(2), 239–250. https://doi.org/10.1046/j.0016-8025.2001.00808.x

Munns, R., & Gilliham, M. (2015). Salinity tolerance of crops—What is the cost? *New Phytologist*, *208*(3), 668–673. https://doi.org/10.1111/nph.13519

Munns, R., & Tester, M. (2008). Mechanisms of salinity tolerance. *Annual Review of Plant Biology*, *59*(1), 651–681. https://doi.org/10.1146/annurev.arplant.59.032607.092911

Muwamba, A., Nkedi-Kizza, P., & Morgan, K. (2018). Effect of water table depth on nutrient concentrations below the water table in a spodosol. *Water, Air, & Soil Pollution*, *229*(3), 1–14. https://doi.org/10.1007/s11270-018-3727-z

Nachshon, U., Shahraeeni, E., Or, D., Dragila, M., & Weisbrod, N. (2011). Infrared thermography of evaporative fluxes and dynamics of salt deposition on heterogeneous porous surfaces. *Water Resources Research*, *47*(12), W12519. https://doi.org/10.1029/2011wr010776

Nachshon, U., & Weisbrod, N. (2015). Beyond the salt crust: On combined evaporation and subflorescent salt precipitation in porous media. *Transport in Porous Media*, *110*(2), 295–310. https://doi.org/10.1007/s11242-015-0514-9

Nachshon, U., Weisbrod, N., Dragila, M. I., & Grader, A. (2011). Combined evaporation and salt precipitation in homogeneous and heterogeneous porous media. *Water Resources Research*, *47*(3), W03513. https://doi.org/10.1029/2010wr009677

Nachshon, U., Weisbrod, N., Katzir, R., & Nasser, A. (2018). Nacl crust architecture and its impact on evaporation: Three-dimensional insights. *Geophysical Research Letters*, *45*(12), 6100–6108. https://doi.org/10.1029/2018gl078363

Nachtergaele, F. O., van Velthuizen, H., Verelst, L., Batjes, N. H., Dijkshoorn, J. A., van Engelen, V. W. P., et al. (2008). Harmonized world soil database (version 1.0).

Nachtergaele, F. O., van Velthuizen, H., Verelst, L., Wiberg, D., Henry, M., Chiozza, F., et al. (2023). *Harmonized world soil database version 2.0*. Food and Agriculture Organization of the United Nations.

Nadim, F., Hoag, G. E., Liu, S., Carley, R. J., & Zack, P. (2000). Detection and remediation of soil and aquifer systems contaminated with petroleum products: An overview. *Journal of Petroleum Science and Engineering*, *26*(1–4), 169–178. https://doi.org/10.1016/s0920-4105(00)00031-0

Naillon, A., Duru, P., Marcoux, M., & Prat, M. (2015). Evaporation with sodium chloride crystallization in a capillary tube. *Journal of Crystal Growth*, *422*, 52–61. https://doi.org/10.1016/j.jcrysgro.2015.04.010

Naillon, A., Joseph, P., & Prat, M. (2018). Ion transport and precipitation kinetics as key aspects of stress generation on pore walls induced by salt crystallization. *Physical Review Letters*, *120*(3), 034502. https://doi.org/10.1103/physrevlett.120.034502

Negacz, K., Malek, Ž., de Vos, A., & Vellinga, P. (2022). Saline soils worldwide: Identifying the most promising areas for saline agriculture. *Journal of Arid Environments*, *203*, 104775. https://doi.org/10.1016/j.jaridenv.2022.104775

Neukom, R., Gergis, J., Karoly, D. J., Wanner, H., Curran, M., Elbert, J., et al. (2014). Inter-hemispheric temperature variability over the past millennium. *Nature Climate Change*, *4*(5), 362–367. https://doi.org/10.1038/nclimate2174

Nevermann, H., Gomez, J. N. B., Fröhle, P., & Shokri, N. (2023). Land loss implications of sea level rise along the coastline of Colombia under different climate change scenarios. *Climate Risk Management*, *39*, 100470, https://doi.org/10.1016/j.crm.2022.100470

Nicolai, A., Grunewald, J., & Zhang, J. S. (2007). Salztransport und phasenumwandlung–modellierung und numerische lösung im simulationsprogramm delphin 5. *Bauphysik*, *29*(3), 231–239. https://doi.org/10.1002/bapi.200710032

Nooraiepour, M., Masoudi, M., & Hellevang, H. (2021). Probabilistic nucleation governs time, amount, and location of mineral precipitation and geometry evolution in the porous medium. *Scientific Reports*, *11*(1), 16397. https://doi.org/10.1038/s41598-021-95237-7

Norouzi Rad, M., & Shokri, N. (2014). Effects of grain angularity on n a c l precipitation in porous media during evaporation. *Water Resources Research*, *50*(11), 9020–9030. https://doi.org/10.1002/2014wr016125

Norouzi Rad, M., Shokri, N., & Sahimi, M. (2013). Pore-scale dynamics of salt precipitation in drying porous media. *Physical Review E Statistical Physics, Plasmas, Fluids, and Related Interdisciplinary Topics*, *88*(3), 032404. https://doi.org/10.1103/physreve.88.032404

Northcote, K. H., & Srene, J. (1972). *Australian soils with saline and sodic properties*. CSIRO.

Nouri, H., Borujeni, S. C., Nirola, R., Hassanli, A., Beecham, S., Alaghmand, S., et al. (2017). Application of green remediation on soil salinity treatment: A review on halophytoremediation. *Process Safety and Environmental Protection*, *107*, 94–107. https://doi.org/10.1016/j.psep.2017.01.021

Nulsen, R. (1981). Critical depth to saline groundwater in non-irrigated situations. *Soil Research*, *19*(1), 83–86. https://doi.org/10.1071/sr9810083

Oki, T., & Kanae, S. (2006). Global hydrological cycles and world water resources. *Science*, *313*(5790), 1068–1072. https://doi.org/10.1126/science.1128845

Oldeman, L. R., Hakkeling, R. T. A., & Sombroek, W. G. (1990). World map of the status of human-induced soil degradation: An explanatory note. Technical report.

Olsson, L., Barbosa, H., Bhadwal, S., Cowie, A., Delusca, K., Flores-Renteria, D., et al. (2019). Land degradation. In P. R. Shukla, J. Skeg, E. C. Buendia, V. Masson-Delmotte, H. O. Pörtner, D. C. Roberts, et al. (Eds.) *Climate change and land: An IPCC special report on climate change, desertification, land degradation, sustainable land management, food security, and greenhouse gas fluxes in terrestrial ecosystems*. Retrieved from https://www.ipcc.ch/site/assets/uploads/2018/07/sr2_background_report_final.pdf

Omuto, C., Nachtergaele, F., & Rojas, R. V. (2013). *State of the art report on global and regional soil information: Where are we? Where to go?* Food and Agriculture Organization of the United Nations.

Oo, A. N., Ando, K., Khaung, T., & Khaing, M. T. (2017). Food security and socio-economic impacts of soil salinization in the central dry zone of Myanmar: A case study. *Journal of Agroforestry and Environment*, *11*(1–2), 149–154.
Oo, A. N., Iwai, C. B., & Saenjan, P. (2013). Food security and socio-economic impacts of soil salinization in northeast Thailand. *Journal of Environmental and Rural Development*, *4*, 76–81.
Or, D., Lehmann, P., Shahraeeni, E., & Shokri, N. (2013). Advances in soil evaporation physics—A review. *Vadose Zone Journal*, *12*(4), 1–16. https://doi.org/10.2136/vzj2012.0163
Orgiazzi, A., Ballabio, C., Panagos, P., Jones, A., & Fernández-Ugalde, O. (2018). Lucas soil, the largest expandable soil dataset for Europe: A review. *European Journal of Soil Science*, *69*(1), 140–153. https://doi.org/10.1111/ejss.12499
Oster, J., & Tanji, K. (1985). Chemical reactions within root zone of arid zone soils. *Journal of Irrigation and Drainage Engineering*, *111*(3), 207–217. https://doi.org/10.1061/(asce)0733-9437(1985)111:3(207)
Ott, H., Andrew, M., Snippe, J., & Blunt, M. J. (2014). Microscale solute transport and precipitation in complex rock during drying. *Geophysical Research Letters*, *41*(23), 8369–8376. https://doi.org/10.1002/2014gl062266
Ott, H., de Kloe, K., Marcelis, F., & Makurat, A. (2011). Injection of supercritical CO_2 in brine saturated sandstone: Pattern formation during salt precipitation. *Energy Procedia*, *4*, 4425–4432. https://doi.org/10.1016/j.egypro.2011.02.396
Oude Essink, G. H., Van Baaren, E. S., & De Louw, P. G. (2010). Effects of climate change on coastal groundwater systems: A modeling study in The Netherlands. *Water Resources Research*, *46*(10), W00F04. https://doi.org/10.1029/2009wr008719
Pang, H.-C., Li, Y.-Y., Yang, J.-S., & Liang, Y.-S. (2010). Effect of brackish water irrigation and straw mulching on soil salinity and crop yields under monsoonal climatic conditions. *Agricultural Water Management*, *97*(12), 1971–1977. https://doi.org/10.1016/j.agwat.2009.08.020
Parihar, P., Singh, S., Singh, R., Singh, V. P., & Prasad, S. M. (2015). Effect of salinity stress on plants and its tolerance strategies: A review. *Environmental Science and Pollution Research*, *22*(6), 4056–4075. https://doi.org/10.1007/s11356-014-3739-1
Parker, V. T., & Boyer, K. E. (2019). Sea-level rise and climate change impacts on an urbanized Pacific coast estuary. *Wetlands*, *39*(6), 1219–1232. https://doi.org/10.1007/s13157-017-0980-7
Parkhurst, D. L., & Appelo, C. (1999). *User's guide to phreeqc (version 2): A computer program for speciation, batch-reaction, one-dimensional transport, and inverse geochemical calculations. Technical report*. US Geological Survey.
Paul, D. (2013). Osmotic stress adaptations in rhizobacteria. *Journal of Basic Microbiology*, *53*(2), 101–110. https://doi.org/10.1002/jobm.201100288
Paulot, F., Paynter, D., Winton, M., Ginoux, P., Zhao, M., & Horowitz, L. W. (2020). Revisiting the impact of sea salt on climate sensitivity. *Geophysical Research Letters*, *47*(3), e2019GL085601. https://doi.org/10.1029/2019gl085601
Pawlowicz, R., & Feistel, R. (2012). Limnological applications of the thermodynamic equation of seawater 2010 (TEOS-10). *Limnology and Oceanography: Methods*, *10*(11), 853–867. https://doi.org/10.4319/lom.2012.10.853
Perri, S., Detto, M., Porporato, A., & Molini, A. (2023). Salinity-induced limits to mangrove canopy height. *Global Ecology and Biogeography*, *32*(9), 1561–1574. https://doi.org/10.1111/geb.13720
Perri, S., Entekhabi, D., & Molini, A. (2018). Plant osmoregulation as an emergent water-saving adaptation. *Water Resources Research*, *54*(4), 2781–2798. https://doi.org/10.1002/2017wr022319
Perri, S., Molini, A., Hedin, L. O., & Porporato, A. (2022). Contrasting effects of aridity and seasonality on global salinization. *Nature Geoscience*, *15*(5), 375–381. https://doi.org/10.1038/s41561-022-00931-4
Perri, S., Suweis, S., Entekhabi, D., & Molini, A. (2018). Vegetation controls on dryland salinity. *Geophysical Research Letters*, *45*(21), 11–669. https://doi.org/10.1029/2018gl079766
Perri, S., Suweis, S., Holmes, A., Marpu, P. R., Entekhabi, D., & Molini, A. (2020). River basin salinization as a form of aridity. *Proceedings of the National Academy of Sciences*, *117*(30), 17635–17642. https://doi.org/10.1073/pnas.2005925117
Peysson, Y., Fleury, M., & Blázquez-Pascual, V. (2011). Drying rate measurements in convection-and diffusion-driven conditions on a shaly sandstone using nuclear magnetic resonance. *Transport in Porous Media*, *90*(3), 1001–1016. https://doi.org/10.1007/s11242-011-9829-3
Pezeshki, E., Moysey, S. M., Manda, A. K., Gibbs, A., Palochak, T., & Gullett, J. P. (2022). Investigation of storm surge versus saltwater intrusion on coastal aquifer salinization in hyde county, North Carolina. *AGU Fall Meeting Abstracts*, *2022*, H25S–H1335.
Pham, S. T., Chareyre, B., Tsotsas, E., & Kharaghani, A. (2022). Pore network modeling of phase distribution and capillary force evolution during slow drying of particle aggregates. *Powder Technology*, *407*, 117627. https://doi.org/10.1016/j.powtec.2022.117627
Pino, V., McBratney, A., O'Brien, E., Singh, K., & Pozza, L. (2022). Citizen science & soil connectivity: Where are we? *Soil Security*, *9*, 100073. https://doi.org/10.1016/j.soisec.2022.100073
Porporato, A., Daly, E., & Rodriguez-Iturbe, I. (2004). Soil water balance and ecosystem response to climate change. *The American Naturalist*, *164*(5), 625–632. https://doi.org/10.1086/424970
Postma, D., & Appelo, C. (2000). Reduction of mn-oxides by ferrous iron in a flow system: Column experiment and reactive transport modeling. *Geochimica et Cosmochimica Acta*, *64*(7), 1237–1247. https://doi.org/10.1016/s0016-7037(99)00356-7
Prat, M. (1995). Isothermal drying on non-hygroscopic capillary-porous materials as an invasion percolation process. *International Journal of Multiphase Flow*, *21*(5), 875–892. https://doi.org/10.1016/0301-9322(95)00022-p
Prat, M. (2002). Recent advances in pore-scale models for drying of porous media. *Chemical Engineering Journal*, *86*(1–2), 153–164. https://doi.org/10.1016/s1385-8947(01)00283-2
Prat, M. (2011). Pore network models of drying, contact angle, and film flows. *Chemical Engineering & Technology*, *34*(7), 1029–1038. https://doi.org/10.1002/ceat.201100056
Prăvălie, R. (2016). Drylands extent and environmental issues. a global approach. *Earth-Science Reviews*, *161*, 259–278. https://doi.org/10.1016/j.earscirev.2016.08.003
Prusty, P., & Farooq, S. (2020). Seawater intrusion in the coastal aquifers of India-a review. *HydroResearch*, *3*, 61–74. https://doi.org/10.1016/j.hydres.2020.06.001
Qadir, M., Ghafoor, A., & Murtaza, G. (2000). Amelioration strategies for saline soils: A review. *Land Degradation & Development*, *11*(6), 501–521. https://doi.org/10.1002/1099-145x(200011/12)11:6<501::aid-ldr405>3.0.co;2-s
Qadir, M., Quillérou, E., Nangia, V., Murtaza, G., Singh, M., Thomas, R. J., et al. (2014). Economics of salt-induced land degradation and restoration. In *Natural resources forum* (Vol. 38, pp. 282–295). Wiley Online Library.
Qazi, M., Salim, H., Doorman, C., Jambon-Puillet, E., & Shahidzadeh, N. (2019). Salt creeping as a self-amplifying crystallization process. *Science Advances*, *5*(12), eaax1853. https://doi.org/10.1126/sciadv.aax1853
Qi, G., Chang, C., Yang, W., Gao, P., & Zhao, G. (2021). Soil salinity inversion in coastal corn planting areas by the satellite-UAV-ground integration approach. *Remote Sensing*, *13*(16), 3100. https://doi.org/10.3390/rs13163100
Rabbani, H. S., Joekar-Niasar, V., Pak, T., & Shokri, N. (2017). New insights on the complex dynamics of two-phase flow in porous media under intermediate-wet conditions. *Scientific Reports*, *7*(1), 4584. https://doi.org/10.1038/s41598-017-04545-4

Rabbani, H. S., Zhao, B., Juanes, R., & Shokri, N. (2018). Pore geometry control of apparent wetting in porous media. *Scientific Reports*, *8*(1), 15729. https://doi.org/10.1038/s41598-018-34146-8

Rad, M. N., Shokri, N., Keshmiri, A., & Withers, P. J. (2015). Effects of grain and pore size on salt precipitation during evaporation from porous media. *Transport in Porous Media*, *110*(2), 281–294. https://doi.org/10.1007/s11242-015-0515-8

Rahimi, A., Metzger, T., Kharaghani, A., & Tsotsas, E. (2016). Interaction of droplets with porous structures: Pore network simulation of wetting and drying. *Drying Technology*, *34*(9), 1129–1140. https://doi.org/10.1080/07373937.2015.1099106

Rahman, M., Penny, G., Mondal, M., Zaman, M., Kryston, A., Salehin, M., et al. (2019). Salinization in large river deltas: Drivers, impacts and socio-hydrological feedbacks. *Water security*, *6*, 100024. https://doi.org/10.1016/j.wasec.2019.100024

Randall, K., Ewing, E. T., Marr, L. C., Jimenez, J. L., & Bourouiba, L. (2021). How did we get here: What are droplets and aerosols and how far do they go? A historical perspective on the transmission of respiratory infectious diseases. *Interface Focus*, *11*(6), 20210049. https://doi.org/10.1098/rsfs.2021.0049

Rath, K. M., & Rousk, J. (2015). Salt effects on the soil microbial decomposer community and their role in organic carbon cycling: A review. *Soil Biology and Biochemistry*, *81*, 108–123. https://doi.org/10.1016/j.soilbio.2014.11.001

Raupach, M. (1992). Drag and drag partition on rough surfaces. *Boundary-Layer Meteorology*, *60*(4), 375–395. https://doi.org/10.1007/bf00155203

Raupach, M., Gillette, D., & Leys, J. (1993). The effect of roughness elements on wind erosion threshold. *Journal of Geophysical Research*, *98*(D2), 3023–3029. https://doi.org/10.1029/92jd01922

Reheis, M. (2006). A 16-year record of eolian dust in southern Nevada and California, USA: Controls on dust generation and accumulation. *Journal of Arid Environments*, *67*(3), 487–520. https://doi.org/10.1016/j.jaridenv.2006.03.006

Rengasamy, P. (2006). World salinization with emphasis on Australia. *Journal of Experimental Botany*, *57*(5), 1017–1023. https://doi.org/10.1093/jxb/erj108

Reynolds, R. L., Yount, J. C., Reheis, M., Goldstein, H., Chavez Jr., P., Fulton, R., et al. (2007). Dust emission from wet and dry playas in the Mojave Desert, USA. *Earth Surface Processes and Landforms: The Journal of the British Geomorphological Research Group*, *32*(12), 1811–1827. https://doi.org/10.1002/esp.1515

Ribeiro, E. C., Batjes, N. H., Leenaars, J. G., Van Oostrum, A., & de Jesus, J. M. (2015). *Towards the standardization and harmonization of world soil data: Procedures manual isric world soil information service (wosis version 2.0). Technical report*. ISRIC.

Richards, L. A. (1954). Diagnosis and improvement of saline and alkali soils. In *Handbook No. 60*. US Department of Agriculture.

Richardson, K., Steffen, W., & Liverman, D. (2011). *Climate change: Global risks, challenges and decisions*. Cambridge University Press.

Rignot, E., Velicogna, I., van den Broeke, M. R., Monaghan, A., & Lenaerts, J. T. (2011). Acceleration of the contribution of the Greenland and Antarctic ice sheets to sea level rise. *Geophysical Research Letters*, *38*(5), L05503. https://doi.org/10.1029/2011gl046583

Rijniers, L., Huinink, H., Pel, L., & Kopinga, K. (2005). Experimental evidence of crystallization pressure inside porous media. *Physical Review Letters*, *94*(7), 075503. https://doi.org/10.1103/physrevlett.94.075503

Ritsema, C. J., & Dekker, L. W. (2012). *Soil water repellency: Occurrence, consequences, and amelioration*. Elsevier.

Rodríguez-Iturbe, I., & Porporato, A. (2007). *Ecohydrology of water-controlled ecosystems: Soil moisture and plant dynamics*. Cambridge University Press.

Rodriguez-Iturbe, I., Porporato, A., Ridolfi, L., Isham, V., & Coxi, D. (1999). Probabilistic modelling of water balance at a point: The role of climate, soil and vegetation. *Proceedings of the Royal Society of London. Series A: Mathematical, Physical and Engineering Sciences*, *455*(1990), 3789–3805. https://doi.org/10.1098/rspa.1999.0477

Rodriguez-Navarro, C., & Doehne, E. (1999). Salt weathering: Influence of evaporation rate, supersaturation and crystallization pattern. *Earth Surface Processes and Landforms: The Journal of the British Geomorphological Research Group*, *24*(3), 191–209. https://doi.org/10.1002/(sici)1096-9837(199903)24:3<191::aid-esp942>3.0.co;2-g

Roels, S. M., Ott, H., & Zitha, P. L. (2014). μ-ct analysis and numerical simulation of drying effects of CO_2 injection into brine-saturated porous media. *International Journal of Greenhouse Gas Control*, *27*, 146–154. https://doi.org/10.1016/j.ijggc.2014.05.010

Rose, D., Konukcu, F., & Gowing, J. (2005). Effect of watertable depth on evaporation and salt accumulation from saline groundwater. *Soil Research*, *43*(5), 565–573. https://doi.org/10.1071/sr04051

Rosenfeld, D., Lohmann, U., Raga, G. B., O'Dowd, C. D., Kulmala, M., Fuzzi, S., et al. (2008). Flood or drought: How do aerosols affect precipitation? *Science*, *321*(5894), 1309–1313. https://doi.org/10.1126/science.1160606

Ross, P., Williams, J., & Bristow, K. (1991). Equation for extending water-retention curves to dryness. *Soil Science Society of America Journal*, *55*(4), 923–927. https://doi.org/10.2136/sssaj1991.03615995005500040004x

Rossiter, D. G., Liu, J., Carlisle, S., & Zhu, A. X. (2015). Can citizen science assist digital soil mapping? *Geoderma*, *259*, 71–80. https://doi.org/10.1016/j.geoderma.2015.05.006

Runyan, C. W., & D'Odorico, P. (2010). Ecohydrological feedbacks between salt accumulation and vegetation dynamics: Role of vegetation-groundwater interactions. *Water Resources Research*, *46*(11), W11561. https://doi.org/10.1029/2010wr009464

Sabbioni, C., Cassar, M., Brimblecombe, P., & Lefevre, R.-A. (2008). Vulnerability of cultural heritage to climate change. In *European and mediterranean major hazards agreement (EUR-OPA)* (pp. 1–24).

Sadeghi, M., Shokri, N., & Jones, S. B. (2012). A novel analytical solution to steady-state evaporation from porous media. *Water Resources Research*, *48*(9), W09516. https://doi.org/10.1029/2012wr012060

Safdar, H., Amin, A., Shafiq, Y., Ali, A., Yasin, R., Shoukat, A., et al. (2019). A review: Impact of salinity on plant growth. *Nature and Science*, *17*(1), 34–40.

Sahab, S., Suhani, I., Srivastava, V., Chauhan, P. S., Singh, R. P., & Prasad, V. (2021). Potential risk assessment of soil salinity to agroecosystem sustainability: Current status and management strategies. *Science of the Total Environment*, *764*, 144164. https://doi.org/10.1016/j.scitotenv.2020.144164

Sahavacharin, A., Sompongchaiyakul, P., & Thaitakoo, D. (2022). The effects of land-based change on coastal ecosystems. *Landscape and Ecological Engineering*, *18*(3), 351–366. https://doi.org/10.1007/s11355-022-00505-x

Sahimi, M. (2011). *Flow and transport in porous media and fractured rock: From classical methods to modern approaches*. John Wiley & Sons.

Sahimi, M. (2012). Dispersion in porous media, continuous-time random walks, and percolation. *Physical Review E*, *85*(1), 016316. https://doi.org/10.1103/physreve.85.016316

Sahimi, M. (2023). *Applications of percolation theory, volume 2 of applied mathematical sciences* (2 ed). Springer.

Sahimi, M. (2024). Physics-informed and data-driven discovery of governing equations for complex phenomena in heterogeneous media. *Physical Review E*, *109*(4), 041001. https://doi.org/10.1103/physreve.109.041001

Sahimi, M., Davis, H. T., & Scriven, L. (1983). Dispersion in disordered porous media. *Chemical Engineering Communications*, *23*(4–6), 329–341. https://doi.org/10.1080/00986448308940483

Sahimi, M., Heiba, A. A., Davis, H. T., & Scriven, L. (1986). Dispersion in flow through porous media—II. Two-phase flow. *Chemical Engineering Science*, *41*(8), 2123–2136. https://doi.org/10.1016/0009-2509(86)87129-9
Sahimi, M., Hughes, B. D., Scriven, L., & Davis, H. T. (1986). Dispersion in flow through porous media—I. One-phase flow. *Chemical Engineering Science*, *41*(8), 2103–2122. https://doi.org/10.1016/0009-2509(86)87128-7
Sahimi, M., & Imdakm, A. (1988). The effect of morphological disorder on hydrodynamic dispersion in flow through porous media. *Journal of Physics A: Mathematical and General*, *21*(19), 3833–3870. https://doi.org/10.1088/0305-4470/21/19/019
Saliba, G., Chen, C.-L., Lewis, S., Russell, L. M., Rivellini, L.-H., Lee, A. K., et al. (2019). Factors driving the seasonal and hourly variability of sea-spray aerosol number in the North Atlantic. *Proceedings of the National Academy of Sciences*, *116*(41), 20309–20314. https://doi.org/10.1073/pnas.1907574116
Salter, S. J., & Mohanty, K. K. (1982). Multiphase flow in porous media: I. Macroscopic observations and modeling. In *SPE annual technical conference and exhibition, SPE-11017*. SPE.
Salvati, L., & Ferrara, C. (2015). The local-scale impact of soil salinization on the socioeconomic context: An exploratory analysis in Italy. *Catena*, *127*, 312–322. https://doi.org/10.1016/j.catena.2015.01.008
Saravanapavan, T., & Salvucci, G. D. (2000). Analysis of rate-limiting processes in soil evaporation with implications for soil resistance models. *Advances in Water Resources*, *23*(5), 493–502. https://doi.org/10.1016/s0309-1708(99)00045-7
Sarkar, S. K., Rudra, R. R., Nur, M. S., & Das, P. C. (2023). Partial least-squares regression for soil salinity mapping in Bangladesh. *Ecological Indicators*, *154*, 110825. https://doi.org/10.1016/j.ecolind.2023.110825
Schatz, V., & Herrmann, H. J. (2006). Flow separation in the lee side of transverse dunes: A numerical investigation. *Geomorphology*, *81*(1–2), 207–216. https://doi.org/10.1016/j.geomorph.2006.04.009
Scherer, G. W. (1990). Theory of drying. *Journal of the American Ceramic Society*, *73*(1), 3–14. https://doi.org/10.1111/j.1151-2916.1990.tb05082.x
Schimel, D. S. (2010). Drylands in the Earth system. *Science*, *327*(5964), 418–419. https://doi.org/10.1126/science.1184946
Schofield, R., & Kirkby, M. (2003). Application of salinization indicators and initial development of potential global soil salinization scenario under climatic change. *Global Biogeochemical Cycles*, *17*(3), 1078. https://doi.org/10.1029/2002gb001935
Schoups, G., Hopmans, J., & Tanji, K. (2006). Evaluation of model complexity and space–time resolution on the prediction of long-term soil salinity dynamics, Western San Joaquin valley, California. *Hydrological Processes: An International Journal*, *20*(13), 2647–2668. https://doi.org/10.1002/hyp.6082
Schoups, G., Hopmans, J. W., Young, C. A., Vrugt, J. A., Wallender, W. W., Tanji, K. K., & Panday, S. (2005). Sustainability of irrigated agriculture in the San Joaquin valley, California. *Proceedings of the National Academy of Sciences*, *102*(43), 15352–15356. https://doi.org/10.1073/pnas.0507723102
Scudiero, E., Skaggs, T. H., & Corwin, D. L. (2017). Simplifying field-scale assessment of spatiotemporal changes of soil salinity. *Science of the Total Environment*, *587*, 273–281. https://doi.org/10.1016/j.scitotenv.2017.02.136
Sekine, K., Okamoto, A., & Hayashi, K. (2011). In situ observation of the crystallization pressure induced by halite crystal growth in a microfluidic channel. *American Mineralogist*, *96*(7), 1012–1019. https://doi.org/10.2138/am.2011.3765
Seltenrich, N. (2023). A terminal case? Shrinking inland seas expose salty particulates and more. *Environmental Health Perspectives*, *131*(6), 062001. https://doi.org/10.1289/ehp12835
Setia, R., Gottschalk, P., Smith, P., Marschner, P., Baldock, J., Setia, D., & Smith, J. (2013). Soil salinity decreases global soil organic carbon stocks. *Science of the Total Environment*, *465*, 267–272. https://doi.org/10.1016/j.scitotenv.2012.08.028
Sghaier, N., Prat, M., & Nasrallah, S. B. (2007). On ions transport during drying in a porous medium. *Transport in Porous Media*, *67*(2), 243–274. https://doi.org/10.1007/s11242-006-9007-1
Shah, S., Vervoort, R., Suweis, S., Guswa, A. J., Rinaldo, A., & Van Der Zee, S. (2011). Stochastic modeling of salt accumulation in the root zone due to capillary flux from brackish groundwater. *Water Resources Research*, *47*(9), 57. https://doi.org/10.1029/2010wr009790
Shahidzadeh, N., & Desarnaud, J. (2012). Damage in porous media: Role of the kinetics of salt (re) crystallization. *The European Physical Journal-Applied Physics*, *60*(2), 24205. https://doi.org/10.1051/epjap/2012120235
Shahidzadeh, N., Schut, M. F., Desarnaud, J., Prat, M., & Bonn, D. (2015). Salt stains from evaporating droplets. *Scientific Reports*, *5*(1), 10335. https://doi.org/10.1038/srep10335
Shahidzadeh-Bonn, N., Azouni, A., & Coussot, P. (2007). Effect of wetting properties on the kinetics of drying of porous media. *Journal of Physics: Condensed Matter*, *19*(11), 112101. https://doi.org/10.1088/0953-8984/19/11/112101
Shahidzadeh-Bonn, N., Desarnaud, J., Bertrand, F., Chateau, X., & Bonn, D. (2010). Damage in porous media due to salt crystallization. *Physical Review E*, *81*(6), 066110. https://doi.org/10.1103/physreve.81.066110
Shahidzadeh-Bonn, N., Rafaı, S., Bonn, D., & Wegdam, G. (2008). Salt crystallization during evaporation: Impact of interfacial properties. *Langmuir*, *24*(16), 8599–8605. https://doi.org/10.1021/la8005629
Shahraeeni, E., Lehmann, P., & Or, D. (2012). Coupling of evaporative fluxes from drying porous surfaces with air boundary layer: Characteristics of evaporation from discrete pores. *Water Resources Research*, *48*(9), W09525. https://doi.org/10.1029/2012wr011857
Shahraeeni, E., & Or, D. (2010). Thermo-evaporative fluxes from heterogeneous porous surfaces resolved by infrared thermography. *Water Resources Research*, *46*(9), 12519. https://doi.org/10.1029/2009wr008455
Shankar, V., & Evelin, H. (2019). Strategies for reclamation of saline soils. In *Microorganisms in saline environments: Strategies and functions* (pp. 439–449).
Shao, Y. (2001). A model for mineral dust emission. *Journal of Geophysical Research*, *106*(D17), 20239–20254. https://doi.org/10.1029/2001jd900171
Shao, Y., Jung, E., & Leslie, L. M. (2002). Numerical prediction of northeast Asian dust storms using an integrated wind erosion modeling system. *Journal of Geophysical Research*, *107*(D24), AAC21. https://doi.org/10.1029/2001jd001493
Shaw, T. (1987). Drying as an immiscible displacement process with fluid counterflow. *Physical Review Letters*, *59*(15), 1671–1674. https://doi.org/10.1103/physrevlett.59.1671
Shaygan, M., & Baumgartl, T. (2022). Reclamation of salt-affected land: A review. *Soil systems*, *6*(3), 61. https://doi.org/10.3390/soilsystems6030061
Sheppard, A. P., Knackstedt, M. A., Pinczewski, W. V., & Sahimi, M. (1999). Invasion percolation: New algorithms and universality classes. *Journal of Physics A: Mathematical and General*, *32*(49), L521–L529. https://doi.org/10.1088/0305-4470/32/49/101
Sherwood, T. (1929a). The drying of solids—I. *Industrial & Engineering Chemistry*, *21*(1), 12–16. https://doi.org/10.1021/ie50229a004
Sherwood, T. (1929b). The drying of solids—II. *Industrial & Engineering Chemistry*, *21*(10), 976–980. https://doi.org/10.1021/ie50238a021
Sherwood, T. (1930). The drying of solids—III1 mechanism of the drying of pulp and paper. *Industrial & Engineering Chemistry*, *22*(2), 132–136. https://doi.org/10.1021/ie50242a009

Sherwood, T. (1931). Application of theoretical diffusion equations to the drying of solids. *Transactions of the American Institute of Chemical Engineers*, *27*, 190–202.
Shimojimaa, E., Yoshioka, R., & Tamagawa, I. (1996). Salinization owing to evaporation from bare-soil surfaces and its influences on the evaporation. *Journal of Hydrology*, *178*(1–4), 109–136. https://doi.org/10.1016/0022-1694(95)02826-9
Shokri, N. (2014). Pore-scale dynamics of salt transport and distribution in drying porous media. *Physics of Fluids*, *26*(1), 012106. https://doi.org/10.1063/1.4861755
Shokri, N., Lehmann, P., & Or, D. (2008). Effects of hydrophobic layers on evaporation from porous media. *Geophysical Research Letters*, *35*(19), L19407. https://doi.org/10.1029/2008gl035230
Shokri, N., Lehmann, P., & Or, D. (2009). Characteristics of evaporation from partially wettable porous media. *Water Resources Research*, *45*(2), W02415. https://doi.org/10.1029/2008wr007185
Shokri, N., Lehmann, P., & Or, D. (2010). Evaporation from layered porous media. *Journal of Geophysical Research*, *115*(B6), 147. https://doi.org/10.1029/2009jb006743
Shokri, N., Lehmann, P., Vontobel, P., & Or, D. (2008). Drying front and water content dynamics during evaporation from sand delineated by neutron radiography. *Water Resources Research*, *44*(6), W06418. https://doi.org/10.1029/2007wr006385
Shokri, N., & Or, D. (2010). Comment on "A simple model for describing hydraulic conductivity in unsaturated porous media accounting for film and capillary flow" by A. Peters and W. Durner. *Water Resources Research*, *46*, W06801. https://doi.org/10.1029/2008WR007136
Shokri, N., & Or, D. (2011). What determines drying rates at the onset of diffusion controlled stage-2 evaporation from porous media? *Water Resources Research*, *47*(9), W09513. https://doi.org/10.1029/2010wr010284
Shokri, N., & Sahimi, M. (2012). Structure of drying fronts in three-dimensional porous media. *Physical Review E*, *85*(6), 066312. https://doi.org/10.1103/physreve.85.066312
Shokri, N., Sahimi, M., & Or, D. (2012). Morphology, propagation dynamics and scaling characteristics of drying fronts in porous media. *Geophysical Research Letters*, *39*(9), L09401. https://doi.org/10.1029/2012gl051506
Shokri, N., & Salvucci, G. (2011). Evaporation from porous media in the presence of a water table. *Vadose Zone Journal*, *10*(4), 1309–1318. https://doi.org/10.2136/vzj2011.0027
Shokri, N., Stevens, B., Madani, K., Grabe, J., Schlüter, M., & Smirnova, I. (2023). Climate informed engineering: An essential pillar of industry 4.0 transformation. *ACS Engineering Au*, *3*(1), 3–6. https://doi.org/10.1021/acsengineeringau.2c00037
Shokri, N., Zhou, P., & Keshmiri, A. (2015). Patterns of desiccation cracks in saline bentonite layers. *Transport in Porous Media*, *110*(2), 333–344. https://doi.org/10.1007/s11242-015-0521-x
Shokri-Kuehni, S. M. (2018). *Dynamics of saline water evaporation from porous media*. The University of Manchester.
Shokri-Kuehni, S. M., Bergstad, M., Sahimi, M., Webb, C., & Shokri, N. (2018). Iodine k-edge dual energy imaging reveals the influence of particle size distribution on solute transport in drying porous media. *Scientific Reports*, *8*(1), 10731. https://doi.org/10.1038/s41598-018-29115-0
Shokri-Kuehni, S. M., Raaijmakers, B., Kurz, T., Or, D., Helmig, R., & Shokri, N. (2020). Water table depth and soil salinization: From pore-scale processes to field-scale responses. *Water Resources Research*, *56*(2), e2019WR026707. https://doi.org/10.1029/2019wr026707
Shokri-Kuehni, S. M., Rad, M. N., Webb, C., & Shokri, N. (2017). Impact of type of salt and ambient conditions on saline water evaporation from porous media. *Advances in Water Resources*, *105*, 154–161. https://doi.org/10.1016/j.advwatres.2017.05.004
Shokri-Kuehni, S. M., Sahimi, M., & Shokri, N. (2022). A personal perspective on prediction of saline water evaporation from porous media. *Drying Technology*, *40*(4), 691–696. https://doi.org/10.1080/07373937.2021.1999256
Shokri-Kuehni, S. M., Vetter, T., Webb, C., & Shokri, N. (2017). New insights into saline water evaporation from porous media: Complex interaction between evaporation rates, precipitation, and surface temperature. *Geophysical Research Letters*, *44*(11), 5504–5510. https://doi.org/10.1002/2017gl073337
Shukla, P. R., Skea, J., Calvo Buendia, E., Masson-Delmotte, V., Portner, H. O., Roberts, D. C., et al. (2019). *Climate change and land: An IPCC special report on climate change, desertification, land degradation, sustainable land management, food security, and greenhouse gas fluxes in terrestrial ecosystems*. IPCC.
Silatsa, F. B., & Kebede, F. (2023). A quarter century experience in soil salinity mapping and its contribution to sustainable soil management and food security in Morocco. *Geoderma Regional*, *34*, e00695. https://doi.org/10.1016/j.geodrs.2023.e00695
Šimůnek, J., Jacques, D., van Genuchten, M., & Mallants, D. (2006). Multicomponent geochemical transport modelling using the hydrus computer software packages. *Journal of the American Water Resources Association*, *42*, 1537–1547.
Šimůnek, J., Šejna, M., & van Genuchten, M. (1998). *The HYDRUS-1D software package for simulating the one-dimensional movement of water, heat, and multiple solutes in variably-saturated media*. IGWMC-TPS 70.
Šimůnek, J., Suarez, D., & Šejna, M. (1996). The unsatchem software package for simulating one-dimensional variably saturated water flow, heat transport, carbon dioxide production and transport, and multicomponent solute transport with major ion equilibrium and kinetic chemistry. *Research Report*, *141*, 186.
Singh, K. (2016). Microbial and enzyme activities of saline and sodic soils. *Land Degradation & Development*, *27*(3), 706–718. https://doi.org/10.1002/ldr.2385
Singh, M., Kumar, J., Singh, S., Singh, V. P., & Prasad, S. M. (2015). Roles of osmoprotectants in improving salinity and drought tolerance in plants: A review. *Reviews in Environmental Science and Biotechnology*, *14*(3), 407–426. https://doi.org/10.1007/s11157-015-9372-8
Singh, P., Sharma, S., Nisar, S., & Choudhary, O. P. (2023). Structural stability and organic matter stabilization in soils: Differential impacts of soil salinity and sodicity. *Journal of Soil Science and Plant Nutrition*, *23*(2), 1751–1773. https://doi.org/10.1007/s42729-023-01136-3
Singh, R. P., & Sirohi, A. (1994). Spectral reflectance properties of different types of soil surfaces. *ISPRS Journal of Photogrammetry and Remote Sensing*, *49*(4), 34–40. https://doi.org/10.1016/0924-2716(94)90045-0
Smeets, P. J., Cho, K. R., Kempen, R. G., Sommerdijk, N. A., & De Yoreo, J. J. (2015). Calcium carbonate nucleation driven by ion binding in a biomimetic matrix revealed by in situ electron microscopy. *Nature Materials*, *14*(4), 394–399. https://doi.org/10.1038/nmat4193
Smits, K. M., Ngo, V. V., Cihan, A., Sakaki, T., & Illangasekare, T. H. (2012). An evaluation of models of bare soil evaporation formulated with different land surface boundary conditions and assumptions. *Water Resources Research*, *48*(12), W12526. https://doi.org/10.1029/2012wr012113
Soares, J., Sofiev, M., Geels, C., Christensen, J. H., Andersson, C., Tsyro, S., & Langner, J. (2016). Impact of climate change on the production and transport of sea salt aerosol on European seas. *Atmospheric Chemistry and Physics*, *16*(20), 13081–13104. https://doi.org/10.5194/acp-16-13081-2016
Soil Science Glossary Terms Committee. (2008). *Glossary of soil science terms*. Soil Science Society of America.

Soltanian, M. R., Amooie, M. A., Cole, D. R., Graham, D. E., Hosseini, S. A., Hovorka, S., et al. (2016). Simulating the cranfield geological carbon sequestration project with high-resolution static models and an accurate equation of state. *International Journal of Greenhouse Gas Control*, *54*, 282–296. https://doi.org/10.1016/j.ijggc.2016.10.002

Sonmez, S., Buyuktas, D., Okturen, F., & Citak, S. (2008). Assessment of different soil to water ratios (1: 1, 1: 2.5, 1: 5) in soil salinity studies. *Geoderma*, *144*(1–2), 361–369. https://doi.org/10.1016/j.geoderma.2007.12.005

Sorensen, L. (2007). A spatial analysis approach to the global delineation of dryland areas of relevance to the CBD Programme of Work on Dry and Subhumid Lands. In *Dataset based on spatial analysis between WWF terrestrial ecoregions (WWF-US, 2004) and aridity zones (CRU/UEA; UNEPGRID, 1991)*. UNEP-WCMC.

Squires, V. R., & Glenn, E. P. (2011). *Salination, desertification and soil erosion* (Vol. 3). EOLSS Publications.

Staff, S. S. (2022). *Keys to soil taxonomy* (13th ed.). USDA-Natural Resources Conservation Service.

Stauffer, D. (1976). Kinetic theory of two-component ("hetero-molecular") nucleation and condensation. *Journal of Aerosol Science*, *7*(4), 319–333. https://doi.org/10.1016/0021-8502(76)90086-0

Stauffer, D., & Aharony, A. (2018). *Introduction to percolation theory*. Taylor & Francis.

Steiger, M. (2005). Crystal growth in porous materials—I: The crystallization pressure of large crystals. *Journal of Crystal Growth*, *282*(3–4), 455–469. https://doi.org/10.1016/j.jcrysgro.2005.05.007

Storlazzi, C. D., Gingerich, S. B., Van Dongeren, A., Cheriton, O. M., Swarzenski, P. W., Quataert, E., et al. (2018). Most atolls will be uninhabitable by the mid-21st century because of sea-level rise exacerbating wave-driven flooding. *Science Advances*, *4*(4), eaap9741. https://doi.org/10.1126/sciadv.aap9741

Suarez, D. L., & Jurinak, J. (2011). The chemistry of salt-affected soils and waters. In *Agricultural salinity assessment and management* (pp. 57–88).

Suarez, D. L., & Šimůnek, J. (1997). Unsatchem: Unsaturated water and solute transport model with equilibrium and kinetic chemistry. *Soil Science Society of America Journal*, *61*(6), 1633–1646. https://doi.org/10.2136/sssaj1997.03615995006100060014x

Sun, Q., Cui, S., & Zhang, M. (2020). Homogeneous nucleation mechanism of nacl in aqueous solutions. *Crystals*, *10*(2), 107. https://doi.org/10.3390/cryst10020107

Sunagawa, I. (1999). Growth and morphology of crystals. *FORMA-TOKYO*, *14*(1/2), 147–166.

Surasani, V., Metzger, T., & Tsotsas, E. (2008). Consideration of heat transfer in pore network modelling of convective drying. *International Journal of Heat and Mass Transfer*, *51*(9–10), 2506–2518. https://doi.org/10.1016/j.ijheatmasstransfer.2007.07.033

Suweis, S., Rinaldo, A., Van der Zee, S., Daly, E., Maritan, A., & Porporato, A. (2010). Stochastic modeling of soil salinity. *Geophysical Research Letters*, *37*(7), L07404. https://doi.org/10.1029/2010gl042495

Szabo, S., Hossain, M. S., Adger, W. N., Matthews, Z., Ahmed, S., Lázár, A. N., & Ahmad, S. (2016). Soil salinity, household wealth and food insecurity in tropical deltas: Evidence from south-west coast of Bangladesh. *Sustainability Science*, *11*(3), 411–421. https://doi.org/10.1007/s11625-015-0337-1

Szabolcs, I. (1989). *Salt-affected soils*. CRC Press.

Szabolcs, I. (1990). Impact of climatic change on soil attributes: Influence on salinization and alkalinization. In *Developments in soil science* (Vol. 20, pp. 61–69). Elsevier. https://doi.org/10.1016/s0166-2481(08)70482-3

Taber, S. (1916). The growth of crystals under external pressure. *American Journal of Science*, *41*(246), 532–556. https://doi.org/10.2475/ajs.s4-41.246.532

Talat, N. (2020). Alleviation of soil salinization and the management of saline soils, climate change, and soil interactions. In *Climate change and soil interactions* (pp. 305–329). Elsevier.

Tegen, I., & Schepanski, K. (2018). Climate feedback on aerosol emission and atmospheric concentrations. *Current Climate Change Reports*, *4*, 1–10. https://doi.org/10.1007/s40641-018-0086-1

TEOS. (2010). The international thermodynamic equation of seawater—2010: Calculation and use of thermodynamic properties. Retrieved from https://www.teos-10.org/pubs/TEOS-10_Manual.pdf

Tomaz, A., Palma, P., Alvarenga, P., & Gonçalves, M. C. (2020). Soil salinity risk in a climate change scenario and its effect on crop yield. In *Climate change and soil interactions* (pp. 351–396). Elsevier.

Toner, J. D., Catling, D. C., & Light, B. (2015). Modeling salt precipitation from brines on Mars: Evaporation versus freezing origin for soil salts. *Icarus*, *250*, 451–461. https://doi.org/10.1016/j.icarus.2014.12.013

Trenberth, K. E., Fasullo, J. T., & Kiehl, J. (2009). Earth's global energy budget. *Bulletin of the American Meteorological Society*, *90*(3), 311–324. https://doi.org/10.1175/2008bams2634.1

Tripathi, R. (2011). Socio-economic impact of reclaiming salt affected lands in India. *Journal of Soil Salinity and Water Quality*, *3*(2), 110–126.

Trites, M., & Bayley, S. E. (2009). Vegetation communities in continental boreal wetlands along a salinity gradient: Implications for oil sands mining reclamation. *Aquatic Botany*, *91*(1), 27–39. https://doi.org/10.1016/j.aquabot.2009.01.003

Tsimpanogiannis, I., Yortsos, Y., Poulou, S., Kanellopoulos, N., & Stubos, A. (1999). Scaling theory of drying in porous media. *Physical Review E*, *59*(4), 4353–4365. https://doi.org/10.1103/physreve.59.4353

Tully, K., Gedan, K., Epanchin-Niell, R., Strong, A., Bernhardt, E. S., BenDor, T., et al. (2019). The invisible flood: The chemistry, ecology, and social implications of coastal saltwater intrusion. *BioScience*, *69*(5), 368–378. https://doi.org/10.1093/biosci/biz027

Ullo, S. L., & Sinha, G. R. (2021). Advances in iot and smart sensors for remote sensing and agriculture applications. *Remote Sensing*, *13*(13), 2585. https://doi.org/10.3390/rs13132585

UNEP factsheet. (2017). Land degradation—factsheet. Retrieved from https://www.unep.org/resources/factsheet/land-degradation-factsheet

US Department of Defense. (2014). Security implications of climate change. Retrieved from https://www.defense.gov/News/News-Stories/Article/Article/612710/

US Soil Salinity Laboratory Staff. (1954). *Diagnosis and improvement of saline and alkali soils* (Vol. 60, p.159). US Government Printing Office.

Ustohal, P., Stauffer, F., & Dracos, T. (1998). Measurement and modeling of hydraulic characteristics of unsaturated porous media with mixed wettability. *Journal of Contaminant Hydrology*, *33*(1–2), 5–37. https://doi.org/10.1016/s0169-7722(98)00063-1

Valipour, M. (2014). Drainage, waterlogging, and salinity. *Archives of Agronomy and Soil Science*, *60*(12), 1625–1640. https://doi.org/10.1080/03650340.2014.905676

van Brakel, J. (1980). Mass transfer in convective drying. *Advanced Drying*, *1*, 217–267.

Vanselow, A. P. (1932). Equilibria of the base-exchange reactions of bentonites, permutites, soil colloids, and zeolites. *Soil Science*, *33*(2), 95–114. https://doi.org/10.1097/00010694-193202000-00002

Van Weert, F., & Van Der Gun, J. (2012). Saline and brackish groundwater at shallow and intermediate depths: Genesis and world-wide occurrence. In *IAH congress*. Niagara Falls.

Varela, M., Benito, E., & De Blas, E. (2005). Impact of wildfires on surface water repellency in soils of northwest Spain. *Hydrological Processes: An International Journal*, *19*(18), 3649–3657. https://doi.org/10.1002/hyp.5850

Veran-Tissoires, S., Marcoux, M., & Prat, M. (2012). Discrete salt crystallization at the surface of a porous medium. *Physical Review Letters*, *108*(5), 054502. https://doi.org/10.1103/physrevlett.108.054502

Vermeer, M., & Rahmstorf, S. (2009). Global sea level linked to global temperature. *Proceedings of the National Academy of Sciences*, *106*(51), 21527–21532. https://doi.org/10.1073/pnas.0907765106

Vicente-Serrano, S. M., Quiring, S. M., Peña-Gallardo, M., Yuan, S., & Domínguez-Castro, F. (2020). A review of environmental droughts: Increased risk under global warming? *Earth-Science Reviews*, *201*, 102953. https://doi.org/10.1016/j.earscirev.2019.102953

Vogelbacher, A., Aminzadeh, M., Madani, K., & Shokri, N. (2024). An analytical framework to investigate groundwater-atmosphere interactions influenced by soil properties. *Water Resources Research*, *60*(4), e2023WR036643. https://doi.org/10.1029/2023wr036643

Volmer, M., & Weber, A. (1926). Nuclei formation in supersaturated states. *Journal of Physical Chemistry*, *119*, 277–301.

Vorhauer, N., Tsotsas, E., & Prat, M. (2018). Drying of thin porous disks from pore network simulations. *Drying Technology*, *36*(6), 651–663. https://doi.org/10.1080/07373937.2017.1319853

Vu, D., Yamada, T., & Ishidaira, H. (2018). Assessing the impact of sea level rise due to climate change on seawater intrusion in Mekong Delta, Vietnam. *Water Science and Technology*, *77*(6), 1632–1639. https://doi.org/10.2166/wst.2018.038

Wagner, W., Naeimi, V., Scipal, K., De Jeu, R., & Martínez-Fernández, J. (2007). Soil moisture from operational meteorological satellites. *Hydrogeology Journal*, *15*(1), 121–131. https://doi.org/10.1007/s10040-006-0104-6

Wang, B., Davenport, R. J., Volkov, V., & Amtmann, A. (2006). Low unidirectional sodium influx into root cells restricts net sodium accumulation in thellungiella halophila, a salt-tolerant relative of arabidopsis thaliana. *Journal of Experimental Botany*, *57*(5), 1161–1170. https://doi.org/10.1093/jxb/erj116

Wang, J., Yang, T., Zhu, K., Shao, C., Zhu, W., Hou, G., & Sun, Z. (2023). A novel retrieval model for soil salinity from CYGNSS: Algorithm and test in the yellow river delta. *Geoderma*, *432*, 116417. https://doi.org/10.1016/j.geoderma.2023.116417

Wang, N., Chen, S., Huang, J., Frappart, F., Taghizadeh, R., Zhang, X., et al. (2024). Global soil salinity estimation at 10 m using multi-source remote sensing. *Journal of Remote Sensing*, *4*, 0130. https://doi.org/10.34133/remotesensing.0130

Wang, X., Zhang, H., Zhang, Z., Zhang, C., Zhang, K., Pang, H., et al. (2023). Reinforced soil salinization with distance along the river: A case study of the Yellow River basin. *Agricultural Water Management*, *279*, 108184. https://doi.org/10.1016/j.agwat.2023.108184

Wang, Y., Hu, B., Hong, Y., Chen, S., Zhao, C., & Peng, J. (2024). Minimize of moisture effects from laboratory simulations of in-situ Vis-NIR spectral for the prediction of soil salinity. *Infrared Physics & Technology*, *137*, 105194. https://doi.org/10.1016/j.infrared.2024.105194

Washburn, E. (1926). The creeping of solutions. *Journal of Physical Chemistry*, *31*(8), 1246–1248. https://doi.org/10.1021/j150278a009

Werner, A. D., Bakker, M., Post, V. E., Vandenbohede, A., Lu, C., Ataie-Ashtiani, B., et al. (2013). Seawater intrusion processes, investigation and management: Recent advances and future challenges. *Advances in Water Resources*, *51*, 3–26. https://doi.org/10.1016/j.advwatres.2012.03.004

West, L. T. (2004). Soil development and properties: Landscape and soil classification for forest management. In J. Burley (Ed.), *Encyclopedia of forest sciences* (pp. 1216–1223). Elsevier.

Whitaker, S. (1977). Simultaneous heat, mass, and momentum transfer in porous media: A theory of drying. In *Advances in heat transfer* (Vol. 13, pp. 119–203). Elsevier. https://doi.org/10.1016/s0065-2717(08)70223-5

White, E., & Kaplan, D. (2017). Restore or retreat? Saltwater intrusion and water management in coastal wetlands. *Ecosystem Health and Sustainability*, *3*(1), e01258. https://doi.org/10.1002/ehs2.1258

Wicke, B., Smeets, E., Dornburg, V., Vashev, B., Gaiser, T., Turkenburg, W., & Faaij, A. (2011). The global technical and economic potential of bioenergy from salt-affected soils. *Energy & Environmental Science*, *4*(8), 2669–2681. https://doi.org/10.1039/c1ee01029h

Wild, A. (2003). *Soils, land and food: Managing the land during the twenty-first century*. Cambridge University Press.

Wilkinson, D., & Willemsen, J. F. (1983). Invasion percolation: A new form of percolation theory. *Journal of Physics A: Mathematical and General*, *16*(14), 3365–3376. https://doi.org/10.1088/0305-4470/16/14/028

Wissmeier, L., & Barry, D. (2008). Reactive transport in unsaturated soil: Comprehensive modelling of the dynamic spatial and temporal mass balance of water and chemical components. *Advances in Water Resources*, *31*(5), 858–875. https://doi.org/10.1016/j.advwatres.2008.02.003

Wolde, P. R. T., & Frenkel, D. (1997). Enhancement of protein crystal nucleation by critical density fluctuations. *Science*, *277*(5334), 1975–1978. https://doi.org/10.1126/science.277.5334.1975

Wondim, G. B., Daba, A. W., & Qureshi, A. S. (2020). Effects of salinity on producers' livelihoods and socio-economic conditions; the case of Afar region, northeastern Ethiopia. *Journal of Sustainable Agricultural Sciences*, *46*(3), 35–46.

Wong, V. N., Greene, R., Dalal, R. C., & Murphy, B. W. (2010). Soil carbon dynamics in saline and sodic soils: A review. *Soil Use & Management*, *26*(1), 2–11. https://doi.org/10.1111/j.1475-2743.2009.00251.x

Wu, R., & Chen, F. (2023). Interplay between salt precipitation, corner liquid film flow, and gas–liquid displacement during evaporation in microfluidic pore networks. *Journal of Applied Physics*, *133*(7), 074701. https://doi.org/10.1063/5.0135135

Wu, R., Zhang, T., Ye, C., Zhao, C., Tsotsas, E., & Kharaghani, A. (2020). Pore network model of evaporation in porous media with continuous and discontinuous corner films. *Physical Review Fluids*, *5*(1), 014307. https://doi.org/10.1103/physrevfluids.5.014307

Wu, W. (2019). A brief review on soil salinity mapping by optical and radar remote sensing. *Research Developments in Saline Agriculture*, 53–65. https://doi.org/10.1007/978-981-13-5832-6_2

Wurtsbaugh, W. A., Miller, C., Null, S. E., DeRose, R. J., Wilcock, P., Hahnenberger, M., et al. (2017). Decline of the world's saline lakes. *Nature Geoscience*, *10*(11), 816–821. https://doi.org/10.1038/ngeo3052

Xiao, C., Ji, Q., Chen, J., Zhang, F., Li, Y., Fan, J., et al. (2023). Prediction of soil salinity parameters using machine learning models in an arid region of northwest China. *Computers and Electronics in Agriculture*, *204*, 107512. https://doi.org/10.1016/j.compag.2022.107512

Xie, L., Feng, X., Zhang, C., Dong, Y., Huang, J., & Cheng, J. (2022). A framework for soil salinity monitoring in coastal wetland reclamation areas based on combined unmanned aerial vehicle (UAV) data and satellite data. *Drones*, *6*(9), 257. https://doi.org/10.3390/drones6090257

Xu, X., Wang, J., Tang, Y., Cui, X., Hou, D., Jia, H., et al. (2023). Mitigating soil salinity stress with titanium gypsum and biochar composite materials: Improvement effects and mechanism. *Chemosphere*, *321*, 138127. https://doi.org/10.1016/j.chemosphere.2023.138127

Yang, H., Wang, Z., Cao, J., Wu, Q., & Zhang, B. (2023). Estimating soil salinity using Gaofen-2 imagery: A novel application of combined spectral and textural features. *Environmental Research*, *217*, 114870. https://doi.org/10.1016/j.envres.2022.114870

Yang, J., Lei, T., Wang, G., Xu, Q., Chen, J., & Luo, K. H. (2023). Lattice Boltzmann modelling of salt precipitation during brine evaporation. *Advances in Water Resources*, *180*, 104542. https://doi.org/10.1016/j.advwatres.2023.104542

Yang, L., Huang, C., Liu, G., Liu, J., & Zhu, A.-X. (2015). Mapping soil salinity using a similarity-based prediction approach: A case study in Huanghe River Delta, China. *Chinese Geographical Science*, *25*(3), 283–294. https://doi.org/10.1007/s11769-015-0740-7

Yin, X., Feng, Q., Liu, W., Zhu, M., Zhang, J., Li, Y., et al. (2023). Assessment and mechanism analysis of plant salt tolerance regulates soil moisture dynamics and controls root zone salinity and sodicity in seasonally irrigated agroecosystems. *Journal of Hydrology*, *617*, 129138. https://doi.org/10.1016/j.jhydrol.2023.129138

Yiotis, A., Boudouvis, A., Stubos, A., Tsimpanogiannis, I., & Yortsos, Y. (2004). Effect of liquid films on the drying of porous media. *AIChE Journal*, *50*(11), 2721–2737. https://doi.org/10.1002/aic.10265

Yiotis, A., Salin, D., & Yortsos, Y. (2015). Pore network modeling of drying processes in macroporous materials: Effects of gravity, mass boundary layer and pore microstructure. *Transport in Porous Media*, *110*(2), 175–196. https://doi.org/10.1007/s11242-015-0529-2

Yiotis, A. G., Stubos, A., Boudouvis, A., & Yortsos, Y. C. (2001). A 2-D pore-network model of the drying of single-component liquids in porous media. *Advances in Water Resources*, *24*(3–4), 439–460. https://doi.org/10.1016/s0309-1708(00)00066-x

Yiotis, A. G., Tsimpanogiannis, I. N., Stubos, A. K., & Yortsos, Y. C. (2006). Pore-network study of the characteristic periods in the drying of porous materials. *Journal of Colloid and Interface Science*, *297*(2), 738–748. https://doi.org/10.1016/j.jcis.2005.11.043

Yu, L., Gao, W., R Shamshiri, R., Tao, S., Ren, Y., Zhang, Y., & Su, G. (2021). Review of research progress on soil moisture sensor technology. *International Journal of Agricultural and Biological Engineering*, *14*(3), 32–42. https://doi.org/10.25165/j.ijabe.20211404.6404

Yu, X., Chang, C., Song, J., Zhuge, Y., & Wang, A. (2022). Precise monitoring of soil salinity in China's yellow river delta using UAV-borne multispectral imagery and a soil salinity retrieval index. *Sensors*, *22*(2), 546. https://doi.org/10.3390/s22020546

Zabbey, N., & Olsson, G. (2017). Conflicts–oil exploration and water. *Global challenges*, *1*(5), 1600015. https://doi.org/10.1002/gch2.201600015

Zahn, D. (2004). Atomistic mechanism of NaCl nucleation from an aqueous solution. *Physical Review Letters*, *92*(4), 040801. https://doi.org/10.1103/physrevlett.92.040801

Zaman, M., Shahid, S. A., & Heng, L. (2018). *Guideline for salinity assessment, mitigation and adaptation using nuclear and related techniques*. Springer Nature.

Zamrsky, D., Oude Essink, G. H., & Bierkens, M. F. (2024). Global impact of sea level rise on coastal fresh groundwater resources. *Earth's Future*, *12*(1), e2023EF003581. https://doi.org/10.1029/2023ef003581

Zanchi, C., & Cecchi, S. (2010). Soil salinisation in the grosseto plain (Maremma, Italy): An environmental and socio-economic analysis of the impact on the agro-ecosystem. In *Coastal water bodies: Nature and culture conflicts in the mediterranean* (pp. 79–90).

Zarei, A., Hasanlou, M., & Mahdianpari, M. (2021). A comparison of machine learning models for soil salinity estimation using multi-spectral Earth observation data. In *ISPRS annals of the photogrammetry, remote sensing and spatial information sciences* (Vol. 3, pp. 257–263). https://doi.org/10.5194/isprs-annals-v-3-2021-257-2021

Zeidouni, M., Pooladi-Darvish, M., & Keith, D. (2009). Analytical solution to evaluate salt precipitation during CO_2 injection in saline aquifers. *International Journal of Greenhouse Gas Control*, *3*(5), 600–611. https://doi.org/10.1016/j.ijggc.2009.04.004

Zekri, S., Al-Rawahy, S. A., & Naifer, A. (2010). Socio-economic considerations of salinity: Descriptive statistics of the Batinah sampled farms.

Zeng, Y., Zhao, C., Shi, F., Schneider, M., Lv, G., & Li, Y. (2020). Impact of groundwater depth and soil salinity on riparian plant diversity and distribution in an arid area of China. *Scientific Reports*, *10*(1), 7272. https://doi.org/10.1038/s41598-020-64045-w

Zhang, G.-L., Feng, L., & Song, X.-D. (2017). Recent progress and future prospect of digital soil mapping: A review. *Journal of Integrative Agriculture*, *16*(12), 2871–2885. https://doi.org/10.1016/s2095-3119(17)61762-3

Zhao, C., Zhang, H., Song, C., Zhu, J.-K., & Shabala, S. (2020). Mechanisms of plant responses and adaptation to soil salinity. *The innovation*, *1*(1), 100017. https://doi.org/10.1016/j.xinn.2020.100017

Zhao, W., Cao, T., Li, Z., & Sheng, J. (2019). Comparison of IDW, cokriging and ARMA for predicting spatiotemporal variability of soil salinity in a gravel–sand mulched jujube orchard. *Environmental Monitoring and Assessment*, *191*(6), 1–15. https://doi.org/10.1007/s10661-019-7499-8

Zhao, Y., Li, T., Shao, P., Sun, J., Xu, W., & Zhang, Z. (2022). Variation in bacterial community structure in rhizosphere and bulk soils of different halophytes in the yellow river delta. *Frontiers in Ecology and Evolution*, *9*, 816918. https://doi.org/10.3389/fevo.2021.816918

Zimmermann, N. E., Vorselaars, B., Quigley, D., & Peters, B. (2015). Nucleation of NaCl from aqueous solution: Critical sizes, ion-attachment kinetics, and rates. *Journal of the American Chemical Society*, *137*(41), 13352–13361. https://doi.org/10.1021/jacs.5b08098